Mechanisms of internal phosphorus loading in lentic ecosystems

By

Ellen A. Albright

A dissertation submitted in partial fulfillment of

the requirements for the degree of

Doctor of Philosophy

(Freshwater and Marine Sciences)

at the

UNIVERSITY OF WISCONSIN-MADISON

2022

Date of final oral examination: 4/29/2022

The dissertation is approved by the following members of the Final Oral Committee:

Grace M. Wilkinson, Assistant Professor, Integrative Biology
Steven J. Hall, Associate Professor, Iowa State University
Matthew Ginder-Vogel, Associate Professor, Civil and Environmental Engineering
Emily Stanley, Professor, Integrative Biology
Hilary Dugan, Assistant Professor, Integrative Biology

TABLE OF CONTENTS

ACKNOWLEDGEMENTS

I owe a debt of gratitude to my mentors, collaborators, friends, and family for their insights, guidance, and support over the last five years. Although a dissertation is the product of an individual's academic training, it also represents the time, energy, and sacrifices of many others, for whom I am truly grateful.

To my advisor and mentor Grace, thank you for taking a chance on me as one of your first graduate students. I've had too many people tell me that grad students are like pancakes – you always mess up the first couple, but I like think we proved them wrong. Thank you for helping me grow as a scientist and as a person. I will not soon forget your patience and compassion during times of turmoil and grief. I have learned so much over the past five years, and I feel very lucky to be a part of the Wilkinson Lab. I hope this is the start of many more collaborations.

Thank you to the other members of my advisory committee, Drs. Hilary Dugan, Matt Ginder-Vogel, Steven Hall, and Emily Stanley, for your helpful input and enthusiastic support of my research endeavors. Thank you also to members of my original committee at Iowa State, Drs. Bill Crumpton, Crystal Lu, and Michael Weber, for feedback during the early formulation of my research projects.

I am grateful for my coauthors Rachel Fleck King, Quin Shingai, Robert Ladwig, Tyler Butts, Jess Briggs, and Danny Szydlowski. This dissertation would not have been possible without your efforts, and I am fortunate to work with all of you. Thank you to all members of the Wilkinson Lab both past and present, especially Haley Grigel for helping me through my first year of grad school. I am also thankful for the EEOB grad student community at ISU, particularly Kathleen Thompson, Alex Walton, Angela Bunning, Lydia English and Brittany

Cavazos, and the CFL community at UW for being so welcoming. Thank you to all of my friends for listening to perhaps too many rants about phosphorus over the past few years, especially Kristen Touhey Jessen, Lena Schaller, Ian Lock, Meredith Bensen, and Alex Bauch.

It certainly would not have been possible for me to complete this degree without the love, support, and inspiration of my family. Thank you to my sister Catherine and brother-in-law John for listening to my grad school tribulations, offering good advice, and sending me funny tweets. Thank you to my partner Nate for always believing in me and for supporting me through very challenging times. I don't have the words to adequately thank my parents Bill and Kathy, but thank you for nurturing my curiosity and raising me to cherish the water, land, plants, and critters around me. And for my dad, thank you for teaching me that, "observation is the key to a good scientist."

ABSTRACT

Effective eutrophication management in freshwater ecosystems requires a holistic understanding of internal phosphorus (P) cycling and how nutrient enrichment will interact with other stressors. These management needs inspired the following dissertation research on internal P loading and compounding stressors in shallow lakes, reservoirs, and ponds. **Chapter 1** used literature synthesis and meta-analysis to quantify the magnitude and variability of sediment P flux rates across different lentic ecosystems. This analysis synthesized findings across studies to understand patterns between flux rates and both ecosystem- and site-scale drivers. **Chapter 2** explored the role of sediment P chemistry as a controlling variable on internal P loading by quantifying spatial heterogeneity in sediment P content and composition within and among lakes. This quantitative understanding of variation in sediment P composition is essential for accurately sampling sediment P pools and inferring likely mechanisms for sediment P release. Building off this understanding of high inter-ecosystem variation in sediment P pools, **chapter 3** quantified both seasonal and spatial variation in sediment P pools and fluxes in a temperate reservoir in order to quantify the ecosystem-level impacts of spatiotemporal heterogeneity in internal P loading and identify mechanisms responsible for hot spots of sediment P release. **Chapter 4** focused on specific physicochemical mechanisms that may influence sediment P fluxes (i.e., thermal stratification and dissolved oxygen dynamics) and the role of aquatic plants in structuring these drivers. This analysis highlighted that small waterbodies are spatially complex and temporally dynamics systems. Overall, this research has advanced our understanding of lacustrine P cycling by synthesizing our current understanding of internal P loading in lentic ecosystems and by generating knowledge on spatiotemporal variation in sediment P fluxes and the underlying mechanisms.

INTRODUCTION

Anthropogenic activities have profoundly altered the global phosphorus (P) cycle, enhancing the flux of this nutrient from terrestrial to aquatic ecosystems (Yuan et al. 2018). In inland waterbodies, P enrichment is associated with blooms of algae and cyanobacteria that alter ecosystem structure and function, often with detrimental consequences for other organisms (Carmichael et al. 2001; Schindler et al. 2016). Regulatory and management efforts to curtail external P inputs to lakes and reservoirs may yield dramatic improvements in algal blooms and other eutrophication symptoms (Edmondson 1970). However, in many waterbodies, internal recycling of P between sediments and the overlying water (i.e., internal P loading) maintains high water column P availability, even after external inputs have been reduced (Søndergaard et al. 1999). As eutrophication continues to present grave threats to freshwater resources (Schindler and Vallentyne 2008), there is a pressing need to reduce total P loads in inland waters, which requires a quantitative and mechanistic understanding of internal P loading.

There are many different pathways through which sediment P may be mobilized and released into the water column, which are controlled by a complex web of interacting biogeochemical mechanisms (Wilkinson and Albright in press; Figure 1). For example, P incorporated into sediment organic matter may be mobilized through microbial decomposition and subsequent mineralization. However, this pathway is mediated by many factors including temperature, dissolved oxygen and alternative electron acceptor concentrations, nutrient availability, microbial community composition, and sediment minerology (Song and Burgin 2017; Orihel et al. 2017). Additionally, whether or not the mobilized P will be released into the water depends on depth in the sediment profile, P concentration gradients across the sediment-water interface, and potential for sediment disturbance. Given the influence of dynamic biogeochemical conditions on sediment P mobilization and release pathways, internal P loading

is expected to vary over space and time within individual waterbodies (Kowalczewska-Madura et al. 2019). Spatiotemporal heterogeneity in sediment P fluxes and the complexity of the underlying mechanisms present challenges for managing lentic P cycles. These challenges guided my dissertation research efforts to constrain current knowledge gaps on internal P loading through research synthesis and then explore gaps in our understanding through field and laboratory studies.

The guiding aim of this dissertation is to contribute to a quantitative and mechanistic understanding of internal P loading in lakes, ponds, and reservoirs by acknowledging the spatial and temporal complexity of these ecosystems. In **chapter 1**, I undertook a systematic literature review and meta-analysis to quantify the magnitude and variability of sediment P fluxes among lentic ecosystems worldwide, synthesize findings across studies to understand the relationship between P flux rates and controlling mechanisms at the ecosystem- and site-scales, and identify remaining data gaps that introduce bias into our understanding of internal P loading (e.g., geographic location, types of waterbodies studied, and mechanisms tested). My analysis revealed that the role of sediment characteristics as a controlling variable on internal loading as well as intra-lake variation in sediment P fluxes and mechanisms were not well-quantified in the literature. I explored these knowledge gaps in subsequent chapters.

Chapter 2 focuses on spatial variation in sediment P speciation (i.e., different chemical forms of P that may be present in lakebed sediments such as P associated with minerals, organic materials, or surface complexes). Different forms of sediment P are susceptible to different internal loading pathways (North et al. 2015). As such, the size and chemical composition of the sediment P pool is a pivotal mechanism controlling internal loading. Sediment P composition is expected to vary among different waterbodies with differences in watershed soils, external P

loading, and *in situ* processing (Stone and English 1992; Carpenter et al., 1998; Kerr et al. 2011) as well as within individual lakes following spatial variation in sediment transport, deposition, and resuspension processes (Mackay et al. 2012; Cardoso-Silva et al., 2018). However, the degree of spatial heterogeneity in sediment P pools within and among lakes remains poorly constrained. I measured sediment P speciation across seven glacial lakes, found spatial variation both within and among lakes, and explored how watershed and lake characteristics influenced the observed heterogeneity. This quantitative understanding of inter- and intra-lake variation in sediment P composition is essential for accurately sampling sediment P pools and inferring likely mechanisms for sediment P release.

Building off this understanding of high inter-ecosystem variation in sediment P pools, **chapter 3** quantifies both seasonal and spatial variation in sediment P pools and fluxes in a temperate reservoir. I completed an intensive study of P cycling in a shallow reservoir by measuring sediment P speciation and flux rates over space (i.e., along the longitudinal gradient of the reservoir) and across seasons (i.e., approximating every other month over the course of a year, capturing ice cover and mixing and stratification events during the open water season). My analysis revealed the influence of sediment P release from littoral sediments under oxic conditions and the risks of ignoring winter internal P loading. This chapter quantifies the ecosystem-level impacts of spatiotemporal heterogeneity in internal P loading and identifies mechanisms responsible for hot spots of sediment P release.

The first three chapters focus on P biogeochemistry at the sediment-water interface to better understand the role that internal P loading plays in freshwater eutrophication. **Chapter 4** focuses on specific physicochemical mechanisms that may influence sediment P fluxes (i.e., thermal stratification and dissolved oxygen dynamics) and the role of aquatic plants in

structuring these drivers. Specifically, I measured spatiotemporal variation in thermal structure and dissolved oxygen saturation in ponds and tested how these waterbodies responded to the compounding stressors of nutrient enrichment and aquatic heatwaves. The frequency of aquatic heatwaves has increased over the past century as a result of anthropogenic climate change, and this trend is expected to continue, even under low green-house-gas-emissions scenarios (Woolway et al. 2022). The effects of aquatic heatwaves are well-documented for marine and coastal systems; however, until recently, lake heatwaves have received little attention (Oliver et al. 2018; Woolway et al. 2021). Leveraging an ecosystem experiment, I tested interactions between nutrient loading and aquatic heatwaves in small ponds and evaluated the role of aquatic vegetation in mediating ecosystem response to these stressors. The results indicate that submersed aquatic plants may buffer small waterbodies from brief heatwaves by restricting vertical heat transport and maintaining cooler bottom water temperatures. However, the heatwave was associated with dramatic declines in dissolved oxygen saturation, which has implications for internal P loading and greenhouse gas production.

This dissertation explores the causes and consequences of spatiotemporal heterogeneity in the biogeochemical cycles of lentic ecosystems with an emphasis on internal P loading and ecosystem response to compounding stressors.

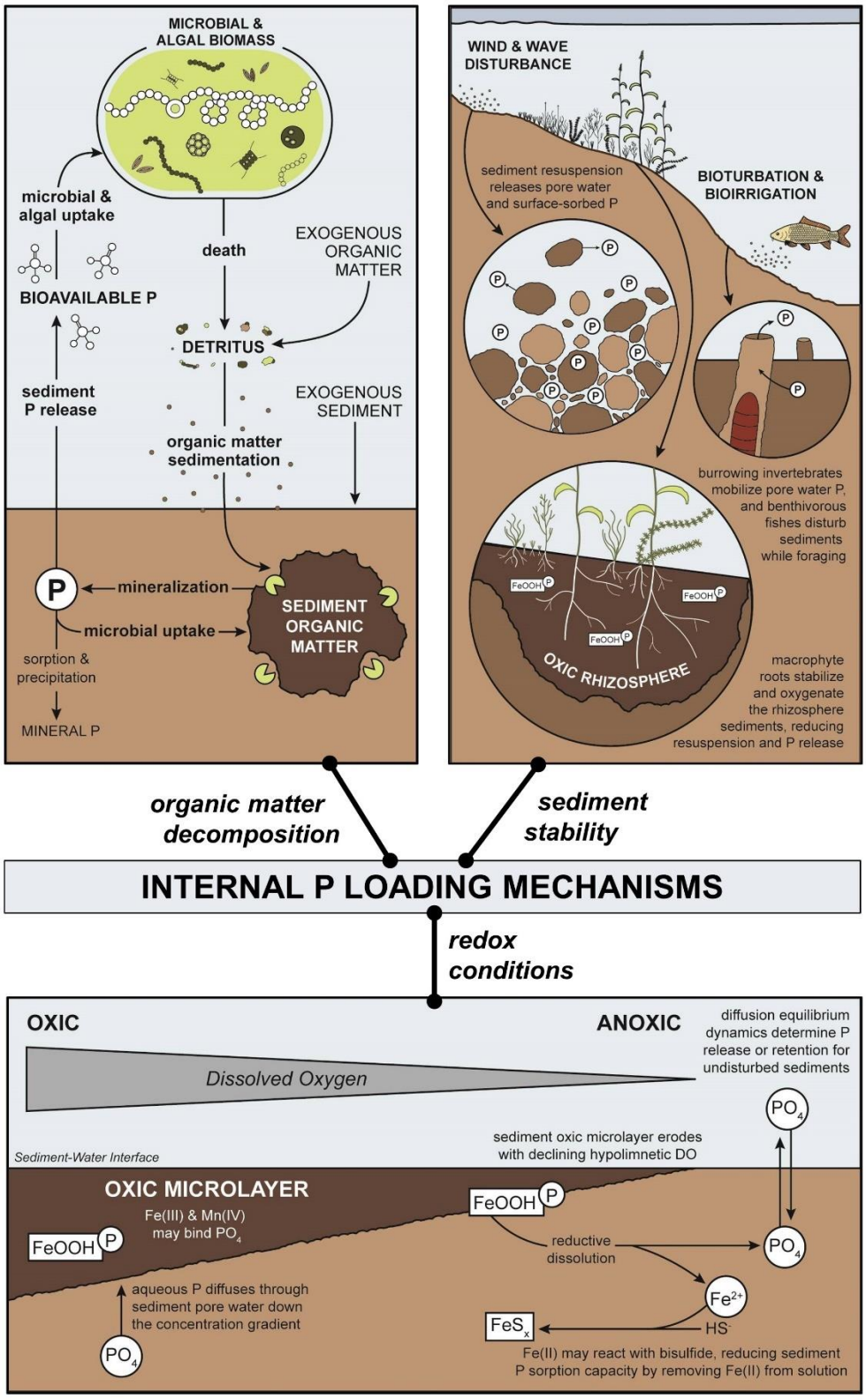

Figure 1. Pathways and controlling mechanisms of internal P loading, modified from Wilkinson and Albright (in press). Illustrations drawn by Albright.

References

1. Cardoso-Silva, S., P.A.d. Ferreira, R.C.L. Figueira, D.C. Silva, V. Moschini-Carlos, and M.L.M. Pompêo. 2018. Factors that control the spatial and temporal distributions of phosphorus, nitrogen, and carbon in the sediments of a tropical reservoir. Environ. Sci. Pollut. Res. 25(31): 31776–31789, doi: 10.1007/s11356-018-2923-0

2. Carmichael, W.W. 2001. Health effects of toxin-producing cyanobacteria: "The CyanoHABs". Hum. Ecol. Risk Assess. **7**(5): 1393-1407, doi: 10.1080/20018091095087

3. Carpenter, S.R., N.F. Caraco, D.L. Correll, R.W. Howarth, A.N. Sharpley, and V.H. Smith. 1998. Nonpoint pollution of surface waters with phosphorus and nitrogen. Ecol. Appl. 8(3): 559-568, doi: 10.1890/1051-0761(1998)008[0559:NPOSWW]2.0.CO;2

4. Edmondson, W.T. 1970. Phosphorus, nitrogen, and algae in Lake Washington after diversion of sewage. Science. 169(3946): 690-691, doi: 10.1126/science.169.3946.690

5. Kerr, J.G., M.A. Burford, J.M. Olley, S.E. Bunn, and J. Udy. 2011. Examining the link between terrestrial and aquatic phosphorus speciation in a subtropical catchment: The role of selective erosion and transport of fine sediments during storm events. Water Res. 45(11): 3331-3340, doi: 10.1016/j.watres.2011.03.048

6. Kowalczewska-Madura, K., R. Gołdyn, J. Bogucka, and K. Strzelczyk. 2019. Impact of environmental variables on spatial and seasonal internal phosphorus loading in a mesoeutrophic lake. Int. J. Sediment Res. 34(1): 14–26, doi: 10.1016/j.ijsrc.2018.08.008

7. Mackay, E.B., I.D. Jones, A.M. Folkard, and P. Barker. 2012. Contribution of sediment focussing to heterogeneity of organic carbon and phosphorus burial in small lakes. Freshw. Biol. 57(2): 290-304, doi:10.1111/j.1365-2427.2011.02616.x

8. North, R.L, J. Johansson, D.M. Vandergucht, L.E. Doig, K. Liber, K. Lindenschmidt, H. Baulch, and J.J. Hudson. 2015. Evidence for internal phosphorus loading in a large prairie reservoir (Lake Diefenbaker, Saskatchewan). J. Great Lakes Res. 41(S2): 91-99, doi: 10.1016/j.jglr.2015.07.003

9. Oliver, E.C.J., et al. 2018. Longer and more frequent marine heatwaves over the past century. Nat. Commun. 9, 1324, doi:10.1038/s41467-018-03732-9

10. Orihel, D.M., H.M. Baulch, N.J. Casson, R.L. North, C.T. Parsons, D.C.M. Seckar, and J.J. Venkiteswaran. 2017. Internal phosphorus loading in Canadian fresh waters: a critical review and data analysis. Can. J. Fish. Aquat. Sci. 74: 2005-2029, doi: 10.1139/cjfas-2016-0500

11. Schindler, D.W., S.R. Carpenter, S.C. Chapra, R.E. Hecky and D.M. Orihel. 2016. Reducing phosphorus to curb lake eutrophication is a success. J. Environ. Sci. Technol. 50(17): 8923-8929., doi: 10.1021/acs.est.6b02204.

12. Schindler, D.W., and J.R. Vallentyne. 2008. *The Algal Bowl: Overfertilization of the World's Freshwaters and Estuaries.* Edmonton: The University of Alberta Press.

13. Song, K., and A.J. Burgin. 2017. Perpetual phosphorus cycling: Eutrophication amplifies biological control on internal phosphorus loading in agricultural reservoirs. Ecosystems. 20(8): 1483-1493, doi: 10.1007/s10021-017-0126-z

14. Stone, M., and M.C. English. 1993. Geochemical composition, phosphorus speciation and mass transport of fine-grained sediment in two Lake Erie tributaries. Hydrobiologia 253: 17-29, doi:10.1007/BF00050719

15. Søndergaard, M., J.P. Jensen, and E. Jeppesen. 1999. Internal phosphorus loading in shallow Danish lakes. Hydrobiologia, 408: 145-152, doi: 10.1023/A:1017063431437

16. Wilkinson, G.M., and E.A. Albright. In press. Phosphorus Cycling in Lacustrine Ecosystems. In the *Encyclopedia of Inland Waters*, 2nd Edition.

17. Woolway, R. I., E. Jennings, T. Shatwell, M. Golub, D.C. Pierson, and S.C. Maberly. 2021. Lake heatwaves under climate change. Nature. 589: 402-407, doi: 10.1038/s41586-020-03119-1

18. Woolway, R.I., C. Albergel, T.L. Frölicher, and M. Perroud. 2022. Severe Lake Heatwaves Attributable to Human-Induced Global Warming. Geophys. Res. Lett. 49(4): e2021GL097031, doi: 10.1029/2021GL097031

19. Yuan, Z.W., S.Y. Jiang, H. Sheng, X. Liu, H Hua, X.W. Liu, and Y. Zhang. 2018. Human perturbation of the global phosphorus cycle: Changes and consequences. J. Environ. Sci. Technol. 52(5): 2438-2450, doi: 10.1021/acs.est.7b03910

CHAPTER 1

INTERNAL PHOSPHORUS LOADING IN LENTIC ECOSYSTEMS: SYNTHESIS, MECHANISMS, AND DATA GAPS

In preparation for submission with coauthors G.M. Wilkinson, J. Briggs, T. Butts, D. Szydlowski

Author Contributions: Albright designed the study; performed the literature search and screening; organized data extraction; cleaned, analyzed, and visualized the data; and wrote the manuscript. Wilkinson contributed to study design, data cleaning, and data analysis and provided writing feedback. Briggs, Butts, and Szydlowski assisted with data extraction.

ABSTRACT

Effective management of freshwater eutrophication requires the ability to forecast internal recycling of phosphorus (P) between sediments and the overlying water. However, this broad predictive capacity is undeveloped, despite a wealth of empirical research on internal P loading. One challenge is that variation in sediment P flux rates and the underlying mechanisms within and among waterbodies remains poorly-constrained. In order to address these uncertainties, we performed a literature synthesis and meta-analysis to quantify sediment P fluxes among lentic ecosystems worldwide, synthesize findings across studies to define relationships between flux rates and controlling mechanisms, and identify remaining data gaps. Our synthesis revealed that sediment P flux rates vary among different ecosystems based on trophic state and basin morphometry. Mean flux rates were approximately 1.5 times greater in eutrophic and hypereutrophic waterbodies compared to oligo-mesotrophic waters. Oxic flux rates decreased with increasing basin depth and surface area while anoxic flux rates followed the

opposite pattern. At the site level, anoxic flux rates were almost twice as great as oxic rates; however, internal P loading was observed under both conditions, demonstrating that aerobic sediment P release is widespread. Sediment P chemistry further modulated site-scale controls on sediment P release with greater total P content and redox-sensitive P concentrations associated with higher release rates under both oxic and anoxic conditions. Our analysis identified future research needs including attention to understudied ecosystems (e.g., reservoirs and tropical waterbodies) and explicit consideration of interactions among internal loading mechanisms. Although further empirical work is needed, our synthesis is an important step in bridging our mechanistic understanding of sediment P fluxes at site and ecosystem scales.

INTRODUCTION

Phosphorus (P) contributing to freshwater eutrophication may enter lakes and reservoirs either through external loading or subsequent internal recycling between sediments and the overlying water (i.e., internal P loading; Carpenter et al. 1998; Søndergaard et al. 2003; Schindler et al. 2016). Effective eutrophication management requires the ability to quantify and forecast the magnitude and mechanisms of internal P loading in a waterbody. However, building this predictive capacity is challenging because internal P loading is typically measured at one spatiotemporal scale yet modeled and managed at another. Direct measurements of sediment P release are commonly made using sediment core incubations (e.g., Ogdahl et al. 2014) at the timescale of hours or days. These *ex-situ* measurements are useful for identifying the mechanisms of sediment P release under controlled conditions; however, scaling these measurements back to the ecosystem can be highly uncertain (Orihel et al. 2017). Alternatively, mass balance or other modeling approaches usually quantify the net P exchange between sediments and the water column for an entire ecosystem on annual or multi-annual scales.

Although this ecosystem-scale perspective is valuable, estimation of internal P loading via mass balance often cannot reveal when or where sediment P release is likely to occur or illuminate the underlying mechanisms for management to act upon.

Sediment P mobilization and release occur across a range of dissolved oxygen conditions at the sediment-water interface and throughout the sediment profile (Hupfer and Lewandowski 2008). The chemical speciation of the sediment P pool in combination with redox conditions mediates the relative importance of anoxic versus oxic mechanisms of P release. Reducing conditions mobilize redox-sensitive P species (i.e., iron- and manganese-bound P), due to dissolution of the host minerals through microbial dissimilatory reduction (Mortimer 1941; Jensen and Andersen 1992). Microbial activity also mobilizes P from sediment organic matter via decomposition and subsequent mineralization, which may occur under anoxia and is enhanced under aerobic conditions (Joshi et al. 2015; Horppila et al. 2017) and warmer temperatures (Jensen and Andersen 1992). This biological pathway is especially influential in hypereutrophic waterbodies, where intense algal production results in substantial labile organic matter inputs to the sediments (Baines and Pace 1994; Jiang et al. 2022), which can be mobilized via enzymatic or photolytic hydrolysis across a range of dissolved oxygen concentrations (Song and Burgin 2017; Frost et al. 2019). Finally, the concentrations of alternative electron acceptors also mediate sediment P release. High nitrate concentrations are thought to prevent the dissolution of manganese and iron oxides under anoxic conditions, thus maintaining sediment P sorption capacity (Parsons et al. 2017; Orihel et al. 2017). Conversely, high sulfate concentrations are associated with increased P release due to sorption site competition, mineralization, and iron sulfide production (Geelhoed et al. 1997; Caraco et al. 1993; Orihel et al. 2015).

The mechanisms mediating sediment P release rates vary both within and among ecosystems and between seasons (Nowlin et al. 2005; Kowalczewska-Madura et al. 2019; Albright and Wilkinson in review, Chapter 3). The relationship between oxygen and sediment P release is expected to vary with sediment P speciation and organic matter content, which are heterogeneous within and among waterbodies (Mackay et al. 2012; Cardoso-Silva et al. 2018). The chemical composition of the sediment P pool varies within individual waterbodies (Albright et al. in review, Chapter 2) because of heterogeneity in sediment transport, deposition, and resuspension (Mackay et al., 2012). Dissolved oxygen availability also varies with the frequency and duration of thermal stratification, the depth of surface water mixing, and the location of macrophyte beds (Wassenaar 2010, Hudson et al. 2015; Han et al. 2018, Albright et al. in prep, Chapter 4). As a result, oxygen-mediated sediment P fluxes are dynamic across space and time and may differ both within and among waterbodies. Organic matter inputs to the sediment also vary within and among different waterbodies following patterns of autochthonous productivity and allochthonous loading (Dietz et al. 2015; Buelo et al. 2018; Ortiz and Wilkinson 2021). In addition to within-ecosystem variability in mechanisms of internal P loading, dominant biogeochemical mechanisms may also vary among lakes and reservoirs, correlated with more static waterbody features such as morphometry, hydrology, and trophic state (Welch and Cooke 1995; Kerr et al. 2011; Song and Burgin 2017).

A wealth of empirical research since the 1940's has revealed the complex and interacting suite of biogeochemical mechanisms that controls internal P loading. However, much of what we know about the magnitude and mechanisms of sediment P fluxes comes from case studies of individual waterbodies, and explicit comparisons of rates among ecosystems have typically been limited in geographic area (e.g., Orihel et al. 2017) or mechanism (e.g., Nürnberg et al. 1986). As

such, there is still uncertainty regarding how observed sediment P fluxes and the underlying mechanisms vary within and across different lentic ecosystems. As a consequence, there is little guidance available for estimating the magnitude and underlying mechanisms of internal loading for ecosystems where direct measurements have not been made, hampering eutrophication management efforts.

We conducted a literature synthesis of sediment P flux rates in freshwater, permanent lentic ecosystems. The primary objectives of our synthesis and meta-analysis were to (1) identify key data gaps based on geographic location, ecosystem type, and dominant mechanisms; (2) quantify the magnitude and variability of sediment P fluxes among lentic ecosystems; (3) synthesize findings across studies to understand the relationship between P flux rates and ecosystem characteristics; and (4) explore the relationship between sediment flux rates and site-scale drivers across a broader range of conditions than typically found in one ecosystem. Our synthesis better quantifies the uncertainty associated with scaling or estimating measurements of sediment P flux within and among waterbodies, informs process-based models of lentic P cycling, and illuminates where targeted empirical research is still needed.

METHODS

Systematic Literature Review and Data Cleaning

In order to synthesize pattens and mechanisms of internal P loading across a diverse population of waterbodies, we performed a systematic review of studies reporting direct measurements of sediment P flux rates from permanent, freshwater lentic ecosystems. We conducted a literature search on 16 June 2021 using the Clarivate Analytics Web of Science database with a targeted search string ("internal p load*" OR "internal phosphor* load*" OR

"sediment P release" OR "sediment phosphor* release" OR "sediment p flux*" OR "sediment phosphor* flux*"). We refined the search to peer-reviewed articles published in English language journals. The initial search returned 543 citations. We evaluated the scope of this search and augmented these returns by using citation-based searches (i.e., backward searches *sensu* Foo et al. 2021) from key reviews and meta-analyses in the field (i.e., Nürnberg et al. 1986, North American and European lakes; Orihel et al. 2017, Canadian and transboundary waters).

Our initial screening followed a decision tree for inclusion based primarily on study system and methods (Figure S1). Our goal was to compare direct measurements of P flux in permanent, inland waters (i.e., lakes, ponds, reservoirs, and permanent wetlands) worldwide. Studies from lotic ecosystems, marine and estuarine areas, and ephemeral wetlands were not considered. We later excluded all wetlands from our analyses due to limited studies (n=4) and combined ponds into the lakes category because the functional transition between the two is gradual (Biggs et al. 2017). Additionally, studies were included only when the source ecosystem was identified and the in-situ sediment structure was not significantly disturbed (e.g., by mixing sediments before placing in an incubation chamber). The focus of our questions was on direct measurements of areal P flux rates between sediments and the overlying water. We defined direct measurements as methods in which any changes in the mass of P in water overlying a discrete area of sediment could be quantified over time (e.g., sediment core incubations or benthic flux chambers). We excluded estimates from modeling, hypolimnetic P accumulation, and measurements of sediment pore water concentrations to infer P diffusion, as these are indirect estimates of P flux and therefore not comparable across methods.

Based on our inclusion criteria, we identified a total of 81 studies (Table S1), from which we extracted data on sediment P flux rates and associated error as well as covariates of interest. Covariates included waterbody features (i.e., location, ecosystem type, morphometric variables, trophic state, mixing regime, water retention time, pH, nitrate concentrations); methodological details (i.e., measurement method, incubation time); incubation conditions (i.e., temperature, dissolved oxygen, pH, nitrate, sulfate); and sediment features (i.e., total P, redox-sensitive P, organic matter content, C:N). As there were few waterbodies classified as either oligotrophic (n=7) or mesotrophic (n=22) in the dataset, we combined these waterbodies into one trophic class, oligo-mesotrophic for further analysis. If data were only presented in figures, we extracted values using Web Plot Digitizer (Rohatgi 2021). We performed additional searches using peer-reviewed literature, technical reports, and websites maintained by agencies or local lake enthusiasts to fill in missing information on waterbody morphometry (i.e., surface area, maximum and minimum depth), water retention time, trophic state, and coordinates for the centroid of the waterbody.

To clean the extracted data, all data were converted to consistent units, as needed (Table S2). We then standardized the type of error associated with flux rate measurements and any continuous covariates by converting any standard error values to standard deviation (i.e., multiply by the square root of the number of samples). Finally, in order to compare studies in which sediment P flux rates were reported using different forms of P (i.e., soluble reactive P, SRP; total reactive P, TRP; total dissolved P, TDP, and total P, TP), we used custom conversions to express all the rates in terms of TP flux following the methods of Orihel et al. (2017). Specifically, we used studies that measured fluxes using both TP and another P form to develop simple linear regressions to estimate TP flux based on a flux rate in another form. We developed

our own equations to convert SRP and TRP to TP (Figures S2-3) and used the equation from Orihel and others (2017) to convert TDP to TP. We were interested in TP flux rates as this measure captures all forms of P that may be exchanged between sediments and the overlying water, including organic forms.

Statistical Methods

Our final dataset included 1,202 observations of sediment P flux rates from 129 waterbodies. Multiple measurements from the same waterbody were either from multiple studies, or in most instances, measurements taken at various locations, times of year, and incubation treatments (e.g., anoxic or oxic). For 495 of the measurements, the mean and error of replicate cores or chambers was reported. We estimated missing error based on the linear relationship estimated with Bayesian regression between mean flux and standard deviation for the studies that reported both values (Figure S4), following the approach of Wilkinson and others (2018).

We used simple linear regressions to explore the relationships between sediment P release rates and continuous ecosystem- and site-scale drivers. There were no clear relationships between raw sediment P flux rates and morphometric variables, incubation conditions, or sediment characteristics (Figure S5). However, given the strong right-skew of both the flux rate values and many of the continuous explanatory variables, we further explored the relationships between sediment P release rates (i.e., positive flux values) and lake basin morphometry and sediment P chemistry using $\log_{10}$-transformed data. At the ecosystem-scale, we regressed P release rates against either waterbody surface area, maximum depth, or mean water residence time. We took a similar approach with site-scale drivers, modeling release rates as a function of

sediment TP or redox-sensitive P concentrations. For analyses at both scales, separate regressions were used for observations made under oxic versus anoxic conditions.

We further tested the effect of dissolved oxygen on sediment P flux rates by calculating the effect size of anoxic versus oxic flux rates at the waterbody level. We selected waterbodies from our dataset in which P flux rates were reported under both oxic and anoxic conditions (n=39). Waterbodies were included in this analysis if there were at least two observations of P flux rates under both oxic and anoxic conditions from the same study, typically under experimental conditions. We calculated effect size as Hedge's *g* to compare the standardized difference in means between P flux rates under oxic versus anoxic conditions and correct for small sample size.

In order to synthesize patterns in P flux rates across different ecosystem characteristics and site-scale conditions, we used Bayesian hierarchical models to estimate mean P flux rates within groups of interest, specifically waterbody type, trophic state, mixing regime, anoxic versus oxic conditions, and littoral versus profundal sediments. Hierarchical models allowed us to account for structure in the data (e.g., variable number of observations from different waterbodies) and the uncertainty of individual observations such that highly uncertain flux rates did not unduly influence the mean estimate. Loosely-informed priors were used for the mean and standard deviation (gamma distribution with shape parameters of 0.001). We ran three Monte Carlo Markov Chains for 300,000 iterations, using a 100,000-iteration burn-in period and then thinning by 10. JAGS (Plumer 2017) was used as a Gibbs sampler to initialize and sample the chains. Trace plots and the Gelman-Rubin diagnostic were used to confirm convergence. The posterior distributions provide a data-informed estimate of mean sediment P flux rate by various waterbody and site characteristics.

All statistical analyses were performed in R version 4.1.2 (R Core Team 2021) using the rjags (Plummer 2021), coda (Plummer et al. 2006), effectsize (Ben-Shachar et al. 2020), and tidyverse (Wickham et al. 2019) packages.

RESULTS AND DISCUSSION

Dimensions of Current Knowledge and Key Data Gaps

Our final dataset included 1,202 observations of sediment P flux rates from 129 individual waterbodies. Lakes comprised the majority of these ecosystems (69% of total waterbodies), while reservoirs were less common (31%). Around half of the waterbodies were eutrophic (51.9%) with the other half divided between hypereutrophic (25.6%) and oligo-mesotrophic (22.5%). Mixing regime was reported for 66 waterbodies, most of which were dimictic or polymictic (56.1 and 40.9%, respectively). There were also two warm monomictic lakes (3.0%); however, due to the paucity of observations from this category, further analyses of mixing regime were limited to dimictic and polymictic systems. The waterbodies included in the dataset represented a wide range of morphometries (Table S3); however, the majority were relatively small (median surface area 2.28 km^2) and shallow (median maximum and mean depths 8.3 m and 6.0 m respectively).

The waterbodies in the data set are located on four continents, without any lakes or reservoirs from South America, Africa, or Antarctica. Waterbodies were overwhelmingly located in Europe and North America (38.8 and 57.4% of waterbodies, respectively), particularly in central and northern Europe as well as the central contiguous United States and along the southern Canadian border (Figure 1). The majority of reservoirs in the dataset were located in the Great Plains and Prairies of the United States and Canada, while lakes were more commonly

studied in Europe. Over half of the European study lakes were located in either Poland or Denmark.

The continuous covariates of interest were unevenly represented across studies (Table S4). Besides lake morphometric features, the most commonly reported mechanistic variables were temperature and dissolved oxygen conditions during sediment incubations (76.5 and 81.5% of studies, respectively). Alternative electron acceptors and pH were rarely reported at either the lake or core incubation level. For example, incubation sulfate concentrations were measured in 1.2% of included studies. Continuous explanatory variables were considered for further analyses if measurements were available for $\geq$ 20% of study waterbodies (Table 1).

Despite extensive research on the myriad biogeochemical mechanisms that may control internal P loading (Orihel et al. 2017), we found that studies reporting direct measurements of sediment P flux rates did not always include potential explanatory variables. Studies that did consider underlying mechanisms were overwhelmingly focused on temperature or dissolved oxygen conditions as an oxic versus anoxic dichotomy. Far less data were available on the role of water chemistry (i.e., pH and alternative electron acceptors) and sediment characteristics. Sediment P speciation as well as organic matter content and quality are expected to mediate the relative importance of other biogeochemical mechanisms because different chemical forms of P are susceptible to different release mechanisms (North et al. 2015), and organic matter quality largely determines if decomposition will result in P mineralization or immobilization (Davis and van der Valk 1978; Guillemette et al. 2013). However, it is difficult to evaluate these interactions across different waterbodies as few studies quantify sediment characteristics in addition to other potential mechanisms. Furthermore, there was a dearth of data from direct measurements on how sulfate concentrations affect P flux rates, despite evidence that high sulfate concentrations likely

enhance sediment P release (Geelhoed et al. 1997; Caraco et al. 1993; Orihel et al. 2015). Although atmospheric sulfur deposition has declined since the 1990's, industrial and agricultural sources continue to provide a flux of sulfur to inland waters (Rappold and Lackner 2010), highlighting the need to better quantify how sulfate pollution affects internal P loading.

We identified clear geographic biases in direct measurements of sediment P flux rates in lakes and reservoirs. To a degree, the concentration of study waterbodies in the mid-latitudes of the northern hemisphere reflects the latitudinal distribution of waterbodies globally (Verpoorter et al. 2014). However, lakes and reservoirs in the northern boreal region, the tropics, and the mid-latitudes of the southern hemisphere are still dramatically underrepresented in our knowledge of the magnitude and mechanisms of internal P loading. Common rationales for studying internal P loading may explain some of the geographic disparities. Specifically, sediment P fluxes are more likely to be measured in waterbodies experiencing eutrophication, which aligns with the high proportion of eutrophic and hypereutrophic waterbodies in the dataset and may explain the high densities of study waterbodies in agricultural regions of North America and Europe. We also found that reservoirs were underrepresented in the dataset overall, and were overwhelmingly located in the central region of the contiguous United States. Given forecasted increases in large, hydro-power reservoirs globally (Zarfl et al. 2015), there is a pressing need to better quantify the magnitude and mechanisms of sediment P release in reservoirs across a broader geographic scope.

Magnitude and Variability of P Flux Rates and Relationship to Ecosystem Characteristics

Sediment P flux rates ranged from -26.60 to 226.97 mg P m^{-2} day^{-1} (Figure 2). Error was reported for 41.2% of the flux rate observations and, as expected, was generally higher for

greater flux values. Negative rates (91 observations, 7.57%) indicate P flux into the sediments from the overlying water while positive values (1111 observations, 92.43%) show sediment P release. Sediment P flux rates varied among different lentic ecosystems based on waterbody type, trophic state, and mixing regime. The posterior probability distributions from our Bayesian hierarchical models provide estimates of average sediment P flux rates based on ecosystem characteristics (Table 2; Figure 3). By waterbody type, mean flux rates are slightly higher in reservoirs than lakes; however, there is overlap in the 95% credible intervals of these two groups, due in part to greater uncertainty in the reservoir posterior distribution (Figure 3A). Sediment P flux rates vary by waterbody trophic status, specifically with mean rates increasing from oligo-mesotrophic waterbodies to eutrophic and hypereutrophic waters (Figure 3B). Posterior distributions from eutrophic and hypereutrophic ecosystems were very similar and included a high degree of overlap in the credible intervals. However, mean flux rates from oligo-mesotrophic waters were much lower and the credible interval did not overlap with those of more productive systems. Additionally, P flux rates were distinct between dimictic and polymictic waterbodies (Figure 3C). Mean rates were greater in polymictic ecosystems and the credible intervals of these two groups did not overlap.

Sediment P release rates further varied among different ecosystems based on morphometric characteristics, and the direction of these relationships differed with dissolved oxygen conditions (Figure 4). Under oxic conditions, there was a significant, negative relationship between P release rates and waterbody surface area ($F_{1,649}$=93.44, p<0.0001, β_1= -0.16 [-0.19, -0.13]; Figure 4A), maximum depth ($F_{1,606}$=166.1, p<0.0001, β_1= -0.56 [-0.65, -0.48]; Figure 4B), and mean residence time ($F_{1,532}$=107.2, p<0.0001, β_1= -0.35 [-0.41, -0.28]; Figure 4C). For anoxic sediments there were significant, positive relationships between P release

and basin surface area ($F_{1,399}$=10.04, p=0.0016, β_1=0.06 [0.02, 0.10]; Figure 4A) and maximum depth ($F_{1,361}$=10.19, p=0.0015, β_1=0.21 [0.08, 0.34]; Figure 4B). Anoxic release rates were consistent across mean residence time. Overall, sediment P release rates under oxic conditions were lower for deeper, larger waterbodies while anoxic release rates increased with basin size.

We determined the effect size of anoxic versus oxic conditions on sediment P flux rates at the waterbody-level, using observations from 39 waterbodies for which flux rates were measured under both conditions. Across waterbodies the effect size (mean $\pm$ standard deviation) ranged from -1.58 $\pm$ 0.47 to 4.51 $\pm$ 0.77 (Figure 5). Negative values indicate that oxic flux rates are greater than anoxic (n=3 waterbodies) while positive effect size values indicate that flux rates are greater under anoxic conditions (n=33). The global standardized mean effect size was 1.02 $\pm$ 0.52, indicating a large effect of anoxia on sediment P flux rates.

Variation in sediment P flux rates among different ecosystems followed patterns with trophic state and basin morphometry. Higher flux rates in eutrophic and hypereutrophic waterbodies are likely linked to differences in both sediment P pools and primary production between oligo-mesotrophic waterbodies and more productive systems. Specifically, eutrophic to hypereutrophic waters have probably experienced greater external P loading, yielding a larger pool of legacy P in the sediments that may be available for release. Additionally, eutrophied lakes and reservoirs have greater phytoplankton production, resulting in enhanced inputs of labile organic materials to the sediments (Baines and Pace 1994; Jiang et al. 2022). A large pool of labile organic materials, coupled with high nutrient availability in productive ecosystems will likely result in P mineralization during microbial decomposition of sediment organic matter, and thus higher sediment P flux rates. Our finding of higher flux rates in more productive waterbodies, across a broad range of lakes and reservoirs, supports empirical research indicating

that hypereutrophic waterbodies may enter a positive feedback loop of "perpetual" internal P cycling (Song and Burgin 2017). Specifically, heightened phytoplankton production in eutrophic systems contributes large detrital inputs to the sediments, where decomposition results in P mineralization and release into the overlying water under a range of oxygen conditions (Joshi et al. 2015; Horppila et al. 2017; Frost et al. 2019). Released P then fuels additional algal blooms, closing the loop. The potential mechanisms underlying observed differences in P flux rates across waterbody trophic state underscore the importance of quantifying sediment P and organic matter characteristics when measuring internal P loading.

Flux rates further varied among ecosystems based on basin morphometry, and dissolved oxygen conditions modulated the direction of the relationship between sediment P release and basin size. Under oxic conditions P release rates declined with increasing basin surface area, maximum depth, and mean water residence times. This pattern may be explained by larger waterbodies tending to be more oligotrophic, resulting in less *in situ* organic matter production and inputs to the sediments to fuel aerobic sediment P mobilization and release. Conversely, anoxic release rates increased in larger and deeper waterbodies, but the relationships were not as strong as those for oxic P release. It is possible that morphometric variables considered covary with sediment P chemistry with larger, deeper waterbodies having greater concentrations of redox-sensitive P, enhancing anoxic release rates. Given the importance of sediment characteristics, along with the strong effect size of dissolved oxygen conditions, we further investigated the effects of these drivers on P flux rates on a site-scale.

Site-Scale Drivers of Sediment P Fux Rates

In addition to synthesizing patterns between P flux rates and ecosystem characteristics, we also explored how fluxes varied with site-scale drivers, specifically sediment P chemistry, dissolved oxygen conditions, and sediment location. We estimated differences in P flux rates based on dissolved oxygen status during the incubation (i.e., oxic versus anoxic) and sediment location (i.e., profundal versus littoral; Table 2; Figure 6). Dissolved oxygen condition was defined for 97.9% of the observations in the dataset, and there were approximately twice as many oxic observations as anoxic (61.6 and 32.3% of observations respectively). Profundal or littoral location was provided for 92.5% of observations, with profundal sediments more commonly sampled than littoral (56.4 and 36% respectively). Mean P flux rates were distinct between oxic and anoxic conditions (Figure 6A). The mean rates were almost twice as great in the anoxic group, and there was no overlap in the 95% credible intervals. When sediment location was crossed with dissolved oxygen conditions, mean P flux rates were lowest in the littoral-oxic group and then increased from profundal-oxic to littoral-anoxic to the highest mean in the profundal-anoxic group (Figure 6B). Profundal-anoxic was the only group for which the credible interval did not overlap with any other group.

Sediment P release rates further varied with sediment P chemistry and dissolved oxygen conditions as a site-scale drivers. There were significant, direct relationships between release rates and sediment TP content under both oxic and anoxic conditions (oxic $F_{1,368}$=64.17, $p<0.0001$, β_1= 0.85 [0.64, 1.06]; anoxic $F_{1,264}$=11.82, p=0.00068, β_1=0.37 [0.16, 0.58]; Figure 7A). Similarly, both dissolved oxygen conditions had a direct relationship with redox-sensitive P concentrations in the sediments (oxic $F_{1,185}$=15.25, p=0.00013, β_1= 0.60 [0.30, 0.90]; anoxic $F_{1,136}$=9.3, p=0.003, β_1= 0.43 [0.15, 0.71]); Figure 7B).

Our analyses of site-scale drivers of internal loading reinforced the central role of the sediment P pool and dissolved oxygen conditions in determining rates. As anticipated from the empirical emphasis on anaerobic internal loading processes, sediment P flux rates were greater under anoxic conditions. However, the credible interval of the estimate for mean oxic flux rates did not include zero. This synthesis supports empirical evidence for the importance of internal P loading under oxic conditions (James et al. 2015; Horppila et al. 2017; Tammeorg et al. 2017) in both the littoral and profundal regions. Under both oxic and anoxic conditions, sediment P release rates increased with higher total sediment P content and redox-sensitive P concentrations. These relationships support a growing appreciation for the complexity of P mobilization under oxic conditions at the sediment-water interface (Hupfer and Lewandowski 2008). Specifically, that the role of an oxidized microlayer of redox-sensitive minerals on the sediment surface preventing P release into the overlying water is likely limited to a brief temporal scale due to sediment disturbance and mobilization of P from deeper in the anoxic sediment profile. Overall, these site-scale analyses suggest the importance of incorporating processes within the sediment profile into our understanding of internal P loading and moving beyond the dichotomy of oxic versus anoxic conditions and considering dissolved oxygen as a continuous variable that may be highly variable over space and time within waterbodies.

Conclusions and Research Needs

Through our literature synthesis and meta-analysis, we have quantified the magnitude of sediment P flux rates across lentic ecosystems and identified sources of variation in rates within waterbodies at a site-scale and among different waterbodies at an ecosystem level. While dissolved oxygen conditions at the sediment-water interface have been a focus of internal P

loading studies for decades (e.g., Nurnberg et al. 1986; Hupfer and Lewandowski 2008), this synthesis demonstrates the widespread persistence of internal loading under oxic conditions in both profundal and littoral habitats, particularly in small, shallow lakes. Across a variety of lakes and reservoirs of varying trophic state and basin morphometry, sediment P chemistry and dissolved oxygen conditions are key drivers of the magnitude of sediment P flux rates. However, this understanding comes from a biased population of waterbodies that is heavily skewed towards temperate lakes in Europe and North America. Large reservoirs and tropical waterbodies are under-represented in direct measurements of sediment P flux rates, limiting our understanding of internal P loading processes across the global population of lentic ecosystems, specifically the roles of large riverine sediment inputs and consistently warmer temperatures.

Additionally, few studies explicitly evaluated interactions between different drivers of sediment P release. As such, there is a need for targeted research to test these interactions, especially between sediment P chemistry and organic matter characteristics under more dynamic biogeochemical conditions. Furthermore, our mechanistic understanding of internal P loading would benefit from additional studies considering dissolved oxygen as a continuous variable, rather than an oxic versus anoxic classification. Such analyses would better define the shape of the relationship between sediment P flux rates and dissolved oxygen availability and potentially identify critical thresholds in oxygen levels for mobilization of different sediment P forms (e.g., organic versus mineral-associated P).

Given the variability observed in both rates and drivers, more attention to spatiotemporal variation in sediment P fluxes and the underlying mechanisms within individual waterbodies is needed. Although further empirical research is necessary to support our mechanistic understanding of internal P loading in lentic ecosystems, our synthesis provides an important

step in bridging our understanding of sediment P fluxes at different scales (i.e., site versus ecosystem) and providing guidance for estimating the magnitude and mechanisms of internal loading for ecosystems where few or no direct measurements are available. Ultimately, this predictive capacity will be necessary to guide eutrophication management by identifying when and where sediment P release is likely to occur and illuminating the underlying mechanisms for management action.

Acknowledgements

Albright was supported by the National Science Foundation Graduate Research Fellowship Program under Grant No. DGE-1747503. Any opinions, findings, and conclusions or recommendations expressed in this material are those of the authors and do not necessarily reflect the views of the National Science Foundation. Support was also provided by the Graduate School and the Office of the Vice Chancellor for Research and Graduate Education at the University of Wisconsin-Madison with funding from the Wisconsin Alumni Research Foundation. Wilkinson was supported by the National Science Foundation Division of Environmental Biology grant #1942256 and #2200391.

REFERENCES

1. Albright, E.A., and G.M. Wilkinson. In review. Sediment phosphorus composition controls hot spots and hot moments of internal loading in a temperate reservoir. Ecosphere.

2. Albright, E.A., R. Fleck King, Q. Shingai, and G.M. Wilkinson. In review. High inter- and intra-lake variation in sediment phosphorus pools in shallow lakes. JGR-Biogeosciences.

3. Albright, E.A., R. Ladwig, and G.M. Wilkinson. In preparation. Effects of macrophyte bed development on stratification and dissolved oxygen dynamics in shallow lakes. Target Journal: Limnology and Oceanography.

4. Baines, S.B., and M.L. Pace. 1994. Relationships between suspended particulate matter and sinking flux along a trophic gradient and implications for the fate of planktonic primary production. Can. J. Fish. Aquat. Sci. 51 (1): 25-36, doi: 10.1139/f94-005

5. Ben-Shachar, M., D. Lüdecke, and D. Makowski. 2020. effectsize: Estimation of Effect Size Indices and Standardized Parameters. J. Open Source Softw. 5(56): 2815, doi: 10.21105/joss.02815

6. Biggs, J., S. von Fumetti, and M. Kelly-Quinn. 2017. The importance of small waterbodies for biodiversity and ecosystem services: implications for policy makers. Hydrobiologia. 793(1): 3-39, doi: 10.1007/s10750-016-3007-0

7. Buelo, C.D., S.R. Carpenter, and M.L. Pace. 2018. A modeling analysis of spatial statistical indicators of thresholds for algal blooms. Limnol. Oceanogr. Lett. 3(5): 384–392, doi: 10.1002/lol2.10091

8. Caraco, N.F., J.J. Cole, and G.E. Likens. 1993. Sulfate control of phosphorus availability in lakes: A test and re-evaluation of Hasler and Einsele's Model. Hydrobiologia. 253(1-3): 275-280, doi: 10.1007/BF00050748

9. Cardoso-Silva, S., P.A.d. Ferreira, R.C.L. Figueira, D.C. Silva, V. Moschini-Carlos, and M.L.M. Pompêo. 2018. Factors that control the spatial and temporal distributions of phosphorus, nitrogen, and carbon in the sediments of a tropical reservoir. Environ. Sci. Pollut. Res. 25(31): 31776–31789, doi: 10.1007/s11356-018-2923-0

10. Carpenter, S.R., N.F. Caraco, D.L. Correll, R.W. Howarth, A.N. Sharpley, and V.H. Smith. 1998. Nonpoint pollution of surface waters with phosphorus and nitrogen. Ecol. Appl. 8(3): 559-568, doi: 10.1890/1051-0761(1998)008[0559:NPOSWW]2.0.CO;2

11. Davis, C.B., and A.G. van der Valk. 1978. Litter decomposition in prairie glacial marshes. In Good, R.E., D.F. Whigham, and R.L. Simpson. (eds), Freshwater wetlands. Ecologial processes and management potential. Academic Press, NY, 99-113.

12. Dietz, R.D., D.R. Engstrom, and N.J. Anderson. 2015. Patterns and drivers of change in organic carbon burial across a diverse landscape: Insights from 116 Minnesota lakes. Global Biogeochem. Cy. 29(5): 708-727, doi: 10.1002/2014GB004952

13. Foo, Y.Z., R.E. O'Dea, J. Koricheva, S. Nakagawa, and M. Lagisz. 2021. A practical guide to question formation, systematic searching and study screening for literature reviews in ecology and evolution. Methods Ecol. Evol. 12(9): 1705-1720, doi: 0.1111/2041-210X.13654

14. Frost, P. C., C. Prater, A.B. Scott, K. Song, and M.A. Xenopoulos. 2019. Mobility and Bioavailability of Sediment Phosphorus in Urban Stormwater Ponds. Water Resour. Res. 55(5): 3680-3688, doi: 10.1029/2018WR023419

15. Geelhoed, J.S., T Hiemstra, and W.H. Van Riemsdijk. 1997. Phosphate and sulfate adsorption on goethite: single anion and competitive adsorption. Geochim. Cosmochim. Acta. 61(12): 2389–2396, doi:10.1016/S0016-7037(97)00096-3

16. Guillemette, F., S.L. McCallister, and P.A. del Giorgio. 2013. Differentiating the degradation dynamics of algal and terrestrial carbon within complex natural dissolved organic carbon in temperature lakes. J. Geophys. Res. Biogeosci. 118(3): 963-973, doi: 10.1002/jgrg.20077

17. Han, C., J. Ren, Z. Wang, S. Yang, F. Ke, D. Xu, and X. Xie. 2018. Characterization of phosphorus availability in response to radial oxygen losses in the rhizosphere of Vallisneria spiralis. Chemosphere. 208: 740-748, doi: 10.1016/j.chemosphere.2018.05.180

18. Horppila, J., H. Holmroos, J. Niemistö, I. Massa, N. Nygrén, P. Schonach, P. Tapio, and O. Tammeorg. 2017. Variations of internal phosphorus loading and water quality in a hypertrophic lake during 40 years of different management efforts. Ecol. Eng. 103: 264-274, doi: 10.1016/j.ecoleng.2017.04.018 0925-8574

19. Hudson, J.J., and D.M. Vandergucht. 2015. Spatial and temporal patterns in physical properties and dissolved oxygen in Lake Diefenbaker, a large reservoir on the Canadian Prairies. J. Great Lakes Res. 41: 22-33. doi: 10.1016/j.jglr.2015.06.007

20. Hupfer, M., and J. Lewandowski. 2008. Oxygen controls the phosphorus release from lake sediments – a long-lasting paradigm in limnology. Int. Rev. Hydrobiol. 93(4-5):415-432, doi: 10.1002/iroh.200711054

21. James, W.F., P.W. Sorge, and P.J. Garrison. 2015. Managing internal phosphorus loading and vertical entrainment in a weakly stratified eutrophic lake. Lake Reserv. Manag. 31: 292-305, doi: 10.1080/10402381.2015.1079755

22. Jensen, H.S., and F.Ø. Andersen. 1992. Importance of temperature, nitrate, and pH for phosphate release from aerobic sediments of four shallow, eutrophic lakes. Limnol. Oceanogr. 37(3): 577-598, doi: 10.4319/lo.1992.37.3.0577

23. Jiang, X.Y., G. Gao, Y. Hu, K.Q. Shao, X.M. Tang, H. Cheng, and J. Li. 2022. The shift from macrophytic to algal particulate organic matter favours dissimilatory nitrate reduction to ammonium over denitrification in a eutrophic lake. Freshw. Biol. 67(3): 564-576, doi: 10.1111/fwb.13863

24. Joshi, S.R., R.K. Kukkadapu, D.J. Burdige, M.E. Bowden, D.L. Sparks, and D.P. Jaisi. 2015. Organic matter remineralization predominates phosphorous cycling in the mid-bay sediments in the Chesapeake Bay. Environ. Sci. Technol. 49(10): 5887-5896, doi: 10.1021/es5059617

25. Kerr, J.G., M.A. Burford, J.M. Olley, S.E. Bunn, and J. Udy. 2011. Examining the link between terrestrial and aquatic phosphorus speciation in a subtropical catchment: The role of selective erosion and transport of fine sediments during storm events. Water Res. 45(11): 3331-3340, doi: 10.1016/j.watres.2011.03.048

26. Kowalczewska-Madura, K., R. Gołdyn, J. Bogucka, and K. Strzelczyk. 2019. Impact of environmental variables on spatial and seasonal internal phosphorus loading in a mesoeutrophic lake. Int. J. Sediment Res. 34(1): 14–26, doi: 10.1016/j.ijsrc.2018.08.008

27. Mackay, E.B., I.D. Jones, A.M. Folkard, and P. Barker. 2012. Contribution of sediment focussing to heterogeneity of organic carbon and phosphorus burial in small lakes. Freshw. Biol. 57(2): 290-304, doi:10.1111/j.1365-2427.2011.02616.x

28. Mortimer, C. 1941. The exchange of dissolved substances between mud and water in lakes. Ecology. 29: 280-239, doi: 10.2307/2256395

29. North, R.L, J. Johansson, D.M. Vandergucht, L.E. Doig, K. Liber, K. Lindenschmidt, H. Baulch, and J.J. Hudson. 2015. Evidence for internal phosphorus loading in a large prairie reservoir (Lake Diefenbaker, Saskatchewan). J. Great Lakes Res. 41(S2): 91-99, doi: 10.1016/j.jglr.2015.07.003

30. Nowlin, W.H., J.L. Evarts, and M.J. Vanni. 2005. Release rates and potential fates of nitrogen and phosphorus from sediments in a eutrophic reservoir. Freshw. Biol. 50(2): 301–322, doi: 10.1111/j.1365-2427.2004.01316.x

31. Nürnberg, G.K., M. Shaw, P.J. Dillon, and D.J. McQueen. 1986. Internal phosphorus loading in an oligotrophic Precambrian shield lake with an anoxic hypolimnion. Can. J. Fish. Aquat. Sci. 43(3): 574-580, doi: 10.1139/f86-068

32. Ogdahl, M.E., A.D. Steinman, and M.E. Weinert. 2014. Laboratory-determined phosphorus flux from lake sediments as a measure of internal phosphorus loading. J. Vis. Exp. 85: e51617, doi: 10.3791/51617.

33. Orihel, D.M., H.M. Baulch, N.J. Casson, R.L. North, C.T. Parsons, D.C.M. Seckar, and J.J. Venkiteswaran. 2017. Internal phosphorus loading in Canadian fresh waters: a critical

review and data analysis. Can. J. Fish. Aquat. Sci. 74: 2005-2029, doi: 10.1139/cjfas-2016-0500

34. Orihel, D. M., D.W. Schindler, N.C. Ballard, M.D. Graham, D.W. O'Connell, L.R. Wilson, and R. D. Vinebrooke. 2015. The "nutrient pump:" Iron-poor sediments fuel low nitrogen-to-phosphorus ratios and cyanobacterial blooms in polymictic lakes. Limnol. Oceanogr. 60(3): 856-871, doi:10.1002/lno.10076

35. Ortiz, D.A., and G.M. Wilkinson. 2021. Capturing the spatial variability of algal bloom development in a shallow temperate lake. Freshw. Biol. 66(11): 2064-2075, doi:10.1111/fwb.13814

36. Parsons, C.T., F. Rezanezhad, D.W. O'Connell, and P. Van Cappellen. 2017. Sediment phosphorus speciation and mobility under dynamic redox conditions. Biogeosciences. 14(14): 3585–3602, doi:10.5194/bg-14-3585-2017

37. Plummer, M. 2017. JAGS: Just another Gibbs Sampler. https://mcmc-jags.sourceforge.io/

38. Plummer, M. 2021. rjags: Bayesian Graphical Models using MCMC. R package version 4-12. https://CRAN.R-project.org/package=rjags

39. Plummer, M., N. Best, K. Cowles, and K. Vines. 2006. CODA: Convergence Diagnosis and Output Analysis for MCMC. R News. 6: 7-11.

40. R Core Team. 2021. R: A language and environment for statistical computing. R Foundation for Statistical Computing, Vienna, Austria. https://www.R-project.org/.

41. Rappold, T.A., and K.S. Lackner. 2010. Large scale disposal of waste sulfur: From sulfide fuels to sulfate sequestration. Energy. 35(3): 1368-1380, doi: 10.1016/j.energy.2009.11.022

42. Rohatgi, A. 2021. WebPlotDigitizer. Version 4.5. https://automeris.io/WebPlotDigitizer

43. Schindler, D.W., S.R. Carpenter, S.C. Capra, R.E. Hecky, and D.M. Orihel. 2016. Reducing phosphorus to curb lake eutrophication a success. Environ. Sci. Technol. 50(17): 8923-8929, doi: 10.1021/acs.est.6b02204

44. Song, K., and A.J. Burgin. 2017. Perpetual phosphorus cycling: Eutrophication amplifies biological control on internal phosphorus loading in agricultural reservoirs. Ecosystems. 20(8): 1483-1493, doi: 10.1007/s10021-017-0126-z

45. Søndergaard, M., J.P. Jensen, and E. Jeppesen. 2003. Role of sediment and internal loading of phosphorus in shallow lakes. Hydrobiologia. 506: 135-145, doi: 10.1023/B:HYDR.0000008611.12704.dd

46. Tammeorg, O., T. Möls, J. Niemistö, H. Holmroos, and J. Horppila. 2017. The actual role of oxygen deficit in the linkage of the water quality and benthic phosphorus release: Potential implications for lake restoration. Sci.Total Environ. 599-600: 732-738, doi: 10.1016/j.scitotenv.2017.04.244

47. Verpoorter, C., K. Tiit, D.A. Seekell, and L.J. Tranvik. 2014. A global inventory of lakes based on high-resolution satellite imagery. Geophys. Res. Letter. 41: 6396-6402, doi: 10.1002/2014GL060641

48. Wassenaar, L.I. 2010. Dissolved oxygen status of Lake Winnipeg: Spatio-temporal and isotopic (delta O-18-O-2) patterns. J. Great Lakes Res. 38: 123-134, doi: 10.1016/j.jglr.2010.12.011

49. Welch, E.B., and G.D. Cooke. 1995. Internal phosphorus loading in shallow lakes: Importance and control. Lake. Reserv. Manag. 11(3): 273-281, doi: 10.1080/07438149 509354208

50. Wickham, H., et al. 2019. Welcome to the tidyverse. J. Open Source Softw. 4(43): 1686, doi: 10.21105/joss.01686

51. Wilkinson, G.M., A. Besterman, C. Buelo, J. Gephart, and M.L. Pace. 2018. A synthesis of modern organic carbon accumulation rates in coastal and aquatic inland ecosystems. Sci. Rep. 18: 15736, doi: 10.1038/s41598-018-34126-y

52. Zarfl, C., A.E. Lumsdon, J. Berlekamp, L. Tydecks, and K. Tocker. 2015. A global boom in hydropower dam construction. Aquat. Sci. 77(1): 161-170, doi: 10.1007/s00027-014-0377-0

TABLES

Table 1. Summary of continuous explanatory variables included in analyses

Variable	Value Range	Median Value	Number of Waterbodies	Percent of waterbodies
Surface Area (km^2)	0.0004 - 59600	2.28	122	94.6%
Incubation DO (mg L^{-1})	0 - 14	0.59	110	85.3%
Incubation Temperature (°C)	2 - 30	16	103	79.8%
Maximum Depth (m)	0.8 - 260	8.3	98	76.0%
Mean Depth (m)	0.41 - 147	6	83	64.3%
Water Residence Time (yr)	0.006 - 191	0.7	72	55.8%
Sediment Total P (mg P g^{-1} DW)	0.14 - 6.8	1.26	63	48.8%
Sediment Redox P (mg P g^{-1} DW)	0 - 2.517	0.064	38	29.5%
Sediment Organic Matter (%)	1.1 - 64.6	15.56	38	29.5%

Table 2. Mean, standard deviation, and 95% credible interval summary of Bayesian posterior distributions of the mean sediment P flux rate among various groups of waterbodies

Waterbody Characteristics				
		Mean	***SD***	***95% Credible Interval***
Waterbody Type	Lake	4.82	0.22	4.40 - 5.25
	Reservoir	5.75	0.51	4.82 - 6.75
Trophic State	Oligo-Mesotrophic	3.54	0.39	2.78 - 4.33
	Eutrophic	5.20	0.27	4.68 - 5.73
	Hypereutrophic	5.79	0.35	5.10 - 6.49
Mixing Regime	Dimictic	3.99	0.28	3.44 - 4.55
	Polymictic	5.67	0.34	5.00 - 6.34
Dissolved Oxygen and Sample Site				
		Mean	***SD***	***95% Credible Interval***
Incubation DO	Anoxic	7.02	0.31	6.42 - 7.63
	Oxic	3.62	0.22	3.19 - 4.07
Sampling Site and DO condition	Littoral, Oxic	3.03	0.31	2.42 - 3.65
	Littoral, Anoxic	5.65	0.58	4.52 - 6.78
	Profundal, Oxic	4.20	0.32	3.58 - 4.82
	Profundal, Anoxic	7.51	0.37	6.79 - 8.24

FIGURES

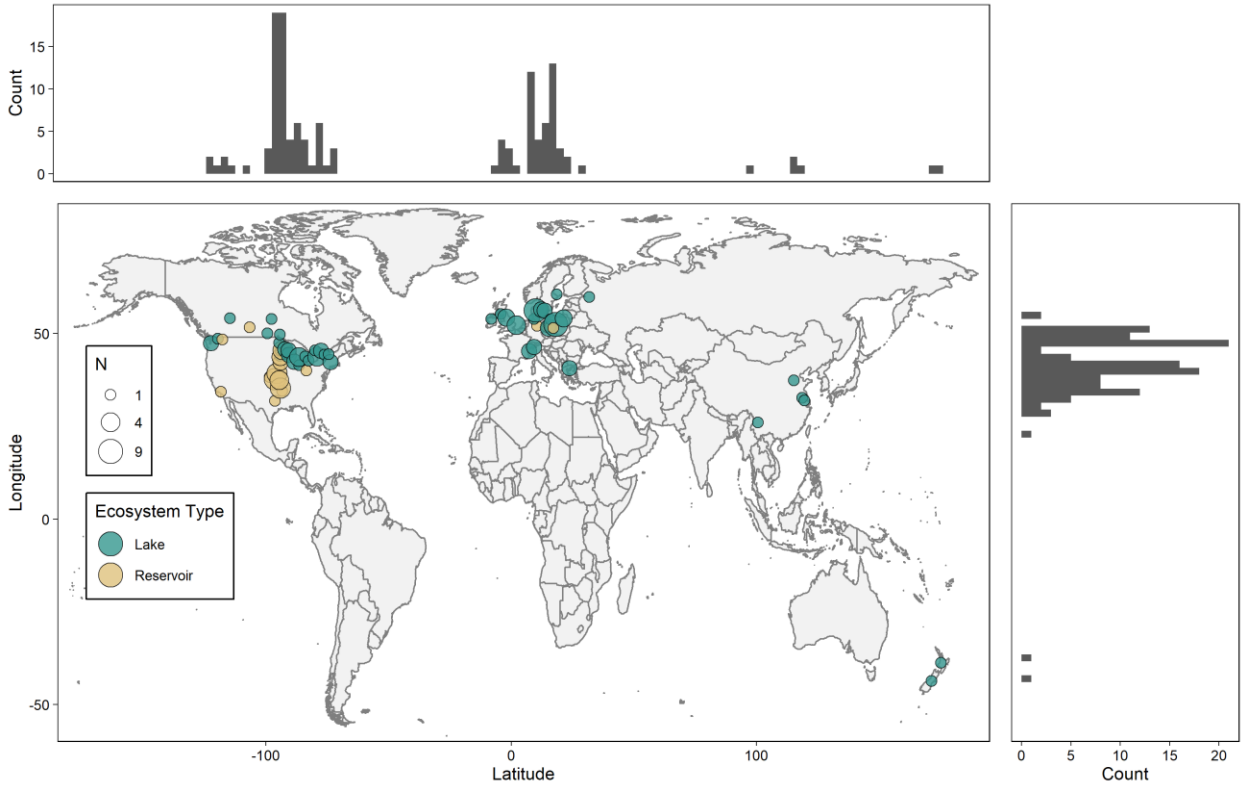

Figure 1. Geographic location and distribution of study lakes and reservoirs. Waterbodies of the same type (lake vs. reservoir) within a 2-degree square grid were aggregated and the location plotted at the center of the grid. The size of each point represents the number of individual waterbodies in that location.

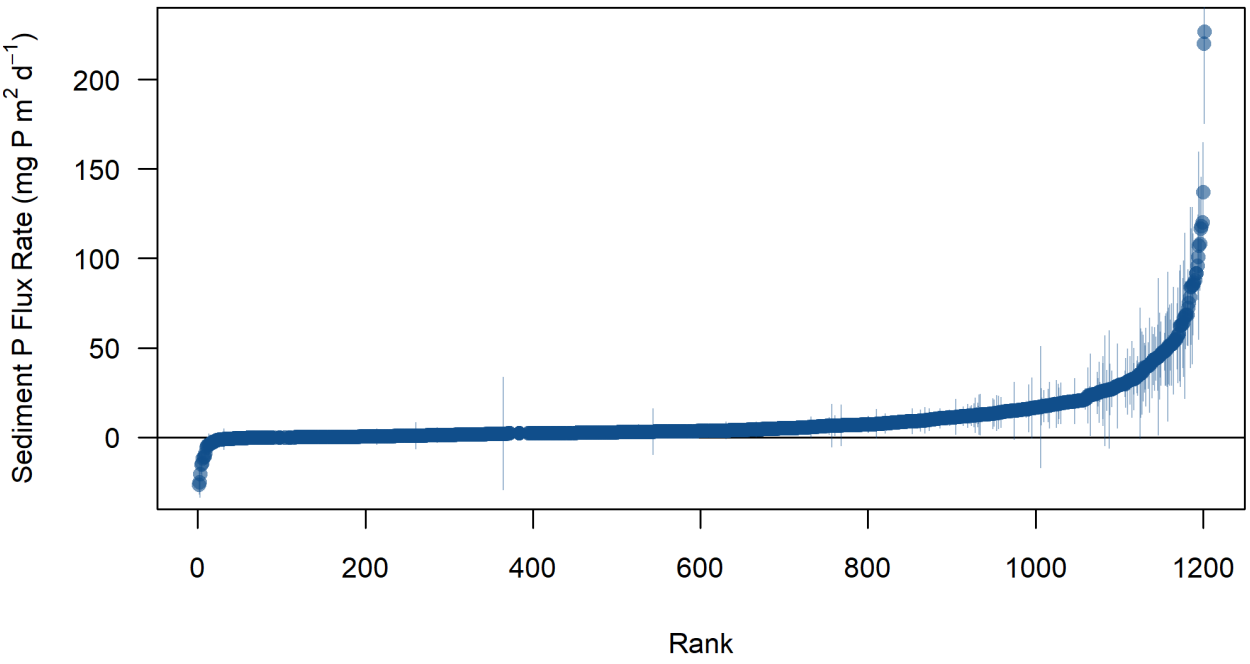

Figure 2. Rank plot of all sediment P flux observations (n=1202). Error bars represent one standard deviation for values where error was reported in the original study (n=495).

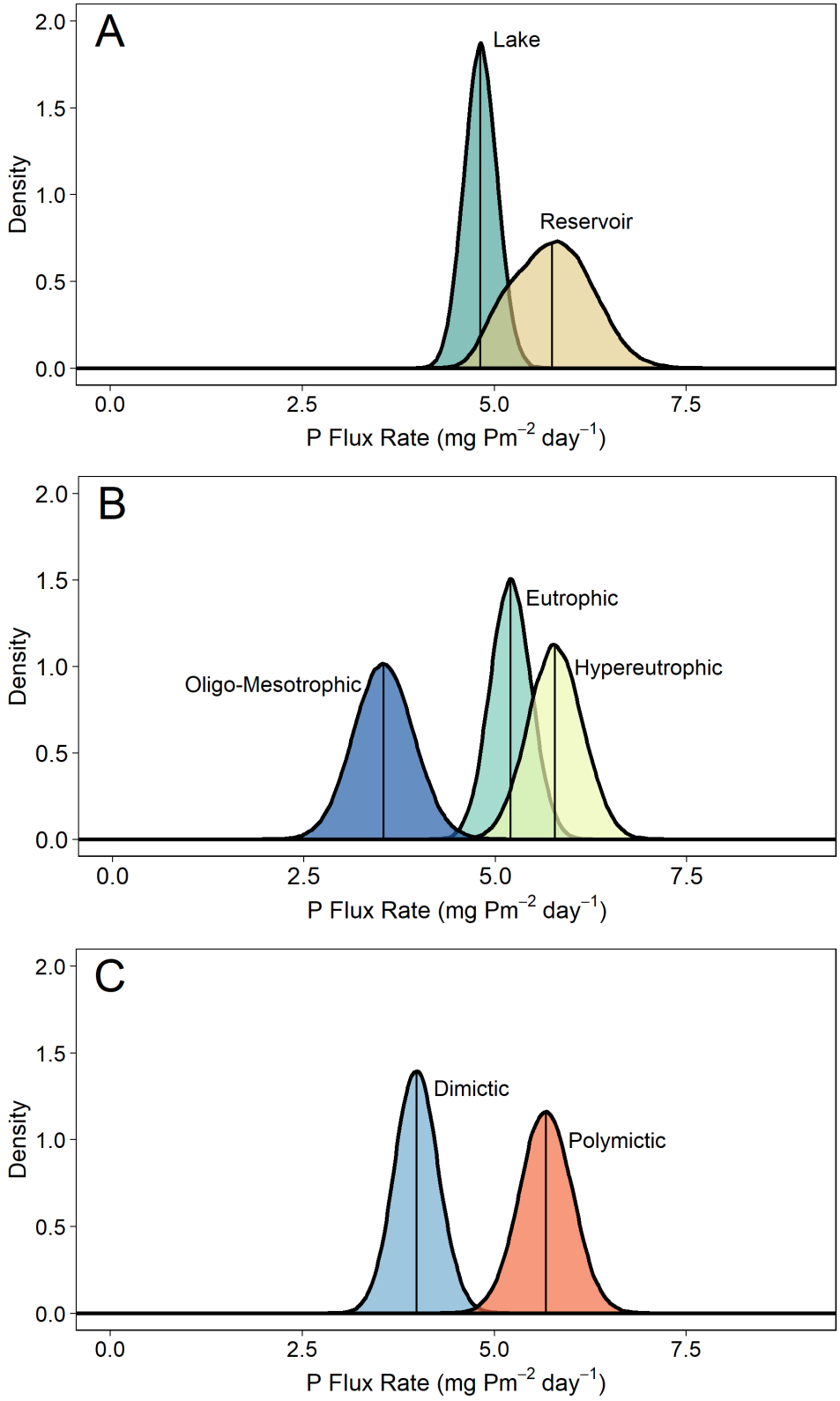

Figure 3. Bayesian posterior estimate of the mean sediment P flux rate (A) between lakes and reservoirs, (B) by trophic state, and (C) by mixing regime. Vertical lines mark the mean value of the posterior estimate.

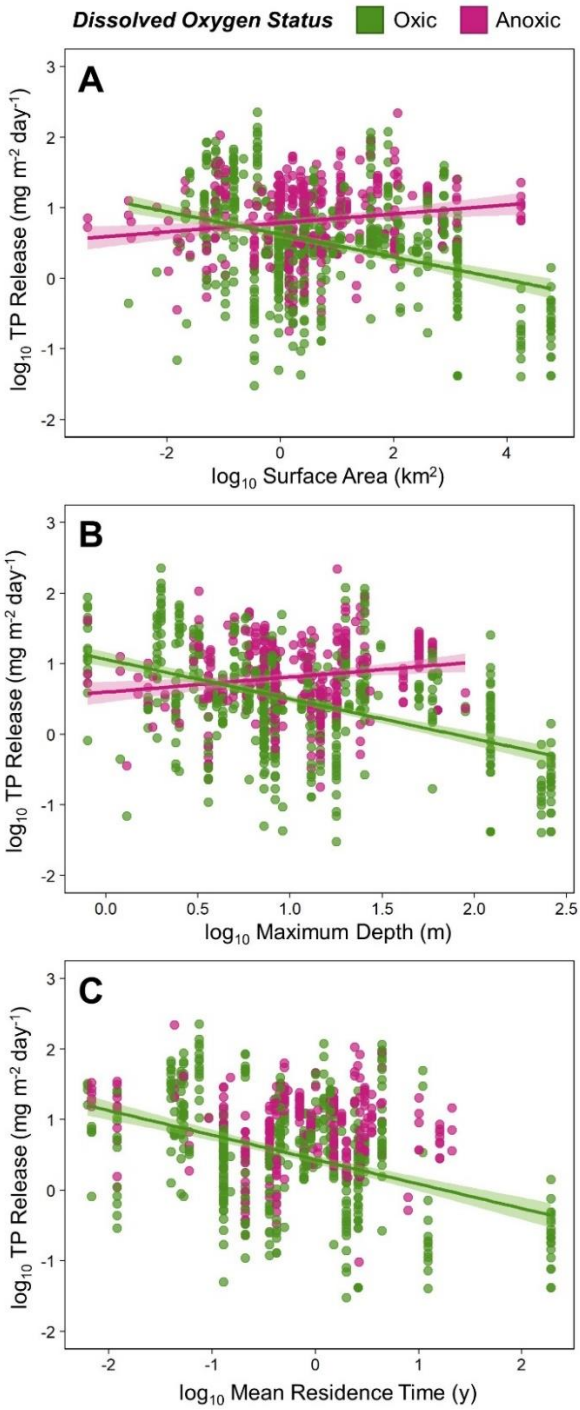

Figure 4. The relationships between log-transformed P release rates and morphometric variables based on oxygen conditions. (A) There were significant relationships between P release rates and water body surface area under both oxic ($F_{1,649}$=93.44, p<0.0001, β_1= -0.16 [-0.19, -0.13]) and anoxic ($F_{1,399}$=10.04, p=0.0016, β_1=0.06 [0.02, 0.10]) conditions as well as between P release and (B) maximum depth (oxic $F_{1,606}$=166.1, p<0.0001, β_1= -0.56 [-0.65, -0.48]; anoxic $F_{1,361}$=10.19, p=0.0015, β_1= 0.21 [0.08, 0.34]). (C) The relationship between P release rates and mean residence time was only significant for oxic sediments ($F_{1,532}$=107.2, p<0.0001, β_1= -0.35 [-0.41, -0.28]).

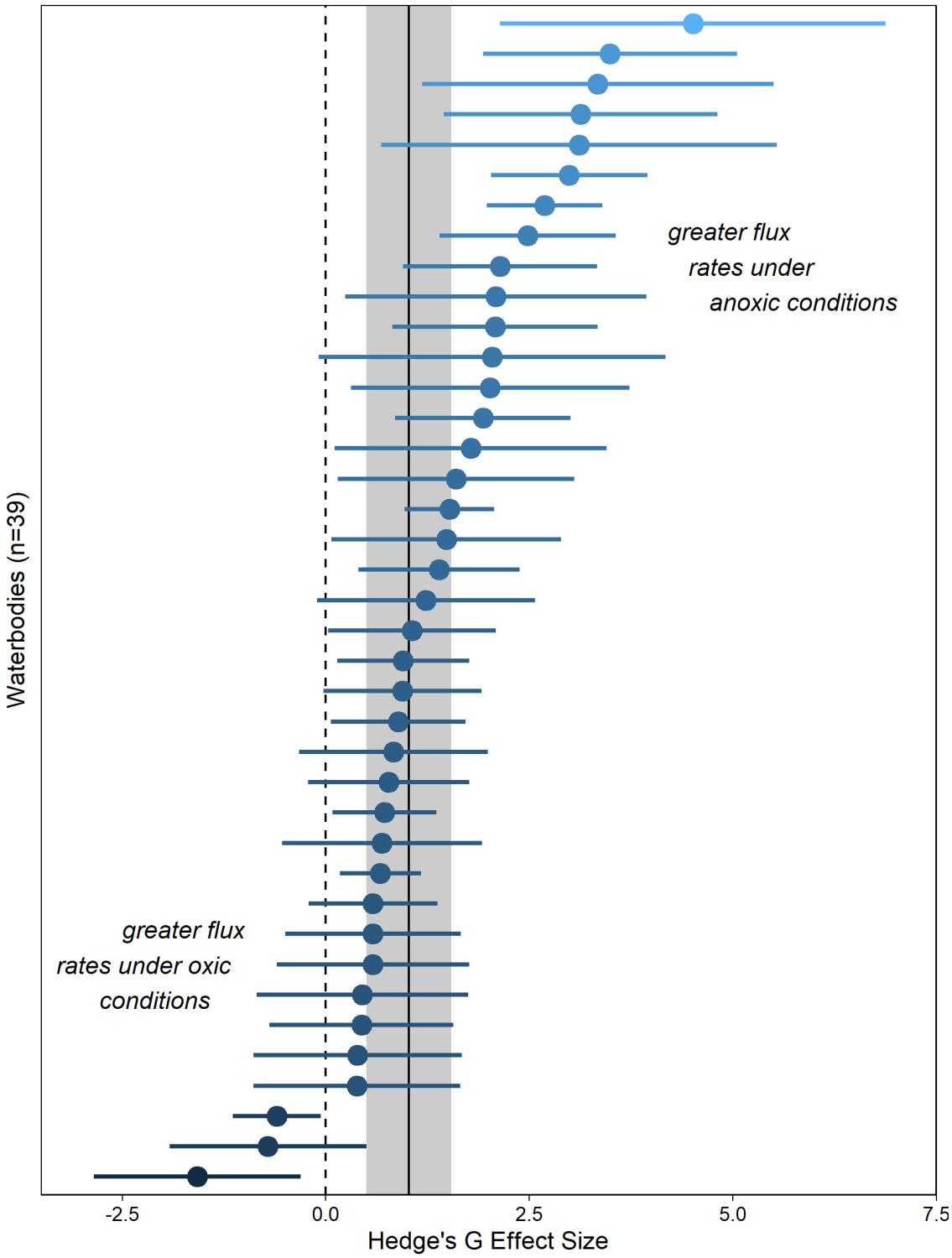

Figure 5. Effect size of dissolved oxygen conditions on mean sediment P flux rates. Standardized mean effect size for 39 waterbodies in which flux rates were reported under both anoxic and oxic conditions are plotted, with error bars indicating the 95% confidence interval of the estimate. The solid vertical line and grey box show the global effect size and its standard deviation respectively.

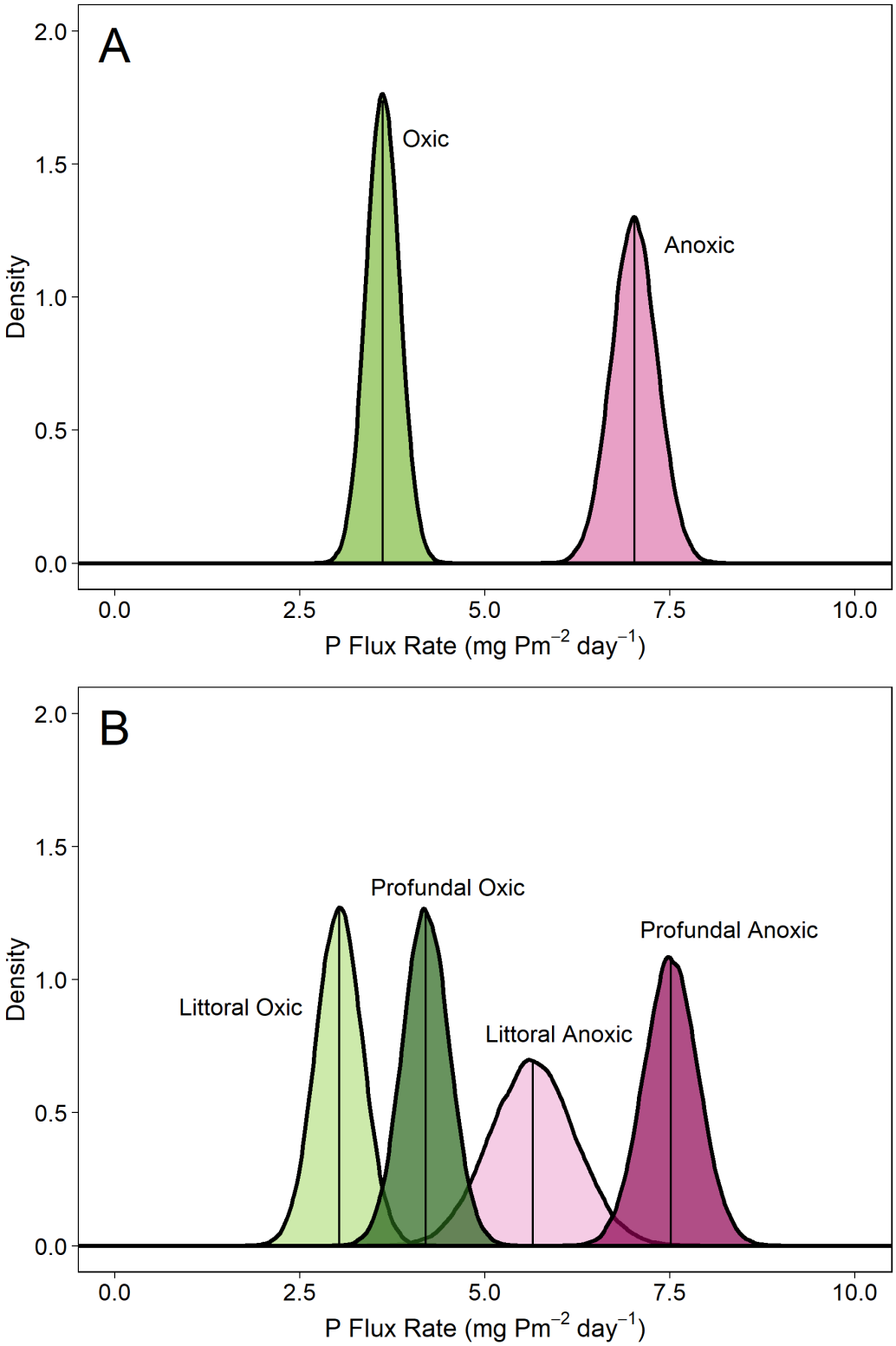

Figure 6. Bayesian posterior estimate of the mean sediment P flux rate (A) by incubation dissolved oxygen conditions and (B) by both sampling location and dissolved oxygen status. Vertical lines mark the mean value of the posterior estimate.

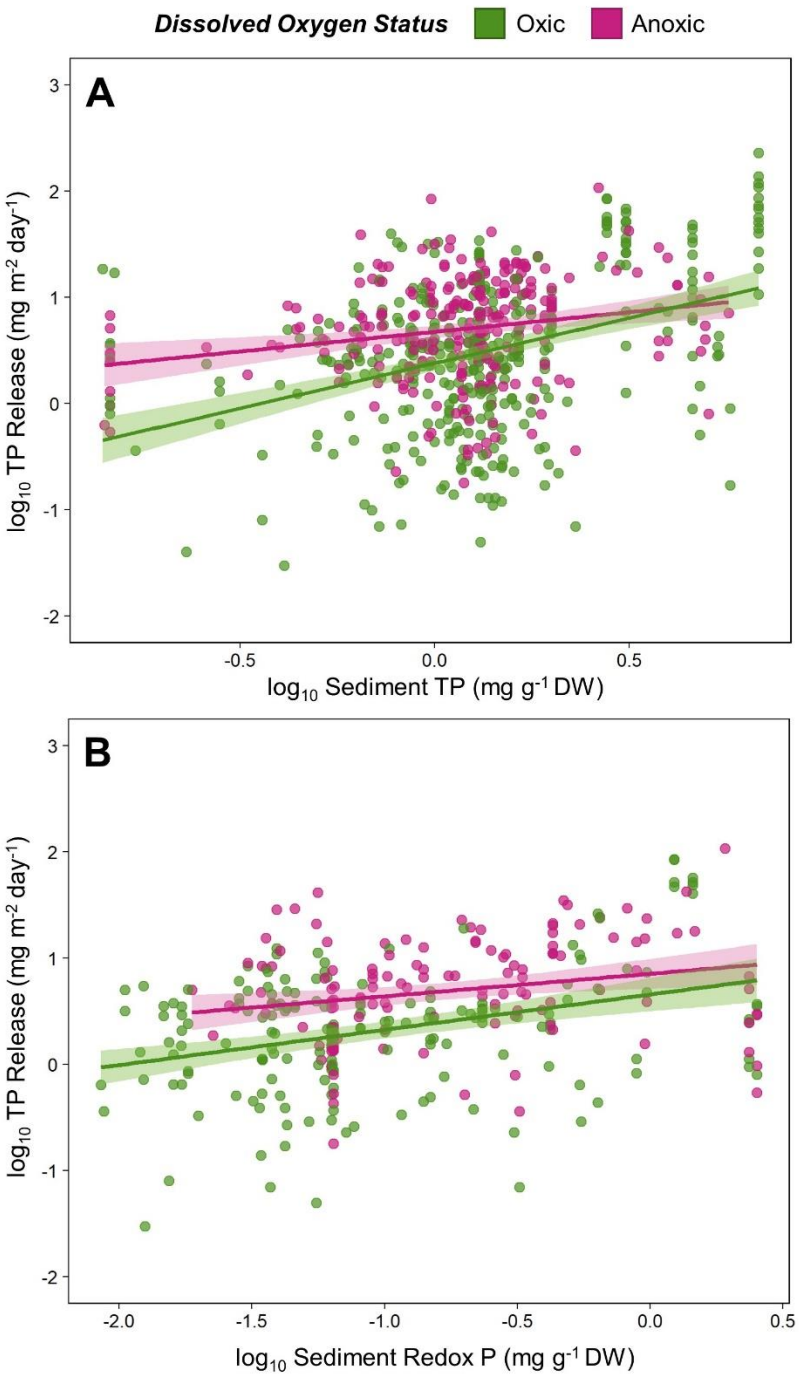

Figure 7. The relationships between log-transformed sediment P release rates and sediment characteristics based on dissolved oxygen conditions. (A) There were significant relationships between P release rates and sediment total P content under both oxic ($F_{1,368}$=64.17, p<0.0001, β_1= 0.85 [0.64, 1.06]) and anoxic ($F_{1,264}$=11.82, p=0.00068, β_1=0.37 [0.16, 0.58]) conditions as well as between P release and (B) sediment redox-sensitive P concentrations (oxic $F_{1,185}$=15.25, p=0.00013, β_1= 0.60 [0.30, 0.90]; anoxic $F_{1,136}$=9.3, p=0.003, β_1= 0.43 [0.15, 0.71]).

SUPPLEMENTARY INFORMATION FOR CHAPTER 1

TABLES

Table S1. Studies from which sediment P flux rates and covariates of interest were extracted

No.	*First Author*	*Year*	*DOI or Other Identifier*	*Title*
1	Andersen	1999	10.1023/a:1017027818233	Comparison of phosphorus release from littoral and profundal sediments in a shallow, eutrophic lake
2	Auer	1993	10.1007/bf00050750	Measurement and verification of rates of sediment phosphorus release for hypereutrophic urban lake
3	Austin	2020	10.4081/jlimnol.2020.1913	Sediment phosphorus release sustains nuisance periphyton growth when nitrogen is not limiting
4	Beklioglu	1999	10.1023/a:1003705518774	Rapid recovery of a shallow hypertrophic lake following sewage effluent diversion: lack of chemical resilience
5	Beutel	2008	10.1080/07438140809354047	Effects of oxygen and nitrate on nutrient release from profundal sediments of a large, oligo-mesotrophic reservoir, Lake Mathews, California
6	Burger	2007	10.1007/s10750-007-0582-0	Benthic nutrient fluxes in a eutrophic, polymictic lake
7	Carter	2012	10.1899/11-177.1	Predicting sediment phosphorus release rates using land use and water-quality data
8	Christensen	2013	10.1080/10402381.2013.831148	Evaluation of internal loading and water level changes: implications for phosphorus, algal production, and nuisance blooms in Kabetogama Lake, Voyageurs National Park, Minnesota
9	Christophoridis	2006	10.2134/jeq2005.0213	Conditions affecting the release of phosphorus from surface lake sediments
10	Cornwell	1999	Lake Champlain Basin Program Technical Report No. 34B	Benthic phosphorus cycling in Lake Champlain: Results of an integrated field sampling/water quality modeling study | Part B: Field Studies
11	Crosa	2013	10.1127/1863-9135/2013/0427	Recovery of Lake Varese: reducing trophic status through internal P load capping
12	Dadi	2020	10.3390/w12041065	Trajectories of Sediment-Water Interactions in Reservoirs as a Result of Temperature and Oxygen Conditions
13	Doig	2017	10.1007/s10750-016-2977-2	Phosphorus release from sediments in a river-valley reservoir in the northern Great Plains of North America
14	Dondajewska	2008	10.2478/v10009-007-0043-0	Internal phosphorus loading from bottom sediments of a shallow preliminary reservoir
15	Dong	2011	10.1007/s10661-010-1740-9	Phosphorus fractions, sorption characteristics, and its release in the sediments of Baiyangdian Lake, China
16	Egemose	2011	10.1139/f2011-016	Changed cycling of P, N, Si, and DOC in Danish Lake Nordborg after aluminum treatment
17	Freedman	1977	ISSN: 0090-3914	Nutrient release from anaerobic sediments
18	Fuchs	2018	10.1016/j.scitotenv.2018.02.059	Evaluation of dried amorphous ferric hydroxide CFH-12 (R) as agent for binding bioavailable phosphorus in lake sediments
19	Gibbons	2020	10.1016/j.watres.2020.116022	Effect of temperature on phosphorus flux from anoxic western Lake Erie sediments
20	Graneli	1979	10.1007/BF00032045	The influence of Chironomus plumosus larvae on the exchange of dissolved substances between sediment and water
21	Haggard	2005	10.2134/jeq2005.0724	Phosphorus flux from bottom sediments in Lake Eucha, Oklahoma
22	Haggard	2006	10.1016/j.ecoleng.2006.07.013	Sediment phosphorus release at a small impoundment on the Illinois River, Arkansas and Oklahoma, USA
23	Haggard	2021	10.1080/07438141.2012.659376	Sediment phosphorus flux in an Oklahoma reservoir suggests reconsideration of watershed management planning
24	Heinen	2004	10.1016/S0380-1330(04)70381-0	Carbon and Nutrient Cycling at the Sediment-water Boundary in Western Lake Superior
25	Hillbricht-Ilkowska	1984	10.1080/03680770.1983.11897422	External and internal loading and retention of phosphorus in the R. Jorka lakes (Masurian Lakeland, Poland) vs their trophic status
26	Holdren & Armstrong	1980	10.1021/es60161a014	Factors affecting phosphorus release from intact lake sediment cores
27	Ignatieva	1996	10.1007/bf00031817	Distribution and release of sedimentary phosphorus in Lake Ladoga
28	James	1995	10.1080/02705060.1995.9663446	Internal Phosphorus Loading in Lake Pepin, Upper Mississippi River
29	James	2000	10.1111/j.1752-1688.2000.tb04294.x	Distribution of sediment phosphorus pools and fluxes in relation to alum treatment
30	James	2001	ISSN: 0003-9136	Changes in sediment characteristics following drawdown of Big

				Muskego Lake, Wisconsin
31	James	2015	10.1080/10402381.2015.1079755	Managing internal phosphorus loading and vertical entrainment in a weakly stratified eutrophic lake
32	James	2017	10.1080/10402381.2017.1346010	Diffusive phosphorus fluxes in relation to the sediment phosphorus profile in Big Traverse Bay, Lake of the Woods
33	James	2017	10.1080/10402381.2017.1312647	Internal phosphorus loading contributions from deposited and resuspended sediment to the Lake of the Woods
34	James	2020	10.1080/10402381.2019.1661554	Sediment aluminum:phosphorus binding ratios and internal phosphorus loading characteristics 12 years after aluminum sulfate application to Lake McCarrons, Minnesota
35	Jensen	1992	10.4319/lo.1992.37.3.0577	Importance of temperature, nitrate, and pH for phosphate release from aerobic sediments of four shallow, eutrophic lakes
36	Jensen	2015	10.1007/s10750-015-2186-4	Evaluation of aluminum treatment efficiency on water quality and internal phosphorus cycling in six Danish lakes
37	Kowalczewska-Madura	2010	10.2478/v10009-010-0035-3	Internal phosphorus loading in selected lakes of the Cybina River valley
38	Kowalczewska-Madura	2017	10.1007/s11356-017-8997-2	The influence of restoration measures on phosphorus internal loading from the sediments of a hypereutrophic lake
39	Kowalczewska-Madura	2018	10.1007/s11270-018-3937-4	Internal Phosphorus Loading from the Bottom Sediments of a Dimictic Lake During Its Sustainable Restoration
40	Kowalczewska-Madura	2019	10.1016/j.ijsrc.2018.08.008	Impact of environmental variables on spatial and seasonal internal phosphorus loading in a mesoeutrophic lake
41	Kowalczewska-Madura	2019	10.1051/limn/2019003	Internal phosphorus loading as the response to complete and then limited sustainable restoration of a shallow lake
42	Krivtsov	2001	10.1002/1521-401x(200109)29:2/3<111::aid-aheh111>3.0.co;2-1	Determination of P release from Rostherne Mere sediment cores
43	Lasater	2017	10.2134/ael2017.06.0017	Sediment Phosphorus Flux at Lake Tenkiller, Oklahoma: How Important Are Internal Sources?
44	Lazoff	1983	US EPA 440/5-83-001: 123-126	Evaluation of internal phosphorus loading from anaerobic sediments
45	Lennox	1984	10.1111/j.1365-2427.1984.tb00032.x	Lough Ennell: laboratory studies on sediment phosphorus release under varying mixing, aerobic and anaerobic conditions
46	Liu	2016	10.1016/j.envpol.2015.12.045	Effects of riverine suspended particulate matter on the post-dredging increase in internal phosphorus loading across the sediment-water interface
47	Liu	2015	10.1007/s12665-015-4715-x	Phosphorus release characteristics of sediments in Erhai Lake and their impact on water quality
48	Loh	2013	10.5268/IW-3.1.533	Evaluating relationships between sediment chemistry and anoxic phosphorus and iron release across three different water bodies
49	Mawson	1983	ISSN: 0043-1303	Phosphorus flux rates in lake sediments
50	McCarty	2019	10.13031/trans.13300	Algal demand drives sediment phosphorus release in a shallow eutrophic cove
51	McCarty	2019	10.13031/trans.13309	Sediment phosphorus release in a shallow eutrophic reservoir cove
52	Natarajan	2021	10.1080/10402381.2020.1862371	Iron filings application to reduce lake sediment phosphorus release
53	Nowlin	2005	10.1111/j.1365-2427.2004.01316.x	Release rates and potential fates of nitrogen and phosphorus from sediments in a eutrophic reservoir
54	Nurnberg	1987	10.4319/lo.1987.32.5.1160	A comparison of internal phosphorus loading in lakes with anoxic hypolimnia – laboratory incubation versus in situ hypolimnetic phosphorus accumulation
55	Oldenborg	2019	10.1016/j.scitotenv.2018.09.298	Impact of sediment dredging on sediment phosphorus flux in a restored riparian wetland
56	Orihel	2015	10.1002/lno.10076	The "nutrient pump:" Iron-poor sediments fuel low nitrogen-to-phosphorus ratios and cyanobacterial blooms in polymictic lakes
57	Orihel	2000	NA	Unpublished data included in Orihel et al. 2017 (DOI: 10.1139/cjfas-2016-0500)
58	Penn	2000	10.1139/cjfas-57-5-1033	Seasonality in phosphorus release rates from the sediments of a hypereutrophic lake under a matrix of pH and redox conditions
59	Phillips	1994	10.1007/bf00026733	The importance of sediment phosphorus release in the restoration of very shallow lakes (The Norfolk Broads, England) and implications for biomanipulation
60	Premazzi	1985	10.1007/bf00034587	Internal P loading in lakes – a different approach to its evaluation
61	Reitzel	2003	10.1023/B:HYDR.0000008624.54844.2d	Testing aluminum addition as a tool for lake restoration in shallow, eutrophic Lake Sonderby, Denmark
62	Reitzel	2005	10.1021/es0485964	Lake restoration by dosing aluminum relative to mobile phosphorus in the sediment
63	Riley	1984	10.1139/f84-101	Role of Internal Phosphorus Loading in Two Shallow, Productive Lakes in Alberta, Canada

64	Sen	2007	10.1007/s11270-006-9214-y	Sediment phosphorus release at Beaver Reservoir, northwest Arkansas, USA, 2002-2003: A preliminary investigation
65	Sondergaard	1992	10.1007/bf00006480	Phosphorus release from resuspended sediment in the shallow and wind-exposed Lake Arresø, Denmark
66	Song	2018	10.1016/j.ecoleng.2017.06.008	Relative importance of external and internal phosphorus loadings on affecting lake water quality in agricultural landscapes
67	Soster	2001	ISBN: 1570034311	In situ effects of organisms on porewater geochemistry in Great Lakes sediments
68	Spears	2007	10.1007/s10750-007-0610-0	Sediment phosphorus cycling in a large shallow lake: spatio-temporal variation in phosphorus pools and release
69	Steinman	2009	10.1007/s10452-007-9147-6	Spatial and temporal variability of internal and external phosphorus loads in Mona Lake, Michigan
70	Steinman	2006	10.1899/0887-3593(2006)25[304:fiipli]2.0.co;2	Factors influencing internal P loading in a western Michigan, drowned river-mouth lake
71	Steinman	2012	10.2134/jeq2011.0476	Macroinvertebrate Response and Internal Phosphorus Loading in a Michigan Lake after Alum Treatment
72	Steinman	2015	10.1080/10402381.2015.1014582	TMDL reevaluation: reconciling internal phosphorus load reductions in a eutrophic lake
73	Steinman	2018	10.1080/10402381.2017.1402834	Alum efficacy 11years following treatment: phosphorus and macroinvertebrates
74	Stephen	1997	10.1023/a:1017019713123	Do rooted macrophytes increase sediment phosphorus release?
75	Suplee	2002	10.1023/a:1020291130333	An evaluation of the importance of sulfate reduction and temperature to P fluxes from aerobic-surfaced, lacustrine sediments
76	Taguchi	2020	10.1002/lol2.10155	Sediment phosphorus release in stormwater ponds
77	Theis	1978	ISSN: 0043-1303	Retardation of sediment phosphorus release by fly ash application
78	Ulen	1978	10.1007/BF02502342	Seston and sediments in Lake Norrviken. III. Nutrient release from sediment
79	Waters	2021	10.1080/00288330.2020.1804408	The release of legacy phosphorus from deforestation-derived sediments in shallow, coastal lake Forsyth/Te Roto o Wairewa
80	Wen	2020	10.1016/j.jhazmat.2020.122548	Does external phosphorus loading diminish the effect of sediment dredging on internal phosphorus loading? An in-situ simulation study
81	Yin	2015	10.1016/j.jenvman.2015.01.003	Reduction of sediment internal P-loading from eutrophic lakes using thermally modified calcium-rich attapulgite-based thin-layer cap

Table S2. Equations used to convert units of P flux rates and covariates

Variable	*Original Units*	*Final Units*	*Full Conversion*	*Simple Conversion*
P Flux Rate	µg P m^{-2} day^{-1}	mg P m^{-2} day^{-1}	$\frac{\mu g}{m^2 d} \times \frac{1\ mg}{1{,}000\ \mu g}$	Divide by 1,000
	µg P m^{-2} $hour^{-1}$		$\frac{\mu g}{m^2 h} \times \frac{1\ mg}{1{,}000\ \mu g} \times \frac{24\ h}{1\ d}$	Multiply by 0.024
	mmol P m^{-2} day^{-1}		$\frac{mmol\ P}{m^2 d} \times \frac{1\ mol}{1{,}000\ mmol} \times \frac{30.97\ g}{1\ mol\ P} \times \frac{1{,}000\ mg}{1\ g}$	Multiply by 30.97
	mmol P m^{-2} $year^{-1}$		$\frac{mmol\ P}{m^2 y} \times \frac{1\ mol}{1{,}000\ mmol} \times \frac{30.97\ g}{1\ mol\ P} \times \frac{1{,}000\ mg}{1\ g} \times \frac{1\ y}{365\ d}$	Multiply by 30.97, divide by 365
	µmol P m^{-2} day^{-1}		$\frac{\mu mol\ P}{m^2 d} \times \frac{1\ mol}{1{,}000{,}000\ \mu mol} \times \frac{30.97\ g}{1\ mol\ P} \times \frac{1{,}000\ mg}{1\ g}$	Multiply by 0.03097
Sediment TP and Redox-Sensitive P	µg g^{-1}	mg P g^{-1}	$\frac{\mu g}{g} \times \frac{1\ mg}{1{,}000\ \mu g}$	Divide by 1,000
	mg kg^{-1}		$\frac{mg}{kg} \times \frac{1\ kg}{1{,}000\ g}$	Divide by 1,000
	µmol P g^{-1}		$\frac{\mu mol\ P}{g} \times \frac{1\ mol}{1{,}000{,}000\ \mu mol} \times \frac{30.97\ g}{1\ mol\ P} \times \frac{1{,}000\ mg}{1\ g}$	Multiply by 0.03097
	mmol P g^{-1}		$\frac{mmol\ P}{g} \times \frac{1\ mol}{1{,}000\ mmol} \times \frac{30.97\ g}{1\ mol\ P} \times \frac{1{,}000\ mg}{1\ g}$	Multiply by 30.97
Surface Area	hectares	km^2	$\frac{ha}{1} \times \frac{1\ km^2}{100\ ha}$	Divide by 100
Dissolved Oxygen	µmol L^{-1}	mg L^{-1}	$\frac{\mu mol\ O_2}{L} \times \frac{1\ mol}{1{,}000{,}000\ \mu mol} \times \frac{32\ g}{1\ mol\ O_2} \times \frac{1{,}000\ mg}{1\ g}$	Multiply by 0.032

Table S3. *Morphometry of waterbodies in dataset*

Morphometric Variable	*Median*	*Range*	*Waterbodies Represented*
Surface Area (km^2)	2.28	0.0004 - 59,600	122 (94.6%)
Maximum Depth (m)	8.3	0.8 - 260	98 (76.0%)
Mean Depth (m)	6.0	0.41 - 147	83 (64.3%)

Table S4. *Representation of explanatory variables in dataset*

Variable	Number of Observations	Number Studies	Percent of Studies	Number of Waterbodies	Percent of waterbodies
Surface Area	1179	80	98.8%	122	94.6%
Incubation DO	691	66	81.5%	110	85.3%
Incubation Temperature	885	62	76.5%	103	79.8%
Maximum Depth	1081	74	91.4%	98	76.0%
Mean Depth	1089	71	87.7%	83	64.3%
Water Residence Time	920	67	82.7%	72	55.8%
Sediment Total P	717	42	51.9%	63	48.8%
Sediment Redox P	395	18	22.2%	38	29.5%
Sediment Organic Matter	442	22	27.2%	38	29.5%
Incubation pH	276	16	19.8%	24	18.6%
Lake pH	223	17	21.0%	17	13.2%
Incubation nitrate	88	7	8.6%	11	8.5%
Lake nitrate	68	7	8.6%	7	5.4%
Sediment C:N	10	2	2.5%	3	2.3%
Incubation sulfate	2	1	1.2%	1	0.8%

FIGURES

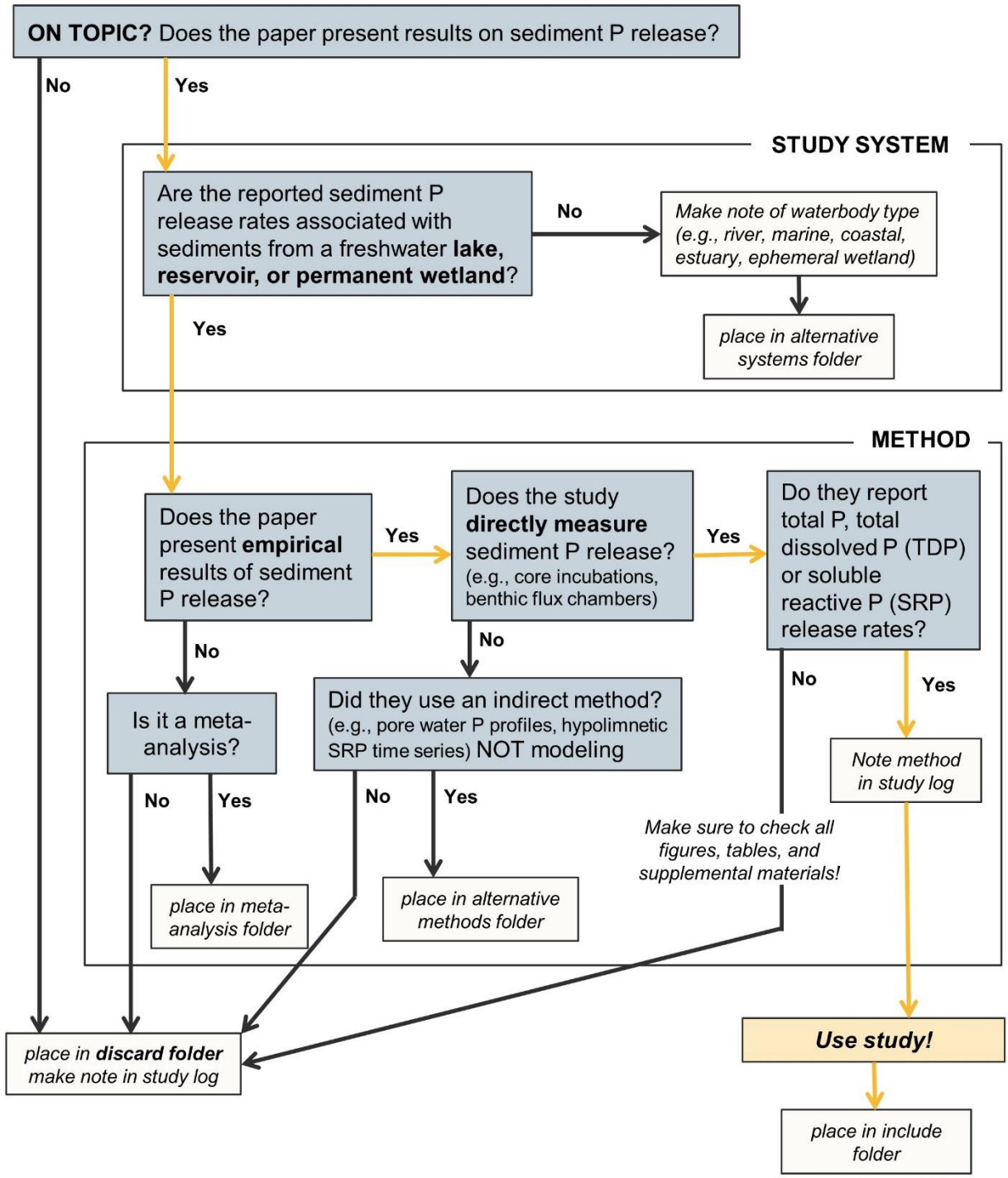

Figure S1. Decision tree for study inclusion during initial and full text screenings.

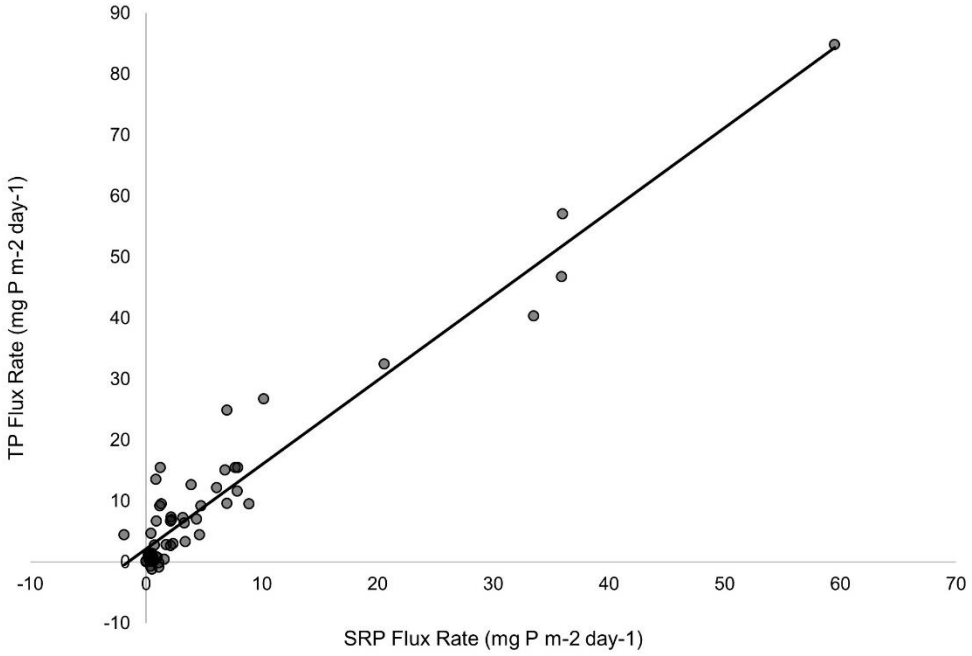

Figure S2. Linear relationship used to convert flux rates measured as soluble reactive P (SRP) to TP flux rates (TP=1.38(SRP)+2.2; R^2=0.92).

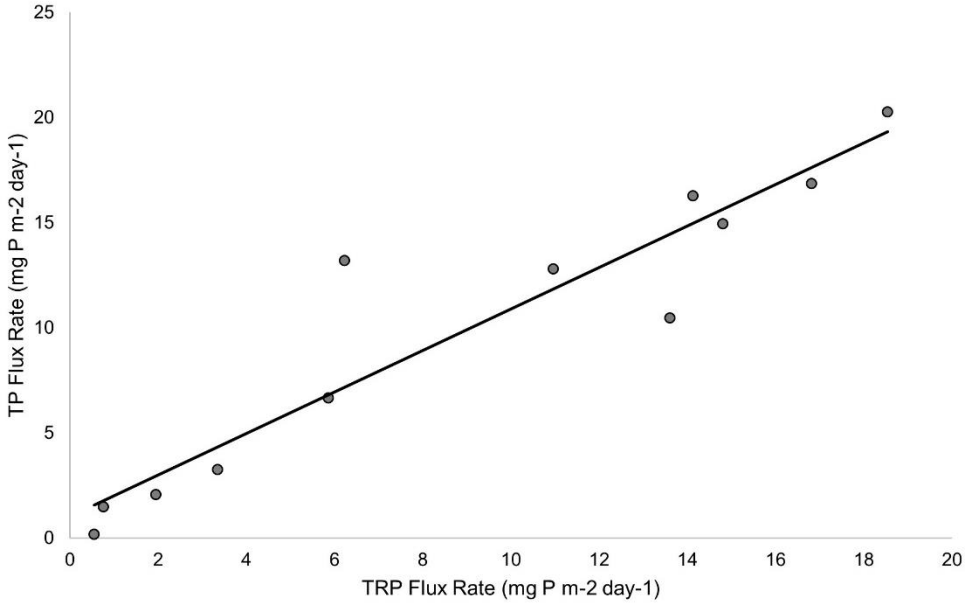

Figure S3. Linear relationship used to convert flux rates measured as total reactive P (TRP) to TP flux rates (TP=0.99(TRP)+1.04; R^2=0.88).

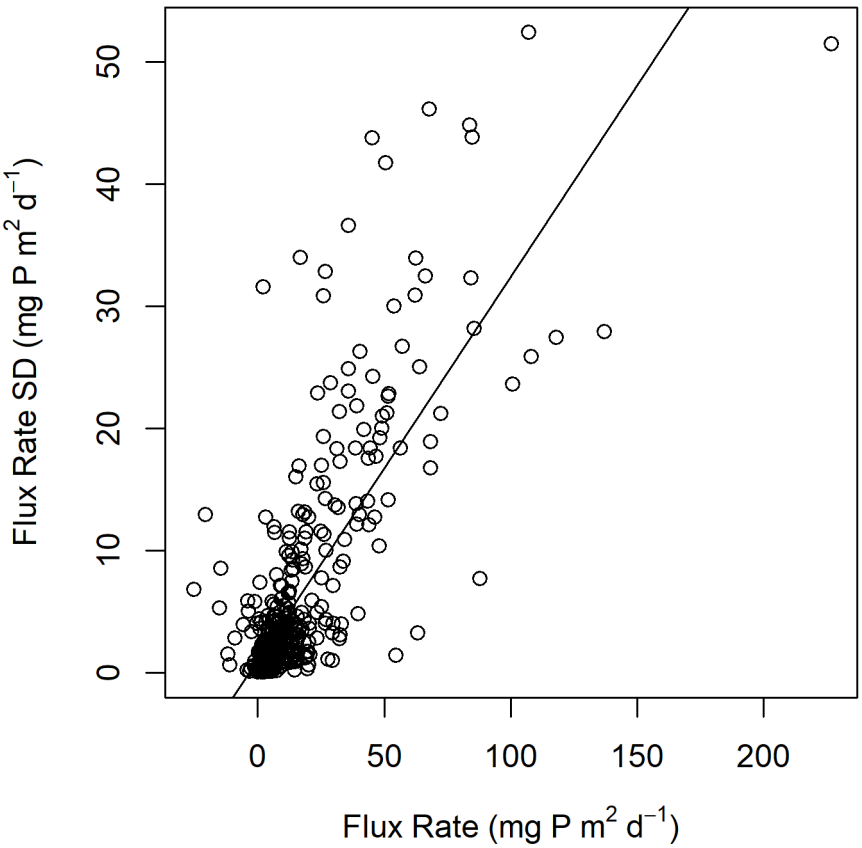

Figure S4. Linear relationship between reported P flux rates and associated standard deviation values ($F_{1,493}$=768, p<0.001, β_1=0.031 [0.29, 0.34]).

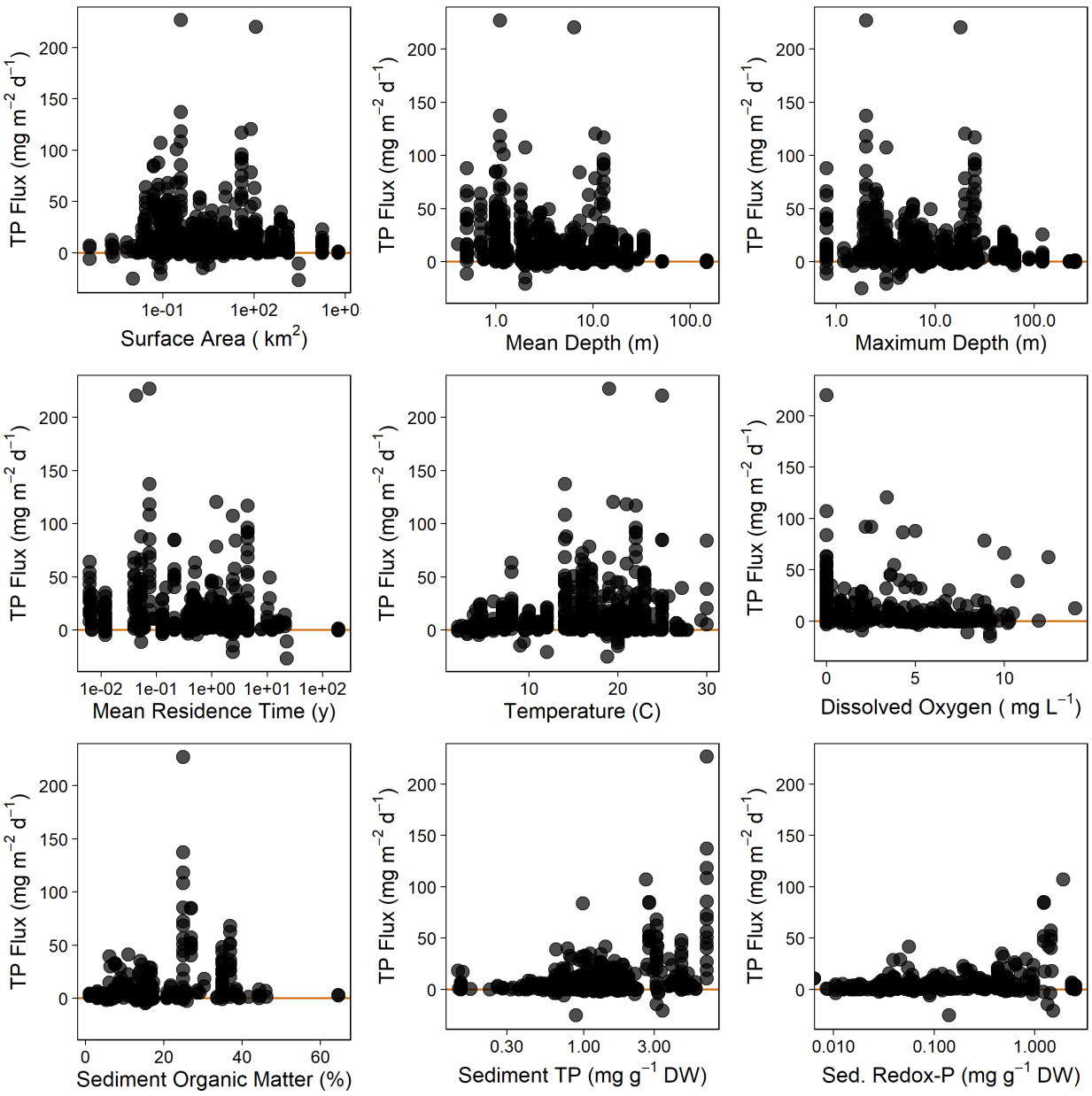

Figure S5. TP flux rates across continuous explanatory variables. Note that the x-axes for waterbody surface area, mean depth, maximum depth, mean residence time, sediment TP concentrations, and sediment redox-sensitive P concentrations are on a log-10 scale.

CHAPTER 2

HIGH INTER- AND INTRA-LAKE VARIATION IN SEDIMENT PHOSPHORUS POOLS IN SHALLOW LAKES

Albright, E.A., R. Fleck King, Q.K. Shingai, and G.M. Wilkinson. In review. High inter- and intra-lake variation in sediment phosphorus pools in shallow lakes. JGR-Biogeosciences.

Author contributions: Albright designed the study; performed all field and laboratory work; cleaned, analyzed, and visualized the data; and wrote the manuscript. Wilkinson contributed to study design and data analysis and provided feedback on writing. Fleck King and Shingai assisted with field and laboratory work and provided writing feedback.

ABSTRACT

Phosphorus (P) release from lakebed sediments may fuel algal blooms, especially in shallow systems. A primary mechanism that controls internal P loading is the size and chemical composition of the sediment P pool. However, variation in sediment P speciation within and among shallow lakes remains poorly quantified, limiting efforts to scale and model sediment P pools. We measured the degree of spatial heterogeneity in the size and composition of the sediment P pool, both within and among lakes, for seven shallow glacial lakes by measuring sediment P fractions from 10 cores in each lake. There was a 1.6x difference in total sediment P among the study lakes, with sediment P composition varying based on the dominant watershed soil series. We also found that higher mobile P (as a fraction of total P) in the profundal sediments was significantly correlated with higher average chlorophyll-*a* concentrations ($p=0.04$), indicating the influence of sediment P composition on algal biomass in shallow lakes.

Additionally, we measured substantial within-lake heterogeneity in total and loosely-bound sediment P among the 10 sites sampled in each lake. Concentrations were positively correlated with the depth of the water column above the sediments such that extrapolating measurements from the deep site alone could overestimate whole-lake mean P concentrations. Our results provide insight into the magnitude and pattern of inter- and intra-lake variation in sediment P pools that should be accounted for when sampling, scaling measurements, and modeling sediment P dynamics.

INTRODUCTION

Sediments are an integral component of aquatic ecosystems, especially shallow lakes. The sediments regulate whole-lake biogeochemical cycles through diagenetic processes and material exchange across the sediment-water interface (Forsberg 1989; Golterman 2004). For example, phosphorus (P) stored in sediments may reenter the water column due to disturbance, microbial activity, or changes in chemical conditions at the sediment surface (Søndergaard et al. 2003). In many ecosystems, this sediment P release (i.e., internal P loading) can maintain high water column P concentrations, even if external nutrient inputs are reduced (Søndergaard et al. 1999; Jeppesen et al. 2005; Søndergaard et al. 2013). Excess P availability supports algal production (Elser et al. 2007; Schindler et al. 2016), which can reach nuisance levels, threatening ecosystem services and public health (Schindler and Vallentyne 2008). The morphometric features of shallow lakes make these systems particularly susceptible to internal P loading. Specifically, shallow basins have a large sediment surface area relative to water volume. As a result, sediment-water interactions are highly influential in determining whole-lake water chemistry (Welch and Cooke 1995; Søndergaard et al. 2003). Although it is known that internal

P loading is an important process in shallow lakes, variation in the underlying mechanisms remains poorly quantified for these ecosystems.

A fundamental mechanism controlling internal P loading in shallow lakes is the size and composition of the sediment P pool. Sediment P may be found in a wide variety of minerals and organic materials as well as sorbed to particle surfaces (North et al. 2015). This chemical speciation determines the conditions in which P is mobilized and released as different P forms are vulnerable to different internal loading processes (Orihel et al. 2017). For example, changes in redox potential due to fluctuations in dissolved oxygen and alternative electron acceptor concentrations can mobilize P associated with redox-sensitive minerals (i.e., iron- and manganese-bound P; Mortimer, 1941; Orihel et al. 2015). Changes in pH may release other mineral-bound P forms (e.g., calcium-, and aluminum-bound; Jensen and Andersen 1992), and microbial decomposition can liberate P incorporated in labile organic materials (Joshi et al. 2015; Song and Burgin 2017; Frost et al. 2019). Sediment resuspension due to wind disturbance or bioturbation releases pore water and surface-sorbed P (i.e., loosely-bound P *sensu* James 2017b; Ekholm et al. 1997). Loosely-bound P is likely an important form of sediment P in shallow lakes as these ecosystems experience frequent water column mixing and wind disturbance (Bengtsson and Hellström 1992). Although internal P loading occurs under a variety of conditions, the dominant mechanisms are determined by the chemical composition of the sediment P pool.

Sediment P content and speciation vary among lakes due to differences in watershed features and external loading as well as autochthonous processing. External P loading includes particulate and dissolved forms that are transported from the watershed into lakes through surface and subsurface flows (Carpenter et al. 1998; Pease et al. 2018). The P speciation in catchment soils will drive the chemical composition of particulate P inputs, in turn influencing

the composition of the sediment P pool (Kerr et al. 2011; Tang et al. 2019). However, selective soil erosion and transport processes may alter sediment composition relative to the soil matrix if various P fractions are not distributed evenly across grain sizes. Fine particles that are more easily transported are often enriched in exchangeable, organic, and iron- and aluminum-bound P and depleted in calcium-bound P relative to larger grain sizes (Stone and English 1992). As a result, lakebed sediments may have more labile P forms than the surrounding soils (Kerr et al. 2011). In addition to exogeneous loading of particulate forms, P may also enter waterbodies in an aqueous form or desorb from settling particles before reaching the sediments (Pease et al. 2018). This soluble P is readily taken up by aquatic primary producers. Following biological uptake, P may be cycled among producers and consumers or it may settle out of the water column as necromass, algal detritus, or macrophyte leaf litter (Orihel et al. 2017). The sources of sedimented organic matter influence sediment P composition and lability (Twilley et al. 1986). For example, if algal detritus dominates organic matter sedimentation, then sediment organic P will be associated with more labile materials. Overall, sediment P content and composition vary among different lakes due to differences in exogeneous inputs and *in situ* processing.

The spatial distribution of the sediment P pool is also heterogeneous within individual shallow lakes following variation in sediment transport, deposition, and resuspension processes (Mackay et al. 2012). Sediment total P generally increases with water depth as a result of sediment focusing, which concentrates fine-grained, P-enriched sediments in deeper portions of the lake basin (White and Stone 1996; Hou et al. 2014; Cardoso-Silva et al. 2018). Dynamic disturbance and biological activity across the lakebed further drive spatial variation in sediment P speciation in shallow waterbodies (Forsberg 1989; Nowlin et al. 2005; Kowalczewska-Madura et al. 2019a). Variable sediment disturbance has the greatest influence on the distribution of

loosely-bound P forms. Smaller stocks of loosely-bound P are expected in shallow sediments that experience wind or wave disturbance while higher loosely-bound P content is expected in deeper, more protected sediments. (James 2017a). Additionally, the location and density of macrophyte beds can influence the spatial distribution of sediment P pools as macrophytes take up pore water P from the sediments and mobilize other P forms in order to meet their nutrient requirements (Xing et al. 2018). Macrophyte root structures also stabilize and oxygenate rhizosphere sediments, which can protect stocks of loosely-bound and redox-sensitive P species by reducing resuspension and maintaining aerobic conditions (Carpenter et al. 1983; Madsen 2001; Lai et al. 2011). Sediment focusing and disturbance as well as the presence of macrophytes are expected in shallow waterbodies (Kelton and Chow-Fraser 2005). As a result, the spatial distribution of sediment P content and composition are expected to be heterogeneous within shallow lakes. Accounting for this spatial variation is essential for accurate inventories of sediment P pools, burial rates, and internal loading potential (Mackay et al. 2012; Orihel et al. 2017). However, the degree of spatial heterogeneity in sediment P content and composition in shallow lakes remains poorly quantified.

In order to quantify the spatial heterogeneity of sediment P species in shallow lakes we measured the sediment P pools of seven shallow, glacial lakes in northwest Iowa. Specifically, we collected sediment cores from ten locations within each lake and analyzed the sediments for total P as well as pore water and loosely-bound P. We quantified spatial variation in these P forms and tested how sampling resolution influenced estimates of mean sediment P concentrations. Water depth is expected to drive horizontal variation in sediment P within lakes, with higher concentrations found in deeper areas of the lake. We further hypothesize that lakes with more variable bathymetry will have greater variability in loosely-bound P, driven by

variation in sediment disturbance and macrophyte occurrence. The sediment core from the deepest site in each study lake was additionally analyzed for total P and five sediment P species (loosely-bound P, redox-sensitive, labile organic, and calcium-, and aluminum-bound fractions). We hypothesize that the variation in the composition of the sediment P pool among lakes will relate to watershed soil composition, land cover, and long-term algal biomass. Understanding spatial variability in sediment P pools within and among shallow lakes is necessary to measure, scale, and model lentic P dynamics. A quantitative understanding of this variation is a critical step to being able to predict internal P loading potential based on lake and watershed characteristics.

METHODS

Study Lakes

We surveyed seven shallow, glacial lakes in northwest Iowa, USA (Table 1). The spatial extent of the study lakes covers approximately 5,600 km^2 on the western edge of the Des Moines Lobe. Although the study systems cover a wide range of basin characteristics, all are shallow (average mean depth = 2.2 m) and follow a discontinuous cold polymictic stratification and mixing pattern (Lewis 1983; Table S1). These lakes were formed from kettle depressions at the end of the Wisconsin glaciation. The watershed soils developed from loamy glacial till and are now heavily influenced by row crop agriculture (Arbuckle and Downing 2001; Tables S2-3). The watersheds of Storm and Swan Lake also contain soils developed from loess deposits as these catchments are located on the boundary of the Des Moines Lobe and the Loess Prairies of western Iowa. All of the study lakes are classified as eutrophic or hypereutrophic due to high phosphorus concentrations (Carlson 1977).

Sediment Core Collection and Analysis

We collected ten sediment cores from each study lake once between mid-June and early July of 2018 using a gravity corer (inner diameter 5 cm). Sampling sites included the deep point of the lake (hereafter "profundal sediments"), from which all sediment P species and total P were measured, as well as nine shallower sites distributed across the lakebed, from which only loosely-bound and total P were measured. These additional sites were selected using a randomized sampling scheme stratified by water depth. Specifically, sites were randomly selected from an evenly spaced grid of potential sites within each depth contour, defined as 0.5 or 1 m intervals depending on the maximum depth of the lake. All sediment cores were sliced in the field immediately following collection. Cores from the profundal site, the zone of sediment accumulation, were sliced every 2 cm up to 10 cm deep and then every 5 cm up to 20 cm deep. One slice from 0-10 cm was collected for each of the other nine shallow sediment cores. Sediment samples were sealed in plastic bags with the air removed and transported and stored at 4°C until analysis. All analyses began within 36 hours of sample collection.

The sediments from all ten collection sites were thoroughly homogenized within the sample bags before subsampling. For analysis of physical characteristics, a 0.4 to 0.5 g subsample was first measured into a pre-weighed, oven-dried aluminum weigh boat. The subsamples were then placed in a drying oven at 104 $\pm$ 1°C for at least 2 hours to dry to a constant mass. The wet and dry masses of each subsample were used to calculate sediment moisture content (MC; Text S1, Eq. 1). The samples were then combusted in a muffle furnace for 2 hours at 550°C and weighed again to calculate organic matter content as loss-on-ignition (Text S1, Eq. 2) and estimate bulk density (Text S1, Eq. 3; Håkanson and Jansson 2002).

An additional sediment subsample was analyzed for P speciation via sequential extraction following the methods of James (2017b). This method was modified from the methods of Nürnberg (1988) and Psenner and Puckso (1988). To begin the sequential P extractions, subsamples of fresh sediment equivalent to 0.2 g of dry sediment (Text S1, Eq. 4) were weighed into 50 mL polyethylene centrifuge tubes. The same sediment pellet was used throughout the sequential extraction procedure. All extractions were performed at 25°C unless otherwise stated. Centrifuge time and speed (30 minutes at 3000 rpm) as well as shaker table speed (120 rpm) were consistent across extractions.

To quantify loosely-bound P (all sampling sites in each lake), sediment was extracted in 25 mL of 1 M NH_4Cl. The samples were placed on a shaker table for two hours and then centrifuged. After pouring off and saving the supernatant, we repeated this extraction on the same sediment pellet. The combined, filtered (0.45µm GF/C filters) supernatants were analyzed for soluble reactive phosphorus (SRP; Standard Methods 4500-P E) to determine the concentration of sediment pore water and loosely-bound P (Text S1, Eq. 5).

For profundal sediment samples, additional extraction steps were performed on each core slice immediately following the NH_4Cl extraction to quantify other P species. Redox-sensitive P species were extracted in 12.5 mL of a 0.11 M bicarbonate – 0.1 M sodium dithionite solution. Sample tubes were placed in a 40°C water bath for 30 minutes and centrifuged. The supernatant was bubbled with air for at least 30 minutes before filtering and analyzing for SRP. Next, we determined the amount of labile organic P and P associated with aluminum oxides with a two-step 0.1 M NaOH extraction. We added 25 mL of the extractant to the sample tubes and shook the samples for 17 hours. After centrifuging, the supernatant pH was adjusted to between 6-8 using 0.1 M HCl. A subsample of the supernatant was filtered and analyzed for SRP to determine

the aluminum-bound P concentration while the remainder underwent a persulfate digestion (Standard Methods 4500-P B.5) before SRP analysis to determine the concentration of both aluminum-bound and labile organic P. The labile organic P fraction was determined as the difference between the total NaOH-extractable P and the subsample analyzed for aluminum-bound P. Unfortunately, the persulfate digestion for total NaOH-extractable P failed for sediments from three of the lakes (Swan, North Twin, and South Twin) due to an autoclave malfunction. As such, we were unable to determine labile organic P for these lakes. Since the error occurred during supernatant processing, we are confident that the sequential extractions for other P fractions were not affected. For the final extraction for calcium-bound P, we added 25 mL of 0.5 M HCl to the remaining sediment pellet, shook for 24 hours, and centrifuged. We then used 0.1 M NaOH to adjust the supernatant pH to within 6-8 before SRP analysis. All SRP concentrations were corrected for pH adjustments and standardized by extractant volume and sediment mass to determine the sediment concentration of each P species (Text S1, Eq. 5-9).

To determine the total P concentration, we performed a hot acid digestion on an additional subsample from every sediment sample (both profundal and shallow sites). Sediments were dried for 24 hours, ground into a fine powder with a mortar and pestle, and stored in glass scintillation vials until analysis. For the acid digestion, we first weighed 0.2 g of the dried, ground sediment and combusted it at 550°C for 2 hours. We then boiled the sediment samples on a digestion block in 50 mL of 1 M HCl for 2 hours at 150°C. Following digestion, we brought the samples back up to volume using 50 mL of deionized water. Samples were then pH adjusted within 6-8 using 0.1 M NaOH before analysis of TP (Standard Methods 4500-P B.5, E). All concentrations were corrected for pH adjustments and dilution and standardized by the sediment mass used (Text S1, Eq. 10).

Aquatic Macrophyte Survey

We evaluated spatial relationships between macrophyte beds and sediment P pools in one of the study lakes, Swan Lake, as there were extensive beds of submersed and floating-leaf macrophytes in this waterbody. High turbidity limited macrophyte colonization in the other study lakes; therefore, we focused our investigation of macrophytes and sediment P pools to Swan Lake. We surveyed aquatic macrophyte community composition and bed density on Swan Lake in July of 2018 (peak of seasonal growth) using the point-intercept method. We followed a grid of 98 sampling sites, evenly-spaced 65 m apart across the lakebed (Ortiz and Wilkinson 2021). At each sampling point, a two-side rake was lowered to the bottom to collect submersed and floating-leaf macrophytes from an approximately 0.4 m^2 area (Mikulyuk et al. 2011). Species presence and a qualitative estimate of density were recorded at each sampling site. We scored bed density on a scale of 0-3 based on whether the site yielded no plants on the sampling rake or in sight of the boat (score of 0), a few plants on the rake or visible within 2 m of the boat (score of 1), enough plants to fill the rake but leave the tines visible (score of 2), or enough plants to completely fill the rake leaving no part of the metal rake head visible (score of 3).

Statistical Analyses

To determine if profundal sediment P speciation varied among study lakes, we used compositional data analysis and principal components analysis (PCA) on the covariance matrix. Compositional data analysis tests for a difference of proportions among multivariate observations that convey relative information (i.e., parts of a whole). This statistical approach allowed us to test differences in the relative abundance of P fractions among the study lakes

without biasing the analysis to the most abundant fractions (Filzmoser et al. 2018). We used the concentrations of sediment P species measured at each depth interval in the core from the deep site of each study lake in this analysis. However, one interval slice from North Twin (0-2cm) and two from Center Lake (2-4cm and 10-15cm) were excluded from the analysis due to insufficient preserved sediment to determine total P. The compositional analysis was defined by the concentrations of loosely-bound (porewater and surface sorbed), redox-sensitive (Fe- and Mn-bound), aluminum-bound, calcium-bound, and total organic P (defined as the sum of labile and refractory organic P). Refractory organic P was calculated as the difference between total P and the sum of loosely-bound, redox-sensitive, aluminum-bound, calcium-bound, and labile organic P. For the study lakes where we were unable to measure labile organic P directly, we calculated total organic P as the difference between total P and the sum of loosely-bound, redox-sensitive, aluminum -bound, and calcium-bound P (Table 2). The sediment P concentrations were center logratio transformed prior to PCA and further analyses. We fit vectors of environmental data to the PCA biplot to explore how watershed land cover, basin morphology, and sediment physical characteristics corresponded to patterns in profundal sediment P speciation among lakes.

In order to understand the effect that the bioavailability of sediment P fractions may have on algal biomass in the study lakes, we performed a linear regression analysis of the percent of the total sediment P pool at the profundal site that is in a mobile form (the combination of the loosely-bound, total organic, and redox-sensitive species) versus the time-averaged chlorophyll-*a* concentrations for the ice-free season, as an index of algal biomass. Chlorophyll-*a* concentrations are determined based on the U.S. EPA method 445 from a depth integrated sample up to the thermocline or 2 m deep, whichever is shallower (Arar and Collins 1997; Standard Methods 10200-H). These measurements are made 3-5 times each summer from May through September

as a part of the Iowa Department of Natural Resources Ambient Lake and Shallow Lakes monitoring programs. Annual monitoring began in 2000 in all lakes except South Twin where monitoring began in 2006.

To quantify spatial heterogeneity in loosely-bound and total P both within and among lakes, we used measures from the nine spatially-distributed shallow sediment cores and the deep site core slices averaged over depth interval slices. To make comparisons of the variability among lakes we calculated the coefficient of variation for both total P and loosely-bound P in each lake. To test if water depth at the sampling site correlated with the concentration of total P and loosely-bound P, we used linear mixed effects regression with lake as a random effect on the intercept. We used likelihood ratio tests to evaluate the importance of random effects of the lake on model intercepts. We further assessed within-lake variation in Swan Lake by mapping spatial patterns in macrophyte bed density and sediment P concentrations.

We used a rarefaction analysis to determine the spatial sampling resolutions needed for accurate inventories of sediment P pools (Ortiz and Wilkinson 2021). Specifically, we tested how the number of sampling sites affected the whole-lake estimate of mean total and loosely-bound P concentrations. For each study lake and P form, the data were randomly subset to between 2 and 9 sites. The mean P concentration for this sampling subset was then calculated and compared to the "true" mean of all 10 sites based on the root mean square error (RMSE). This analysis was repeated for 1000 iterations and RMSE values were averaged for each sampling subset and normalized to the mean for all 10 sites to express the estimated error a proportion of the "true" mean concentration.

All data are available in Albright et al. (2020). All statistical analyses were completed in R version 3.6.0 (R Core Team 2019) using the tidyverse (Wickham et al. 2019),

robCompositions (Filzmoser et al. 2018), vegan (Oksanen et al. 2019), lmerTest (Kuznetsova et al. 2017), infer (Bray et al. 2021),and sf packages (Pebesma 2018).

RESULTS

Inter-lake Variation in Profundal Sediment P

The size and composition of the profundal sediment P pool varied considerably among the study lakes. Total sediment P concentrations, averaged across the depth intervals of profundal cores, ranged from 738.2 to 1,164.7 µg P g^{-1} dry sediment. The chemical speciation of the profundal sediment P pool also differed among the study lakes (Table 2). Redox-sensitive and organic P fractions were consistently the most abundant components of the total sediment P pool while aluminum and calcium-bound P were usually present in the lowest concentrations. We used PCA as part of a compositional analysis to explore patterns in profundal sediment P chemistry among our study lakes and to identify lakes with similar sediment P composition (Figure 1A). The first principal component (PC1) explained 45.27% of the variation in the dataset and was most closely associated with the prevalence of redox-sensitive and aluminum-bound P. The second principal component (PC2) explained 36.42% of the variation and was highly correlated with organic P content. Together, the first two principal components explained 81.69% of the variance in the dataset. Sediment P speciation defined groups of similar lakes (Table 2, Figure 1A). Center, Five Island, Storm, and Silver Lake formed the largest group, based on higher calcium-bound P concentrations. Silver Lake was slightly separated from this group due to higher concentrations of loosely-bound P. Abundant organic and loosely-bound P placed North and South Twin Lake in a group together. Swan Lake was distinguished from the other study lakes due to high redox-sensitive and aluminum-bound P concentrations.

The grouping of study lakes based on sediment P composition followed patterns in dominant watershed soil series (Table S2). North and South Twin Lake had very similar watershed soil composition, primarily characterized by Webster, Nicollet, Clarion, and Canisteo soil series. Additionally, Swan Lake, which was unique in sediment P speciation, had a different watershed soil composition, the majority of which were Marshall, Colo-Judson, and Exira series formed in loess, rather than glacial till. There was variation in dominant watershed soils within the Center, Five Island, Silver and Storm Lake group. Soils in the Storm Lake catchment were predominantly Sac, Primghar, Marcus, and Galva series formed in loess while the other watershed soils were composed of series formed in glacial till.

In addition to watershed soils, some landcover classes corresponded to the observed groups of study lakes based on profundal sediment P chemistry (Table S3, Figure 1B). Specifically, the proportions of grassland and forest cover in the catchment were strong predictors of sediment P composition, separating Swan Lake from the other waterbodies. Lake basin morphology and sediment characteristics were also strong predictors of lake groupings. The Center, Five Island, Storm, and Silver Lake group was associated with greater maximum lake depth and higher sediment bulk density. The North and South Twin Lake group was associated with higher sediment organic matter content and greater volume development, indicating bowl-shaped basins. The spread of lakes along PC1 seems to be driven by watershed characteristics while variation along PC2 was more closely associated with lake basin and sediment features.

In order to evaluate the ecosystem-level implications of the observed variation in profundal sediment P speciation among our study lakes, we tested the relationship between the relative availability of mobile P fractions in the sediment and algal biomass in each lake. We

performed a linear regression of the percent of total sediment P that is mobile (loosely-bound, total organic, and redox-sensitive) versus time-averaged chlorophyll-*a* concentrations. There was a significant positive relationship between the percentage of total P that is mobile and chlorophyll-*a* concentrations among the seven study lakes ($F_{1,5} = 7.584$, $p = 0.0401$, adjusted $R^2 = 0.52$, $\beta_1 = 3.953$ [0.263, 7.642]; Figure 2).

Intra-lake Variation in Sediment P

There was substantial spatial variation in total and loosely-bound P within individual study lakes. Loosely-bound P had greater spatial heterogeneity than total P within most lakes. There was a 1.2 to 2.2-fold within-lake difference in sediment total P and a 1.7 to 11.3-fold difference in loosely-bound P. Values for the coefficient of variation for loosely-bound P (range = 11.4 to 39.7%, mean = 25.7%) were also greater than the values for total P (range = 6.4 to 22.4%, mean = 14.0%; Table 2). South Twin was the only lake for which the coefficient of variation for loosely-bound P was less than the coefficient of variation for total P. The depth of the water column at the coring location explained 63.1% of the variation in sediment total P and 84.6% of the variation in loosely-bound P when lake was included as a random effect on the intercept (Figure 3). Including random effects on the model intercepts substantially improved the model fits ($p<0.0001$ for both models). For both the total sediment P and loosely-bound fractions, concentrations increased with depth. The increase in P with water depth was greater for total P ($\beta_1 = 65.28$ [27.57, 102.49]) than loosely-bound P ($\beta_1 = 12.79$ [7.18, 18.33]).

We further explored the influence of lake basin morphology on spatial variation in loosely-bound P through an analysis of volume development (D_v). The D_v score is a ratio of the volume of a lake basin to the volume of a perfect cone with a base area equal to the surface area

of the lake and a height equal to the maximum water depth. The D_v ratio is used to characterize lake basin shape. Lakes with low D_v values have cone-shaped basins with localized deep holes while higher D_v ratios correspond to shallow, bowl-shaped bathymetries (Hutchinson 1957). We found an inverse relationship between D_v and the variability in loosely-bound P, measured as the coefficient of variation (Figure S1). Five Island, Storm, and Swan Lakes had the greatest within-lake variation in loosely-bound P (CV range = 32.0 to 39.7%), and these waterbodies also had low D_v values (range = 0.65 to 1.36). Conversely, we found much less variability in loosely-bound P (CV range = 11.4 to 24.4%) in Center, Silver, North and South Twin Lakes, which all had higher D_v scores near 2 (range = 1.98 to 2.12).

To evaluate additional explanations for within-lake variation in sediment P, we surveyed spatial relationships between macrophyte colonization and sediment P in Swan Lake. Swan Lake had high variation in both loosely-bound and total P across the lakebed (Figure 4). There were extensive beds of sago pondweed (*Stuckenia pectinata*) within the 1-2 m depth contour across the northern half of Swan Lake and along the eastern shoreline. These beds were especially dense on the east side of the lake. There was also an isolated but dense bed of American lotus (*Nelumbo lutea*) in the center of the northern half of the lake rooted in 1.7 m of water. Both total and loosely-bound sediment P concentrations were lowest in the shallow, northern portion of the lake. Concentrations increased in the deeper, southern portion of the lake. There was no clear pattern between sediment P concentration and macrophyte bed density.

A better understanding of intra-lake variation in sediment P concentrations will inform appropriate spatial sampling resolutions to accurately quantify sediment P pools. We used a rarefaction analysis to test how the number of sampling sites affected the estimate of mean total and loosely-bound P in each study lake. For sediment total P, normalized RMSE values began to

plateau when 6 or more sampling sites were included (Figure 5A). In subsets of 6 or more sampling sites, the normalized RMSE was less than 5 percent for all study lakes (range = 1.37 to 4.71%). Some study lakes had relatively low normalized RMSE values regardless of how many sites were included while others demonstrated sharp declines in normalized RMSE as the number of sites increased. These differences among lakes did not follow patterns with basin D_v or maximum water depth. Compared to total P, the number of sampling sites had a greater impact on the estimate of mean loosely-bound P within each study lake (Figure 5B). Normalized RMSE values did not reach obvious plateaus for any study lakes. Lakes with low D_v values (i.e., Five Island, Storm, and Swan Lakes) had higher normalized RMSE values and more drastic improvements in RMSE with increasing number of sample sites. Conversely, lakes with higher D_v values (i.e., Center, Silver, North and South Twin Lakes) had lower normalized RMSE and more gradual improvements in RMSE with more sampling sites.

In addition to quantifying the effects of spatial sampling resolution on P pool estimates, we also tested the influence of sample site location, specifically whether P concentrations at the deep site were representative of mean P concentrations across the lakebed. We compared total and loosely-bound P concentrations from the deep site of each lake to the whole-lake mean (Table S4). For sediment total P, concentrations at the deep site exceeded the whole-lake average for all lakes except Swan Lake. Normalized RMSE values ranged from 0.3 to 11.3 percent (mean = 4.6 %). Loosely-bound P concentrations at the deep site were consistently greater than whole-lake means. Normalized RMSE values were much greater than for total P (range = 2.2 to 52.5%, mean = 26.2%).

DISCUSSION

Inter-lake Variation in Sediment P Content and Composition

We quantified spatial heterogeneity in sediment P content and composition in shallow lakes and found high variation both within individual waterbodies and among different systems. Whole-lake means of sediment total P content ranged from 897.0 to 1,184.9 μg P g^{-1} dry sediment across the study lakes, with a grand mean of 946.2 μg P g^{-1} dry sediment. These concentrations align with observed ranges in other shallow, eutrophic lakes (Søndergaard et al. 2013) as well as other productive waterbodies (Doig et al. 2017; Kowalczewska-Madura et al. 2019b; Tao and Lu 2020). Overall, sediment total P concentrations from our study lakes tend to be either similar to or lower than average values reported for other productive waterbodies (Table S5). The chemical composition of the profundal sediment P pool also varied among our study lakes; however, redox-sensitive and organic P were consistently the most abundant components. Other eutrophic waterbodies also have high levels of redox-sensitive P (Song and Burgin 2017; Randall et al. 2019; Papera et al. 2021) and organic P forms (Nowlin et al. 2005; Frost et al. 2019). More generally, aquatic sediments tend to be enriched in redox-sensitive, organic, loosely-bound, and aluminum-bound P because these forms are commonly associated with fine sediments, which are more easily eroded and transported from the source material (i.e., terrestrial soils; Stone and English 1992; Kerr et al. 2011).

In order to compare sediment P composition among our study lakes, we used PCA as part of a compositional analysis to explore patterns and identify lakes with similar sediment P chemistry. The analysis grouped Center, Five Island, Storm, and Silver Lake together based on higher calcium-bound P levels. Abundant organic and loosely-bound P grouped North and South Twin Lake together while high redox-sensitive and aluminum-bound P concentrations placed Swan Lake apart from the other study lakes. The North and South Twin Lake and Swan Lake

groupings reflect patterns in dominant watershed soil series. However, there was variation in watershed soil characteristics within the Center, Five Island, Silver and Storm Lake group as soils in the Storm Lake catchment were formed in loess while the other watershed soils were formed in glacial till. Variation in watershed soils within this group reinforces that aquatic sediment P composition is not a direct reflection of the bulk soil matrix due to selective erosional and sediment transport processes as well as *in situ* processing (Kerr et al. 2011).

The dominant mechanisms that drive internal P loading in a given waterbody depend on the chemical composition of the sediment P pool (Orihel et al. 2017). Our finding that sediment P composition varies among different lakes implies that the processes driving sediment P release also vary across systems. For example, redox-sensitive P was the dominant fraction in Swan Lake while North and South Twin Lake a higher prevalence of organic P. Based on these differences in sediment P composition, we would expect sediment P release in these lakes to respond differently to dissolved oxygen levels at the sediment-water interface. Specifically, we would anticipate that anoxia would prompt sediment P release in Swan Lake due to the dissolution of redox-sensitive minerals under reducing conditions (Mortimer 1941; Orihel et al. 2015). Anaerobic sediment P release from redox-sensitive P minerals could also occur in North and South Twin Lake; however, due to high organic P levels, we would also expect to see sediment P release under oxic conditions due to decomposition of sediment organic matter and subsequent P mineralization (Joshi et al. 2015; Song and Burgin 2017; Frost et al. 2019). Hypolimnetic aeration, a management approach to limit anaerobic internal P loading, might protect redox-sensitive minerals and reduce sediment P release in Swan Lake, but the same approach in North and South Twin Lakes could stimulate decomposition and enhance aerobic P release (Horppila et al. 2017, Tammeorg et al. 2017). Inter-lake variation in sediment P

composition means that management strategies to prevent and control internal P loading are unlikely to translate well across lakes with different sediment P chemistry.

Across the study lakes we found a strong relationship between the average contribution of mobile P fractions to the total sediment P pool and long-term, average chlorophyll-*a* concentrations, as an index of algal biomass. This relationship indicates the substantial contribution of internally-loaded P to algal production in these shallow lakes. Total organic P was the largest fraction of total sediment P in all of the study lakes, driving the among-lake variability in mobile P contributions. Given the prevalence of organic P in the sediments, it is likely that decomposition of sediment organic matter and subsequent P mineralization are key processes for internal P loading in the study lakes (Joshi et al. 2015; Frost et al. 2019). In hypereutrophic waterbodies rampant algal production and detritus enhance organic matter sedimentation, increasing organic P in lakebed sediments. Large pools of organic P are associated with high extracellular enzyme activities, which mobilize and release sediment P (Song and Burgin 2017). Our study lakes are likely examples of systems in which biologically-mediated cycling of organic P pools drives internal P loading.

Intra-lake Variation in Sediment P Pools

In addition to variation in sediment P content and composition across different lakes, we also identified spatial heterogeneity in total and loosely-bound P pools within individual lakes. Consistent with our expectations, loosely-bound P concentrations were most variable in lakes with low volume development indices, indicative of conical basins with localized deep holes. This bathymetric variability produces both shallow regions where frequent sediment disturbance releases loosely-bound P and deeper areas where loosely-bound P is protected (James 2017a). As

a result, loosely-bound P concentrations are more variable in lake basins with more complex bathymetry. In contrast, lakes with high volume development scores, associated with shallow, bowl-shaped basins, had more consistent loosely-bound P concentrations, as sediment disturbance was likely more uniform across the lakebed. We also hypothesized that greater water depths would correlate with higher concentrations of total and loosely-bound sediment P across the lakebed, which was supported by the mixed model analysis. In fact, the depth of the water at the sediment sampling location described the vast majority (84.1%) of the variation in loosely-bound P and over half of the variation (63.1%) in total P concentrations. The pattern of higher concentrations at greater depths is likely driven by sediment focusing and greater net sediment deposition in deeper portions of the lake (White and Stone 1996; Hou et al. 2014; Cardoso-Silva et al. 2018). The direct relationship that we observed between water depth and sediment P concentrations is consistent with other studies of spatial variation in sediment P pools (Nowlin et al. 2005; Kowalczewska-Madura et al. 2019b). However, water depth did not fully explain the observed variation in sediment total and loosely-bound P, indicating that factors beyond basin morphology contribute to spatial variation in sediment P pools.

A factor that may influence the spatial distribution of the sediment P pool is the location and density of macrophyte beds. In most of the study lakes, macrophytes were limited to emergent taxa; therefore, the macrophyte beds did not overlap with sediment sampling sites. However, extensive submersed and floating-leaf vegetation across Swan Lake allowed us to sample sediment P across a gradient of macrophyte bed density. We found no clear evidence of a spatial pattern between macrophyte bed density and sediment P. Total and loosely-bound P concentrations were lowest in the shallow, heavily-vegetated northern portion of the lake. Sediment P concentrations were generally higher in the deeper, non-vegetated areas of the lake.

However, there were two vegetated sites along the eastern edge of the lake that also had high sediment total and loosely-bound P concentrations. Thus, it is difficult to establish a spatial relationship between macrophyte beds and sediment P. Macrophytes could be expected to either increase sediment P stocks by stabilizing sediments and reducing resuspension (Carpenter et al. 1983; Madsen 2001) or decrease sediment P pools via biological uptake (Xing et al. 2018). Exploring the balance of this complex relationship is an avenue for future research. Specifically, quantifying sediment resuspension could better explain the spatial distribution of P stocks in Swan Lake (James 2017a). Sediment resuspension is expected to interact with both water depth and macrophytes as shallow, non-vegetated sediments are the most susceptible to disturbance (Horppila and Nurminen 2001; Nurminen and Horppila 2009). Quantifying sediment disturbance on Swan Lake could further illuminate interactions between water depth and macrophyte bed density and the resultant effects on sediment P pools.

Our study provides a valuable characterization of spatial heterogeneity in sediment P pools. Although sediment P content and chemical composition are expected to vary over time as a balance of sedimentation, mobilization and release into the water column, and post depositional transformations (Ostrofsky 2012; Heathcote et al. 2013;), other studies of natural, productive lakes have found limited temporal variation in sediment P concentrations on intra-annual scales (Kowalczewka-Madura et al. 2019a; Kowalczewka-Madura et al. 2019b). As such, our results provide a fair snapshot of expected spatial variation in sediment P pools within shallow lakes. A natural progression of this research is to explore temporal variation in sediment P content and composition.

Applications and Significance

A quantitative understanding of intra-lake heterogeneity in sediment P concentrations reveals the spatial sampling resolutions necessary for accurate inventories of sediment P pools. Our rarefaction analysis suggests that sampling six or more locations across the lakebed may be sufficient to estimate the mean, whole-lake concentration of sediment total P. When six or more sites were included, estimate error (normalized RMSE) dropped below five percent for all study lakes and remained stable even as more sampling sites were included. This result aligns with research on lacustrine burial rates that proposes as few as five sediment cores can be used to accurately assess sediment P accumulation rates (Rippey et al. 2008; Engstrom and Rose 2013). Compared to the rarefaction analysis for total P, estimate errors for mean loosely-bound P concentrations were greater for most study lakes, and there were no clear plateaus in error values as more sampling sites were considered. However, the relationship between sampling sites and estimate error did follow a pattern with basin morphology. Lakes with more complex bathymetry (low D_v; Five Island, Storm, Swan Lake) had more drastic improvements in RMSE values as more sampling sites were considered. Lakes with simple, bowl-shaped basins (high D_v; Silver, Center, South Twin, North Twin Lake) had lower RMSE values overall and more gradual improvements with increased sampling resolution. This pattern makes sense in light of our finding that lakes with more complex basin morphology had greater spatial variation in loosely-bound P concentrations and suggests that more sampling sites are needed to inventory loosely-bound P stocks compared to total P, especially in lakes with complex bathymetry.

Comparing P concentrations at the deep site of each study lake to whole-lake means demonstrates that scaling values from the deep site to the entire lakebed will tend to overestimate sediment P stocks. We found that total P concentrations at the deep site were greater than the whole-lake average for all lakes except for Swan Lake, where the values were very similar, and

that extrapolating values from the deep site could overestimate the whole-lake mean by as much as 11.3 percent. Loosely-bound P concentrations at the deep site were consistently greater than the whole-lake mean and extrapolating from the deep site overestimated loosely-bound P stocks by 2.2 to 52.5 percent (mean 26.2%). Our findings support other studies suggesting that single-core analyses produce unreliable estimates of whole lake carbon and nutrient stocks (Mackay et al. 2012; Lin et al. 2022). Our analysis further reinforces that a good approach for addressing this bias and obtaining an accurate estimate of whole-lake sediment P stocks is to collect multiple sediment cores across a range of water depths (Engstrom and Rose 2013). Accurate inventories of sediment P stocks are necessary to parameterize models of lentic P cycling (Hansen et al. 2020). Lake response to simulated changes in external P loading will be sensitive to the mass of P held in the sediments that is available for recycling. As such, accurate estimates of sediment P stocks, accounting for spatial variation, are critical for modeling lentic P cycles and forecasting lake response to changes in watershed nutrient loading.

A quantitative understanding of inter- and intra-lake variation in sediment P content and composition is essential for accurately sampling, scaling, and modeling sediment P pools, yet this variability has been largely undescribed for shallow lakes. Our study builds on our understanding of regional patterns in lacustrine sediment P speciation and contributes novel perspectives on the causes and consequences of spatial heterogeneity in sediment P pools within shallow lakes. Our finding of inter-lake variation in sediment P composition reinforces that management strategies to control internal P loading will also differ among lakes and that effective solutions will consider site-specific features, including sediment P chemistry. Our analysis further supports that shallow lakes are spatially heterogenous ecosystems, and accounting for this variation is necessary to accurately characterize sediment P pools. The large

within-lake variability in loosely-bound and total P documented in this study reinforces the importance of sampling multiple sites across the lakebed when possible and using caution when extrapolating measures from the deep site to the whole system. Accurate sediment P inventories will allow for more empirical parameterization of sediment-water interactions in models of lake P cycling. Our quantification of spatial heterogeneity in sediment P pools within and among lakes is a critical step to being able to predict internal P loading potential based on lake and watershed characteristics.

Acknowledgments

We thank David Ortiz and Elena Sandry for their assistance with sample collection and analysis, and Dr. Jonathan Walter, Dr. Philip Dixon and Audrey McCombs for helpful discussions regarding analyses. All authors and the research were supported with funds from Iowa Department of Natural Resources (Contract No. 18CRDLWBMBALM-0013). Albright was additionally supported by the National Science Foundation Graduate Research Fellowship under Grant No. (1744592).

Data Availability Statement

The data supporting the conclusions are publicly available in Albright et al. (2020), with a CC0 1.0 Universal Public Domain Dedication license. The analysis code is available in the Github repository https://github.com/AlbrightE/Sediment_P_2018, which will be archived using Zenodo upon acceptance of the manuscript.

REFERENCES

1. Albright, E.A., G.M. Wilkinson, R.E. Fleck, and Q. Shingai. 2020. Analysis of Sediment Phosphorus Pools in Shallow Lakes. figshare. doi, 10.6084/m9.figshare.13362971.v1
2. Arar, E.J., and G.B. Collins. 1997. Method 445.0 *in vitro* determination of chlorophyll a and pheophytin a in marine and freshwater algae by fluorescence. U.S. Environmental Protection Agency, Washington, DC.
3. Arbuckle, K.E., and J.A. Downing. 2001. The influence of watershed land use on lake N:P in a predominantly agricultural landscape. Limnol. Oceanogr. 46(4): 970-975, doi: 10.4319/lo.2001.46.4.0970
4. Bengtsson, L., and T. Hellström. 1992. Wind-induced resuspension in a small shallow lake. Hydrobiologia. 241: 163-172, doi: 10.1007/BF00028639
5. Bray, A., C. Ismay, E. Chasnovski, B. Baumer, and M. Cetinkaya-Rundel. 2021. infer: Tidy Statistical Inference. R package version 0.5.4. https://CRAN.R-project.org/package=infer
6. Cardoso-Silva, S., P.A.d. Ferreira, R.C.L. Figueira, D.C. Silva, V. Moschini-Carlos, and M.L.M. Pompêo. 2018. Factors that control the spatial and temporal distributions of phosphorus, nitrogen, and carbon in the sediments of a tropical reservoir. Environ. Sci. Pollut. Res. 25(31): 31776–31789, doi: 10.1007/s11356-018-2923-0
7. Carlson, R.E. 1977. A trophic state index for lakes. Limnol. Oceanogr. 22(2): 361-369, doi: 10.4319/lo.1977.22.2.0361
8. Carpenter, S.R., N.F. Caraco, D.L. Correll, R.W. Howarth, A.N. Sharpley, and V.H. Smith. 1998. Nonpoint pollution of surface waters with phosphorus and nitrogen. Ecol. Appl. 8(3): 559-568, doi: 10.1890/1051-0761(1998)008[0559:NPOSWW]2.0.CO;2
9. Carpenter, S.R., J.J. Elser, and K.M. Olson. 1983. Effects of roots of *Myriophyllum verticuillatum* L. on sediment redox conditions. Aquat. Bot. 17(3-4): 243-249, doi: 10.1016/0304-3770(83)90060-8
10. Doig, L.E., R.L. North, J.J. Hudson, C. Hewlett, K.-E. Lindenschmidt, and K. Liber. 2017. Phosphorus release from sediments in a river-valley reservoir in the northern Great Plains of North America. Hydrobiologia 78(1): 323-339, doi: 10.1007/s10750-016-2977-2
11. Ekholm, P., O. Malve, and T. Kirkkala. 1997. Internal and external loading as regulators of nutrient concentrations in the agriculturally loaded Lake Pyhäjärvi (southwest Finland). Hydrobiologia. 345: 3-14, doi: 10.1023/A:1002958727707
12. Elser, J.J., et al. 2007. Global analysis of nitrogen and phosphorus limitation of primary producers in freshwater, marine and terrestrial ecosystems. Ecol. 10: 1135-1142, doi: 10.1111/j.1461-0248.2007.01113.x
13. Engstrom, D.R., and N.L. Rose. 2013. A whole-basin, mass-balance approach to paleolimnology. J. Paleolimnol. 49: 333–347, doi:10.1007/s10933-012-9675-5
14. Filzmoser, P., K. Hron, and M. Templ. 2018. *Applied Compositional Data Analysis with Worked Examples in R.* Spring Series in Statistics. Spring International Publishing, Cham, Switzerland.

15. Forsberg, C. 1989. Importance of sediments in understanding nutrient cyclings in lakes. Hydrobiologia. 176/177:263-277, doi: 10.1007/BF00026561

53. Frost, P. C., C. Prater, A.B. Scott, K. Song, and M.A. Xenopoulos. 2019. Mobility and Bioavailability of Sediment Phosphorus in Urban Stormwater Ponds. Water Resour. Res. 55(5): 3680-3688, doi: 10.1029/2018WR023419

16. Golterman, H.L. 2004. *The Chemistry of Phosphate and Nitrogen Compounds in Sediments.* Springer Science+Business Media, B.V.

17. Hanson, P.C., et al. 2020. Predicting lake surface water phosphorus dynamics using process-guided machine learning. Ecol. Modell. 430: 109136, doi: 10.1016/j.ecolmodel.2020.109136

18. Heathcote, A.J., C.T. Filstrup, and J.A. Downing. 2013. Watershed sediment losses to lakes accelerating despite agricultural soil conservation efforts. PLoS One. 8(1): e 53554, doi: 10.1371/journal.pone.0053554

19. Hou, D., J. He, C. Lü, S. Dong, J. Wang, Z. Xie, F. Zhang. 2014. Spatial variation and distributions of phosphorus and nitrogen in bottom sediments from a typical north-temperate lake, China. Environ. Earth Sci. 71: 3063-3079, doi: 10.1007/s12665-013-2683-6

20. Horppila, J., H. Holmroos, J. Niemistö, I. Massa, N. Nygrén, P. Schonach, P. Tapio, and O. Tammeorg. 2017. Variations of internal phosphorus loading and water quality in a hypertrophic lake during 40 years of different management efforts. Ecol. Eng. 103: 264-274, doi: 10.1016/j.ecoleng.2017.04.018 0925-8574

21. Horppila, J., and L. Nurminen. 2001. The effect of an emergent macrophyte (Typha angustifolia) on sediment resuspension in a shallow north temperate lake. Freshw. Biol. 46(11): 1447-1455, doi: 10.1046/j.1365-2427.2001.00765.x

22. Hutchinson, G.E. 1957. *A treatise on limnology.* Volume 1. New York, NY: Wiley.

23. Håkanson, L., and M. Jansson. 2002. *Principles of lake sedimentology*. Caldwell, NJ: The Blackburn Press. doi: 10.1002/iroh.19850700318

24. James, W.F. 2017a. Internal phosphorus loading contributions from deposited and resuspended sediment to the Lake of the Woods. Lake Reserv. Manag. 34(4): 347-359, doi: 10.1080/10402381.2017.1312647

25. James, W.F. 2017b. Diffusive phosphorus fluxes in relation to the sediment phosphorus profile in Big Traverse Bay, Lake of the Woods. Lake Reserv. Manag. 33(4): 360-368, doi: 10.1080/10402381.2017.1346010

26. Jensen, H.S., and F.Ø. Andersen. 1992. Importance of temperature, nitrate, and pH for phosphate release from aerobic sediments of four shallow, eutrophic lakes. Limnol. Oceanogr. 37(3): 577-598, doi: 10.4319/lo.1992.37.3.0577

27. Jeppesen, E., et al. 2005. Lake responses to reduced nutrient loading — an analysis of contemporary long-term data from 35 case studies. Freshw. Biol. 50(10): 1747–1771, doi: 10.1111/j.1365-2427.2005.01415.x

28. Joshi, S.R., R.K. Kukkadapu, D.J. Burdige, M.E. Bowden, D.L. Sparks, and D.P. Jaisi. 2015. Organic matter remineralization predominates phosphorous cycling in the mid-bay sediments in the Chesapeake Bay. Environ. Sci. Technol. 49(10): 5887-5896, doi: 10.1021/es5059617

29. Kelton, N., and P. Chow-Fraser. 2005. A simplified assessment of factors controlling phosphorus loading from oxygenated sediments in a very shallow eutrophic lake. Lake Reserv. Manag. 21(3): 223-230, doi: 10.1080/07438140509354432

30. Kerr, J.G., M.A. Burford, J.M. Olley, S.E. Bunn, and J. Udy. 2011. Examining the link between terrestrial and aquatic phosphorus speciation in a subtropical catchment: The role of selective erosion and transport of fine sediments during storm events. Water Res. 45(11): 3331-3340, doi: 10.1016/j.watres.2011.03.048

31. Kowalczewska-Madura, K., R. Gołdyn, J. Bogucka, and K. Strzelczyk. 2019. Impact of environmental variables on spatial and seasonal internal phosphorus loading in a mesoeutrophic lake. Int. J. Sediment Res. 34(1): 14–26, doi: 10.1016/j.ijsrc.2018.08.008

32. Kowalczewska-Madura, K., A. Kozak, M. Dera, and R. Gołdyn. 2019b. Internal loading of phosphorus from bottom sediments of two meso-eutrophic lakes. Int. J. Environ. Res. 13: 325-251, doi: 10.1007/s41742-019-00167-y

33. Kuznetsova, A., P.B. Brockhoff, and R.H.B. Christensen. 2017. lmerTest package: Tests in linear mixed effects models. J. Stat. Softw. 82(13): 1-26, doi: 10.18637/jss.v082.i13

34. Lai, W., Y. Zhang, and Z. Chen. 2011. Radial oxygen loss, photosynthesis, and nutrient removal of 35 wetland plants. Ecol. Eng. 39: 24-30, doi: 10.1016/j.ecoleng.2011.11.010

35. Lewis, W.M. 1983. A revised classification of lakes based on mixing. Can. J. Fish. Aquat. Sci. 40(10): 1779-1787, doi: 10.1139/f83-207

36. Lin, Q., E. Liu, E. Zhang, R. Bindler, B. Nath, K. Zhang, and J. Shen. 2022. Spatial variation of organic carbon sequestration in large lakes and implications for carbon stock quantification. CATENA. 208: 105768, doi: 10.1016/j.catena.2021.105768

37. Lukkari, K., H. Hartikainen and M. Leivuori. 2007. Fractionation of sediment phosphorus revisited. I: Fractionation steps and their biogeochemical basis. Limnol. Oceanogr-meth. 5: 433-444, doi: 10.4319/lom.2007.5.433

38. Mackay, E.B., I.D. Jones, A.M. Folkard, and P. Barker. 2012. Contribution of sediment focussing to heterogeneity of organic carbon and phosphorus burial in small lakes. Freshw. Biol. 57(2): 290-304, doi:10.1111/j.1365-2427.2011.02616.x

39. Madsen, J.D., P.A. Chambers, W.F. James, E.W. Koch, and D.F. Westlake, D.F. 2001. The interactions between water movement, sediment dynamics and submersed macrophytes. Hydrobiologia. 444: 71-84, doi: 10.1023/A:1017520800568

40. Mortimer, C. 1941. The exchange of dissolved substances between mud and water in lakes. Ecology. 29: 280-239, doi: 10.2307/2256395

41. Mikulyuk, A., S. Sharma, S. Van Egeren, E. Erdmann, M.E. Nault, and J. Hauxwell. 2011. The relative role of environmental, spatial, and land-use patterns in explaining aquatic macrophyte community composition. Can. J. Fish. Aquat. Sci. 68(10): 1778-1789, doi: 10.1139/f2011-095

42. North, R.L, J. Johansson, D.M. Vandergucht, L.E. Doig, K. Liber, K. Lindenschmidt, H. Baulch, and J.J. Hudson. 2015. Evidence for internal phosphorus loading in a large prairie reservoir (Lake Diefenbaker, Saskatchewan). J. Great Lakes Res. 41(S2): 91-99, doi: 10.1016/j.jglr.2015.07.003

43. Nowlin, W.H., J.L. Evarts, and M.J. Vanni. 2005. Release rates and potential fates of nitrogen and phosphorus from sediments in a eutrophic reservoir. Freshw. Biol. 50(2): 301–322, doi: 10.1111/j.1365-2427.2004.01316.x

44. Nurminen, L., and J. Horppila. 2009. Life form dependent impacts of macrophyte vegetation on the ratio of resuspended nutrients. Water Res. 43(13): 3217-3226, doi: 10.1016/j.watres.2009.04.041

45. Nürnberg, G.K. 1988. Prediction of phosphorus release rates from total and reductant-soluble phosphorus in anoxic lake sediments. Can. J. Fish. Aquat. Sci. 45: 453–46, doi: 10.1139/f88-054

46. Oksanen, J., et al. 2019. vegan: Community Ecology Package. R package version 2.5-6. https://CRAN.R-project.org/package=vegan

47. Orihel, D.M., H.M. Baulch, N.J. Casson, R.L. North, C.T. Parsons, D.C.M. Seckar, and J.J. Venkiteswaran. 2017. Internal phosphorus loading in Canadian fresh waters: a critical review and data analysis. Can. J. Fish. Aquat. Sci. 74: 2005-2029, doi: 10.1139/cjfas-2016-0500

48. Orihel, D. M., D.W. Schindler, N.C. Ballard, M.D. Graham, D.W. O'Connell, L.R. Wilson, and R. D. Vinebrooke. 2015. The "nutrient pump:" Iron-poor sediments fuel low nitrogen-to-phosphorus ratios and cyanobacterial blooms in polymictic lakes. Limnol. Oceanogr. 60(3): 856-871, doi:10.1002/lno.10076

49. Ortiz, D.A., and G.M. Wilkinson. 2021. Capturing the spatial variability of algal bloom development in a shallow temperate lake. Freshw. Biol. 66(11): 2064-2075, doi: 10.1111/fwb.13814

50. Ostrofsky, M.L. 2012. Differential post-depositional mobility of phosphorus species in lake sediments. J. Paleolimnol. 48: 559-569, doi: 10.1007/s10933-012-9631-4

51. Papera, J., F. Araújo, and V. Becker. 2021. Sediment phosphorus fractionation and flux in a tropical shallow lake. Acta Limnol. Bras. 33: e5, doi: 10.1590/S2179-975X9020

52. Pease, L.A., K.W. King, M.R. Williams, G.A. LaBarge, E.W. Duncan, and N.R. Fausey. 2018. Phosphorus export form artificially drained fields across the Eastern Corn Belt. J. Great Lakes Res. 44(1): 43-53, doi: 10.1016/j.jglr.2017.11.009

53. Pebesma, E. 2018. Simple features for R: Standardized support for spatial vector data. The R Journal. 10(1): 439-446, doi: 10.32614/RJ-2018-009

54. Psenner, R., and R. Puckso. 1988. Phosphorus fractionation: advantages and limits of the method for the study of sediment P origins and interactions. Archiv fur Hydrobiologie. 30: 43–59. ISSN: 0071-1128.

55. R Core Team. 2019. R: A language and environment for statistical computing. R Foundation for Statistical Computing, Vienna, Austria. https://www.R-project.org/

56. Randall, M.C., et al. 2019. Sediment potentially controls in-lake phosphorus cycling and harmful cyanobacteria in shallow, eutrophic Utah Lake. PLoS One. 14(2): e0212238, doi: 10.1371/journal.pone.0212238

57. Rippey, B., N.J. Anderson, I. Renberg, and T. Korsman. 2008. The accuracy of methods used to estimate the whole-lake accumulation rate of organic carbon, major cations, phosphorus and heavy metals in sediment. J. Paleolimnol. 39: 83–99, doi: 10.1007/s10933-007-9098-x

58. Schindler, D.W., S.R. Carpenter, S.C. Chapra, R.E. Hecky and D.M. Orihel. 2016. Reducing phosphorus to curb lake eutrophication is a success. J. Environ. Sci. Technol. 50(17): 8923-8929., doi: 10.1021/acs.est.6b02204.

59. Schindler, D.W., and J.R. Vallentyne. 2008. *The Algal Bowl: Overfertilization of the World's Freshwaters and Estuaries.* Edmonton: The University of Alberta Press.

60. Song, K., and A.J. Burgin. 2017. Perpetual phosphorus cycling: Eutrophication amplifies biological control on internal phosphorus loading in agricultural reservoirs. Ecosystems. 20(8): 1483-1493, doi: 10.1007/s10021-017-0126-z

61. *Standard Methods for the Examination of Water and Wastewater*, 20th Edition, Method 4500-P (1998).

62. *Standard Methods for the Examination of Water and Wastewater*, 20th Edition, Method 10200-H (1998).

20. Stone, M., and M.C. English. 1993. Geochemical composition, phosphorus speciation and mass transport of fine-grained sediment in two Lake Erie tributaries. Hydrobiologia 253: 17-29, doi:10.1007/BF00050719

63. Søndergaard, M., J.P. Jensen, and E. Jeppesen. 1999. Internal phosphorus loading in shallow Danish lakes. Hydrobiologia, 408: 145-152, doi: 10.1023/A:1017063431437

54. Søndergaard, M., J.P. Jensen, and E. Jeppesen. 2003. Role of sediment and internal loading of phosphorus in shallow lakes. Hydrobiologia. 506: 135-145, doi: 10.1023/B:HYDR.0000008611.12704.dd

64. Søndergaard, M., R. Bjerring, and J.P Jensen. 2013. Persistent internal phosphorus loading during summer in shallow eutrophic systems. Hydrobiologia. 710 (1): 95-107, doi: 10.1007/s10750-012-1091-3

65. Tammeorg, O., T. Möls, J. Niemistö, H. Holmroos, and J. Horppila. 2017. The actual role of oxygen deficit in the linkage of the water quality and benthic phosphorus release: Potential implications for lake restoration. Sci.Total Environ. 599-600: 732-738, doi: 10.1016/j.scitotenv.2017.04.244

66. Tang, Q., L. Peng, Y. Yang, Q. Lin, S.S. Qian, and B. Han. 2019. Total phosphorus-precipitation and chlorophyll α-phosphorus relationships of lakes and reservoirs mediated by soil iron at regional scale. Water Re. 154: 136-143, doi: 10.1016/j.watres.2019.01.038

67. Tao, Y.Q, and J. Lu. 2020. Occurrence of total phosphorus in surface sediments of Chinese lakes and its driving factors and implications. J. Hydrol. 580: 124345, doi: 10.1016/j.jhydrol.2019.124345

68. Twilley, R.R., G. Ejdung, P. Romare, and W.M. Kemp. 1986. A comparative study of decomposition, oxygen consumption and nutrient release for selected aquatic plants occurring in an estuarine environment. Oikos. 47: 190-198, doi: 10.2307/3566045

69. Welch, E.B., and G.D. Cooke. 1995. Internal phosphorus loading in shallow lakes: Importance and control. Lake Reserv. Manag. 11(3): 273-281, doi: 10.1080/07438149509354208

70. White, A., and M. Stone. 1996. Spatial variation and distribution of phosphorus forms in bottom sediments of two Canadian Shield Lakes. Can. Geogr. 40(3): 258-265, doi: 10.1111/j.1541-0064.1996.tb00452.x

71. Wickham, H., et al. 2019. Welcome to the tidyverse. J. Open Source Softw. 4(43): 1686, doi: 10.21105/joss.01686

72. Xing, X.G., et al. 2018. Direct evidence for the enhanced acquisition of phosphorus in the rhizosphere of aquatic plants: A case study on *Vallisneria natans.* Sci. Total Environ. 616: 386-396, doi: 10.1016/j.scitotenv.2017.10.304

73. Yu, Z., and C. Lu. 2018. Historical cropland expansion and abandonment in the continental U.S. during 1850 to 2016. Glob. Ecol. Biogeogr. 27(3): 322-333, doi: 10.1111/geb.12697

TABLES

Table 1. *Location, Basin Morphology, and Watershed Features of the Study Lakes*

	Center Lake	Five Island	Silver Lake	Storm Lake	North Twin	South Twin	Swan Lake
Latitude	43.41263	43.1545	43.44145	42.61977	42.47563	42.45847	42.03568
Longitude	-95.1357	-94.648	-95.3353	-95.1857	-94.6405	-94.6536	-94.8416
Surface area (ha)	104	405.6	431.4	1270.7	187.4	224.6	48.6
Maximum depth (m)	5.5	8	3	6.2	3.7	1.6	3.8
Mean depth (m)	3.7	1.7	2	2.6	2.7	1.1	1.7
Catchment/surface area	2.7	9.2	10.7	4.4	4.6	6	6.1
Chlorophyll-*a* (μg L^{-1})	36.64	45.42	28.38	15.94	51.2	87.2	75.71
% Cropland	14.3	75.5	78.1	60.2	82.5	78.4	45.1
Dominant soil origin	Glacial till	Glacial till	Glacial till	Loess	Glacial till	Glacial till	Loess

Note. Chlorophyll-*a* values are the 20-year mean (2000-2019) of measurements made during the ice-free season (n=55-57 measurements per lake) with the exception of South Twin Lake which is the 14-year mean (2006-2019) of measurements made during the ice-free season (n=55)

Table 2. *Variation in Profundal Sediment P Among Lakes and Within-Lake Heterogeneity*

	Center Lake	Five Island	Silver Lake	Storm Lake	North Twin	South Twin	Swan Lake
Total P (µg P g^{-1} dry sediment)	938.3 (±191.4)	1,013.5 (±160.9)	936.5 (±97.0)	738.2 (±29.5)	1,134.1 (±288.3)	939.1 (±113.1)	1,164.7 (±306.2)
% Redox-sensitive	24.45	30.30	22.81	31.16	9.62	11.81	35.58
% Labile organic	31.45	25.02	21.79	19.06	--	--	--
% Refractory organic	21.85	15.98	17.53	22.35	--	--	--
% Total Organic	53.31	41.00	39.32	41.41	74.81	70.48	50.14
% Loosely-bound	7.75	15.04	21.79	9.88	10.74	12.09	3.16
% Al-bound	7.02	8.21	7.50	6.91	2.79	1.96	9.72
% Ca-bound	7.47	5.44	8.58	10.64	2.04	3.64	1.40
CV Total P (%)	10.2	19.0	6.4	17.5	7.3	22.4	15.2
CV Loosely-bound (%)	17.5	32.0	17.7	37.3	24.4	11.4	39.7

Note. Total P values are the mean (± standard deviation) for all intervals of the deep site core. The precent contribution of each P species to the total sediment P pool is an average value across the deep site core profile. The coefficient of variation for total and loosely-bound P was calculated for all ten sediment cores collected across each study lake.

FIGURES

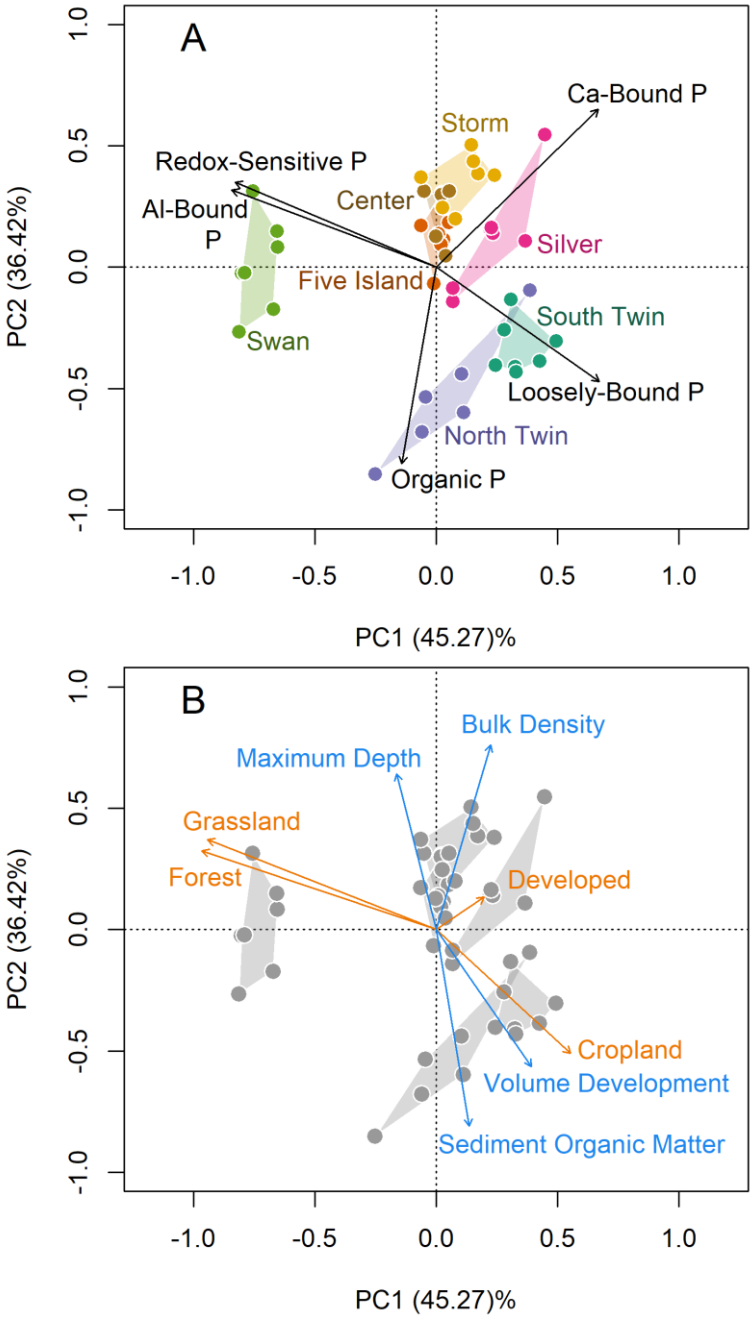

Figure 1. (A) PCA biplot based on a compositional data analysis of profundal sediment P pools. The compositional analysis was defined by the concentrations of loosely-bound (porewater and surface sorbed), redox-sensitive (Fe- and Mn-bound), aluminum-bound, calcium-bound, and organic P (including labile and refractory components). Arrows represent center log-ratio transformed concentrations of the P fractions. **(B)** Interpretation of PCA biplot with key environmental variables. Watershed land cover classes are shown in orange while lake and sediment characteristics are plotted in blue.

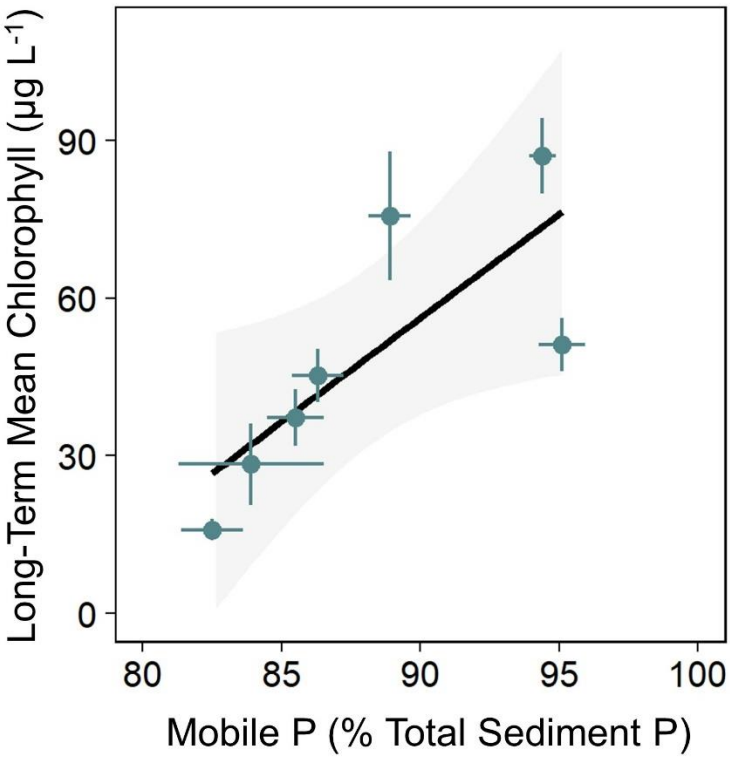

Figure 2. The relationship between the fraction of the total sediment P pool that is comprised of mobile species and the long-term average chlorophyll-*a* concentrations in each study lake ($F_{1,5}$ = 7.584, p = 0.0401, adjusted R^2 = 0.52, β_1 = 3.953 [0.263, 7.642]).

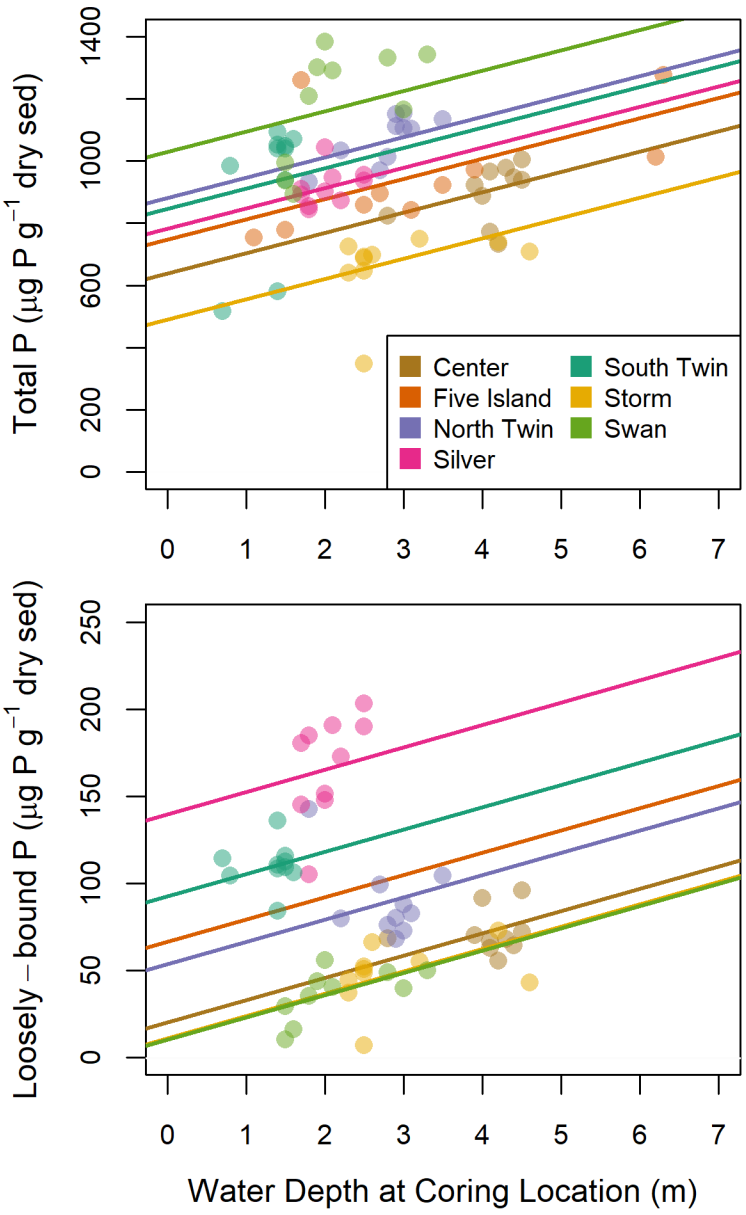

Figure 3. Mixed model regression effects of water depth at the coring location on total sediment P (β_1=65.28 [27.5661, 102.4886]; top panel) and loosely-bound sediment P (β_1=12.787 [7.180, 18.334]; bottom panel) by lake.

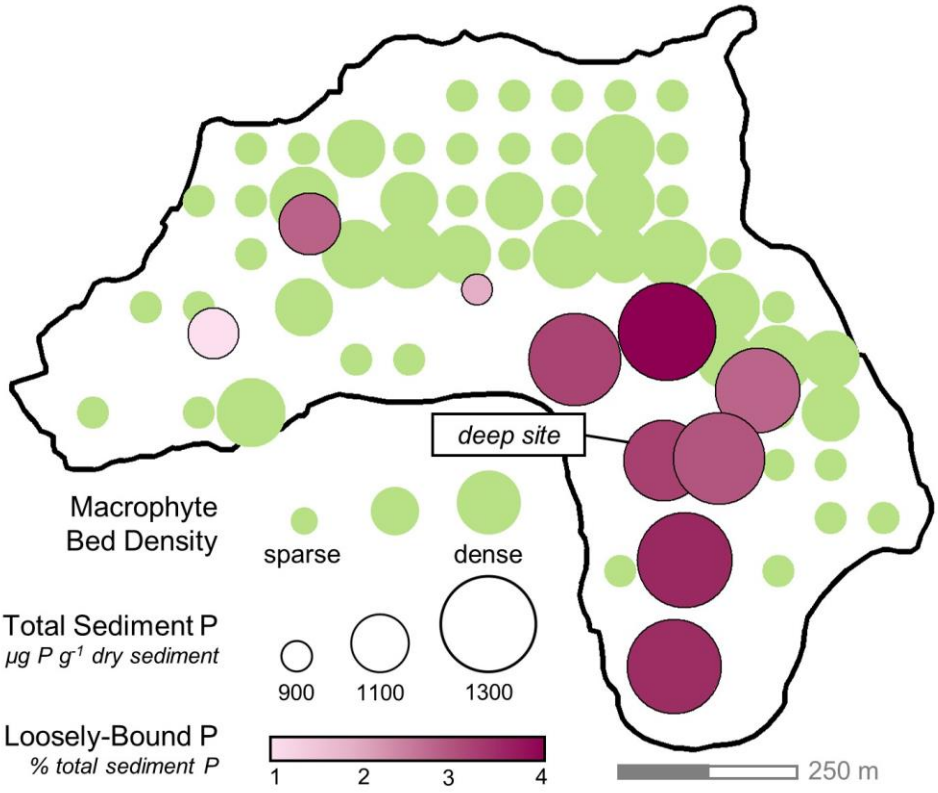

Figure 4. Within-lake variation in sediment loosely-bound and total P in Swan Lake. The ten sediment cores collected across Swan Lake are plotted with pink circles. The point size corresponds to total sediment P concentration which the shade of pink represents the relative proportion of loosely-bound P at that site. The qualitative estimate (1-3) of macrophyte bed density is shown in green circles. Blank areas of the map indicated bare sediment while areas with larger green dots represent very dense beds of *Stuckenia pectinata* and *Nelumbo lutea.*

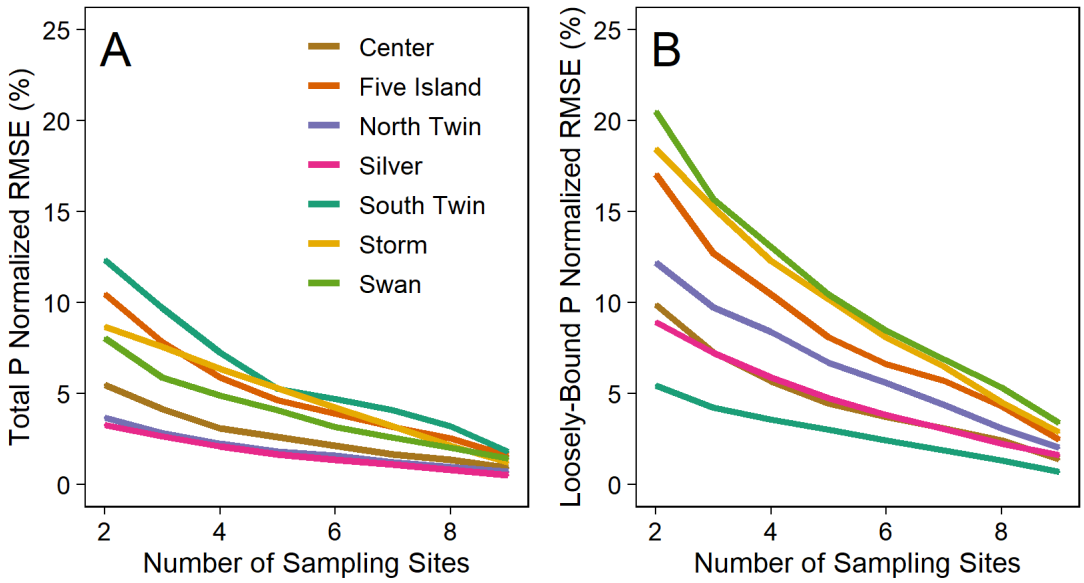

Figure 5. Rarefaction analysis of mean total **(A)** and loosely-bound **(B)** P concentrations based on the number of sampling sites. RMSE values are normalized as a percent of the mean P concentration when all 10 sampling sites are included.

SUPPLEMENTARY INFORMATION FOR CHAPTER 2

Contents of this file

Text S1

Tables S1 to S5

Figure S1

Introduction

The supporting information contains detailed explanations of the equations used to determine the sediment physical characteristics and the concentrations of sediment phosphorus (P) fractions (Text S1). Table S1 details the frequency of thermal stratification in the study lakes as well as dissolved oxygen conditions at the sediment-water interface. Tables S2 and S3 contain more detailed information on watershed soil series and landcover respectively. Table S4 compares the total and loosely-bound P concentrations at the deep site of each study lake to the whole-lake mean values. Table S5 summarizes how sediment total P concentrations in our study lakes compare to other values in the literature. We have also included a visualization of the relationship between the coefficient of variation in loosely-bound P across the lakebed and lake basin volume development for the study lakes (Figure S1).

TEXT S1.

Eq. 1 Moisture Content (MC)

$$\text{Moisture Content (\%)} = \left[\frac{(W_w - W_t) - (W_d - W_t)}{W_w - W_t}\right] \times 100 \quad (1)$$

Where W_t is the weight of the aluminum weigh boat, W_w is the weight of the weigh boat and fresh sediment sample, and W_d is the weight of the weigh boat and dry sediment.

Eq. 2 – Organic Matter Content as Loss-on-Ignition (LOI)

$$\text{LOI Organic Matter Content (\%)} = \left[\frac{(W_d - W_t) - (W_a - W_t)}{W_d - W_t}\right] \times 100 \quad (2)$$

Where W_a is the weight of the weigh boat and the ashed sediment after combustion.

Eq. 3 – Bulk Density

$$\text{Bulk Density } \left(g/cm^3\right) = \frac{260}{100 + 1.6 \times \left[MC + \left(\frac{LOI}{100 \times (100\text{-}MC)}\right)\right]} \quad (3)$$

Eq. 4 – Dry Mass Equivalent of Fresh Sediment Used

$$\text{Dry Mass Equivalent (g)} = \text{Mass Fresh Sediment (g)} \times (100 - MC) \quad (4)$$

Eq. 5 – Loosely sorbed and pore water P

$$\text{Loosely-Bound P (mg P/g dry sediment)} = \frac{\text{Concentration SRP (mg/L)} \times \text{Extractant Volume (L)}}{\text{Dry Mass Equivalent of Sediment Used (g)}} \quad (5)$$

The concentration of SRP used should reflect the average of lab duplicate measures. The extractant volume should equal the total volume of 1M NH_4Cl used across both extractions, (0.05 L). The dry mass equivalent of the fresh sediment used is estimated based on MC (Eq. 4) and will be the same for the calculations of each subsequent extraction (Eq. 6-9).

Eq. 6 – Redox-sensitive P (Fe- and Mn-bound)

$$\text{Redox-Sensitive P (mg P/g dry sediment)} = \frac{\text{Concentration SRP (mg/L)} \times \text{Extractant Volume (L)}}{\text{Dry Mass Equivalent of Sediment Used (g)}} \quad (6)$$

The concentration of SRP used should reflect the average of lab duplicate measures. The extractant volume should equal the volume of 0.11 M bicarbonate – 0.1 M sodium dithionate solution used (0.0125 L).

Eq. 7 – Aluminum-Bound P

$$\text{Al-Bound P (mg P/g dry sed.)} = \frac{\left[\text{Concentration SRP}\left(\frac{\text{mg}}{\text{L}}\right)\times\frac{\text{(Post pH (g)-Tare (g))}}{\text{(Pre pH (g)-Tare (g))}}\right]}{1.00152}\times\text{Extractant Volume (L)}}{\text{Dry Mass Equivalent of Sediment Used (g)}} \quad (7)$$

The concentration of SRP used should reflect the average of lab duplicate measures and must be corrected for the pH adjustment. Tare is the mass of the I-chem jar in which the adjustment is performed; Pre pH is the mass of the jar and the extraction supernatant; and Post pH is the mass of the jar, supernatant, and titrant used for the pH adjustment. The constant 1.00152 is used for 0.1 M HCl as the titrant. The corrected SRP concentration can then be corrected for the extractant volume (0.025 L) and sediment mass.

Eq. 8 – Labile Organic P

$$\text{Labile Organic P (mg P/g dry sed.)} = \left[\frac{\text{Concentration SRP, digested (mg/L)} \times \text{Extractant Volume (L)}}{\text{Dry Mass Equivalent of Sediment Used (g)}}\right] - \text{Al-Bound P} \quad (8)$$

The concentration of SRP from the *digested* supernatant should first be corrected for the volume of NaOH used (0.05 L) and the sediment mass. This value represents the concentration of aluminum-bound and labile organic P in the sediment pellet. The concentration of labile organic P is calculated as the difference between this value and the Al-bound P concentration (Eq. 7).

Eq. 9 – Calcium-Bound P

$$\text{Ca-Bound P (mg P/g dry sed.)} = \frac{\left[\text{Concentration SRP}\left(\frac{\text{mg}}{\text{L}}\right)\times\frac{\text{(Post pH (g)-Tare (g))}}{\text{(Pre pH (g)-Tare (g))}}\right]}{1.00452}\times\text{Extractant Volume (L)}}{\text{Dry Mass Equivalent of Sediment Used (g)}} \quad (9)$$

The concentration of SRP used should reflect the average of lab duplicate measures and must be corrected for the pH adjustment. The constant 1.00452 is used for 0.1 M NaOH as the titrant. The corrected SRP concentration can then be corrected for the extractant volume (0.025 L) and sediment mass.

Eq. 10 – Total P

$$\text{Total P (mg P/g dry sediment)} = \frac{\left[\text{Concentration TP}\left(\frac{\text{mg}}{\text{L}}\right)\times\frac{\text{(Post pH (g)-Tare (g))}}{\text{(Pre pH (g)-Tare (g))}}\right]}{1.00452}\times\text{Dilution Volume (L)}}{\text{Dry Mass of Sediment Used (g)}} \quad (10)$$

The concentration of TP used should reflect the average of lab duplicate measures and must be corrected for the pH adjustment. The constant 1.00452 is used for the 0.1 M NaOH as the titrant. This corrected SRP concentration can then be corrected for the volume to which the sample was diluted after boiling (0.05 L) and the mass of dry sediment used.

TABLES

Table S1. Long-term stratification patterns and dissolved oxygen conditions

	Frequency of Summer Thermal Stratification (%)		Dissolved Oxygen at Sediment-Water Interface (mg L^{-1})
Lake Name	Long-Term Record*	2018 Field Season†	2018 Summer Mean‡
Center	26.2	28.9	4.81
Five Island	26.8	18.9	1.28
North Twin	9.3	21.4	7.26
Silver	8.1	26.7	8.20
South Twin	NA	0.8	9.18
Storm	2.5	NA	4.72
Swan	17.4	30.8	2.87

* Obtained from the Iowa Department of Natural Resources AQuIA data repository. Records are from 2006-2018 for Storm and Silver Lakes and from 2005-2018 for the remaining study lakes. The frequency of stratification was determined as the percent of observations where a thermocline was present at the deep site of the lake out of the total observations in the long-term monitoring record. Lakes were sampled three times between May and October each year.

† Determined from high-frequency water temperature loggers deployed at regular depth intervals at the deep site of each study lake from around May to August of 2018. The frequency of stratification was determined as the number of days when a thermocline was present as a percent of the total days the sensors were deployed. Sensors on Storm Lake were lost during a Storm and never recovered.

‡ Data were obtained from the Iowa Department of Natural Resources Ambient Lake Monitoring Program's profile data. Dissolved oxygen concentrations from early and mid-summer sampling events were averaged to estimate conditions at the time of our sampling. South Twin is not monitored in this program, so dissolved oxygen values were obtained from a surface dissolved oxygen logger and assumed to represent conditions at the sediment-water interface since the lake was well-mixed at this time.

Table S2. Dominant watershed soil texture and series

Lake name	Dominant watershed soil texture	Dominant watershed soil series
Center	Loam, clay loam, silty clay loam	Webster, Nicollet, Clarion, Canisteo, Okabena, Waldorf
Five Island	Loam, clay loam, silty clay loam	Webster, Nicollet, Clarion, Canisteo, Okoboji
North Twin	Loam, clay loam,	Webster, Nicollet, Clarion, Canisteo
Silver	Loam, clay loam, silty clay loam	Webster, Nicollet, Clarion, Canisteo, Okabena, Waldorf
South Twin	Loam, clay loam,	Webster, Nicollet, Clarion, Canisteo
Storm	Silty clay loam	Sac, Primghar, Marcus, Galva
Swan	Silty clay loam	Marshall, Colo-Judson, Exira

Table S3. Watershed land cover

Lake name	Cropland (%)	Grassland (%)	Water (%)	Forest (%)	Urban (%)
Center	14.3	26.6	34.3	7.5	17.2
Five Island	75.5	9.6	12.0	1.8	1.7
North Twin	82.5	11.9	19.8	0.5	2.2
Silver	78.1	12.8	7.5	0.8	0.8
South Twin	78.4	2.2	30.7	0.1	10.4
Storm	60.2	12.6	18.5	1.4	7.2
Swan	45.1	28.8	13.8	8.5	3.9

Table S4. RMSE of deep site P concentrations

	Total P (µg P g dw^{-1})				Loosely-Bound P (µg P g dw-1)			
Lake	Whole-Lake Mean	Deep Site	RMSE	Normalized RMSE (%)	Whole-Lake Mean	Deep Site	RMSE	Normalized RMSE (%)
Center	897.0	938.3	41.3	4.6	71.6	100.6	29.0	40.5
Five Island	956.7	1013.5	56.8	5.9	108.3	156.9	48.6	44.9
Silver	915.6	936.5	20.9	2.3	167.2	203.3	36.1	21.6
Storm	663.1	738.2	75.1	11.3	47.7	72.8	25.1	52.5
North Twin	1070.4	1134.1	63.7	5.9	89.4	101.7	12.3	13.8
South Twin	936.0	939.1	3.1	0.3	110.2	112.6	2.4	2.2
Swan	1184.9	1164.7	20.2	1.7	37.0	39.9	2.9	7.7
	AVERAGE		40.1	4.6	AVERAGE		22.3	26.2

Table S5. Literature comparison of sediment total P concentrations

			Whole-lake Total P across study lakes (µg P g-1 dw)	
Reference	Waterbodies	Location	Range	Grand Mean
This Study	7 shallow lakes	Iowa, USA	897.0 - 1,184.9	946.2
Søndergaard et al., 2013	6 shallow lakes	Denmark	740 - 4,100	2,397
Doig et al., 2017	9 eutrophic lakes reservoirs	Canadian Prairie Provinces	533 - 2,310	1,594
Tao & Lu, 2020	83 lakes and reservoirs	Yangtze, Huaihe River catchments, Eastern China	360 - 2,180	820
Kowalczewska-Madura et al., 2019b	2 meso-eutrophic lakes	Poland	840 - 1,300	1,072

FIGURES

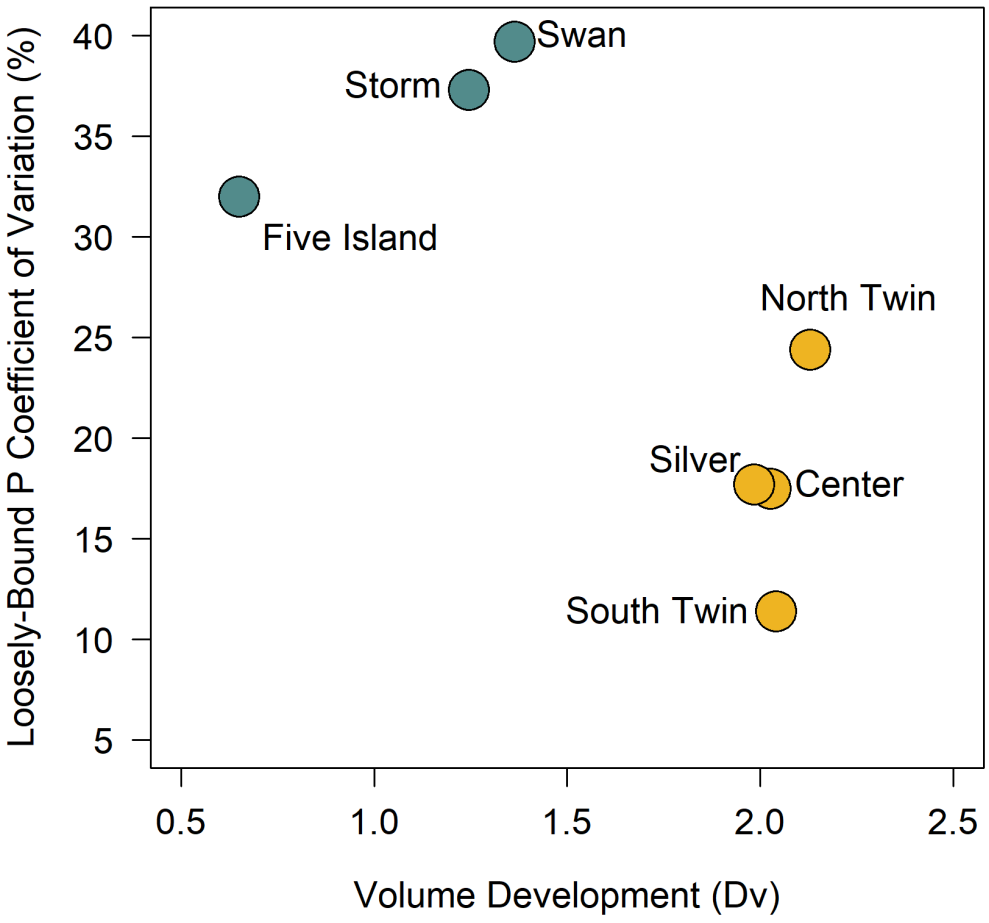

Figure S1. Variation in sediment loosely-bound P across lake basin volume development. The coefficient of variation for loosely-bound P was highest in lakes with low volume development scores (blue points), indicating more variable basin shape. Lakes with higher volume development ratios (yellow points) had less intra-lake variation in loosely-bound P.

CHAPTER 3

SEDIMENT PHOSPHORUS COMPOSITION CONTROLS HOT SPOTS AND HOT MOMENTS OF INTERNAL LOADING IN A TEMPERATE RESERVOIR

Albright, E.A., and G.M. Wilkinson. In review. Sediment phosphorus composition controls hot spots and hot moments of internal loading in a temperate reservoir. Ecosphere.

Author contributions: Albright designed the study; performed all field and laboratory work; cleaned, analyzed, and visualized the data; and wrote the manuscript. Wilkinson contributed to study design and data analysis and provided feedback on writing.

ABSTRACT

Phosphorus (P) flux across the sediment-water interface in lakes and reservoirs responds to external perturbations within the context of sediment characteristics. Lentic ecosystems experience spatiotemporal heterogeneity in the mechanisms that control sediment P fluxes, likely producing hot spots and hot moments of internal loading. However, spatiotemporal variation in P fluxes remains poorly quantified, particularly in the context of sediment chemistry as a controlling variable. We measured P flux rates and mobile sediment P forms along the longitudinal gradient of a temperate reservoir every two months from February to October of 2020. Both aerobic and anaerobic processes mobilized sediment P throughout the year. High flux rates at littoral sampling sites (8.4 and 9.7 mg P m^{-2} day^{-1}) occurred in late summer under oxic conditions and mobilized labile organic P. High fluxes at the profundal site coincided with hypolimnetic anoxia under ice cover and in mid-summer (11.2 and 17.2 mg P m^{-2} day^{-1}, respectively) and released redox-sensitive P. Several high fluxes substantially skewed the flux

rate distribution, providing evidence of hot spots and hot moments of internal loading. We further scaled the measured sediment P flux rates to representative areas of the lakebed to estimate internal P loads at an ecosystem scale. We found that aerobic P release from littoral sites had an outsized impact on total loads. Our findings demonstrate the importance considering spatial and seasonal variation in sediment P pools and fluxes in order to more accurately estimate internal loads and identify the dominant biogeochemical mechanisms involved.

INTRODUCTION

An ecosystem's response to external perturbations results from the interaction of fast- and slow-acting state variables, which fall along a gradient of turnover times from short to long, respectively (Carpenter and Turner 2000). Slow variables determine ecosystem context and control how fast variables respond to external drivers (Walker et al. 2012). Understanding how slow and fast variables interact is necessary for the study and management of complex systems (Crépin 2007; Ward et al. 2019). For example, eutrophication in lakes and reservoirs is often influenced by interacting slow and fast variables at the sediment-water interface. Sediments hold a pool of phosphorus (P), which is the legacy of past external loading and subsequent sedimentation (Søndergaard et al. 2003; Walsh et al. 2019). This P may be retained in the sediments or mobilized and released into the overlying water (i.e., internal P loading; Orihel et al. 2017). Within the sediments there are many different P-containing minerals, organic compounds, and surface complexes, which are vulnerable to different mechanisms of internal loading (North et al. 2015; Orihel et al. 2017). As such, the chemical composition of the sediment P pool is a pivotal slow variable that shapes how the rate of P flux from the sediments (i.e., the fast variable) responds to fluctuations in external drivers (Carpenter 2003).

The response of sediment P flux rates to changing dissolved oxygen availability, the result of external drivers, is shaped by the forms of P present in the sediment. For example, if redox-sensitive P forms (i.e., those associated with iron or manganese oxides) dominate the sediment P pool, then hypolimnetic oxygen depletion will trigger P release due to reductive dissolution of the host minerals (Mortimer 1941; Jensen and Andersen 1992). When water column mixing delivers dissolved oxygen to the sediment surface, oxidized iron and manganese minerals can stabilize P, which may result in sediment P retention. The idea that oxic conditions prevent P release and that internal loading primarily occurs under anoxia is a persistent paradigm in limnology. However, there is ample evidence that internal P loading occurs under a range of dissolved oxygen conditions based on sediment characteristics (Hupfer and Lewandowski 2008). If sediments hold a large pool of labile organic P, then oxic conditions are expected to mobilize and release P via microbial decomposition and mineralization (Joshi et al. 2015; Horppila et al. 2017). A mixing event that delivers dissolved oxygen to the sediments may also result in sediment resuspension, which releases pore water P and increases diffusive P flux through the sediment profile into the overlying water (Tammeorg et al. 2016). In this example, an influx of dissolved oxygen to the lakebed would stimulate rather than suppress internal loading, especially if the sediments were disturbed. The relationship between dissolved oxygen and P flux is expected to vary with the composition of the sediment P pool, which is heterogenous across the lakebed and over time (Nowlin et al. 2005; Kowalczewska-Madura et al. 2019). However, it is unclear how the interaction between this slow variable and external drivers influences spatiotemporal variability in sediment P fluxes and what the consequences of this variation are at the ecosystem scale.

Lentic ecosystems are highly variable in space and time. Temperate reservoirs are particularly variable due to longitudinal gradients in basin morphometry as well as strong spatial and seasonal variation in thermal mixing, hypolimnetic dissolved oxygen, and organic matter sedimentation (Nowlin et al. 2005; Hayes et al. 2017; Cardoso-Silva et al. 2018). Increasing water depth from riverine to lacustrine regions of a reservoir yields spatial variation in water column mixing and thus chemical conditions at the sediment-water interface (Kimmel and Groeger 1984; Hudson and Vandergucht 2015). Specifically, shallow riverine and transitional sections remain mixed throughout the open water season, usually maintaining oxygenated conditions above the sediments. Conversely, the deeper lacustrine region will likely experience at least intermittent thermal stratification, which may result in hypolimnetic dissolved oxygen depletion (Hayes et al. 2017). In short, basin morphometry produces spatial variation in the dynamics of external drivers that influence internal P loading. Organic matter sedimentation also varies along the longitudinal gradient and may impact the composition of the sediment P pool. Riverine segments receive more allochthonous organic matter inputs while autochthonous material dominates sedimentation in the lacustrine region (Hayes et al. 2017; Cardoso-Silva et al. 2018). Autochthonous organic matter inputs also vary over space and time due to seasonal algal dynamics and spatial heterogeneity in bloom formation (Buelo et al. 2018; Ortiz and Wilkinson 2021). When combined, spatial and seasonal variation in both redox conditions and the composition of the sediment P pool likely produce hot spots and hot moments of sediment P release.

Hot spots and hot moments are high rates of biogeochemical activity that occur when two reactants are brought together in space and time within an ecosystem (McClain et al. 2003). This biogeochemical phenomenon can be understood within the conceptual framework of fast and

slow variables. Specifically, a hot spot-hot moment is the product of an external perturbation delivering a reactant that interacts with the slow variable resulting in a high rate in the fast variable at that moment and location. For example, sudden water column mixing due to a storm delivers dissolved oxygen to the sediment surface, which is rich in labile organic P, resulting in a spike of sediment P release due to aerobic decomposition and mineralization as well as increased diffusive P flux due to sediment disturbance (Tammeorg et al. 2016). This external perturbation interacts with the slow variable (i.e., the sediment P pool) and brings two reactants together (i.e., dissolved oxygen and labile organic P), resulting in the hot spot-hot moment. Hot spots and hot moments disproportionately influence elemental cycles at the ecosystem-scale. For example, temperate waterbodies likely experience hot spots and hot moments of sediment P release such that the majority of the total internal P load may be associated with a few key areas of the lakebed and times throughout the year. As such, efforts to control internal P loading would have the greatest impact by focusing on hot spots and hot moments of P release. However, doing so requires an understanding of the underlying mechanisms. Although hot spots and hot moments have been well-documented, most studies have focused on carbon and nitrogen cycles in streams and riparian soils, and there has been little consideration of both hot spots and hot moments of P cycling, especially in lentic ecosystems (Bernhardt et al. 2017). Additionally, analyses of the mechanisms that produce hot spots and hot moments in biogeochemical cycles remain scarce, undermining our understanding of these extreme events and how they impact ecosystem function. While the environmental conditions that may produce high rates of sediment P flux in lakes and reservoirs have been well-documented, no study to date has explicitly delineated hot spots and hot moments of sediment P release and, more importantly, identified the causal mechanisms of these extreme events.

In order to quantify hot spots and hot moments of sediment P flux and explore the underlying mechanisms, we measured mobile sediment P pools and fluxes over the course of a year and across the lakebed of a temperate reservoir (Figure 1). Specifically, we measured sediment P composition and flux rates at three sites along the longitudinal gradient of the reservoir approximately every other month over the course of 2020, capturing conditions under the ice as well as thermal mixing and stratification events during the open water season. We asked, (Q1) When and where do hot spots and hot moments of sediment P flux rates occur, and what are the underlying mechanisms? (Q2) How does the slow variable (i.e., the composition of the sediment P pool) change over space and time, and how do these changes relate to P flux rates? (Q3) How do hot spots and hot moments of internal loading scale to the ecosystem level? We hypothesize that there are hot spots and hot moments in the rates of P flux from the sediments that arise from interactions between P speciation and biogeochemical conditions at the sediment-water interface. Over the course of the year, we anticipate that P will be mobilized and released from a variety of sediment P sources. We anticipate that temperature and dissolved oxygen concentrations will be key mechanisms driving internal loading but that the specific effects of these variables will depend on the composition of the sediment P pool. Predicting the occurrence of hot spots and hot moments of internal loading and identifying the causal mechanisms is essential for effectively managing whole-lake P cycling. Our findings demonstrate that the mechanisms driving hot spots and hot moments of internal P loading cannot be understood without capturing both seasonal and spatial variation in fluxes and the composition of the sediment P pool.

METHODS

Study Site

Green Valley Lake (GVL) is a hypereutrophic reservoir located in southwest Iowa, USA (41°05'58.9"N 94°23'04.7"W, Figure 1), with a discontinuous cold polymictic stratification and mixing pattern. The reservoir lies in the rolling loess prairie region of the western corn belt plains. Row crop agriculture dominates the GVL watershed with 68.4% of the land cover in a corn-soybean rotation. GVL is relatively small (surface area 156.2 ha) and shallow (maximum depth 6.8 m and mean depth 3.2 m), with two main branches meeting at the southern end of the basin above the dam outflow. As an impoundment of several small tributaries, GVL has a highly irregular shape (shoreline development factor 3.44), characterized by numerous shallow bays and an extensive littoral zone.

We measured spatial variation in sediment P pools and fluxes at three sampling sites distributed along the longitudinal gradient of the west branch of the reservoir. We selected the western branch as this inflow is the main tributary to the reservoir and drains the majority of the watershed. The shallow sampling site (2.5 m) was located near the west inlet, and the water column remained mixed throughout the open water season. The intermediate depth site (4.0 m) was in the middle of the western branch of GVL. Thermal stratification developed under ice and intermittently throughout the open water season. The deep sampling site (maximum water depth 6.8 m) was located at the deepest hole of the reservoir near the dam. Water column stratification and mixing followed the same pattern as the intermediate site (Table 1).

In order to evaluate seasonal patterns in P dynamics, we sampled these sites throughout 2020 on day of year (DOY) 39, 117, 181, 223, and 298 (winter, spring, mid-summer, late summer, and autumn, respectively). The timing of the sampling events was designed to capture ice cover, thermal stratification in spring, and mixing events in the summer and autumn (Table

1). The shallow site was not sampled in February due to unsafe ice conditions created by a congregation of Canada geese (*Branta canadensis*). The sampling event in late summer occurred immediately following a derecho, an intense windstorm affecting a large geographic area (Corfidi et al. 2016; Goff et al. 2021). Although GVL lay at the edge of the derecho's path, windspeeds at the reservoir are estimated to have exceeded 65 kph, fully mixing the water column at all sites (Table 1).

Vertical Profiles and Water Chemistry

To monitor thermal mixing patterns in GVL, we deployed vertical strings of temperature sensors at the shallow and deep sites (HOBO 8K Pendant Temperature Data Logger). Sensors were placed every 0.5 m up to 3 m deep and then every 1 m to the lakebed. The sensors logged water temperature every 30 minutes from spring to late summer. At each sampling site and event, we also measured water column profiles of temperature and dissolved oxygen using a YSI ProDSS Multiparameter Digital Water Quality Meter. Additionally, we collected water samples 0.25 m below the water surface and 0.5 m above the sediment-water interface for analysis of total P (TP), soluble reactive P (SRP), total nitrogen, nitrate, and suspended solids (see Appendix S1 for full methods and data). Subsamples were filtered in the lab (0.45µm GF/C filters) for SRP analysis, and all samples were preserved with concentrated sulfuric acid to pH 2. TP samples underwent persulfate digestion prior to analysis (Standard Methods 4500-P B.5). We measured SRP and TP concentrations with the molybdenum blue method modified from Murphy and Riley (1962; Standard Methods 4500-P E) using a SEAL Analytical AQ2 Discrete Analyzer.

Sediment P Fluxes

To quantify sediment P fluxes, we collected intact sediment cores and incubated them under ambient conditions in the lab while measuring P exchange with the overlying water. For each sampling site and event, three replicate sediment cores were collected using a gravity corer (inner diameter 5 cm, length 50 cm), such that there were approximately 25 cm of sediment and 25 cm of overlying water. The sediment cores and the overlying water were sealed in clear, acrylic core sleeves and transported at 4°C. In the laboratory, we exposed cores to temperature and dissolved oxygen treatments corresponding to ambient conditions at each site (Appendix Table S1, Figure S1). Temperature treatments were achieved by securing the cores in either a water bath or an incubation chamber. Dissolved oxygen levels were manipulated by bubbling either air mixtures or N_2 through the overlying water. A slow, consistent bubble rate was used to gently mix the water column without disturbing the sediment surface. After the cores were placed in the incubation system, we measured the height of the water column within each core tube to calculate the water volume.

Samples of the overlying water were collected 12, 36, 60, and 84 hours after the initial incubation set-up. For each daily sampling, 50 mL of water was removed for analysis of TP. An equivalent volume of hypolimnetic water, collected from 0.5 m above the sediment surface at the corresponding site, was used to replace the volume removed. The replacement hypolimnetic water was also analyzed for TP daily to account for changes in water column P due to sampling and water replacement. Samples were preserved with concentrated sulfuric acid to pH 2 and stored at 4°C before undergoing persulfate digestion and analysis for TP (Standard Methods 4500-P B.5, E). We monitored water temperature, dissolved oxygen, and pH (YSI ProDSS Multiparameter Digital Water Quality Meter) daily to ensure that the overlying water remained representative of ambient conditions in the reservoir at the time of sampling.

The change in TP in the overlying water was used to calculate daily, areal P flux rates for each core. We determined flux rates based on TP in order to capture all forms of P that may be exchanged between sediments and the overlying water including phosphate, dissolved organic P forms, and particulate P. We first calculated the mass of P in the overlying water immediately following the collection of the daily water sample as well as the mass of P in the replacement water. We then determined how the addition of the replacement water changed the TP concentration of the overlying water. The daily change in TP concentration was calculated as the difference between this new TP concentration after the addition of replacement water and the TP concentration measured in the water column the next day (see Appendix S1 for equations). The P flux rate was then calculated as:

$$\text{P flux rate (mg P m}^{-2}\text{ day}^{-1}) = (C_t - C_0) * V / A / d \quad \text{(Eq. 1)}$$

Where C_t is the water column TP concentration (mg L^{-1}) on a given day, C_0 is the TP concentration (mg L^{-1}) from the previous day after the addition of replacement water, V is the total volume (L) of water overlying the sediment core, A is the area (m^2) of the sediment surface, and d is the number of days between measurements (Ogdahl et al. 2014). Over a 4-day incubation, we calculated three daily P flux rates for each sediment core. We took the mean of these temporal replicates to yield one P flux rate per core, per incubation. Mean flux rate and standard error of the mean for the three replicate sediment cores from each sampling site and event were then used to estimate P flux rate through time at the various sites.

Sediment P Content and Composition

At each sampling site and event, we collected an additional sediment core for analysis of sediment P composition, total P content, and physical characteristics (see Appendix S1 for

sediment physical characteristics methods). We extruded the first 10 cm of the sediment profile into an acrylic core sleeve, which was sealed immediately to maintain ambient redox conditions. The top 10 cm of sediment is considered actively exchanging with the overlying water as diffusive processes and turbulent disturbance can occur in sediments this deep (Forsberg 1989). This surface sediment layer also holds P forms that are likely to be transformed or released on relatively short timescales (Orihel et al. 2017). Samples were transported and stored at 4°C until analysis, which began within 18 to 36 hours of sample collection. Sediments were handled under N_2-atmosphere in a glove bag and thoroughly homogenized before removing three replicate subsamples from each core. The replicates were analyzed for three mobile P species (loosely-bound, redox-sensitive, and labile organic P) as well as a more stable P fraction (aluminum-bound P) via sequential extraction following Lukkari et al. (2007). Dried sediments were used to quantify total P.

To begin the sequential P extractions, subsamples of fresh sediment equivalent to 0.5 g of dry sediment were weighed into polyethylene centrifuge tubes. This same sediment pellet was used throughout the sequential extraction procedure. All extractions were performed on an orbital shaker table at 25°C. Extractant and rinse solution volumes (50 mL), shaker table speed (200 rpm), and centrifuge time and speed (30 minutes at 3000 rpm) were consistent across all extractions. In general, each extraction involved shaking the sediment pellet in the extraction solution, centrifuging, and pouring off the supernatant. All extractions included at least one rinse, in which the sediment pellet would shake for 15 minutes in a rinse solution to minimize tailing. The supernatant of the rinse extractions was combined with the primary extraction supernatant. Following each extraction, the total supernatant was preserved with concentrated sulfuric acid to pH 2 to keep metals soluble and achieve the required pH for color development during SRP and

TP analyses. All SRP and TP concentrations were corrected for the extractant volume and the mass of sediment used to determine the P concentration per gram of dry sediment (See Appendix S1 for all equations).

Loosely-sorbed and pore water P were extracted in 0.46 M N_2-purged sodium chloride (NaCl) for one hour. One rinse in 0.46 M N_2-purged NaCl was used, and the combined extract solution was preserved for TP analysis (Standard Methods 4500-P B.5, E). Redox-sensitive P species were extracted in a 0.11 M bicarbonate – 0.1 M sodium dithionite (BD) solution for one hour. This extraction included two rinses with BD solution and one NaCl rinse. The combined extract supernatant was bubbled with compressed air for at least 90 minutes to remove dithionite before being preserved for TP analysis. Labile organic P and P associated with aluminum oxides were determined with an 18-hour extraction in 0.1 M sodium hydroxide (NaOH). One NaOH rinse was used, followed by one NaCl rinse. The combined extract supernatant was analyzed in two portions. First, a portion was filtered (0.45µm GF/C filters) and analyzed for SRP (Standard Methods 4500-P E). This SRP concentration was used to calculate the sediment concentration of aluminum-bound P. The remaining supernatant was digested and analyzed for TP. The labile organic P fraction was determined as the difference between the total NaOH-extractable P and the aluminum-bound P. Total sediment P concentrations were measured following a hot acid digestion on dried, ground, and homogenized sediments. Three replicate subsamples (0.2 g) of the dried sediment were combusted it at 550°C for 2 hours and then boiled on a digestion block in 50 mL of 1 M HCl for 2 hours at 150°C. Following digestion, samples were diluted to 50 mL with deionized water, and adjusted to pH 2 using 0.1 M NaOH before TP analysis.

Statistical Analyses

As there is no universal, quantitative method for delineating hot spots and hot moments of biogeochemical fluxes in a distribution of flux measurements (Bernhardt et al. 2017), we used a variety of approaches to explore the distribution of P flux rates and determine whether the observed spatiotemporal variation indicated hot spots or hot moments. We first identified statistical outliers in the distribution, defined as flux measurements falling above or below 1.5 times the interquartile range. We further quantified the shape of the P flux distribution by calculating skewness (m_3; see Appendix S1 for equation), which identifies whether the distribution is symmetric ($m_3 < 0.5$) or if extreme flux rates, presumably due to hot spots or moments, skew the distribution ($m_3 > 0.5$). We further evaluated the influence of high flux rates on the distribution by iteratively removing the highest flux rates and recalculating skewness. Through this process, we determined how many of the highest flux rates would need to be removed to produce a nearly symmetric distribution (Gakuruh 2017).

In order to evaluate how the composition of the sediment P pool varied across sites and seasons, we performed a compositional data analysis. Compositional data analysis tests for a difference of proportions among multivariate observations, allowing us to test differences in the relative abundance of P fractions across different sites and events (Filzmoser et al. 2018). The compositional analysis was defined by the concentrations of loosely-bound (porewater and surface sorbed), redox-sensitive (Fe- and Mn-bound), aluminum-bound, and labile organic P. The sediment P concentrations were center logratio transformed prior to a principal components analysis (PCA) on the covariance matrix, as not to bias the analysis to the most abundant sediment P fractions.

To estimate the total sediment P load (kg day^{-1}) in the reservoir for each sampling event, we multiplied the mean P flux rate (mg m^{-2} day^{-1}) at each sampling site by the lakebed area (m^{-2})

within representative depth contours corresponding to each site. The shallow site measurements were assigned to the 1.2 – 3.6 m depth contour, the intermediate depth site measurements were assigned the 3.6 – 5.6 m depth contour, and the deep site measurements were assigned the 5.6 – 6.8 m depth contour. The threshold of 5.6 m was determined based on the historical mean depth of hypoxia in the water column. We excluded areas shallower than 1.2 m, including the sediment retention basins north of the reservoir, because these areas are mainly in secluded, wind-protected bays (Figure 1). Our sampling sites, which were centrally located along a branch of the reservoir, cannot reasonably be extrapolated to these shallow areas due to expected differences in wave disturbance and the depositional environment (Kleeberg et al. 2013). To calculate the lakebed area within the representative depth contours, we used the length of each depth contour from a bathymetric map produced by the Iowa Department of Natural Resources. The area between depth contours is a trapezoid-shaped area of lakebed wrapping around the reservoir basin. We calculated this area as:

$$A = \left(\frac{length\ 1 + length\ 2}{2}\right) \times h \qquad \text{(Eq. 2)}$$

Where length 1 and 2 are the lengths of the bounding depth contours, and *h* is the assumed average distance between the depth contours across the lakebed, estimated using the Pythagorean theorem:

$$h = \sqrt{(depth\ 2 - depth\ 1)^2 + \left(\sqrt{area\ 1} - \sqrt{area\ 2}\right)^2} \qquad \text{(Eq. 3)}$$

Where depth 1 and 2 refer to the water depth of the top and bottom depth contours, and area 1 and 2 represent the planar areas at the top and bottom depth contours. This method assumes that the lakebed follows a linear slope between the bounding depth contours, so it is likely an underestimate of the true area of the sediment surface. After determining the lakebed area corresponding to each sampling site, we multiplied this area by the flux rates and then summed

across all three load estimates for the total load for that sampling event. To propagate the uncertainty of this estimate, we added the standard error of the mean values in quadrature.

All data are available in Albright and Wilkinson (2021). All analyses were completed in R version 3.6.0 (R Core Team 2019) using the sf (Pebesma 2018), spData (Bivand et al. 2021), fGarch (Wuertz et al. 2020), robCompositions (Filzmoser et al. 2018), and vegan packages (Oksanen et al. 2019).

RESULTS

Physicochemical Conditions

Water column chemistry and thermal structure varied across sampling sites and over the course of the year (Table 1). At the shallow site, the water column remained mixed throughout the open water season and the sediment-water interface remained oxic (dissolved oxygen range 5.4-10.2 mg L^{-1}). At the intermediate and deep sites, thermal stratification first developed after ice-off. Intermittent stratification continued through late summer, after which the water column was mixed at both sites. The sediment-water interface at the intermediate depth site remained oxic throughout the study period (dissolved oxygen range 4.8-12.6 mg L^{-1}), but the deep site experienced periodic hypoxia (dissolved oxygen range 0.3-8.7 mg L^{-1}). On the day of the late summer sampling (DOY 223), a derecho passed over the lake, prompting a mixing event, as evidenced by an isothermal water column at all sampling sites. Following the derecho, the relative contribution of inorganic solids to the total suspended solids pool was much greater than any other point throughout the year in both surface and bottom waters, suggesting that the storm resulted in sediment disturbance and a well-mixed water column (Appendix Table S2).

Hypolimnetic P concentrations followed a similar seasonal pattern across sampling sites (Figure 2). At the deep and intermediate sites, hypolimnetic TP concentrations remained stable between under-ice sampling (DOY 39) and early spring (DOY 117). Hypolimnetic concentrations of both TP and SRP then increased from spring through late summer, peaking at 318.0 to 370.9 µg L^{-1} and 116.3 to 168.5 µg L^{-1}, respectively, before declining in autumn. Although these nutrient concentrations are quite high, the dynamics of P in the water column in 2020 are consistent with concentrations and seasonal patterns previously measured in GVL (Appendix Figure S2).

Sediment P Fluxes

Sediment P flux rates varied substantially among sampling sites and across seasons (Figure 2, Appendix Table S3). Flux rates were most variable over time at the deep site; however, these profundal sediments consistently released P to the overlying water from winter to mid-summer (DOY 39, 117, 181), and then had moderate retention or release rates in the late summer and autumn (DOY 223, 298). Sediments from the intermediate depth site retained P under ice cover (DOY 39), but released P in spring and late summer (DOY 117, 223). The shallow site followed a similar seasonal pattern with sediment P release in spring and late summer (DOY 117, 223) and negligible fluxes in mid-summer and autumn (DOY 181, 298). Overall, the highest rates of P release occurred at the shallow and intermediate sites in late summer (DOY 223) and in winter and mid-summer (DOY 39, 181) at the deep site.

Over the course of the year, sediment P release occurred under a broad range of dissolved oxygen concentrations at the sediment-water interface (Figure 3, Table 1). At the deep site, nearly anoxic conditions were associated with elevated rates of P release in winter and mid-

summer (DOY 39, 181; dissolved oxygen 1.1 and 0.3 mg L^{-1}, respectively). However, most of the observed instances of P release occurred when oxygen was available at the sediment-water interface. For example, sediments across all three sampling sites released P under oxic conditions in spring (DOY 117; dissolved oxygen range 5.8-9.4 mg L^{-1}), and high rates of oxic P release occurred at the intermediate and shallow sites in late summer (DOY 223; dissolved oxygen 4.8 and 7.2 mg L^{-1}, respectively). The effect of dissolved oxygen availability on sediment P flux rates differed between the deep site and more shallow sampling sites, and elevated P release rates were observed under both oxic and anoxic conditions.

The shape of the distribution of sediment P flux rates over the course of 2020 provides evidence of hot spots and hot moments of sediment P release in GVL. The distribution of P flux rates was centered near 0 mg P m^{-2} day^{-1} with the majority of the rates falling between -10 and 10 mg P m^{-2} day^{-1} (Appendix Figure S3). The first statistical moment, or mean, of the distribution was 3.4 mg P m^{-2} day^{-1}. The distribution was moderately positively-skewed (third standardized statistical moment $m_3 = 0.818$) due to five high release rates (range 16.2-23.6 mg P m^{-2} day^{-1}). The four highest of these points were classified as statistical outliers. The high release rates were from the deep sampling site in winter and mid-summer (DOY 39, 181) as well as fluxes in late summer (DOY 223) from the intermediate and shallow sites (Appendix Figure S4). Subsampling the dataset to exclude the five highest flux rates resulted in an approximately symmetric distribution ($m_3 = 0.462$; Appendix Table S4). The mean flux rate with the five highest rates excluded was 1.2 mg P m^{-2} day^{-1}, which is almost a third of the mean flux rate for the whole distribution. The presence of high flux rates that skew the distribution indicate hot spots and hot moments of sediment P release.

Sediment P Composition

To understand spatiotemporal variation in sediment P fluxes, we also measured changes in the sediment P pool, the slow variable, across seasons and sampling sites. The total sediment P pool varied among sites and seasons. Total P concentrations increased along the longitudinal gradient of the reservoir and were far greater at the deep site than the intermediate and shallow sites (Figure 4A). At the deep site, sediment total P increased slightly from winter to spring (DOY 39-117), decreased between spring and mid-summer (DOY 117-181), and then increased through autumn (DOY 298). At the intermediate side, total P also increased from winter to spring (DOY 39-117), but then decreased through late summer (DOY 223) before increasing in autumn (DOY 298). Sediment total P decreased gradually from spring to autumn at the shallow site, except for a slight increase between mid- and late summer (DOY 181-223; Appendix Figure S5).

Across all sampling sites, redox-sensitive P was the dominant pool of mobile P found in the reservoir sediments constituting an average of 40.9-51.3 % of the total P pool across sites (Figure 4A). The concentrations of all measured sediment P species were dynamic over time across the reservoir. Redox-sensitive P concentrations decreased over the course of the year at the shallow site. At the intermediate depth site, redox-sensitive P concentrations increased from winter to spring (DOY 39-117), declined through late summer (DOY 223), and increased until autumn (DOY 298). Redox-sensitive P at the deep site declined from winter through late summer (DOY 39-223), before increasing through autumn (DOY 223-298; Figure 4B).

Overall, concentrations of labile organic P increased from spring to autumn at all study sites, except for slight declines between mid-summer and late summer (DOY 181-223) at the intermediate and shallow sites (Figure 4C). Aluminum-bound P concentrations declined from

spring through autumn at the shallow site. At the intermediate depth site, concentrations increased from winter to spring (DOY 39-117), declined through late summer (DOY 223), and then increased again. At the deep site, aluminum-bound P followed an inverse pattern to that of redox-sensitive P, increasing from winter through late summer (DOY 39-223) and decreasing from late summer to autumn (DOY 223-298; Figure 4D). Temporal patterns in loosely-bound P varied across sites with declines over the study period at the shallow site, a gradual increase over time at the intermediate site, and steady concentrations at the deep site except for an increase from late summer to autumn (DOY 223-298; Figure 4E).

We used PCA as part of a compositional data analysis to explore spatiotemporal variation in overall sediment P composition. The compositional analysis was defined by the concentrations of loosely-bound, redox-sensitive, aluminum-bound, and labile organic P (Figure 5). The first principal component (PC1) explained 76.77% of the variation in the dataset and was highly correlated with loosely-bound and redox-sensitive P content. The second principal component (PC2) explained (14.35%) of the variation and was more closely associated with labile organic P content. The first two principal components explained 91.12% of the variance in the dataset. Overall, sediment samples from the shallow site had lower loosely-bound and redox-sensitive P content, whereas these species were more prevalent in the deep site sediments. The composition of the sediments from the intermediate site fell between that of the deep and shallow sites. Over the course of the study period, sediment composition from all study sites generally decreased in loosely-bound and redox-sensitive P content and increased in labile organic P content.

Sediment physical characteristics remained relatively stable over time but varied along the longitudinal gradient of the reservoir (Appendix Table S5). Loss on ignition organic matter content was greatest at the deep site (13.08 ± 0.98 %) and similar between the shallow and

intermediate sites (8.83 ± 0.75 and 8.54 ± 0.71 %, respectively). Water content was also highest at the deep site (86.18 ± 0.49 %) and comparable between the shallow and intermediate sites (71.83 ± 0.75 and 75.72 ± 3.0 %, respectively). Bulk density decreased from the shallow (1.19 ± 0.006 g cm^{-3}), to intermediate (1.16 ± 0.024 g cm^{-3}), to deep site (1.07 ± 0.003 g cm^{-3}).

Total P Load

We estimated daily sediment P loads for each sampling event by scaling the measured flux rates to representative areas of the lakebed to better understand the ecosystem-scale consequences of the P fluxes. The estimated total P load across the lakebed varied over time, with higher loads occurring under oxic conditions in spring and late summer (DOY 117, 223; Figure 6, Table 2). The greatest total P load occurred in late summer (DOY 223) due to high flux rates from the shallow and intermediate sites under oxic conditions (Figure 3). Oxic conditions were also associated with high total P loads in spring (DOY 117), when low P release rates across all sampling sites resulted in a substantial total P load due to the large area of the lakebed releasing P. In contrast, high rates of sediment P release under anoxic conditions at the deep site in winter and mid-summer (DOY 39, 181) did not translate into a high total P load due to the small area of lakebed involved. The greatest P loads were associated with aerobic sediment P release across a broad area of the lakebed. The seasonal trend in the estimated total P load mirrors the observed time series for hypolimnetic TP and SRP (Figure 2).

DISCUSSION

Hot Spots and Hot Moments of Sediment P Flux Rates

There was clear evidence of hot spots and hot moments of sediment P release in the study reservoir over the course of 2020. These elevated rates of sediment P flux occurred in late

summer at the shallow and intermediate depth sites as well as in winter and mid-summer at the deep site. While the highest rates of sediment P release occurred under anoxic conditions at the deep site, the other elevated flux rates at the shallow and intermediate sites happened when dissolved oxygen was available at the sediment-water interface. Other studies of hypereutrophic reservoirs have also observed aerobic sediment P release, which was associated with intense algal production and P mobilization during decomposition of sediment organic matter (Song and Burgin 2017; McCarty 2019). As a hypereutrophic waterbody, GVL also experiences severe algal blooms throughout the summer months, so it is likely that microbial decomposition of algal detritus contributed to the observed aerobic P release.

However, sediment P release when the overlying water is oxic is very complex and may involve both aerobic and anaerobic processes in the sediment profile. The depth of dissolved oxygen penetration into the sediments is typically very shallow such that much of the sediment profile remains anoxic (Hupfer and Lewandowski 2008). Therefore, P mobilization via aerobic decomposition and subsequent mineralization is limited to a thin, surficial layer of sediment. Anaerobic processes of P mobilization, such as the reductive dissolution of redox-sensitive P minerals, can still occur deeper within the sediment profile. The P mobilized via anaerobic processes will diffuse upward and may be released into the overlying water. The P sorption capacity of the sediments and the availability of alternative electron acceptors will influence whether mobilized P will diffuse into the overlying water or remain in the sediments (Caraco et al. 1993). The observed P release under oxic conditions at the shallow and intermediate depth sites likely represents P mobilized via aerobic decomposition of sediment organic matter as well as anaerobic processes within the sediment profile.

A severe storm disturbance on the late summer sampling date could have further exacerbated internal loading at the shallow and intermediate sites. The late summer sampling event occurred immediately following a derecho, which mixed the reservoir water column and disturbed sediments. Sediment resuspension has been shown to increase diffusive P flux from sediments into the overlying water, even after the sediments have settled following the disturbance (Tammeorg et al. 2016). Resuspension dilutes the pore water near the sediment surface, prompting diffusion of soluble P from deeper within the sediment profile and thus enhancing diffusive P fluxes into the water column. It is likely that the high rates of aerobic P release observed at the shallow and intermediate sites in late summer resulted from both P mineralization from organic matter and sediment disturbance brought on by the storm event. Bottom water TP and SRP concentrations also peaked at this time, indicating that these high flux rates influenced whole-reservoir P dynamics.

The highest rates of P flux from the deep site occurred under ice cover and in mid-summer under nearly anoxic conditions at the sediment-water interface. Profundal sediment P release during summer anoxia has been recorded in many other waterbodies and attributed to reductive dissolution of redox-sensitive P minerals (Mortimer 1941; Nowlin et al. 2005; Kowalczewka-Madura et al. 2019). However, winter measurements of sediment P fluxes are uncommon (Cavaliere and Baulch 2020). Of those measurements that have been made under ice, many studies report low flux rates in the winter (Orihel et al. 2017), while others have measured substantial winter loading (Reedyk et al. 2001; North et al. 2015). Our results provide further evidence that mobilization and release of sediment P is still possible under ice cover. Despite the high flux rates measured under ice, hypolimnetic TP concentrations did not increase from winter to the next sampling event in spring. The winter P fluxes may not have been sustained long

enough to cause a noticeable increase in water column P. Alternatively, the P released under ice-cover could have been exported downstream before the spring sampling event or diluted during ice melt (Cavaliere and Baulch 2020). The relative importance of winter internal loading is likely system-specific, but to assume that winter P fluxes are negligible risks biasing estimates of annual internal loading.

Sediment core incubations are a common tool for measuring sediment P flux rates (Orihel et al. 2017); however, the approach also has limitations (Oghdal et al. 2014). The main assumption when using core incubations to quantify sediment flux dynamics is that the conditions in the core are representative of the conditions in the lake. In an effort to meet this assumption, we incubated cores at ambient temperature and oxygen conditions at the time of collection, monitoring the temperature, dissolved oxygen, and pH daily in the cores. Overall, the experimental set-up mimicked ambient conditions (Appendix Table S1, Figure S1). We also used measurements from replicate cores and multiple days of incubation to estimate daily mean flux rates at a site for a given sampling event in order to capture small-scale spatiotemporal variability in the estimate while comparing across larger spatial and temporal scales. Additionally, we limited our incubations to 3.5 days in order to minimize artifacts that can occur in long-term incubations such as the depletion of organic matter or other key nutrients. Finally, we compared our core incubation-based flux measurements to TP dynamics in the reservoir as another way to verify that the qualitative patterns we observed in flux rates matched the changes in TP concentration measured in the reservoir. These strategies combined provide confidence that the broad-scale spatiotemporal patterns in sediment P flux we measured in GVL reflect the dynamics occurring across sites and seasons in the ecosystem.

Sediment P Composition Controls Flux Response to Dissolved Oxygen

Over the course of the year, we measured internal P loading under a wide range of dissolved oxygen concentrations at the sediment-water interface. Although the dominance of aerobic versus anaerobic internal loading shifted over sites and seasons, both processes were important pathways for P recycling between sediments and the overlying water. In order to understand why sediment P fluxes responded differently to dissolved oxygen conditions across space and time, we measured the chemical composition of the sediment P pool. We hypothesized that this slow variable shapes how fluxes respond to external drivers that alter dissolved oxygen availability. Spatiotemporal variation in sediment P composition corresponded to variation in sediment P flux rates. Specifically, instances of P release under oxic conditions mainly coincided with declines in labile organic P. Sediment P release during hypolimnetic anoxia and the deep site corresponded to decreasing redox-sensitive P concentrations in the sediments.

A change in the concentration of a sediment P fraction over time could indicate flux across the sediment-water interface or a transformation within the sediments. Evaluating temporal change in both total sediment P and various P fractions helps to distinguish between these processes. At the deep site of the reservoir, change in total and redox-sensitive P concentrations mirrored P flux rates over time. Redox-sensitive P declined steadily from winter to mid-summer, and then sharply decreased (35% decrease) from mid- to late summer. The mid-summer sampling event was a hot spot-hot moment of P release from the profundal sediments that coincided with hypolimnetic anoxia at the deep site. The decline in redox-sensitive P from spring to late summer suggests that the high flux rates in mid-summer were the result of reductive dissolution of redox-sensitive P minerals under anoxic conditions. However, total P only declined from spring to mid-summer, suggesting that some of the redox-sensitive P

mobilized between mid- to late summer remained in the sediments. The concentration of aluminum-bound P at the deep site followed the inverse pattern of redox-sensitive P. This temporal pattern suggests that a portion of the P mobilized from redox-sensitive minerals may have sorbed to available aluminum oxides rather than being released into the overlying water.

Concentrations of labile organic P in the sediments generally increased over the course of the year at all sampling sites, likely due to organic matter sedimentation. However, declines were measured at the shallow and intermediate sites from mid- to late summer, indicating that the elevated rates of aerobic P release measured at these sites in late summer involved P mineralization following decomposition of labile organic materials. Sediment total P generally decreased during this time as well, specifically from spring to late summer at the intermediate site and from spring to autumn at the shallow site. The decline in total P at these sites extends beyond the short period of decreasing labile organic P concentrations and is likely driven by declines in redox-sensitive P at these sites over the same time. Temporal coherence between sediment P release and declines in sediment total, labile organic, and redox-sensitive P underscores to the complexity of P mobilization under oxic conditions and the variety of P species that may be released.

Our hypothesis that there are hot spots and hot moments of internal loading resulting from interactions between sediment P composition and biogeochemical conditions at the sediment-water interface was supported in our study reservoir. We found that anoxic conditions can trigger the rapid mobilization and release of P from redox-sensitive P pools regardless of water temperature. We also measured P release originating from labile organic materials as well as redox-sensitive minerals under aerobic conditions and found that these fluxes were enhanced following a storm disturbance. Our findings underscore the importance of considering both

aerobic and anaerobic pathways of internal loading, especially in productive waterbodies. Our work supports the idea of a "perpetual cycle of internal P loading" in hypereutrophic waterbodies, as proposed by Song and Burgin (2017). The perpetual cycle describes a positive feedback loop that develops as lakes become increasingly eutrophic. Increased algal production enhances inputs of detritus to the sediments, producing a large pool of sediment labile organic P that is susceptible to aerobic release (Baines and Pace 1994; Frost et al. 2019). Sediment P release may then occur under both anoxic and oxic conditions. High internal P loads sustain frequent algal blooms, the detritus of which further fuels aerobic sediment P release via decomposition and mineralization. This positive feedback loop likely introduces hysteresis to maintain waterbodies in a hypereutrophic state. Clear evidence of sediment P release under both oxic and anoxic conditions in GVL indicates that the reservoir has entered this proposed cycle in which both aerobic and anaerobic internal loading will continue to fuel intense algal blooms.

Scaling Fluxes to the Whole Ecosystem

A hot spot-hot moment is defined as having a disproportionate influence on elemental cycles at the ecosystem-scale (McClain et al. 2003). As such, we scaled measured P flux rates to representative areas of the lakebed to estimate P loads and determine how the fluxes we classified as hot spots-hot moments actually influenced reservoir-wide internal loading. Hot spots and hot moments of aerobic P release from the shallow and intermediate depth sites in late summer produced the greatest total sediment P load to the reservoir over the study period. This substantial P load resulted from both the high flux rates and the broad spatial extent of sediments releasing P at this time. In contrast, high rates of P release from the deep site in winter and mid-summer did not result in large total P loads due to the small area of lakebed represented by the

deep site as well as sediment P retention at other sampling sites. The scaling results further illustrate how even low rates of P release can result in elevated total P loads if sustained over the entire lakebed. Specifically, we found that low rates of P release across all sampling sites in spring resulted in a high total P load.

Focusing on rates alone may not be sufficient to understand how extreme values of biogeochemical fluxes actually effect ecosystem structure and function. It is essential to scale measurements to the whole system. At the same time, scaling measurements from a single sampling station to an area of the lakebed is fraught with uncertainty. However, we took a conservative approach in assigning representative areas of the lakebed. We also took care in accurately describing the reservoir basin geometry and calculating sediment surface area. As such, we have produced conservative estimates of sediment P loads that can be used to evaluate the ecosystem effects of spatiotemporal variation in P fluxes. Other studies have scaled discrete measurements of sediment P fluxes to larger areas of the lakebed, generally based on waterbody surface area (Scicluna et al. 2015; Noffke and others 2016). Our approach to characterizing basin geometry allows for more accurate estimates of sediment surface area and thus scaling at finer spatial resolutions based on water depth.

Conclusions

Hot spots and hot moments of sediment P release in the study reservoir arose from interactions between the composition of the sediment P pool and external drivers that determined dissolved oxygen conditions at the sediment-water interface. Our findings demonstrate that the magnitude and mechanisms of internal P loading cannot be understood without capturing both seasonal and spatial variation in fluxes as well as the composition of the sediment P pool as a

slow variable. Our understanding of internal P loading in the reservoir would have been very different had we only sampled at one site or in one season. Additionally, scaling flux rates across the lakebed to estimate internal load revealed that even low rates of P release can result in elevated total P loads if sustained over the entire lakebed. Conversely, very high P flux rates do not necessary produce high total P loads if these fluxes occur over a small area or are balanced by P retention in other regions of the lakebed. These findings illustrate how focusing solely on flux rates without scaling to the whole ecosystem could lead to the misidentification of the main sources and mechanisms of internal loading and ultimately hamper eutrophication management.

Acknowledgements

This research was supported by the Iowa Water Center's Graduate Student Supplemental Research Competition. Albright was supported by the National Science Foundation Graduate Research Fellowship Program under Grant No. DGE-1747503 and 1744592. Any opinions, findings, and conclusions or recommendations expressed in this material are those of the authors and do not necessarily reflect the views of the National Science Foundation. Support was also provided by the Graduate School and the Office of the Vice Chancellor for Research and Graduate Education at the University of Wisconsin-Madison with funding from the Wisconsin Alumni Research Foundation. Wilkinson was supported by the National Science Foundation Division of Environmental Biology grant #1942256 and #2200391.

Open research statement

The data supporting the conclusions are publicly available in Albright and Wilkinson (2021), under a Creative Commons Attribution license (CC-BY). The analysis code is available in the Github repository https://github.com/AlbrightE/GVL_Internal_P_Cycling, which will be archived on Zenodo after manuscript acceptance.

REFERENCES

1. Albright, E.A., and G.M. Wilkinson. 2021. Spatiotemporal variation in internal phosphorus loading, sediment characteristics, water column chemistry, and thermal mixing in a hypereutrophic reservoir in southwest Iowa, USA (2019-2020) ver 1. Environmental Data Initiative. https://doi.org/10.6073/pasta/d3a70c1f0d534cca8bdebd7f7483ef38 (Accessed 2021-10-14).
2. Baines, S.B., and M.L. Pace. 1994. Relationships between suspended particulate matter and sinking flux along a trophic gradient and implications for the fate of planktonic primary production. Can. J. Fish. Aquat. Sci. 51 (1): 25-36, doi: 10.1139/f94-005
3. Bernhardt, E.S., J.R. Blaszczak, C.D. Ficken, M.L. Fork, K.E. Kaiser, and E.C. Seybold. 2017. Control points in ecosystems: Moving beyond the hot spot hot moment concept. Ecosystems. 20: 665–82, doi: 10.1007/s10021-016-0103-y
4. Bivand, R., J. Nowosad, and R. Lovelace. 2021. spData: Datasets for Spatial Analysis. R package version 0.3.10.
5. Buelo, C.D., S.R. Carpenter, and M.L. Pace. 2018. A modeling analysis of spatial statistical indicators of thresholds for algal blooms. Limnol. Oceanogr. Lett. 3(5): 384–392, doi: 10.1002/lol2.10091
6. Caraco, N.F., J.J. Cole, and G.E. Likens. 1993. Sulfate control of phosphorus availability in lakes: A test and re-evaluation of Hasler and Einsele's Model. Hydrobiologia. 253(1-3): 275-280, doi: 10.1007/BF00050748
7. Cardoso-Silva, S., P.A.d. Ferreira, R.C.L. Figueira, D.C. Silva, V. Moschini-Carlos, and M.L.M. Pompêo. 2018. Factors that control the spatial and temporal distributions of phosphorus, nitrogen, and carbon in the sediments of a tropical reservoir. Environ. Sci. Pollut. Res. 25(31): 31776–31789, doi: 10.1007/s11356-018-2923-0
8. Carpenter, S.R. 2003. Regime Shifts in Lake Ecosystems: Pattern and Variation. Oldendorf/Luhe, Germany: Ecology Institute.
9. Carpenter, S.R., and M.G. Turner. 2000. Hares and tortoises: Interactions of fast and slow variables in ecosystems. Ecosystems. 3: 495-497, doi: 10.1007/s100210000043
10. Cavaliere, E., and H.M. Baulch. 2020. Winter in two phases: Long-term study of a shallow reservoir in winter. Limnol. Oceanogr. 66: 1335-1352, doi: 10.1002/lno.11687
11. Corfidi, S.F., M.C. Coniglio, A.E. Cohen, and C.M. Mead. 2016. A Proposed Revision to the Definition of "Derecho". Bull. Am. Meteorol. Soc. 97: 935-949, doi: 10.1175/BAMS-D-14-00254.1
12. Crépin, A. 2007. Using fast and slow processes to manage resources with thresholds. Environ. Resour. Econ. 36: 191-213, doi: 10.1007/s10640-006-9029-8
13. Filzmoser, P., K. Hron, and M. Templ. 2018. Applied Compositional Data Analysis with Worked Examples in R. Spring Series in Statistics. Spring International Publishing, Cham, Switzerland.
14. Forsberg, C. 1989. Importance of sediments in understanding nutrient cyclings in lakes. Hydrobiologia 176/177: 263-277, doi: 10.1007/978-94-009-2376-8_24

15. Frost, P. C., C. Prater, A.B. Scott, K. Song, and M.A. Xenopoulos. 2019. Mobility and Bioavailability of Sediment Phosphorus in Urban Stormwater Ponds. Water Resour. Res. 55(5): 3680-3688, doi: 10.1029/2018WR023419.

16. Gakuruh, H. 2017. Essentials of Data Analysis and Graphics Using R. https://helleng.github.io/Data_Mgt_Analysis_and_Graphics_R/Data_Analysis

17. Goff, T.C., M.D. Nelson, G.C. Liknes, T.E. Feeley, S.A. Pugh, and R.S. Morin. 2021. Rapid assessment of tree damage resulting from a 2020 windstorm in Iowa, USA. Forests 12: 555, doi: 10.3390/f12050555

18. Hayes, N.M., B.R. Deemer, J.R. Corman, N.R. Razavi, and K.E. Strock. 2017. Key differences between lakes and reservoirs modify climate signals: A case for a new conceptual model. Limnol. Oceanogr. Let. 2: 47-62, doi: 10.1002/lol2.10036

19. Horppila, J., H. Holmroos, J. Niemistö, I. Massa, N. Nygrén, P. Schonach, P. Tapio, and O. Tammeorg. 2017. Variations of internal phosphorus loading and water quality in a hypertrophic lake during 40 years of different management efforts. Ecol. Eng. 103: 264-274, doi: 10.1016/j.ecoleng.2017.04.018 0925-8574

20. Hudson, J.J., and D.M. Vandergucht. 2015. Spatial and temporal patterns in physical properties and dissolved oxygen in Lake Diefenbaker, a large reservoir on the Canadian Prairies. J. Great Lakes Res. 41: 22-33. doi: 10.1016/j.jglr.2015.06.007

55. Hupfer, M., and J. Lewandowski. 2008. Oxygen controls the phosphorus release from lake sediments – a long-lasting paradigm in limnology. Int. Rev. Hydrobiol. 93(4-5):415-432, doi: 10.1002/iroh.200711054

21. Jensen, H.S., and F.Ø. Andersen. 1992. Importance of temperature, nitrate, and pH for phosphate release from aerobic sediments of four shallow, eutrophic lakes. Limnol. Oceanogr. 37(3): 577-598, doi: 10.4319/lo.1992.37.3.0577

22. Joshi, S.R., R.K. Kukkadapu, D.J. Burdige, M.E. Bowden, D.L. Sparks, and D.P. Jaisi. 2015. Organic matter remineralization predominates phosphorous cycling in the mid-bay sediments in the Chesapeake Bay. Environ. Sci. Technol. 49(10): 5887-5896, doi: 10.1021/es5059617

23. Kimmel, B.L., and A.W. Groeger. 1984. Factors controlling primary production in lakes and reservoirs: A perspective. Lake Reserv. Manag. 1: 277-281, doi: 10.1080/07438148409354524

24. Kleeberg, A., A. Freidank, and K. Jöhnk. 2013. Effects of ice cover on sediment resuspension and phosphorus entrainment in shallow lakes: Combining in situ experiments and wind-wave modeling. Limnol. Oceanogr. 58: 1819-1833, doi: 10.4319/lo.2013.58.5.1819

25. Kowalczewska-Madura, K., R. Gołdyn, J. Bogucka, and K. Strzelczyk. 2019. Impact of environmental variables on spatial and seasonal internal phosphorus loading in a mesoeutrophic lake. Int. J. Sediment Res. 34(1): 14–26, doi: 10.1016/j.ijsrc.2018.08.008

26. Lukkari, K., H. Hartikainen, and M. Leivuori. 2007. Fractionation of sediment phosphorus revisited. I: Fractionation steps and their biogeochemical basis. Limnol. Oceanogr-meth. 5: 433-444, doi: 10.4319/lom.2007.5.433

27. McCarty, J.A. 2019. Sediment phosphorus release in a shallow eutrophic reservoir cove. Trans. ASABE. 62:1269-1281, doi: 10.13031/trans.13309

28. McClain, M.E., et al. 2003. Biogeochemical hot spots and hot moments at the interface of terrestrial and aquatic ecosystems. Ecosystems. 6: 301-312, doi: 10.1007/s10021-003-0161-9

56. Mortimer, C. 1941. The exchange of dissolved substances between mud and water in lakes. Ecology. 29: 280-239, doi: 10.2307/2256395

29. Murphy, J., and J.P. Riley. 1962. A modified single solution method for the determination of phosphate in natural waters. Anal. Chim. Acta. 27: 31-36, doi: 10.1016/S0003-2670(00)88444-5

30. North, R.L, J. Johansson, D.M. Vandergucht, L.E. Doig, K. Liber, K. Lindenschmidt, H. Baulch, and J.J. Hudson. 2015. Evidence for internal phosphorus loading in a large prairie reservoir (Lake Diefenbaker, Saskatchewan). J. Great Lakes Res. 41(S2): 91-99, doi: 10.1016/j.jglr.2015.07.003

31. Nowlin, W.H., J.L. Evarts, and M.J. Vanni. 2005. Release rates and potential fates of nitrogen and phosphorus from sediments in a eutrophic reservoir. Freshw. Biol. 50(2): 301–322, doi: 10.1111/j.1365-2427.2004.01316.x

32. Ogdahl, M.E., A.D. Steinman, and M.E. Weinert. 2014. Laboratory-determined phosphorus flux from lake sediments as a measure of internal phosphorus loading. J. Vis. Exp. 85: e51617, doi: 10.3791/51617.

33. Oksanen, J., et al. 2019. vegan: Community Ecology Package. R package version 2.5-6.

34. Orihel, D.M., H.M. Baulch, N.J. Casson, R.L. North, C.T. Parsons, D.C.M. Seckar, and J.J. Venkiteswaran. 2017. Internal phosphorus loading in Canadian fresh waters: a critical review and data analysis. Can. J. Fish. Aquat. Sci. 74: 2005-2029, doi: 10.1139/cjfas-2016-0500

35. Ortiz, D.A., and G.M. Wilkinson. 2021. Capturing the spatial variability of algal bloom development in a shallow temperate lake. Freshw. Biol. 66(11): 2064-2075, doi:10.1111/fwb.13814

36. Pebesma, E. 2018. Simple features for R: Standardized support for spatial vector data. The R Journal 10:439-446.

37. Reedyk, S., E.E. Prepas, and P.A. Chambers. 2001. Effects of single $Ca(OH)_2$ doses on phosphorus concentration and macrophyte biomass of two boreal eutrophic lakes over 2 years. Freshw. Biol. 46: 1075-1087, doi: 10.1046/j.1365-2427.2001.00790.x

38. R Core Team. 2019. R: A language and environment for statistical computing. R Foundation for Statistical Computing, Vienna, Austria. https://www.R-project.org/

39. Song, K., and A.J. Burgin. 2017. Perpetual phosphorus cycling: Eutrophication amplifies biological control on internal phosphorus loading in agricultural reservoirs. Ecosystems. 20(8): 1483-1493, doi: 10.1007/s10021-017-0126-z

40. Standard Methods for the Examination of Water and Wastewater. 1998. 20th Edition. Method 4500-P B.5.

41. Standard Methods for the Examination of Water and Wastewater. 1998. 20th Edition. Method 4500-P E.

42. Søndergaard, M., J.P. Jensen, and E. Jeppesen. 2003. Role of sediment and internal loading of phosphorus in shallow lakes. Hydrobiologia. 506: 135-145, doi: 10.1023/B:HYDR.0000008611.12704.dd

43. Tammeorg, O., T. Möls, J. Niemistö, H. Holmroos, and J. Horppila. 2017. The actual role of oxygen deficit in the linkage of the water quality and benthic phosphorus release: Potential implications for lake restoration. Sci.Total Environ. 599-600: 732-738, doi: 10.1016/j.scitotenv.2017.04.244

44. Walker, B.H., S.R. Carpenter, J. Rockstrom, A. Crépin, and G.D. Peterson. 2012. Drivers, "slow" variables, "fast" variables, shocks and resilience. Ecol. Soc. 17:30, doi: 10.5751/ES-05063-170330

45. Ward, N.K., et al. 2019. Integrating fast and slow processes is essential for simulating human–freshwater interactions. Ambio. 48:1169-1182, doi: 10.1007/s13280-018-1136-6

46. Walsh, J.R., J.R. Corman, and S.E. Munoz. 2018. Coupled long-term limnological data and sedimentary records reveal new control on water quality in a eutrophic lake. Limnol. Oceanogr. 64: S34-S48, doi: 10.1002/lno.11083

47. Wuertz, D., T. Setz, Y. Chalabi, C. Boudt, P. Chausse, and M. Miklovac. 2020. fGarch: Rmetrics - Autoregressive Conditional Heteroskedastic Modelling. R package version 3042.83.2.

TABLES

Table 1. Thermal stratification and oxygen conditions at the sediment-water interface.

				Sediment-Water Interface Conditions		
DOY	Season	Site	Water Column Thermal Structure	Temperature (°C)	DO (mg L^{-1})	DO Saturation (%)
39	Winter	Intermediate	Stratified	3.2	12.6	94.3
		Deep	Stratified	4.2	1.1	8.6
117	Spring	Shallow	Isothermal	14.6	9.4	92.5
		Intermediate	Stratified	14.1	8.9	86.4
		Deep	Stratified	11.9	5.8	54.3
181	Mid-Summer	Shallow	Isothermal	26.5	5.4	67.4
		Intermediate	Isothermal	26.3	6.3	78.0
		Deep	Isothermal	24.2	0.3	3.3
223	Late Summer	Shallow	Isothermal	26.1	7.2	88.7
		Intermediate	Isothermal	25.4	4.8	58.0
		Deep	Isothermal	24.9	4.5	54.2
298	Autumn	Shallow	Isothermal	6.7	10.2	83.3
		Intermediate	Isothermal	8.1	8.7	73.7
		Deep	Isothermal	8.4	8.7	73.8

Table 2. Estimated mean P load by site and total load.

	Lakebed Information		Estimated Mean P Load ± Standard Error (kg P day^{-1})				
Site	Depth Contour	Sediment Area (m^2)	Winter	Spring	Mid-Summer	Late Summer	Autumn
Shallow	1.2-3.6 m	3,014,983.6	n.a.	6.2 ± 2.8	-0.3 ± 10.3	25.2 ± 10.1	-2.2 ± 3.4
Intermediate	3.6-5.6 m	1,593,676.1	-2.5 ± 1.7	1.9 ± 0.3	-5.8 ± 9.3	15.4 ± 13.7	0.4 ± 1.1
Deep	> 5.6 m	801,995.5	9.0 ± 5.0	1.9 ± 0.2	13.8 ± 0.9	1.9 ± 3.0	-1.2 ± 1.3
Estimated Total Load (kg Pday^{-1})			6.5 ± 1.7	10.0 ± 2.8	7.8 ± 10.3	42.5 ± 10.1	-2.9 ± 3.4

FIGURES

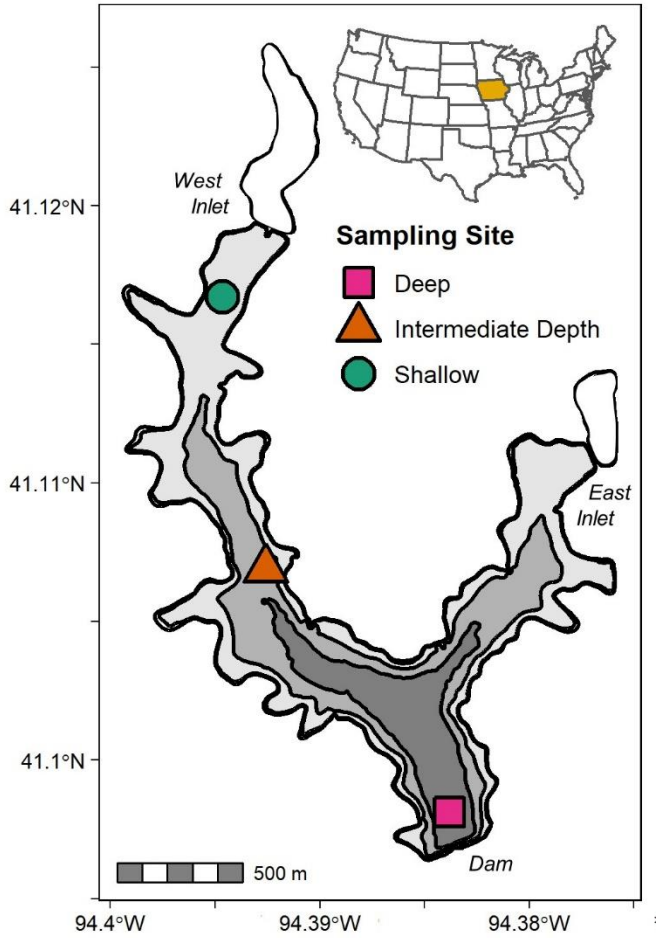

Figure 1. Sampling sites in Green Valley Lake, Iowa, USA. The three sampling sites are representative of different areas of the lakebed based on water depth. The shaded polygons illustrate these areas. The shallow site is representative of the 1.2-3.6 m depth contour. The intermediate depth site is representative of the 3.6-5.6 m interval, and the deep site is representative of the area deeper than 5.6 m.

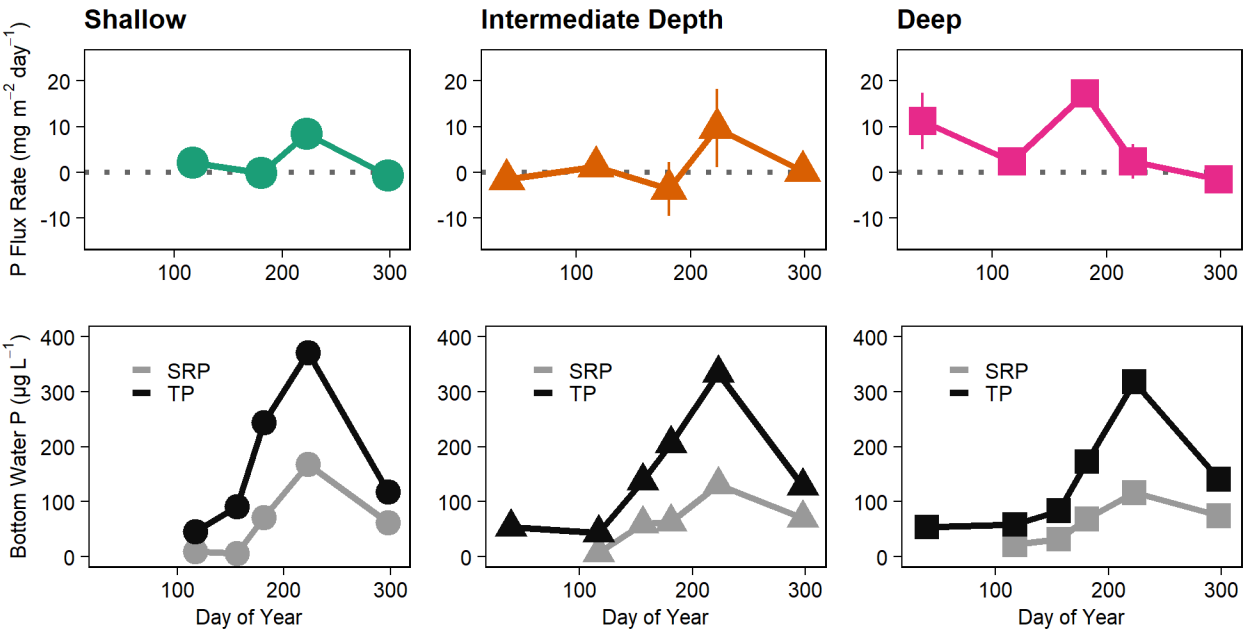

Figure 2. Sediment P flux rates and bottom water P concentrations. (Top row of panels) Time series of mean sediment total P flux (± standard deviation among replicate cores) from February to October of 2020. The shallow site was not sampled in February due to unsafe ice conditions. Negative values indicate sediment P retention while positive values show P release. (Bottom row of panels) Time series of bottom water total P (TP) and soluble reactive P (SRP) concentrations for each sampling site over the study period.

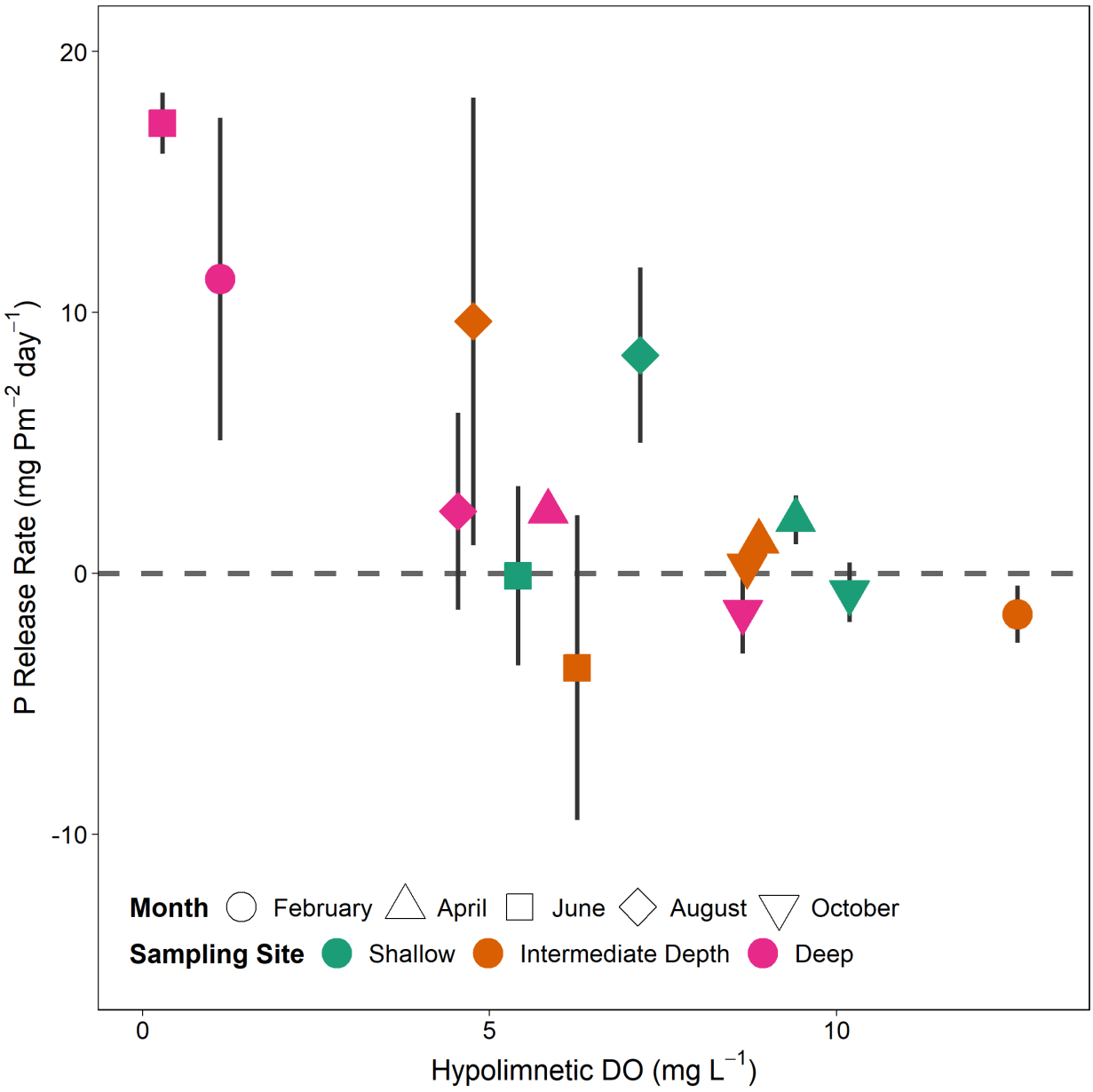

Figure 3. Mean sediment P flux rates (± standard deviation among replicate cores) across the range of observed hypolimnetic dissolved oxygen concentrations.

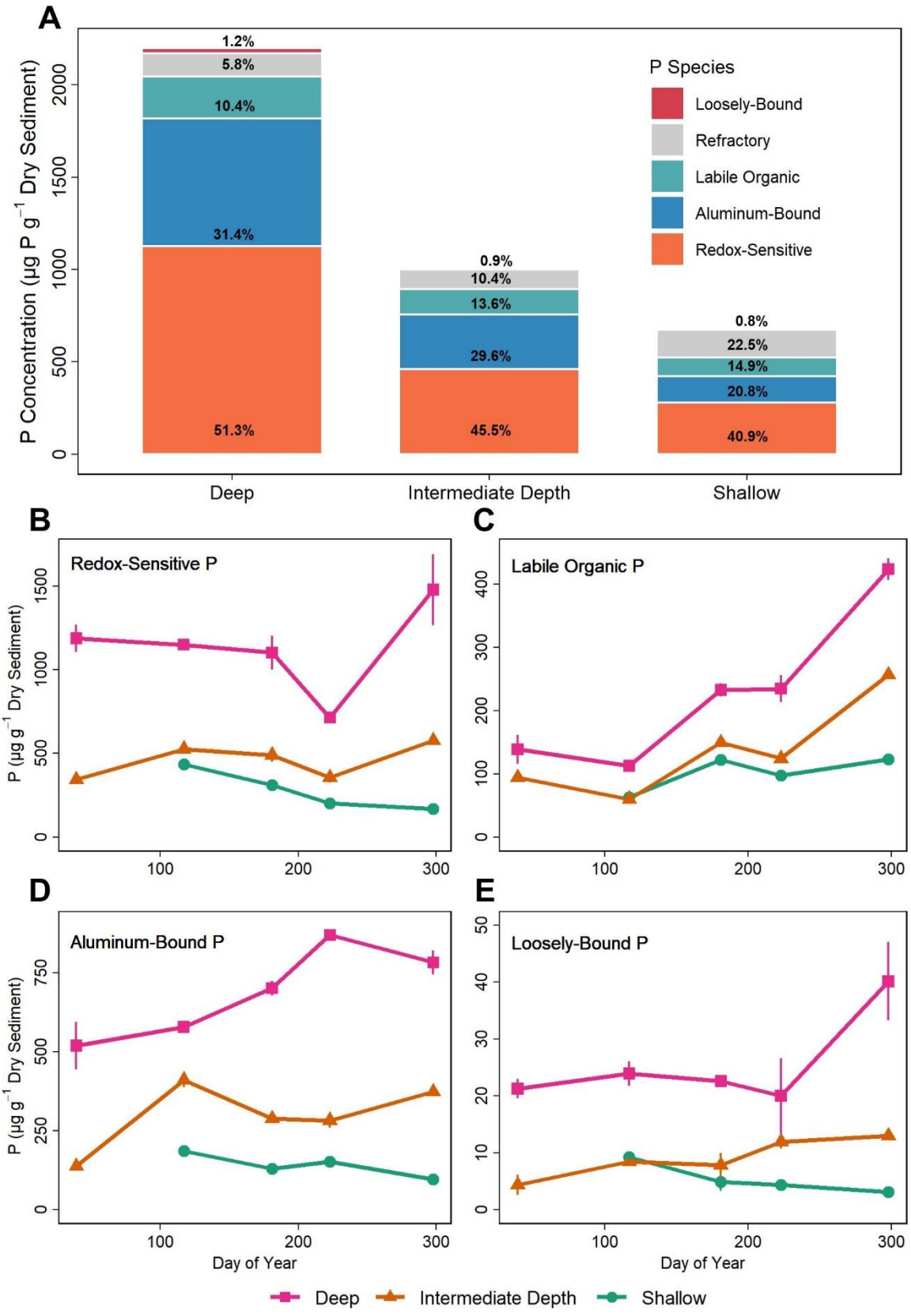
A
P Concentration (µg P g^{-1} Dry Sediment)
0
500
1000
1500
2000
1.2%
5.8%
10.4%
31.4%
51.3%
0.9%
10.4%
13.6%
29.6%
45.5%
0.8%
22.5%
14.9%
20.8%
40.9%
P Species
Loosely-Bound
Refractory
Labile Organic
Aluminum-Bound
Redox-Sensitive
Deep
Intermediate Depth
Shallow
B
Redox-Sensitive P
C
Labile Organic P
D
Aluminum-Bound P
E
Loosely-Bound P
P (µg g^{-1} Dry Sediment)
Day of Year
100
200
300
Deep
Intermediate Depth
Shallow

Figure 4. Spatiotemporal variation in sediment P species. (A) Average, annual sediment P composition by sampling site. Refractory P is estimated as the difference between total P and the sum of the measured P fractions. The relative abundance of each P species as a percent of the total sediment P pool is noted. Time series of mean (± standard deviation of replicate samples) (A) redox-sensitive P, (B) labile organic P, (C) aluminum-bound, and (D) loosely-bound P concentrations across sampling sites and over the course of the year. Note different y-axis scales across plots to depict more versus less abundant P fractions.

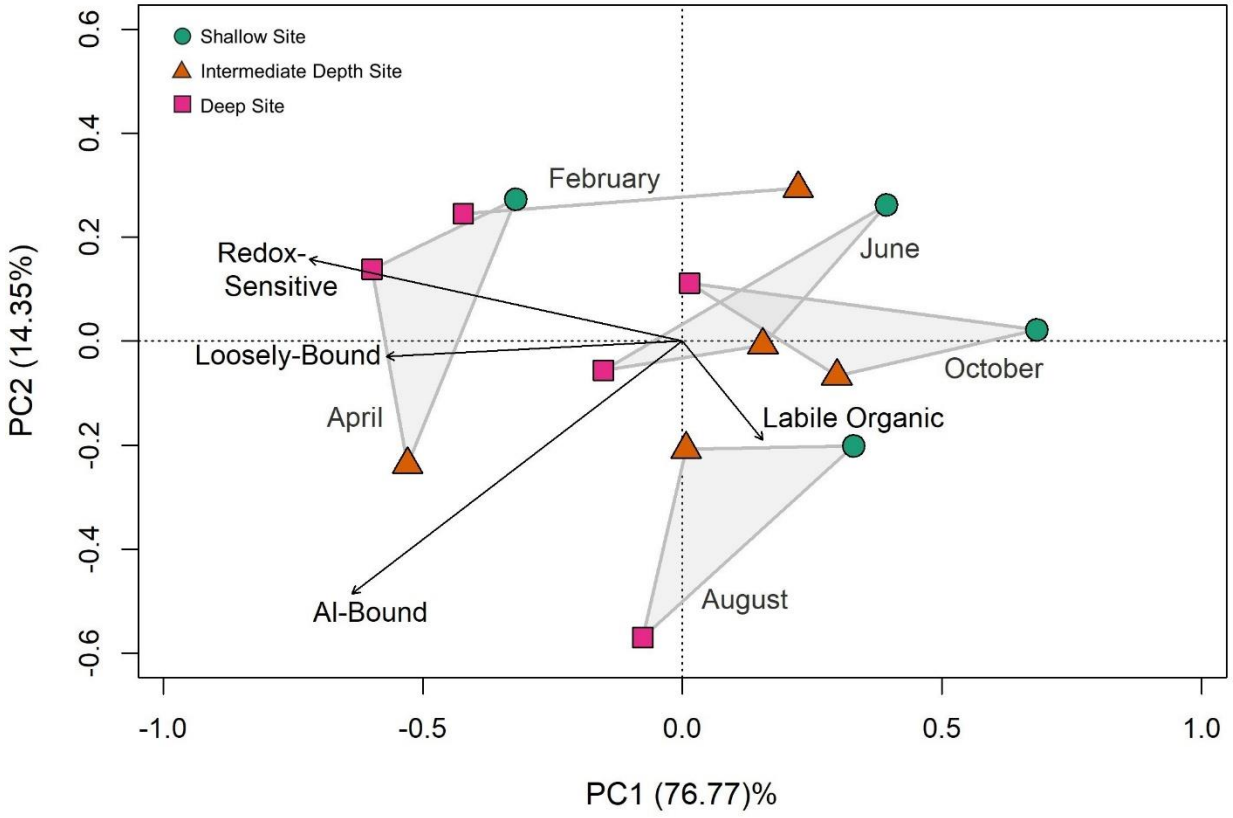

Figure 5. Spatiotemporal variation in sediment P composition. PCA biplot based on a compositional data analysis of sediment P pools over the course of the year across the reservoir.

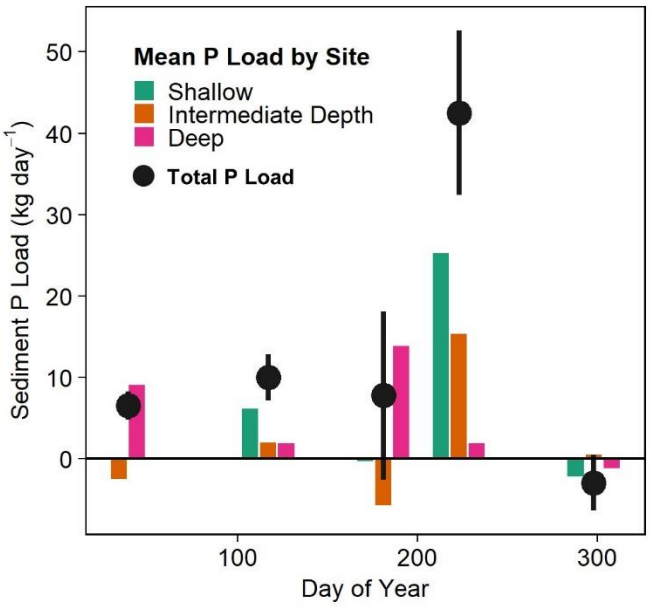

Figure 6. Estimated mean P load at the time of sampling by site (bars) and total load across the lakebed (points; error bars are ± standard error). Bar plots show the mean, estimated P load for each sampling site at the time of sampling. Points represent the sum of the estimated loads across the lakebed.

SUPPLEMENTARY INFORMATION FOR CHAPTER 2

Introduction

The appendix contains additional methods text detailing analysis of suspended solids, total nitrogen, and nitrate as well as use of previous monitoring data. We provide the equations used to determine sediment phosphorus (P) flux rates as well as sediment physical characteristics and the concentrations of sediment total P and various P species. We have also provided the standard equation for determining the third statistical moment. Table S1 compares temperature and dissolved oxygen conditions between the core incubations and ambient conditions in the reservoir for each sampling site and event. Table S2 details surface and bottom water chemistry including total, volatile, and involatile suspended solids; total and soluble reactive P; total nitrogen; and nitrate concentrations. Table S2 reports the mean P flux rates by site and day of year, as presented in Figure 2 in the main manuscript. Table S4 demonstrates the effects of excluding high flux rates on the skewness of the P flux distribution, as quantified by the standardized third statistical moment. Table S5 provides loss on ignition organic matter, moisture content, and bulk density data for each sampling site and event.

Figure S1 plots temperature and dissolved oxygen conditions in the incubating cores against ambient conditions in the reservoir for each sampling site and event. We included a visualization that compares 2020 epi- and hypolimnetic total P and soluble reactive P concentrations to the P dynamics from previous years (Figure S2). Figure S3 illustrates the distribution of sediment P flux rates across sampling sites and seasons, with statistical outliers noted. Figure S4 breaks down the sediment P flux rate data by site and sampling event to identify the points in space and time associated with high flux rates. Figure S5 displays the average, annual sediment P composition by sampling site. We include citations for all references included in the appendix as well as citations for additional R packages used solely for data cleaning and visualizations.

Vertical profiles and water chemistry

Suspended solids

Total suspended solids were determined by filtering a known volume of sample water through a prepared filter (0.45µm GF/C filters) and drying to a constant weight. Volatile suspended solids were determined via loss-on-ignition, and involatile solids were assumed to be the difference between volatile and total suspended solids.

Total nitrogen and nitrate

Subsamples were filtered (0.45µm GF/C filters) in the lab for nitrate analysis, and all samples were preserved with concentrated sulfuric acid to pH 2. Total nitrogen samples underwent digestion prior to analysis (Standard Methods 4500-N.C). Total nitrogen and nitrate were measured via second-derivative ultraviolet spectroscopy (Crumpton and others 1992, Childress and others 1999) using an HP 8453 Spectrophotometer.

Use of previous monitoring data

In order to compare water column nutrient dynamics in 2020 to previous years, we used publicly-available nutrient monitoring data from the Iowa Department of Natural Resources AQuIA database (Figure S1).

Sediment P fluxes

Eq. 1 – *Mass of P in the Overlying Water*

$$\text{Water Column Mass P (mg)} = \text{Water column [TP] (mg/L)} * (\text{Total Water Volume (L)} - \text{Replacement Water Volume (L)}) \quad (1)$$

Eq. 2 – *Mass of P in the Replacement Water*

$$\text{Replacement Water Mass P (mg)} = \text{Replacement Water [TP] (mg/L)} * \text{Replacement Water Volume (L)} \quad (2)$$

Eq. 3 – *New TP Concentration Following Addition of Replacement Water*

$$\text{New [TP] (mg/L)} = (\text{Water Column Mass P (mg)} + \text{Replacement Water Mass P (mg)}) / \text{Total Water Volume (L)} \quad (3)$$

Eq. 4 – *Daily Change in TP Concentration*

$$\Delta\,[\text{TP}]\ (\text{mg/L}) = \text{Water Column } [\text{TP}]_{\text{day n}}\ (\text{mg/L}) - \text{New } [\text{TP}]_{\text{day n-1}}\ (\text{mg/L}) \quad (4)$$

Sediment P content and composition

Additional subsamples of fresh sediment were used for analysis of physical characteristics. For each site, three replicate subsamples were dried to a constant mass and the wet and dry masses were used to determine sediment moisture content (MC). The subsamples were then combusted and weighed again to calculate organic matter content as loss-on-ignition (LOI) and estimate bulk density (Håkanson and Jansson 2002).

Eq. 1 – *Moisture Content (MC)*

$$\text{Moisture Content (\%)} = \left[\frac{(W_w - W_t) - (W_d - W_t)}{W_w - W_t}\right] \times 100 \quad (1)$$

Where W_t is the weight of the aluminum weigh boat, W_w is the weight of the weigh boat and fresh sediment sample, and W_d is the weight of the weigh boat and dry sediment.

Eq. 2 – *Organic Matter Content as Loss-on-Ignition (LOI)*

$$\text{LOI Organic Matter Content (\%)} = \left[\frac{(W_d - W_t) - (W_a - W_t)}{W_d - W_t}\right] \times 100 \quad (2)$$

Where W_a is the weight of the weigh boat and the ashed sediment after combustion.

Eq. 3 – *Bulk Density*

$$\text{Bulk Density } \left(g/cm^3\right) = \frac{260}{100 + 1.6 \times \left[MC + \left(\frac{LOI}{100 \times (100 - MC)}\right)\right]} \quad (3)$$

Eq. 4 – *Dry Mass Equivalent of Fresh Sediment Used*

$$\text{Dry Mass Equivalent (g)} = \text{Mass Fresh Sediment (g)} \times (100 - MC) \quad (4)$$

Eq. 5 – *Loosely-Sorbed and Pore Water P*

$$\text{Loosely-Bound P (mg P/g dry sediment)} = \frac{\text{Concentration TP (mg/L)} \times \text{Solution Volume (L)}}{\text{Dry Mass Equivalent of Sediment Used (g)}} \quad (5)$$

The concentration of TP used should reflect the average of lab duplicates, corrected for any dilutions. The solution volume should equal the total amount of 0.46 M NaCl extractant and rinse solutions (0.1 L total). The dry mass equivalent of the fresh sediment used is estimated based on MC (Eq. 4) and will be the same for the calculations of each subsequent extraction.

Eq. 6 – *Redox-Sensitive P*

$$\text{Redox-Sensitive P (mg P/g dry sediment)} = \frac{\text{Concentration TP (mg/L)} \times \text{Solution Volume (L)}}{\text{Dry Mass Equivalent of Sediment Used (g)}} \quad (6)$$

The concentration of TP used should reflect the average of lab duplicates, corrected for any dilutions. The solution volume should equal the total volume of the 0.11 M bicarbonate – 0.1 M sodium dithionate solution and the rinse solutions (0.2 L total).

Eq. 7 – *Aluminum-Bound P*

$$\text{Al-Bound P (mg P/g dry sediment)} = \frac{\text{Concentration SRP (mg/L)} \times \text{Solution Volume (L)}}{\text{Dry Mass Equivalent of Sediment Used (g)}} \quad (7)$$

The concentration of SRP used should reflect the average of lab duplicates, corrected for any dilutions. The solution volume should equal the total volume of 0.1 M NaOH used and the rinse solutions (0.150 L total).

Eq. 8 – *Labile Organic P*

$$\text{Labile Organic P (mg P/g dry sediment)} = \left[\frac{\text{Concentration TP (mg/L)} \times \text{Solution Volume (L)}}{\text{Dry Mass Equivalent of Sediment Used (g)}}\right] - \text{Al-Bound P} \quad (8)$$

The concentration of TP from the supernatant should first be corrected for the volume of NaOH and rinse solutions used (0.15 L total) and the sediment mass. This value represents the concentration of aluminum-bound and total labile organic P in the sediment pellet. The concentration of labile organic P is calculated as the difference between this value and the Al-bound P concentration (Eq. 7).

Eq. 9 – *Total P*

$$\text{Total P (mg P/g dry sediment)} = \frac{\left[\text{Concentration TP}\left(\frac{\text{mg}}{\text{L}}\right) \times \frac{\text{(Post pH (g)-Tare (g))}}{\text{(Pre pH (g)-Tare (g))}}\right] \times \text{Dilution Volume (L)}}{\text{Dry Mass of Sediment Used (g)}} \quad (9)$$

The concentration of TP used should reflect the average of lab duplicate measures and must be corrected for the pH adjustment. The corrected TP concentration can then be corrected for the volume to which the sample was diluted after boiling (0.05 L) and the mass of dry sediment.

Statistical Analyses

Eq. 1 – *Skewness, third statistical moment (m_3)*

$$m_3 = \frac{\sum(x-\mu)^3}{n} \quad \text{(Eq. 1)}$$

The third statistical moment quantifies skewness and can be standardized by dividing by the cube of the standard deviation. Perfectly symmetric distributions have an m3 value of zero.

Table S1. Incubation versus reservoir temperature and dissolved oxygen conditions

		Temperature (°C)			Dissolved Oxygen (mg L^{-1})		
Month	Site	Reservoir Bottom Water	Core Mean	Core SEM	Reservoir Bottom Water	Core Mean	Core SEM
February	Intermediate	3.2	6.4	0.1	12.6	12.0	0.1
	Deep	4.2	5.4	0.1	1.1	1.8	0.6
April	Shallow	14.6	11.4	0.2	9.4	10.3	0.1
	Intermediate	14.1	11.1	0.1	8.9	10.2	0.1
	Deep	11.9	11.4	0.2	5.8	7.5	0.4
June	Shallow	26.5	23.0	0.1	5.4	7.3	0.1
	Intermediate	26.3	22.8	0.1	6.3	6.2	0.4
	Deep	24.2	22.8	0.1	0.3	1.4	0.1
August	Shallow	26.1	24.6	0.3	7.2	6.6	0.2
	Intermediate	25.4	24.6	0.3	4.8	1.9	0.1
	Deep	24.9	24.8	0.3	4.5	1.6	0.2
October	Shallow	6.7	10.2	0.2	10.2	10.7	0.1
	Intermediate	8.1	10.4	0.1	8.7	10.3	0.2
	Deep	8.4	11.1	0.3	8.7	10.4	0.1

Table S2. Epi- and hypolimnetic water chemistry by site and sampling event

			Suspended Solids ($mg\ L^{-1}$)			Phosphorus ($\mu g\ L^{-1}$)		Nitrogen ($mg\ L^{-1}$)	
DOY	Site	Water Column	TSS	VSS	ISS	TP	SRP	TN	No_x
39	Intermediate	Surface	NA	NA	NA	49.6	NA	NA	NA
		Bottom	7.5	4.5	3.0	54.2	NA	NA	0.4
	Deep	Surface	NA	NA	NA	42.7	NA	NA	NA
		Bottom	5.5	NA	NA	53.9	NA	NA	0.3
117	Shallow	Surface	1.1	NA	NA	39.5	7.1	1.0	0.7
		Bottom	9.5	NA	NA	45.6	9.3	0.9	0.7
	Intermediate	Surface	12.2	NA	NA	33.7	5.5	0.8	0.6
		Bottom	3.0	NA	NA	43.7	7.3	0.8	0.7
	Deep	Surface	5.5	NA	NA	35.0	1.9	0.6	0.6
		Bottom	1.5	NA	NA	58.5	22.0	0.7	0.4
181	Shallow	Surface	36.7	25.7	11.0	251.2	66.9	1.3	0.1
		Bottom	30.3	18.7	11.7	243.6	71.6	1.0	0.1
	Intermediate	Surface	22.0	17.0	5.0	327.4	63.0	0.9	0.1
		Bottom	22.1	15.3	6.8	206.0	63.3	1.0	0.0
	Deep	Surface	15.0	13.0	2.0	178.7	59.6	0.7	0.1
		Bottom	16.4	14.8	1.7	173.0	68.7	0.9	0.1
223	Shallow	Surface	51.0	28.5	22.5	376.4	173.1	1.3	0.1
		Bottom	43.5	21.0	22.5	370.9	168.5	1.3	0.1
	Intermediate	Surface	41.0	29.5	11.5	343.6	134.0	1.4	0.1
		Bottom	40.0	20.0	20.0	334.0	131.2	1.2	0.1
	Deep	Surface	38.0	19.0	19.0	330.3	116.6	1.1	0.1
		Bottom	32.0	17.5	14.5	318.0	116.3	1.3	0.1
298	Shallow	Surface	6.6	NA	NA	115.9	61.6	1.0	0.3
		Bottom	3.2	NA	NA	118.1	62.3	0.9	0.3
	Intermediate	Surface	8.0	NA	NA	131.6	69.2	1.0	0.3
		Bottom	17.6	NA	NA	128.4	69.7	1.0	0.3
	Deep	Surface	6.2	NA	NA	138.4	71.0	1.0	0.2
		Bottom	2.4	NA	NA	141.1	74.3	1.0	0.3

Surface water samples were taken 0.25 m below the surface and bottom water samples were taken 0.5 m above the sediment-water interface. Suspended solid constituents measured include total (TSS), volatile (VSS) and involatile (ISS).

Table S3. Mean P flux rates across sampling sites and seasons.

	Mean P Flux Rate ± Standard Error (mg P m^{-2} day^{-1})				
Sampling Site	***February***	***April***	***June***	***August***	***October***
Shallow		2.0 ± 0.9	-0.1 ± 3.4	8.4 ± 3.4	-0.7 ± 1.1
Middle	-1.6 ± 1.1	1.2 ± 0.2	-3.6 ± 5.8	9.6 ± 8.6	0.3 ± 0.7
Deep	11.3 ± 6.2	2.4 ± 0.3	17.2 ± 1.2	2.4 ± 3.8	-1.5 ± 1.6

Values indicate the mean P flux rate ± standard error across three replicate sediment cores. Blue cells indicate sediment P retention, orange cells corresponded to sediment P release, and either retention or release may have occurred during times indicated in grey.

Table S4. Influence of excluding high flux rates on distribution skewness.

Dataset Subsample	***Standardized Third Statistical Moment (m_3)***	***Distribution Shape***
Full dataset	0.818	Moderately positively skewed
Exclude highest flux	0.734	Moderately positively skewed
Exclude 2 highest fluxes	0.718	Moderately positively skewed
Exclude 3 highest fluxes	0.666	Moderately positively skewed
Exclude 4 highest fluxes	0.584	Moderately positively skewed
Exclude 5 highest fluxes	0.462	approximately symmetric

Table S5. Sediment physical characteristics

		LOI Organic Matter (%)		Moisture Content (%)		Bulk Density (g cm^{-3})	
Site	Month	Mean	SEM	Mean	SEM	Mean	SEM
Shallow	April	9.28	0.42	71.70	0.31	1.19	0.0034
	June	9.37	0.01	71.49	0.18	1.19	0.0014
	August	8.96	0.34	73.24	0.35	1.18	0.0034
	October	7.13	1.95	70.42	1.22	1.20	0.0049
Intermediate	February	7.49	0.29	69.36	0.32	1.21	0.0028
	April	8.54	0.30	78.15	0.58	1.14	0.0048
	June	9.71	0.08	77.12	0.21	1.15	0.0016
	August	9.53	0.36	79.79	0.34	1.13	0.0026
	October	8.42	2.00	82.95	0.67	1.11	0.0021
Deep	February	12.32	0.36	85.25	0.23	1.09	0.0013
	April	14.97	1.28	86.07	0.19	1.08	0.0017
	June	12.73	1.18	86.81	0.31	1.08	0.0010
	August	14.03	0.14	87.21	0.07	1.07	0.0003
	October	11.65	1.43	86.67	0.10	1.08	0.0008

The shallow site was not sampled in February due to unsafe ice conditions. Mean and standard error values represent either three laboratory replicates (February-August) or two replicates (October sampling event).

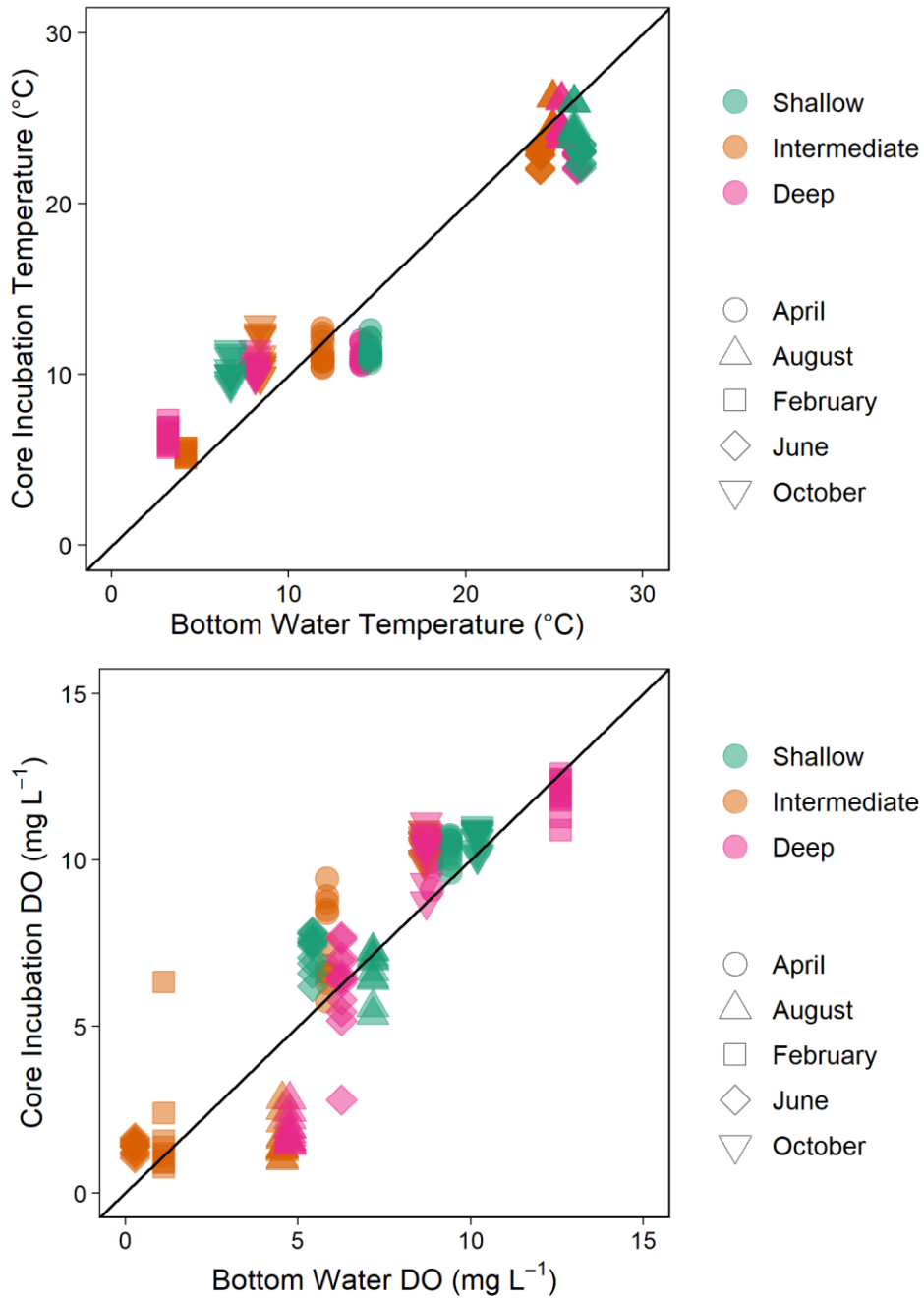

Figure S1. *Comparison of core incubation conditions to reservoir conditions.* The mean temperature (top panel) and dissolved oxygen concentration (bottom panel) across replicate cores are plotted against bottom water conditions at the corresponding sampling sites for each sampling event.

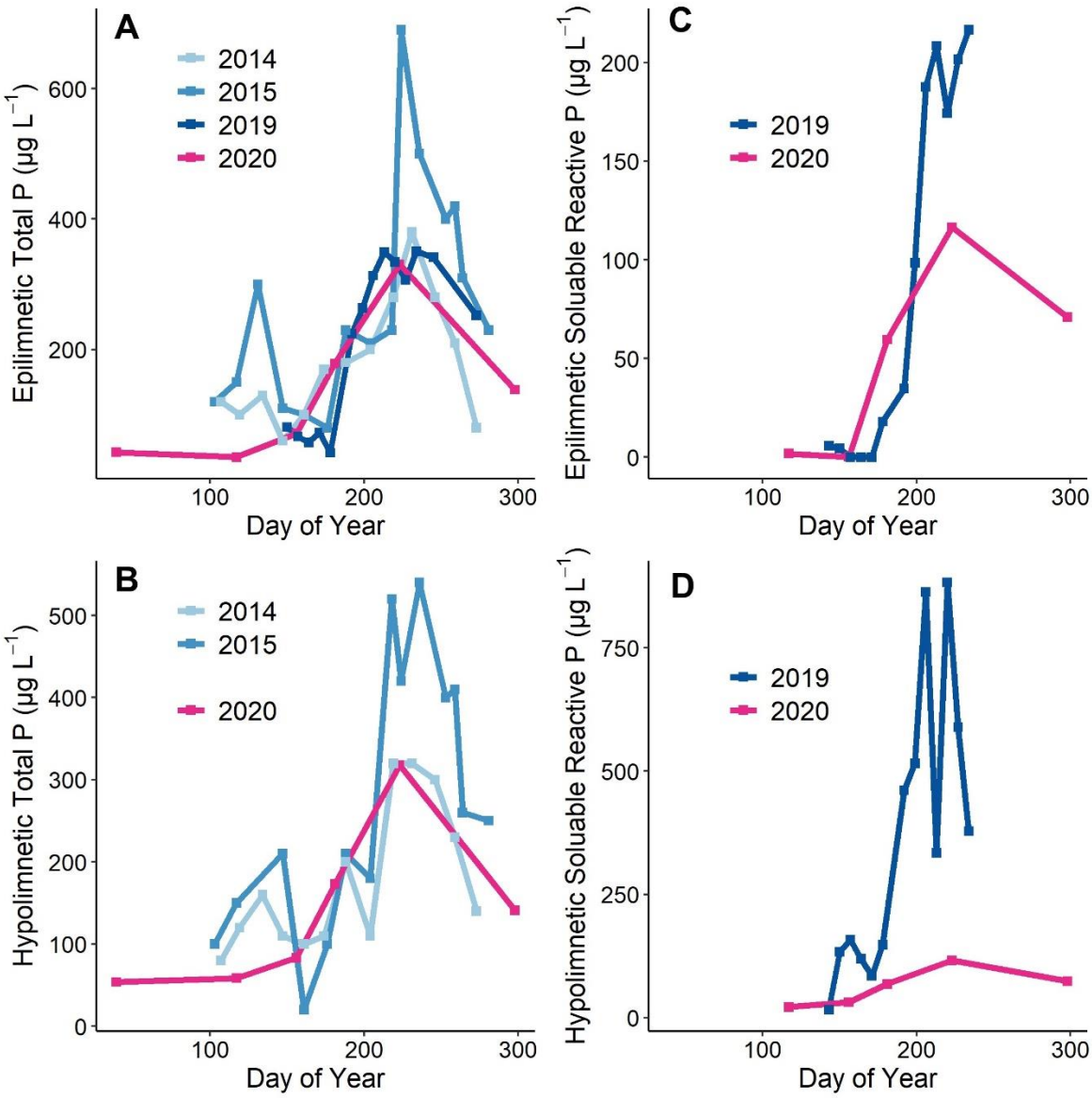

Figure S2. *Comparing 2020 epi- and hypolimnetic P dynamics to previous years (2014, 2015, 2019).* The 2020 P dynamics followed similar seasonal trends as past years in epilimnetic TP (A) and hypolimnetic TP (B) concentrations. Epilimnetic and hypolimnetic SRP concentrations were higher in 2019 than in 2020 (C-D).

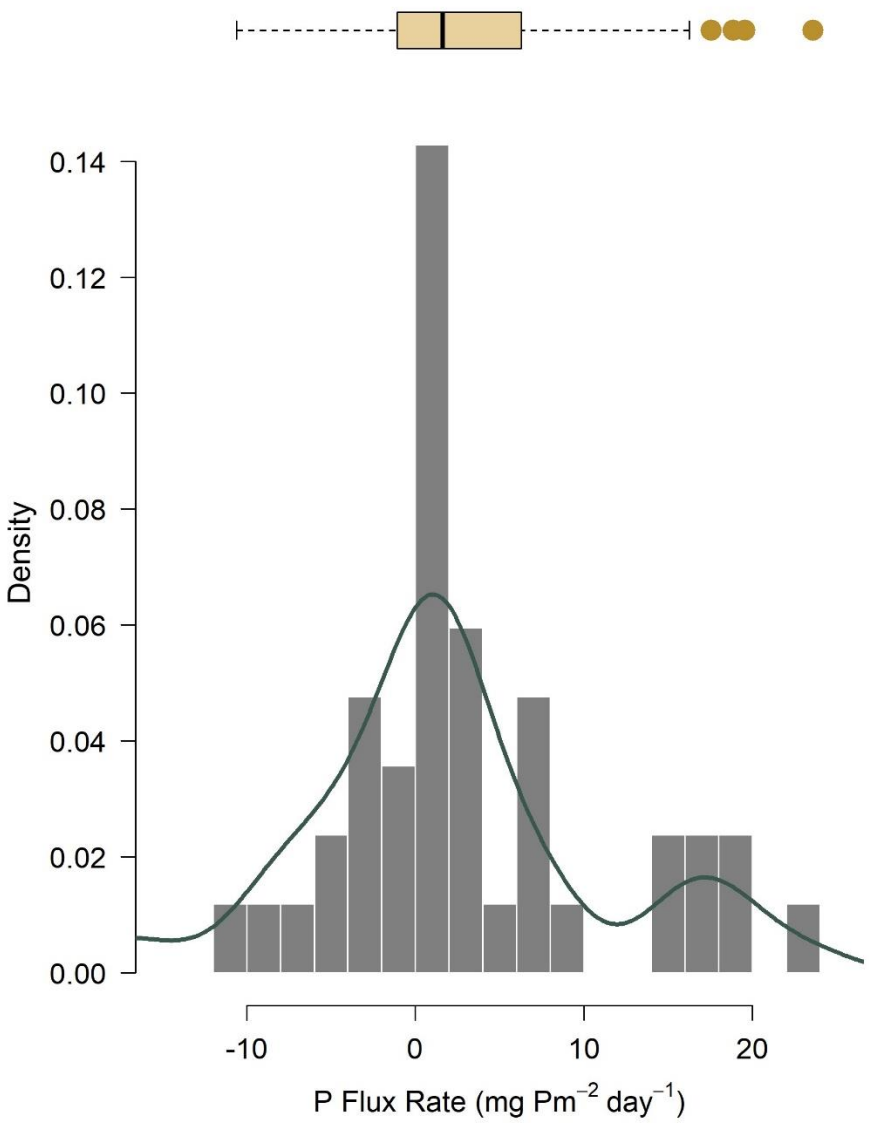

Figure S3. *Distribution of sediment P flux rates.* The histogram details measured sediment P flux rates over all sampling sites and seasons while the density curve provides a kernel density estimation. The distribution and statistical outliers are further summarized with a boxplot.

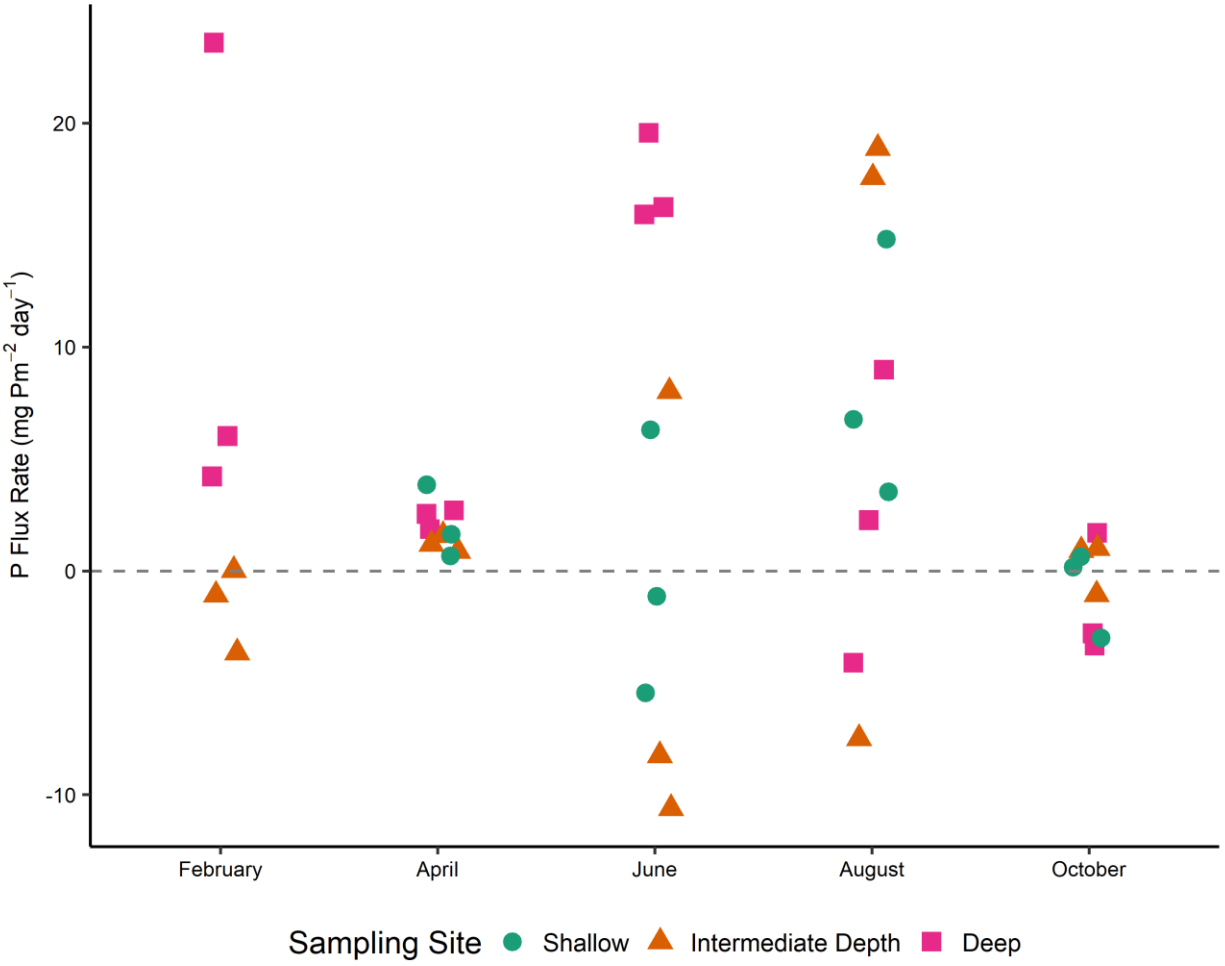

Figure S4. *Sediment P flux rates by site and sampling event, 2020.* The distribution of all measured sediment P flux rates is visualized by sampling site and month. The highest observed release rates were associated with sediments from the deep sampling site in February and June as well as August fluxes from the middle and shallow sites. The four highest rates are statistical outliers.

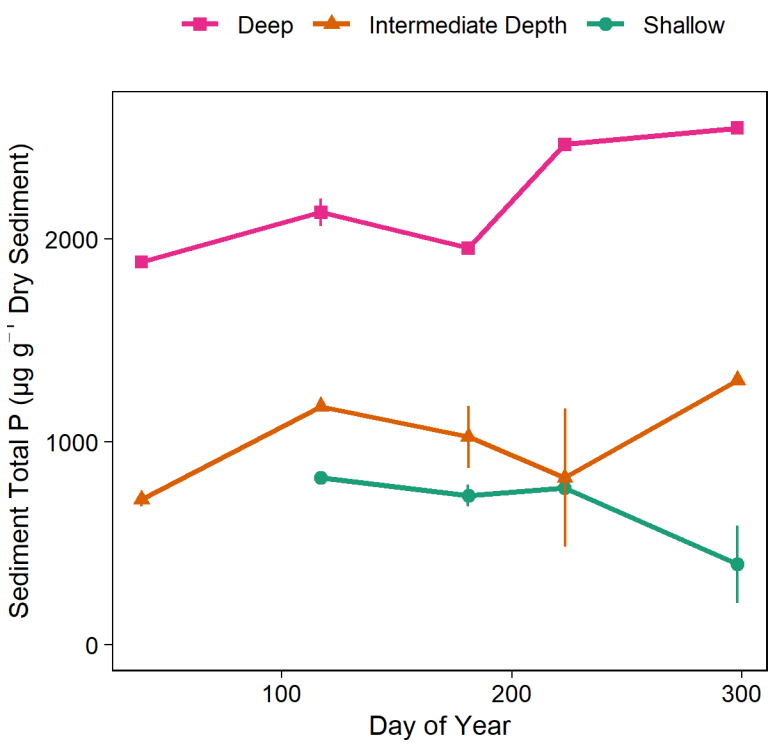

Figure S5. Spatiotemporal variation in sediment total P. Time series of mean total P concentrations over time for each sampling site. Error bars represent one standard error

Supplementary Materials References

1. Childress, C.J.O., W.T. Foreman, B.F. Conner, and T.J. Maloney. 1999. New Reporting Procedures Based on Long-Term Method Detection Levels and Some Considerations for Interpretations of Water-Quality Data Provided by the U.S. Geological Survey National Water Quality Laboratory. U.S. Geological Survey Open File Report 99-193. 24 p.
2. Crumpton, W.G., T.M. Isenhart, and P.D. Mitchel. 1992. Nitrate and organic N analyses with second-derivative spectroscopy. Limnology and Oceanography 37:907-913.
3. Håkanson, L., and M. Jansson. 2002. Principles of lake sedimentology. Caldwell, NJ: The Blackburn Press.
4. Standard Methods for the Examination of Water and Wastewater. 1998. 20th Edition. Method 4500-N N.C.

R packages used for data cleaning and visualizations

1. Auguie, B.. 2017. gridExtra: Miscellaneous Functions for "Grid" Graphics. R package version 2.3.
2. Dunnington, D. 2021. ggspatial: Spatial Data Framework for ggplot2. R package version 1.1.5.
3. Neuwirth, E. 2014. RColorBrewer: ColorBrewer Palettes. R package version 1.1-2.
4. Wickham, H., et al. 2019. Welcome to the tidyverse. Journal of Open Source Software 4:1686.
5. Wilke, C.O. 2020. cowplot: Streamlined Plot Theme and Plot Annotations for 'ggplot2'. R package version 1.1.1.

CHAPTER 4

MACROPHYTE-INDUCED STRATIFICATION MEDIATES POND RESPONSE TO AN AQUATIC HEATWAVE

In preparation for submission with coauthors R. Ladwig, G.M. Wilkinson

Author contributions: Albright designed the study; performed all field and laboratory work; cleaned, analyzed, and visualized the data; and wrote the manuscript. Wilkinson contributed to study design and data analysis and provided feedback on writing. Ladwig designed the hydrodynamic model and provided feedback on data visualizations and writing.

ABSTRACT

Small lakes and ponds are sensitive to external stressors such as nutrient enrichment and heatwaves; however, when present, aquatic macrophytes may mediate the effects of compounding stressors. Leveraging an ecosystem experiment and hydrodynamic model, we tested interactions between episodic nutrient loading and aquatic heatwaves on macrophyte biomass and the subsequent changes in the physicochemical environment in two temperate ponds. We monitored water column thermal structure, dissolved oxygen (DO), and macrophytes in each pond over a growing season, while experimentally pulsing one of the ponds with nutrients to simulate storm-driven external loading (the other pond served as an unmanipulated reference). Both ponds experienced a natural aquatic heatwave following the nutrient pulse. Macrophytes in the nutrient addition pond began to senescence mid-summer as a result of phytoplankton-shading and heat stress while macrophytes in the reference pond followed expected seasonal patterns, senescing in early autumn. Our field observations and model results

indicate that macrophytes structure the thermal environment in shallow ponds through vertical attenuation of light and turbulent kinetic energy. Macrophytes reduced the vertical extent of water column warming during the aquatic heatwave and maintained cooler bottom water temperatures throughout the course of the summer, suggesting that macrophytes may buffer small waterbodies from brief heatwaves. Seasonal patterns in DO saturation also followed trends in macrophyte biomass; however, during the heatwave, DO saturation fell sharply in both ponds and remained depressed through the remainder of the summer. With this experiment and modeling exercise, we have demonstrated that through their physical structure, macrophytes play a pivotal role in mediating how small waterbodies respond to compound extreme events.

INTRODUCTION

Small lakes and ponds are the most abundant lentic ecosystems worldwide and sites of critical importance for freshwater biodiversity and biogeochemical cycles (Scheffer et al. 2006; Cole et al. 2007; Verpoorter et al. 2014). Small waterbodies are active components of regional- and global-scale carbon cycling, both as sites of burial and storage (Wilkinson et al. 2018; Taylor et al. 2019) and as sources of atmospheric carbon dioxide and methane (Holgerson and Raymond 2016; Peacock et al. 2021). Small lakes and ponds enhance local and regional biodiversity, due in part to abundant macrophytes (Van Geest et al. 2003). Robust macrophyte communities support greater diversity of other taxa by providing food resources and habitat structure (Williams et al. 2004; Scheffer et al. 2006). In addition to these biotic interactions, macrophytes play a pivotal role in the ecosystem structure and function of small waterbodies by influencing water column thermal structure and sediment stability as well as whole-lake productivity and nutrient cycling (Carpenter and Lodge 1986; Scheffer et al. 1993; Licci et al. 2019). Despite the

prevalence and importance of small, vegetated lakes and ponds, these ecosystems remain understudied (Downing 2010; Biggs et al. 2017), particularly with regards to the role the macrophytes play in mediating ecosystem response to compounding stressors.

The characteristic morphometry of small waterbodies makes these ecosystems more susceptible to stressors. For example, limited water volume and shallow mean depth reduce both dilution potential and thermal inertia making small waterbodies sensitive to nutrient loading and intense heatwaves (Biggs et al. 2017; Woolway et al. 2021a; Polazzo et al. 2022). As a result, eutrophication and aquatic heatwaves may act as compounding stressors for small lakes and ponds. Aquatic heatwaves are periods of sustained high surface water temperatures relative to local and seasonal baseline conditions (Hobday et al. 2016; Tassone et al. 2021; Woolway et al. 2021a). The frequency, duration, and intensity of aquatic heatwaves have increased over the past century as a result of anthropogenic climate change, a trend which is anticipated to continue, even under low green-house-gas-emissions scenarios (Oliver et al. 2018; Woolway et al. 2021a, Woolway et al. 2022). Aquatic heatwaves may lower dissolved oxygen (DO) concentrations directly through reduced gas solubility in warmer waters and indirectly through increased ecosystem respiration (Tassone et al. 2021). Low DO concentrations and thermal stress have been linked to coral bleaching, declines in kelp forests, and mass seagrass mortality in marine systems (Wernberg et al. 2016; Hughes et al. 2017; Strydom et al. 2020). Although heatwaves are well-studied in coastal and marine systems, research on the effects of heatwaves in lakes is relatively nascent (Woolway et al. 2021a; Woolway et al. 2022). As such, it remains unclear how aquatic heatwaves affect the structure and function of lentic ecosystems, especially small, vegetated waterbodies.

Though aquatic heatwaves are projected to be more severe in small, shallow waterbodies (Woolway et al. 2021a), if present, macrophytes may buffer small lakes and ponds from extreme temperatures by restricting vertical heat transfer. Canopy-forming macrophyte beds attenuate incoming solar radiation and dissipate wind-driven turbulence, thus limiting the depth of heat transport and creating a shallow mixed surface layer separated from cooler bottom waters (Herb and Stefan 2004; Andersen et al. 2017a; Sand-Jensen et al. 2019). In short, macrophytes induce thermal stratification in small waterbodies, which may isolate bottom waters from rising surface temperatures during an aquatic heatwave. Stratification is also expected to restrict dissolved gas transport and may produce a vertically heterogenous chemical environment within macrophyte beds (Andersen et al. 2017b; Vilas et al. 2017). As a result, macrophyte structure could also influence how DO responds to aquatic heatwaves. Rising surface water temperatures during a heatwave are expected to lower DO concentrations; however, in maintaining cooler bottom water temperatures, macrophyte-induced stratification may dampen the effects of a heatwave on gas solubility and ecosystem respiration. Altogether, macrophytes play a key role in the thermal structure and DO environment of small lakes and ponds, potentially mediating the effect of temporary external stressors on these ecosystem's structure and function.

The abundance and growth of macrophytes in small waterbodies is driven by temperature and the availability of light and nutrients (Carpenter and Lodge 1986; Phillips et al. 2016), making them sensitive to environmental stressors such as nutrient loading and heatwaves (Wu et al. 2021). Warmer water temperatures can enhance macrophyte growth (Olesen and Madsen 2001, Bertani et al. 2016; Hansson et al. 2020); however, high temperatures may also induce heat stress, impeding reproduction (Li et al. 2017) or prompting senescence (Hao et al. 2018). Similarly, nutrient loading may have either a positive or negative effect on macrophyte growth.

Although macrophytes can benefit from enhanced nutrient availability through foliar uptake (DeMarte and Hartman 1974; Twilley et al. 1977), nutrient loading can also increase algal biomass and subsequently reduce light availability through shading (Scheffer et al. 1993; Short et al. 1995). The effect of shading from phytoplankton-associated turbidity is expected to vary across macrophyte growth forms, as submersed species are more vulnerable to light limitation than emergent or floating-leaf species (Szabo et al. 2010). While the individual responses of macrophytes to nutrient enrichment and heat stress have been established, it remains unclear how macrophytes respond to simultaneous, compounding stressors and what the consequences are for the thermal and chemical structure of small lentic ecosystems.

We experimentally evaluated the interacting effects of episodic external nutrient loading and aquatic heatwaves on macrophyte biomass and the subsequent changes in the physicochemical environment in two shallow, vegetated ponds. Specifically, we monitored spatiotemporal variation in water column thermal structure, DO profiles, and macrophyte biomass and canopy height in each pond and over the course of a growing season. We experimentally pulsed one of the ponds with nutrients to simulate a typical storm-driven external loading event, while the other pond served as a reference. Both ponds experienced a mid-summer aquatic heatwave following the first experimental nutrient pulse. In the absence of severe environmental stressors, the phenology of the macrophyte communities in these temperate ponds follows a pattern of spring emergence from over-wintering rhizomes, growth throughout the summer, and then senescence of the leaves and stems in early autumn. However, we hypothesized that the combined stress of the nutrient addition and heatwave in the experimentally eutrophied pond would induce early macrophyte senescence due to increased shading from phytoplankton and heat stress, thus reducing macrophyte biomass and subsequently

altering the temperature and DO gradients in the water column. To further test the mechanistic relationship between macrophytes and thermal structure, we applied a hydrodynamic model for one-dimensional heat transport in vegetated ponds and simulated pond response to an aquatic heatwave across a range of macrophyte biomass and canopy height.

Leveraging our ecosystem experiment and hydrodynamic model, we asked (Q1) How do macrophyte biomass and canopy height influence pond thermal structure, and how do macrophytes alter the temperature profile response to an aquatic heatwave? (Q2) How does spatiotemporal variation in DO relate to macrophyte biomass and canopy height, and does macrophyte presence alter the DO response to an aquatic heatwave? We anticipated that greater macrophyte biomass and canopy height would be associated with stronger thermal stratification and greater differences in DO between surface and bottom waters. We also hypothesized that macrophyte presence would maintain cool water habitat and stable DO concentrations during an aquatic heatwave. Through the combination of our experiment, observations, and numerical modeling, we found that macrophyte structure can be a source of spatial and seasonal variation in the thermal and chemical environments of shallow systems. Greater macrophyte biomass and canopy height reduced the depth of water column warming during the aquatic heatwave; however, DO saturation fell sharply in both pond during the heatwave, regardless of macrophyte coverage. Through their physical structure, macrophytes play a pivotal role in mediating how small, vegetated waterbodies respond to the compounding stressors of eutrophication and heatwaves.

METHODS

Study Site and Field Measurements

We studied how macrophyte structure influences spatiotemporal variation in both the thermal and DO environments of shallow waterbodies using two experimental ponds at the Iowa State University Horticulture Research Station (42.110005, -93.580454) during the summer of 2020. The ponds are rectangular, relatively small (surface area 400 m^2 at the water line; Figure 1), and shallow (maximum depth 2 m and mean depth 0.8 m), with simple, bowl-shaped bathymetries. Water balance is driven solely from precipitation and evaporation as there are no surface inflows or outflows and the ponds are lined with bentonite to prevent groundwater interactions. As there is effectively no watershed for these ponds, we experimentally controlled all external inputs of nutrients. The ponds were initially filled with water from the research station's irrigation reservoir to seed natural phytoplankton and zooplankton communities. Early in the spring the ponds were stocked with yellow perch (*Perca flavescens*) and bluegill (*Lepomis macrochirus*) at roughly 20 kg ha^{-1} for both species, which is within the range of densities for temperature waterbodies (Carlander 1977; Schneider 1999). The macrophyte community in both ponds was composed of longleaf pond weed (*Potamogeton nodosus*; hereafter "floating-leaf") and leafy pondweed (*Potamogeton foliosus*; hereafter "submerged").

The external nutrient loading that occurs following large storm events was simulated by adding nitrogen and phosphorus to one of the experimental ponds (hereafter "nutrient addition pond") twice over the course of the summer. Nitrogen was added as ammonium nitrate (NH_4NO_3), and phosphorus was added as sodium phosphate monobasic dihydrate ($(NaH_2PO_4 \bullet (H_2O)_2$) in a ratio of 24N:1P. The first nutrient addition (day of year, DOY, 176) raised the mass of phosphorus in the pond by 3 percent, and the second addition (DOY 211) raised the mass by 5 percent. These increases are consistent with the expected nutrient loading from a large storm event (Vanni et al. 2001; Lürling et al. 2018). Nutrients were not added to the

other pond (hereafter “reference pond”). To assess and compare the effects of the nutrient additions on algal biomass, we measured chlorophyll-*a* concentrations daily at the deep site of each pond (Figure 1) using the Total Algae sensor as a part of the YSI ProDSS multiparameter sonde (Yellow Springs Instruments, Yellow Springs, Ohio USA). The sensor logged continuously and was slowly lowered through the water column. Surface concentrations of chlorophyll-*a* were averaged over 0-0.3 m depth in the water column. To minimize drift, the sensor was calibrated regularly against laboratory standards.

To monitor thermal structure and dynamics across the ponds, we deployed vertical strings of high frequency temperature sensors (HOBO 8K Pendant Temperature Data Logger) at three sites, aligned from the deep (2 m) to shallow (1.5 m) ends of each pond (Figure 1A). Temperature loggers were distributed throughout the water column every 0.25 m until 1.5 m deep and then every 0.5 to the bottom. Water temperature was logged every 30 minutes from May to August (DOY 143-233). We also took high frequency measurements of surface water DO concentration and saturation at the deep site of both ponds (miniDOT Clear Logger; logging every 30 minutes). In order to quantify the three-dimensional DO environment, manual profiles of DO concentration, DO saturation, and water temperature were taken weekly (13 sampling events total) on a grid of 18 sites across each study pond using a kayak (Figure 1). Measurements were taken in the late morning, between 10:00AM and 12:00PM. A continuous profile was logged at each site as the YSI ProDSS multiparameter sonde was slowly lowered through the water column.

We quantified variation in macrophyte structure over space and time by monitoring community composition, canopy height, and biomass from May to August (DOY 143-233) across the study ponds. Species presence-absence and canopy height were measured weekly at

the three sites established from the deep to shallow ends of the ponds (Figure 1). Canopy height was measured as the distance from the sediment-water interface to the top of the canopy. Water depth was also measured at these points so that canopy height could be expressed as a proportion of the water column. Macrophyte dry biomass was sampled every other week (6 sampling events total) on a grid of 18 sites across each pond where manual profiles were also taken (Figure 1A). Profiles were always taken before biomass was sampled. To collect a biomass sample, a two-side rake was lowered to the bottom and used to remove submersed and floating-leaf macrophytes from an approximately 0.4 m^2 area (Mikulyuk et al., 2011). All the above-sediment tissue was collected from the rake to determine dry biomass. Samples were dried at 60°C to a constant mass before weighing.

Hydrodynamic Modeling

In order to explore the mechanisms by which changes in macrophyte biomass and canopy height influence pond thermal structure, we applied a one-dimensional hydrodynamic model for vegetated waterbodies. Our model builds upon the one-dimensional, integral energy model by Herb and Stefan (2004) for heat transport in lakes with submersed macrophytes. Macrophytes are incorporated into the model through two key parameters: a light extinction coefficient due to macrophyte shading and a term for how macrophytes dissipate external turbulent kinetic energy based on their surface area and drag. Our contributions to the original model include adding convective overturn to address density instabilities over the diurnal cycles, a dynamic macrophyte growth and senescence boundary condition over time, dynamic light attenuation coefficient for water based on daily Secchi depth field data, and coding the model for use

through open-source software (R; see Appendix S1 for more details on model algorithms and additional citations).

For boundary conditions, the model requires an initial water temperature profile, timeseries of meteorological drivers (air temperature, relative humidity, air pressure, wind speed, and short-wave radiation), and waterbody hypsography (depth-area relationship). We determined the hypsography of the study ponds through manual calculations based off depth measurements from the profiles taken at 18 sites across each pond. We obtained the necessary meteorological data at an hourly timestep from a weather station located approximately 550 meters from the study ponds and maintained by the Iowa State University Soil Moisture Network (Iowa Environmental Mesonet, ISU Soil Moisture Network 2021). The initial temperature profile was supplied from a single reading from the temperature chain located at the middle site of the nutrient addition pond (Figure 1). Macrophyte data were incorporated into the model through weekly measurements of canopy height at the middle site of the nutrient addition pond as well as biomass density measurements taken every two weeks. Biomass density standardizes the measured macrophyte biomass to the volume of water sampled (g m^{-3}). We used the average biomass density from the two sampling sites closest to the middle site temperature sensors, in the central region of the pond.

The model was run on a 1-hour timestep from late May-August (DOY 143-241; 99 days total). The observed, high frequency water temperature profiles from the middle site of the nutrient addition pond were used to calibrate 9 model parameters (Table S1) and assess model fit (quantified as root mean square error, RMSE). For calibration, we applied the evolutionary Covariance Matrix Adaptation Evolution Strategy (CMA-ES) algorithm. Once the model was well-calibrated to the full duration of the observed field data, we manipulated the input

macrophyte data to simulate the effect of different macrophyte biomass and canopy dynamics on thermal structure (Table S2). Specifically, we tested the outcomes of no macrophytes present in the pond as well as a natural phenology (i.e., similar canopy height and biomass to the reference pond, rather than the early senescence observed in the nutrient addition pond) for bottom water temperatures and the vertical extent of water column warming during an aquatic heatwave. All modeling analyses were completed in R version 4.1.2 (R Core Team 2021) using the gotmtools (https://github.com/aemon-j/gotmtools), rLakeAnalyzer (Winslow et al. 2019), lubridate (Garrett and Wickham 2011), adagio (Borchers 2021), and tidyverse (Wickham et al. 2019) packages.

Statistical Methods

To inform our delineation of aquatic heatwaves in shallow ponds, we used the definition developed for marine heatwaves (Hobday et al. 2016) and applied more recently to estuarine environments (Tassone et al. 2021) and lakes (Woolway et al. 2021a). Following this definition, a heatwave occurs when daily mean water temperatures exceed the seasonal 90th percentile threshold for at least 5 days, without dropping below that threshold for 2 or more days. Since we did not have long-term data on summer water temperatures in the experimental ponds, we used temperature monitoring data for the study period only, but a more stringent definition of a heatwave threshold (i.e., 95th percentile). To determine the 95^{th} percentile surface water temperature for each pond, we used temperature loggers placed at 0 and 0.25 m at the middle at deep sites. For each site, we averaged the readings from these surface loggers, calculated a daily mean, and then averaged values from the middle and deep sites. These steps produced a daily mean surface water temperature for each pond, which we used to calculate the 95^{th} percentile threshold. We then identified any days in which the daily mean surface water temperature

exceeded this threshold. A period with at least five days above this threshold was classified an aquatic heatwave.

To visualize pond thermal structure from our high frequency water temperature data, we used a linear interpolation to estimate temperature for depths at which we either did not place sensors (1.75m deep for both ponds) or for depths at which sensors ceased to function during the summer (1m at the middle and deep sites of the nutrient addition pond, 0.25-0.75m at the shallow site of the nutrient addition pond, and 0.25m at the middle site of the reference pond). The interpolated values were used solely for visualization. Only empirical measurements of water temperature were used in the model and to calculate indices of pond thermal structure (i.e., thermocline depth and Schmidt's stability). Thermocline depth and Schmidt's stability index were calculated using the rLakeAnalyzer package. (Winslow et al. 2019). We defined surface water temperature as the average from the 0 and 0.25m sensors. We used the deepest sensors (2m at the middle and deep sites, 1.5m at the shallow sites) for measurements of bottom water temperature.

In order to compare macrophyte biomass between the study ponds, we calculated the mean macrophyte biomass across 18 sampling sites for each sampling event. However, we weighted this average so that sampling sites around the perimeter of the pond (n=14) had the same weight was sites in the interior or the pond (n=4; Figure 1) so that the mean value would not be biased by water depth. Weighted, pond-averaged macrophyte biomass values were used to plot seasonal changes and explore the relationship between biomass and water column thermal stability. We also standardized macrophyte canopy height as a percent of the water column depth for each sampling site and event to aid comparisons between shallow and deeper sites.

To analyze the manual DO profiles, we first determined that there were no instances of mid-depth DO maximum for any sites or sampling events. The vertical distribution of DO saturation was either uniform, highest in the surface waters, or highest in the bottom waters depending on the site and time of year (Figure S1). Therefore, we focused on DO dynamics in the surface and bottom layers of ponds by averaging values from 0-0.25 m and 0.25 m from the sediment-water interface respectively. Surface and bottom water DO values were used to explore temporal variation, calculate the difference between surface and bottom DO, and quantify variation over space and time. We used coefficients of variation to quantify temporal and spatial variation in surface and bottom water DO saturation. Specifically, spatial variation was defined as the coefficient of variation for DO for each sampling day within each pond, so variation was due to differences among the 18 sampling sites (Figure 1), standardized by the pond-mean for that day. Temporal variation was calculated based on the coefficient of variation in DO for each sampling site, so variation was due to differences in DO over time, standardized by the summer mean DO saturation for that site.

A generalized additive model (GAM) was used to smooth the daily time series of chlorophyll concentrations and weekly time series of DO saturation to highlight differences in trends over time between the nutrient addition and reference pond. All statistical analyses were completed in R version 4.1.2 (R Core Team 2021) using the mgcv (Wood 2017), rLakeAnalyzer (Winslow et al. 2019), lubridate (Garrett and Wickham 2011), and tidyverse (Wickham et al. 2019) packages.

RESULTS

Experimental Context and Environmental Stressors

Chlorophyll-*a* concentrations were variable in both ponds throughout the experiment, but there was a clear increase in chlorophyll-*a* following the sequential additions of nutrients in the experimental pond (Figure 2A). Early in the season, chlorophyll-*a* concentrations were low in the reference pond, likely due to high *Daphnia sp.* biomass (Butts et al., *in prep*). Following this early clear-water phase and prior to the experimental nutrient additions, chlorophyll-*a* concentrations were similarly low in both ponds (DOY 160). Nutrient additions on DOY 176 and 211 resulted in chlorophyll-*a* concentrations 2-3 times higher in the nutrient amended pond compared to the reference pond. Heightened chlorophyll-*a* concentrations in the nutrient addition pond are indicative of higher algal biomass and thus phytoplankton-associated turbidity, likely resulting in reduced light availability in the nutrient addition pond.

Both ponds experienced an aquatic heatwave from DOY 185-190 (Figure 2B). During this period, mean daily surface water temperatures exceeded the seasonal 95th percentile in each pond (greater than 29.8 °C in the nutrient addition pond and 30.6 °C in the reference pond). Maximum daily surface water temperatures ranged from 34.5-37.1 °C in the nutrient addition pond and 33.7-38.6 °C in the reference pond. Although both ponds had brief periods of high surface water temperatures at other points throughout the summer, DOY 185-190 was the only period where high temperatures were sustained long enough to qualify as an aquatic heatwave. The heatwave began 9 days after the first nutrient pulse, creating multiple stressors (i.e., reduced light availability and prolonged heat stress) for macrophytes in the nutrient addition pond.

Spatiotemporal patterns in macrophyte biomass differed between the ponds and macrophyte growth forms (Figure 2C, 3). The floating-leaf species was largely limited to a ring around the shallower edges of the ponds where the floating leaves could easily reach the surface. The submerged species was present across a range of depths but reached the highest biomass in

the deeper, central region of each pond. In the reference pond, macrophytes followed expected phenology with increasing biomass through late summer and then senescence of both growth forms beginning in early autumn (Figure 2C, 3). The aquatic heatwave did not affect macrophyte biomass or assembly in the reference pond. However, in the nutrient addition pond, submerged macrophytes growing in 1.75 to 2 m of water quickly began to senesce following the initial nutrient addition and heatwave such that no plants were present in the deepest areas of the nutrient addition pond 9 days (DOY 199) after the heatwave and the middle site of the pond 23 days (DOY 213) after the heatwave ended (Figure 3). Early senescence of submersed macrophytes in the nutrient addition pond resulted in rapid declines in both biomass (Figure 2C) and canopy height (Figure 4). Both submersed and floating-leaf plants persisted in shallow water around the edge of the pond through the end of the summer. The early senescence of submersed macrophytes in deeper regions of the nutrient addition pond likely arose from light limitation following the nutrient pulse, compounded by sustained heat stress during the aquatic heatwave.

Spatiotemporal Variation in Pond Thermal Structure

Both ponds experienced intermittent thermal stratification during the study period and similar spatial patterns of stratification over depth (Figure 4). Early in the summer, both ponds were cool and isothermal. As surface waters began to warm, the middle and deep sites of both ponds began to stratify while the shallow sites remained fairly well-mixed. At the center of the ponds, a stable thermocline between 1-1.5 m depth was observed in the reference pond between DOY 155-161, and almost constantly between DOY 168-210 (Figure S2A), while the thermocline in the nutrient addition pond was more intermittent (DOY 157-159, 170-174, and 178-192; Figure S2B). When present, pond thermoclines cooled and deepened slightly (0.05-0.1

m) during the night, indicating nighttime convective cooling and mixing in the surface layer. During periods of thermal stratification, differences between surface and bottom water temperatures ranged from 4.3 to 11.5 °C (mean 8.1°C) in the reference pond and 4.5 to 10.2 °C (mean 7.3 °C) in the nutrient addition pond (Figure S3).

Seasonal patterns in thermal structure differed between the ponds, and these dissimilarities were related to differences in the timing of macrophyte senescence (Figure 4). There was a prolonged period of stable thermal stratification from DOY 180-210 in the reference pond, with only brief instability between DOY 198-199. A stable thermocline set-up in the nutrient addition pond around the same time (DOY 178); however, stratification began to break down approximately 18 days earlier (DOY 192) than in the reference pond (Figure S2). The timing of destratification in the nutrient addition pond coincides with declines in macrophyte biomass (Figure 3) and canopy height (Figure 4) in the center of the pond. Destratification in the reference pond also followed patterns of biomass senescence and loss of canopy height, although this did not occur until later in the summer in this pond. Temporal patterns in the Schmidt's stability index reveals that the thermal structure of the ponds began to diverge soon after the initial nutrient addition, with relatively greater stability in the reference pond (Figure S4). Differences in water column stability between the ponds were related to macrophyte biomass, with declines in Schmidt's stability in the nutrient addition pond coinciding with declines in mean macrophyte biomass across the pond (Figure 2C). Despite this temporal coherence, there was not a strong statistical relationship between Schmidt's stability and either macrophyte biomass or macrophyte canopy height (Figure S5). Overall, the observational data revealed strong seasonal patterns in thermal structure coinciding with the timing of macrophyte senescence, which was driven by the compounding stress of eutrophication and an aquatic

heatwave in the nutrient addition pond and typical seasonal senescence in the reference pond. The declines in canopy cover and biomass were associated with increased thermal mixing and warmer bottom water temperatures, especially in the nutrient addition pond.

Thermal Structure During an Aquatic Heatwave

During the aquatic heatwave (DOY 185-190), both ponds experienced a dramatic increase in surface water temperatures and water column thermal stability (Figure 2B, Figure 4, Figure S4). However, there was a stark difference in the response of bottom water temperatures at the deep and middle sites between the ponds (Figure 5). During the aquatic heatwave, bottom water temperature remained consistent at both the deep and middle sites of the reference pond. The daily mean bottom water temperature increased by only 0.2 °C at both sites. In contrast, bottom water temperatures in the nutrient addition pond did respond to the heat wave, increasing by 1.3 °C and 1.4 °C at the deep and middle sites, respectively. At the shallow site in both ponds bottom water temperatures increased 1-1.3 °C during the heatwave. The different response of bottom water temperature to the aquatic heatwave related to differences in macrophyte biomass between the two ponds. At the time of the aquatic heatwave, macrophyte biomass (Figure 2C) and canopy height (Figure 4) were greater in the reference pond because submersed macrophytes in the center of the nutrient addition pond began to senesce following the first nutrient pulse (DOY 176; Figure 3). Overall, bottom waters in the nutrient addition pond warmed over the course of the heatwave while cooler bottom water temperatures were maintained in the reference pond, despite significant warming in the surface layers.

Mechanisms of Macrophyte Control of Thermal Structure

We used a one-dimensional hydrodynamic model to illuminate the mechanistic relationship between macrophytes and pond thermal structure and test how macrophyte presence mediates the degree to which bottom water temperatures warm in response to an aquatic heatwave. We based our model on the middle site of the nutrient addition pond, where macrophytes began to senesce around DOY 200. The model projections were fairly consistent with the observed temperature profiles (mean RMSE 2.46 °C over 7 discrete depths; Figure S6). Error was greatest in the surface waters (RMSE 3.15 °C), where the model did not capture the full range of observed diel oscillations in water temperature, especially early in the season. The model underpredicted water temperature in the surface 1.25m of the water column in early summer and overpredicted temperatures at 1.5 m in the middle of the summer. However, overall, the model captured diel and seasonal trends in water temperature, and there was a good representation of bottom temperatures (2 m; RMSE 1.15 °C).

We simulated water column thermal structure under contrasting scenarios of macrophyte density (Figure 6). Specifically, we tested the temperature profile response to an aquatic heatwave had there been (1) no macrophytes present in the pond versus (2) macrophyte biomass and canopy height values that aligned with the natural phenology we observed in the reference pond (Table S2). Under the natural phenology scenario, bottom water temperatures increased by 0.88 °C over the course of the aquatic heatwave and remained below 25 °C through the rest of the summer (Figure 6B, C). In contrast, the scenario without any macrophyte coverage resulted in a 1.68 °C increase in bottom water temperatures during the heatwave and much higher maximum water temperatures (28.3 °C) later in the summer (Figure 6A, C). The model simulations demonstrate that greater macrophyte density and canopy height result in cooler

bottom water temperatures, even during aquatic heatwave, and that no macrophyte coverage is associated with warming deeper in the water column and higher water temperatures overall.

Spatiotemporal Variation in Dissolved Oxygen

In both ponds, DO varied across sites, vertically in the water column, and over time. Surface waters were supersaturated with DO early in the summer (Figure 6A). In the reference pond, surface DO declined through DOY 170, remained fairly stable, and then declined again during the aquatic heatwave (DOY 185-190). In the nutrient addition pond, surface DO saturation was similar to the reference pond before the nutrient addition. Surface DO then decreased after the nutrient addition and through the aquatic heatwave. After the aquatic heatwave, surface DO in both ponds was generally below saturation, with increased instances of DO saturation below 25%. Weekly DO profiles captured broad seasonal trends in surface DO saturation as similar temporal patterns were observed between weekly and high-frequency values (Figure S7A, 6A). Bottom water DO saturation mirrored the seasonal pattern in surface DO (Figure 6B). For both ponds the difference in DO saturation between surface and bottom waters was most pronounced early in the season (reference pond range -87.1 to 23.3%; nutrient addition pond range -56.8 to 58.8%). Surface and bottom water DO saturation became more similar throughout the summer, especially following the aquatic heatwave (reference pond range -2.1 to 17.0%; nutrient addition pond range -0.3 to 12.2%; Figure S7B).

For both surface and bottom water DO saturation, temporal variation on a seasonal scale was greater than spatial variation across the ponds (Table 1). The coefficient of variation at a given site in the pond over time was 3.6-5.2 times greater than the variation among sites on a given sampling day. The magnitude of temporal versus spatial variation was similar between

ponds. Seasonal patterns in DO saturation followed some trends with declining macrophyte biomass in the center of the pond following the nutrient addition; however, the aquatic heatwave had the most pronounced impact on seasonal DO patterns. There was not a significant relationship between any DO measures (surface, bottom saturation, and the difference between surface and bottom saturation) and either macrophyte biomass or canopy height (Figure S8). The strong effect of the aquatic heatwave on DO saturation may have masked a relationship between macrophyte growth versus senescence and DO concentrations (Figure S9).

DISCUSSION

We leveraged an ecosystem experiment and complimentary hydrodynamic model to test macrophyte response to compounding stressors (i.e., stochastic external nutrient loading and aquatic heatwaves) and evaluate the consequences of stress-induced macrophyte senescence for the physicochemical environment in two shallow, vegetated ponds. The type and severity of environmental stressors differed between the study ponds, producing distinct temporal patterns in macrophyte assembly and coverage. In the reference pond, both submersed and floating-leaf macrophytes followed the expected phenology of spring emergence, summer growth, and then senescence beginning in late summer. This natural phenology may be attributed to the lack of severe physiological stressors in the reference pond. Although this pond did experience an aquatic heatwave, dense macrophyte beds limited the depth of water column warming and maintained stable bottom water temperatures. In contrast, submersed macrophytes in the nutrient addition pond began to senesce in mid-summer after the first experimental nutrient pulse and continuing after the heatwave. This early senescence was dominated by submersed macrophytes in the deeper, central region of pond, suggesting that light limitation from phytoplankton shading

was a key stressor (Scheffer et al. 1993; Short et al. 1995; Phillips et al. 2016). Light limitation may have been exacerbated by heat stress, which was likely more acute in the nutrient addition pond as declining macrophyte biomass following the nutrient pulse allowed temperatures to rise throughout the water column rather than just the surface layers. Early senescence of submersed macrophytes in the nutrient addition pond as a result of compounding stressors altered the thermal environment and DO saturation in relation to the reference pond.

Thermal Structure

On a seasonal scale, we observed strong temporal coherence between macrophyte growth and senescence and pond thermal structure. Both ponds began to experience intermittent thermal stratification in early summer, once macrophytes had grown to fill the majority of the water column. This threshold is consistent with the expectation that canopy-forming macrophyte beds may induce diurnal stratification once they occupy at least 50 percent of the water column (Vilas et al. 2017). By mid-summer we observed strong thermal stratification, characterized by large differences (around 10°C) between surface and bottom water temperatures, comparable to stratification in other small, vegetated ponds (Andersen et al. 2017a; Vilas et al. 2017). However, in other studies, macrophyte-induced stratification followed diel cycles, with daytime stratification and nighttime overturn due to convective mixing (Martinsen et al. 2019; Sand-Jensen et al. 2019), which can move through macrophyte structure more readily than external turbulent mixing (Herb and Stefan 2005; Andersen et al. 2017b). Although we observed nighttime convective cooling and mixing in the surface of the ponds during periods of macrophyte-induced stratification, convective cooling did not mix the entire the water column. Stable thermal stratification began to break down in both study ponds during macrophyte

senescence. Declining macrophyte canopy height and biomass removed structural barriers that had previously attenuated incoming solar radiation and dissipated wind-driven turbulent mixing (Herb and Stefan 2004), allowing the warm, mixed surface layer to deepen and eventually mix the entire water column. However, the timing of both destratification and macrophyte senescence differed between the study ponds, driven by compounding stressors in the nutrient addition pond and typical seasonal senescence in the reference pond. In the nutrient addition pond, destratification and consistent water column mixing began when macrophyte biomass and canopy height in the center of the pond began to decline in response to phytoplankton-shading following the experimental nutrient pulse and the aquatic heatwave.

Macrophyte presence mediated how pond thermal structure responded to an aquatic heatwave by restricting vertical heat transfer and maintaining cooler bottom water temperatures. Both study ponds saw high surface water temperatures during the aquatic heatwave. However, as anticipated, the depth of water column warming and overall change in bottom water temperature differed between the ponds as a result of differences in macrophyte coverage. At the time of the heatwave, macrophyte canopy height and biomass were rapidly declining in center of the nutrient addition pond due to phytoplankton-shading. In the reference pond, macrophyte biomass was still increasing and the canopy reached to fill over 75 percent of the water column. During the heatwave, a layer of cooler water between 0.25 and 0.5 m thick remained in the reference pond, with only subtle increases in daily mean temperature (+0.2 °C). In contrast, the nutrient addition pond saw increasing water temperatures throughout the water column, including a 1.3°C increase in daily mean temperatures in the deepest waters of the pond over the 5-day heatwave. Given the observed differences between the study ponds, it is very likely that macrophyte structure played a pivotal role in mediating the depth and degree of water column warming during the aquatic

heatwave. Nevertheless, thermal structure in small waterbodies arises from complex interactions between waterbody features and external forces (Herb and Stefan 2004; Branco and Torgersen 2009). In order to explicitly test the mechanisms underpinning the differences we saw between the study ponds and evaluate the role of macrophytes, we used a hydrodynamic model for heat transport in vegetated waterbodies and simulated water column thermal structure during a heatwave under contrasting scenarios of macrophyte density.

The model results support our field observations and demonstrate that macrophytes structure the thermal environment in shallow ponds through vertical attenuation of both light and turbulent kinetic energy. Simulations of seasonal patterns in pond thermal structure under variable macrophyte density revealed that macrophyte presence reduces the depth and degree of water column warming both during and after an aquatic heatwave and maintains cooler bottom water temperatures throughout the course of the summer. Our experimental observations and model simulations provide evidence that macrophytes may buffer small waterbodies from brief aquatic heatwaves, at least with the vertical extent of warming in the water column. As aquatic heatwaves become more widespread and frequent, heatwaves in small waterbodies are expected to be shorter but more intense compared to larger waters (i.e., due to lower thermal inertia; Woolway et al. 2021a; Polazzo et al. 2021; Woolway et al. 2022). Our findings suggest that macrophytes can mediate the intensity of brief aquatic heatwaves in small lakes and ponds. As such, managing for robust macrophyte communities is a potential tool for mitigating heatwave effects in small waterbodies and promoting thermal heterogeneity to support other aquatic organisms (Carpenter and Lodge 1986; Till et al. 2019).

Our hydrodynamic model enhances a conceptual and analytical framework for incorporating biological structure into one-dimensional heat transport models (Herb and Stefan

2004). Overall, there was good agreement between the model predications and the observed temperature profiles. The largest discrepancies between the model output and field data occurred in early summer when the model underpredicted temperatures in the surface waters and in mid-summer when the model overpredicted the temperature at 1.5 m. These periods coincide with times of rapid and dramatic change in macrophyte biomass and canopy height due to growth (early summer) and stress-induced senescence (mid-summer). It is possible that the temporal resolution of our field data during these times was insufficient to accurately capture biological dynamics in the pond for the model input. Canopy height was measured weekly while biomass was collected every two weeks. More frequent observations could have fit the macrophyte input data closer to conditions captured by the high frequency temperature profiles. Additionally, other one-dimensional heat transport models (i.e., Simstrat, GOTM, GLM) have been shown to have greater error during extreme meteorological events, including atmospheric heatwaves (Mesman et al. 2020). This tendency could explain some of the disparities between model output and field data during a brief period of high air temperatures around DOY 155, reflected in rapid increases in water temperature in the first 1.25 m of the profile. Our model would benefit from additional testing across a variety of vegetated waterbodies to inform best practices for applying this approach in other waters. However, our findings indicate that macrophytes should be incorporated into hydrodynamic models for vegetated systems, and our modeling approach provides an example of how to do so.

Dissolved Oxygen

Within both study ponds, DO saturation varied on a seasonal scale and responded to the experimental nutrient pulse as well as the aquatic heatwave. We had anticipated greater spatial

variation in DO saturation within each pond as a result of macrophyte-induced thermal stratification. This expectation was based on evidence of steep vertical gradients of DO and dissolved inorganic carbon in other shallow, vegetated waterbodies (Andersen et al. 2017a; Vilas et al. 2017). However, most of the DO profiles were uniform with depth, suggesting that the balance of processes releasing and consuming oxygen (e.g., gross primary production versus respiration) were similar throughout the ponds or that DO was able to diffuse readily throughout the water column. Temporal patterns in surface and bottom water DO saturation were connected to the compounding environmental stressors, beginning with the initial experimental nutrient addition. Following the first nutrient pulse, DO remained stable in the reference pond but declined below 100 percent saturation in the experimental pond. We might have expected to see increased DO after the nutrient addition as a result of enhanced phytoplankton production, but the observed decline in DO suggests that ecosystem respiration was stimulated by the added nutrients, outweighing any increases in gross primary production. Stress-induced macrophyte senescence likely contributed to this pattern through reduced macrophyte photosynthesis and dramatic increases in macrophyte necromass, the decomposition of which would consume oxygen. Although we observed differences in DO saturation between the ponds after the nutrient addition, the most pronounced temporal shift in DO occurring following the aquatic heatwave.

During the heatwave, DO saturation feel sharply in both ponds and remained depressed through the remainder of the study period. We had expected macrophyte structure to maintain stable DO saturation in the bottom waters of the reference pond; however, both ponds responded similarly, regardless of the differences in macrophyte coverage and thermal structure. Our observations support findings from freshwater and marine systems that aquatic heatwaves are associated with declines in DO due to reduced gas solubility and increased respiration rates (Ali

et al. 2016; Brauko et al. 2020; Tassone et al. 2021). Reduced DO availability has consequences for nutrient and carbon cycling as well as greenhouse gas production. For example, anoxia within the sediment profile can mobilize phosphorus from redox-sensitive minerals (i.e., anaerobic internal phosphorus loading; Orihel et al. 2017). Anoxic conditions in the sediments also promote denitrification and methanogenesis, two microbial processes that can produce potent greenhouse gases (i.e., nitrous oxide and methane respectively; Fonseca et al. 2017; Ming et al. 2022). Both denitrification and methanogenesis require organic carbon substrate, which was augmented by macrophyte necromass in the nutrient addition pond (Boon et al. 1995; Bastviken et al. 2005; Deng et al. 2020). Although both ponds likely experienced shifts in other elemental cycles as a result of reduced DO saturation during the aquatic heatwave, the consequences for greenhouse gas production were likely more pronounced in the nutrient addition pond due to early macrophyte senescence increasing organic matter inputs to the sediments. This difference between the study ponds highlights the complex interactions that may arise from compounding stressors in lentic ecosystems.

Conclusions

Lake heatwaves are becoming more frequent and are likely to co-occur with chlorophyll-*a* maxima (i.e., algal blooms; Woolway et al. 2021b). As such, there is a growing need to understand and forecast how lentic ecosystems will respond to compound, extreme events. Our findings illuminate the role that submersed macrophytes play in mediating ecosystem response to multiple stressors. Overall, dense macrophyte structure can buffer small waterbodies from brief aquatic heatwaves by restricting vertical heat transport. However, declines in DO saturation are expected during heatwaves, regardless of macrophyte coverage. Our findings also reinforce that

small lakes and ponds are vulnerable to nutrient loading and temperature extremes. Given the prevalence and importance of small waterbodies for biodiversity and biogeochemical processing, it is essential that we continue to build our mechanistic understanding of the effects of compound, extreme events in these ecosystems and the role that macrophytes can play in ameliorating stressors.

Acknowledgements

Albright was supported by the National Science Foundation Graduate Research Fellowship Program under Grant No. DGE-1747503. Any opinions, findings, and conclusions or recommendations expressed in this material are those of the authors and do not necessarily reflect the views of the National Science Foundation. Support was also provided by the Graduate School and the Office of the Vice Chancellor for Research and Graduate Education at the University of Wisconsin-Madison with funding from the Wisconsin Alumni Research Foundation. Wilkinson was supported by the National Science Foundation Division of Environmental Biology grant #1942256 and #2200391.

REFERENCES

1. Ali, S., P.K. Mishra, A. Islam, and N.M. Alam. 2016. Simulation of water temperature in a small pond using parametric statistical models: Implications of climate warming. J. Environ. Eng. 143(3): 04015085, doi: 10.1061/(ASCE)EE.1943-7870.0001050
2. Andersen, M.R., T. Kragh, and K. Sand-Jensen. 2017a. Extreme diel dissolved oxygen and carbon cycles in shallow vegetated lakes. Proc. Biol. Sci. 284: 20171427, doi: 10.1098/rspb.2017.1427
3. Andersen, M.R., K. Sand-Jensen, R.I. Woolway, I.D. and Jones. 2017b. Profound daily vertical stratification and mixing in a small, shallow, wind-exposed lake with submerged macrophytes. Aquat. Sci. 79: 395-406, doi: 10.1007/s00027-016-0505-0
4. Bastviken, S.K., P.G. Eriksson, A. Premrov, and K. Tonderski. 2005. Potential denitrification in wetland sediments with different plant species detritus. Ecol. Eng. 24(2): 183-190, doi: 10.1016/j.ecoleng.2005.04.013
5. Battin, T. J., S. Luyssaert, L.A. Kaplan, A.K. Aufdenkampe, A. Richter, and L.J. Tranvik. 2009. The boundless carbon cycle. Nat. Geosci. 2: 598-600, doi: 10.1038/ngeo618
6. Bertani, I., R. Primicerio., and G. Rossetti. 2016. Extreme climatic event triggers a lake regime shift that propagates across multiple trophic levels. Ecosystems. 19(1): 16–31, doi:10.1007/s10021-015-9914-5
7. Biggs, J., S. von Fumetti, and M. Kelly-Quinn. 2017. The importance of small waterbodies for biodiversity and ecosystem services: implications for policy makers. Hydrobiologia. 793: 3-39, doi: 10.1007/s10750-016-3007-0
8. Boon, P.I., and A. Mitchell. 1995. Methanogenesis in the sediments of an Australian freshwater wetland: Comparison with aerobic decay, and factors controlling methanogenesis. FEMS Microbiol. Ecol. 18(3): 175-190, doi: 10.1016/0168-6496(95)00053-5
9. Borchers, H.W. 2021. adagio: Discrete and Global Optimization Routines. R package version 0.8.4. https://CRAN.R-project.org/package=adagio
10. Branco, B.F., and T. Torgersen. 2009. Predicting the onset of thermal stratification in shallow inland waterbodies. 71(1): 65-79, doi: 10.1007/s00027-009-8063-3
11. Brauko, K.M., et al. 2020. Marine Heatwaves, Sewage and Eutrophication Combine to Trigger Deoxygenation and Biodiversity Loss: A SW Atlantic Case Study. Front. Mar. Sci. 7, doi: 10.3389/fmars.2020.590258
12. Carlander, K.D. 1977. Biomass, Production, and Yields of Walleye (Stizostedion vitreum vitreum) and Yellow Perch (Perca flavescens) in North American Lakes. J. Fish. Res. Board Can. 34(10): 1602-1612, doi: 10.1139/f77-225

13. Carpenter, S.R., and D.M. Lodge. 1986. Effects of submersed macrophytes on ecosystem processes. Aquat. Bot. 26: 341-370, doi: 10.1016/0304-3770(86)90031-8

14. Cole, J.J., et al. 2007. Plumbing the global carbon cycle: Integrating inland waters into the terrestrial carbon budget. Ecosystems. 10(1): 171-184, doi: 10.1007/s10021-006-9013-8

15. DeMarte, J.A., and R.T. Hartman. 1974. Studies of Absorption of ^{32}P, ^{59}Fe, and ^{45}Ca by Water-Milfoil (Myriophyllum Exalbescens Fernald). Ecology, 55(1): 188-194, doi: 10.2307/1934635

16. Deng, H.G., J. Zhang, J.J. Wu, X. Yao, and L.W. Yang. 2020. Biological denitrification in a macrophytic lake: implications for macrophytes-dominated lake management in the north of China. Environ. Sci. Pollut. Res. 27(34): 42460-42471, doi: 10.1007/s11356-020-10230-3

17. Downing, J. 2010. Emerging global role of small lakes and ponds: little things mean a lot. Limnetica. 29(10): 9-24.

18. Fonseca, A.L.D., C.C. Marinho, and F.D. Esteves. 2017. Potential methane production associated with aquatic macrophytes detritus in a tropical coastal lagoon. Wetlands. 37(4): 763-771, doi: 10.1007/s13157-017-0912-6

19. Hao, B., A.F. Roejkjaer, H. Wu, Y. Cao, E. Jeppesen, and W. Li. 2018. Responses of primary producers in shallow lakes to elevated temperature: a mesocosm experiment during the growing season of Potamogeton crispus. Aquat. Sci. 80: 34, doi: 10.1007/s00027-018-0585-0

20. Hansson, L.-A., M.K. Ekvall., L. He, Z. Li, M. Svensson, P. Urrutia-Cordero, and H. Zhang. 2020. Different climate scenarios alter dominance patterns among aquatic primary producers in temperate systems. Limnol. Oceanogr. 65(10): 2328–2336, doi:10.1002/lno.11455

21. Herb, W.R., and H.G. Stefan. 2004. Temperature stratification and mixing dynamics in a shallow lake with submersed macrophytes. Lake Reserv. Manag. 20(4): 296-308, doi: 10.1080/07438140409354159

22. Herb, W.R., and H.G. Stefan. 2005. Model for Wind-Driven Vertical Mixing in a Shallow Lake with Submersed Macrophytes. J. Hydraul. Eng. 131(6): 488-496, doi: 10.1061/(ASCE)0733-9429(2005)131:6(488)

23. Hobday, A.J., et al. 2016. A hierarchical approach to defining marine heatwaves. Prog. Oceanogr. 141: 227-238, doi: 10.1016/j.pocean.2015.12.014

24. Holgerson, M.A., and P. A. Raymond. 2016. Large contribution to inland water CO_2 and CH_4 emissions from very small ponds. Nat. Geosci. 9: 222-226, doi: 10.1038/ngeo2654

25. Hughes, T.P., et al. 2017. Global warming and recurrent mass bleaching of corals. Nature. 543: 373-377, doi: 10.1038/nature21707

26. Iowa Environmental Mesonet. 2020. Iowa State University Soil Moisture Network. https://mesonet.agron.iastate.edu/agclimate/hist/hourly.php. Accessed 15 November 2021.

27. Li, Z., L. He, H. Zhang, P. Urrutia-Cordero, M.K. Ekvall, J. Hollander, and L.-A. Hansson. 2017. Climate warming and heat waves affect reproductive strategies and interactions between submerged macrophytes. Glob. Chang. Biol. 23: 108–116, doi: 10.1111/gcb.13405

28. Licci, S., H. Nepf, C. Delolme, P. Marmonier, T.J. Bouma, and S. Puijalon. 2019. The role of patch size in ecosystem engineering capacity: a case study of aquatic vegetation. Aquat. Sci. 81(3), doi: 10.1007/s00027-019-0635-2.

29. Lürling, M., M. M. Mello, F. van Oosterhout, L. de S. Domis, and M. M. Marinho. 2018. Response of natural cyanobacteria and algae assemblages to a nutrient pulse and elevated temperature. Front. Microbiol. 9: 1–14, doi:10.3389/fmicb.2018.01851

30. Martinsen, K.T., M.R. Andersen, and K. Sand-Jensen. 2019. Water temperature dynamics and the prevalence of daytime stratification in small temperate shallow lakes. Hydrobiologia. 826: 247–262, doi:10.1007/s10750-018-3737-2

31. Mesman, J.P., et al. 2020. Performance of one-dimensional hydrodynamic lake models during short-term extreme weather events. Environ. Modell. Softw. 133: 104852, doi: 10.1016/j.envsoft.2020.104852

32. Ming, N., X. Liang, L.J. Hou, W.P. Li, and C.Q. He. 2022. Submerged macrophytes regulate diurnal nitrous oxide emissions from a shallow eutrophic lake: A case study of Lake Wuliangsuhai in the temperate arid region of China. Sci. Total. Environ. 811: 152451, doi: 10.1016/j.scitotenv.2021.152451

33. Olesen, B., and T.V. Madsen. 2001. Growth and physiological acclimation to temperature and inorganic carbon availability by two submerged aquatic macrophyte species, Callitriche cophocarpa and Elodea canadensis. Funct. Ecol. 14(2): 252-260, doi: 10.1046/j.1365-2435.2000.00412.x

34. Oliver, E.C.J., et al. 2018. Longer and more frequent marine heatwaves over the past century. Nat. Commun. 9, 1324, doi:10.1038/s41467-018-03732-9

35. Orihel, D.M., H.M. Baulch, N.J. Casson, R.L. North, C.T. Parsons, D.C.M Seckar, and J.J. Venkiteswaran. 2017. Internal phosphorus loading in Canadian fresh waters: a critical review and data analysis. Can. J. Fish. Aquat. Sci. 74: 2005-2029, doi: 10.1139/cjfas-2016-0500

36. Peacock, M., et al. 2021. Small artificial waterbodies are widespread and persistent emitters of methane and carbon dioxide. Glob. Chang. Biol. 27(20): 5109-5123, doi: 10.1111/gcb.15762

37. Phillips, G., N. Willby, and B. Moss. 2016. Submerged macrophyte decline in shallow lakes: What have we learnt in the last forty years? Aquat. Bot. 135: 37-45, doi: 10.1016/j.aquabot.2016.04.004

38. Polazzo, F., S.K. Roth, M. Hermann, A. Mangold-Döring, A. Rico, A. Sobek, P.J. Van den Brink, M.C. Jackson. 2022. Combined effects of heatwaves and micropollutants on freshwater ecosystems: Towards an integrated assessment of extreme events in multiple stressors research. Glob. Chang. Biol. 28: 1248-1267, doi 10.1111/gcb.15971

39. Sand-Jensen, K., M.R. Andersen, K.T. Martinsen, J. Borum, E. Kristensen, and T. Kragh. 2019. Shallow plant-dominated lakes – extreme environmental variability, carbon cycling and ecological species challenges. Ann. Bot. 124: 35-366. doi: 10.1093/aob/mcz084.

40. Scheffer, M., et al. 2006. Small habitat size and isolation can promote species richness: second-order effects on biodiversity in shallow lakes and ponds. Oikos. 112(1): 227-231, doi:10.1111/j.0030-1299.2006.14145.x

41. Scheffer, M., S.H. Hosper, M.L. Meijer, B. Moss, and E. Jeppesen. 1993. Alternative equilibria in shallow lakes. Trends. Ecol. Evol. 8 (8): 275-279, doi: 10.1016/0169-5347(93)90254-M

42. Schneider, J.C. 1999. Dynamics of quality bluegill populations in two Michigan lakes with dense vegetation. N. Am. J. Fish. Manage. 19(1): 97-109, doi: 10.1577/1548-8675(1999)019<0097:DOQBPI>2.0.CO;2

43. Short, F.T., D.M. Burdick, and J.E. Kaldy III. 1995. Mesocosm experiments quantify the effects of eutrophication on eelgrass, Zostera marina. Limnol. Oceanogr. 40(4): 740-749, doi: 10.4319/lo.1995.40.4.0740

44. Strydom, S., et al. 2020. Too hot to handle: Unprecedented seagrass death driven by marine heatwave in a World Heritage Area. Glob. Change. Biol. 26(6): 3525-3538, doi: 10.1111/gcb.15065

45. Szabo, S., M. Scheffer, R. Roijackers, B. Waluto, M. Braun, P.T. Nagy, G. Borics, and L. Zambrano. 2010. Strong growth limitation of a floating plant (Lemna gibba) by the submerged macrophyte (Elodea nuttallii) under laboratory conditions. Freshwater. Biol. 55(3): 681-690, doi: 10.1111/j.1365-2427.2009.02308.x

46. Tassone, S.J., A.F. Besterman, C.D. Buelo, J.A. Walter, and M.L. Pace. 2021. Co-occurrence of Aquatic Heatwaves with Atmospheric Heatwaves, Low Dissolved Oxygen, and Low pH Events in Estuarine Ecosystems. Estuar. Coast. 45: 707-720, doi:10.1007/s12237-021-01009-x

47. Taylor, S., P.J. Gilbert, D.A. Cooke, M.E. Deary, and M.J. Jeffries. 2019. High carbon burial rates by small ponds in the landscape. Front. Ecol. Environ. 17(1): 25-31, doi: 10.1002/fee.1988

48. Till, A., A.L. Rypel, A. Bray, and S.B. Fey. 2019. Fish die-offs are concurrent with thermal extremes in north temperate lakes. Nat. Clim. Chang. 9, 637–641, doi: 10.1038/s41558-019-0520-y

49. Twilley, R.R., M.M., Brinson, and G.J. Davis. 1977. Phosphorus absorption, translocation, and secretion in Nuphar luteum. Limnol. Oceanogr. 22(6): 1022-1032, doi: 10.4319/lo.1977.22.6.1022

50. Van Geest, G.J., F.C.J.M. Roozen, H. Coops, R.M.M. Roijackers, A.D. Buijse, E.T.H.M. Peeters, and M. Scheffer. 2003. Vegetation abundance in lowland flood plan lakes determined by surface area, age and connectivity. Freshw. Biol. 48(3): 440-454, doi: 10.1046/j.1365-2427.2003.01022.x

51. Vanni, M. J., W. H. Renwick, J. L. Headworth, J. D. Auch, and M. H. Schaus. 2001. Dissolved and particulate nutrient flux from three adjacent agricultural watersheds: A five-year study. Biogeochemistry 54: 85–114, doi:10.1023/A:1010681229460

52. Verpoorter, C., K. Tiit, D.A. Seekell, and L.J. Tranvik. 2014. A global inventory of lakes based on high-resolution satellite imagery. Geophys. Res. Letter. 41: 6396-6402, doi: 10.1002/2014GL060641

53. Vilas, M.P, C.L. Marti, M.P. Adams, C.E. Oldham, and M.R. Hipsey. 2017. Invasive macrophytes control the spatial and temporal patterns of temperature and dissolved oxygen in a shallow lake: A proposed feedback mechanism of macrophyte loss. Front. Plant. Sci. 8: 2097. doi: 10.3389/fpls.2017.02097.

54. Wilkinson, G.M., A. Besterman, C. Buelo, J. Gephart, and M.L. Pace. 2018. A synthesis of modern organic carbon accumulation rates in coastal and aquatic inland ecosystems. Sci. Rep. 8: 15736, doi: 10.1038/s41598-018-34126-y

55. Williams, P., M. Whitfield, J. Biggs, S. Bray, G. Fox, P. Nicolet, and D. Sear. 2004. Comparative biodiversity of rivers, streams, ditches and ponds in an agricultural landscape in Southern England. Biol. Conserv. 115(2): 329-341, doi: 10.1016/S0006-3207(03)00153-8

56. Wernberg, T., et al. 2016. Climate-driven regime shift of a temperate marine ecosystem. Science. 353(6295): 169-172, doi: 10.1126/science.aad8745

57. Woolway, R. I., E. Jennings, T. Shatwell, M. Golub, D.C. Pierson, and S.C. Maberly. 2021a. Lake heatwaves under climate change. Nature. 589: 402-407, doi: 10.1038/s41586-020-03119-1

58. Woolway, R.I., B.M. Kraemer, J. Zscheischler, and C. Albergel. 2021b. Compound hot temperature and high chlorophyll extreme events in global lakes. Environ. Res. Lett. 16(12): 124066, doi: 10.1088/1748-9326/ac3d5a

59. Woolway, R.I., C. Albergel, T.L. Frölicher, and M. Perroud. 2022. Severe Lake Heatwaves Attributable to Human-Induced Global Warming. Geophys. Res. Lett. 49(4): e2021GL097031, doi: 10.1029/2021GL097031

60. Wu, H., B. Hao, H. Jo, Y. Cai. 2021. Seasonality and species specificity of submerged macrophyte biomass in shallow lakes under the influence of climate warming and eutrophication. Front. Plant Sci. 12: 678259, doi: 10.3389/fpls.2021.678259

TABLES

Table 1. *Temporal versus spatial variation in DO Saturation*

		Temporal Variation in DO Saturation		***Spatial Variation in DO Saturation***	
Layer	*Pond*	*CV (%)* Mean	*CV (%)* Range	*CV (%)* Mean	*CV (%)* Range
Surface	Reference	28.9	20.2 – 34.4	5.9	1.8 – 11.3
	Nutrient Addition	22.8	20.6 – 28.8	4.4	2.1 – 9.5
Bottom	Reference	34.4	24.1 – 45.6	7.5	2.0 – 16.3
	Nutrient Addition	26.8	22.1 – 40.3	7.5	2.0 – 16.9

FIGURES

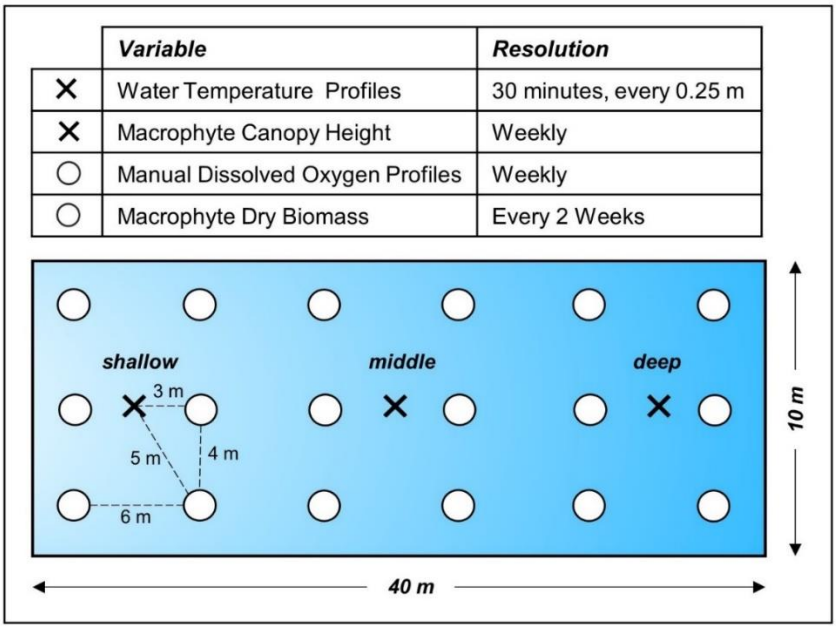

Figure 1. *Spatial and temporal resolution of measured variables and sample site locations.*

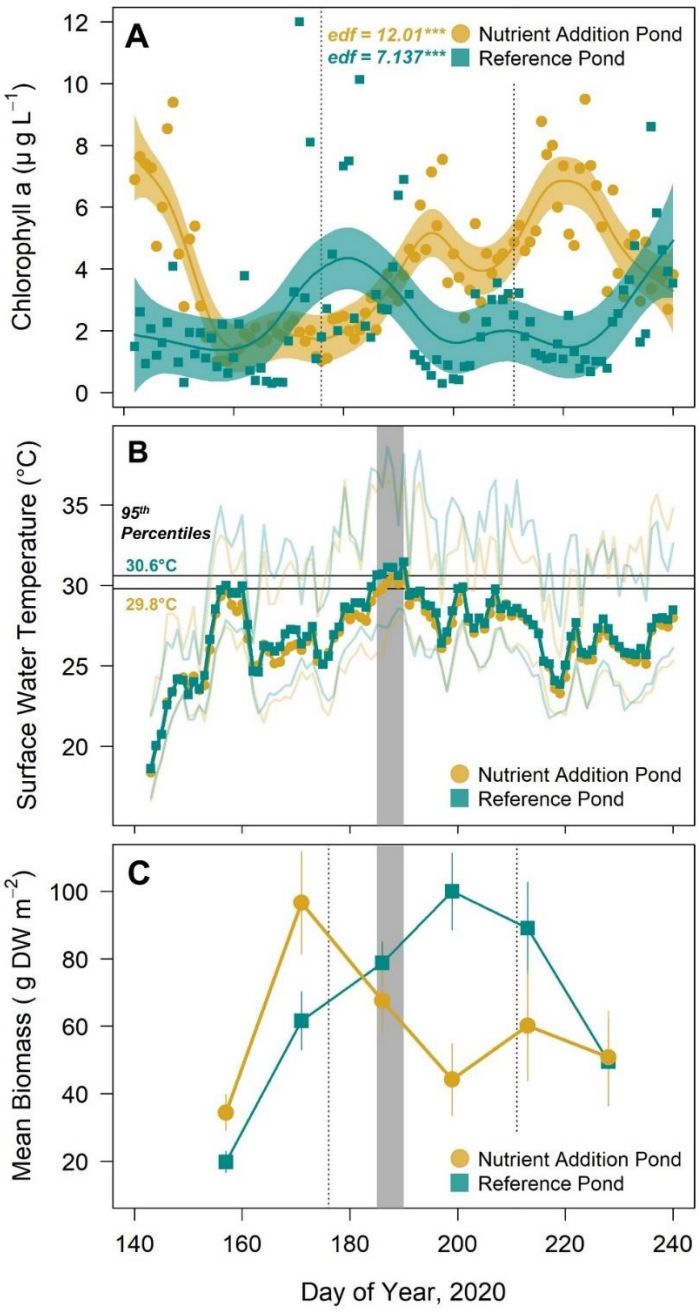

Figure 2. *Experimental Context.* (A) Timeseries of surface chlorophyll-*a* concentrations. Values from each pond were GAM-fit to highlight temporal trends. The asterisks next to the effective degrees of freedom (edf) correspond to the estimated p-value, with *** denoting $p < 0.001$. (B) Timeseries of mean daily surface (0-0.25 m) water temperature. Surface sensors at the deep and middle sites were used for these pond averages. The 95th percentile surface water temperature thresholds are noted in horizontal lines for the nutrient addition (29.8°C) and reference (30.6°C) ponds. (C) Time series of mean macrophyte biomass in each pond. Error bars mark the standard error of the mean. Across panels, dashed lines mark the timing of nutrient additions (DOY 176, 211) and the grey box highlights the aquatic heatwave (DOY 185-190).

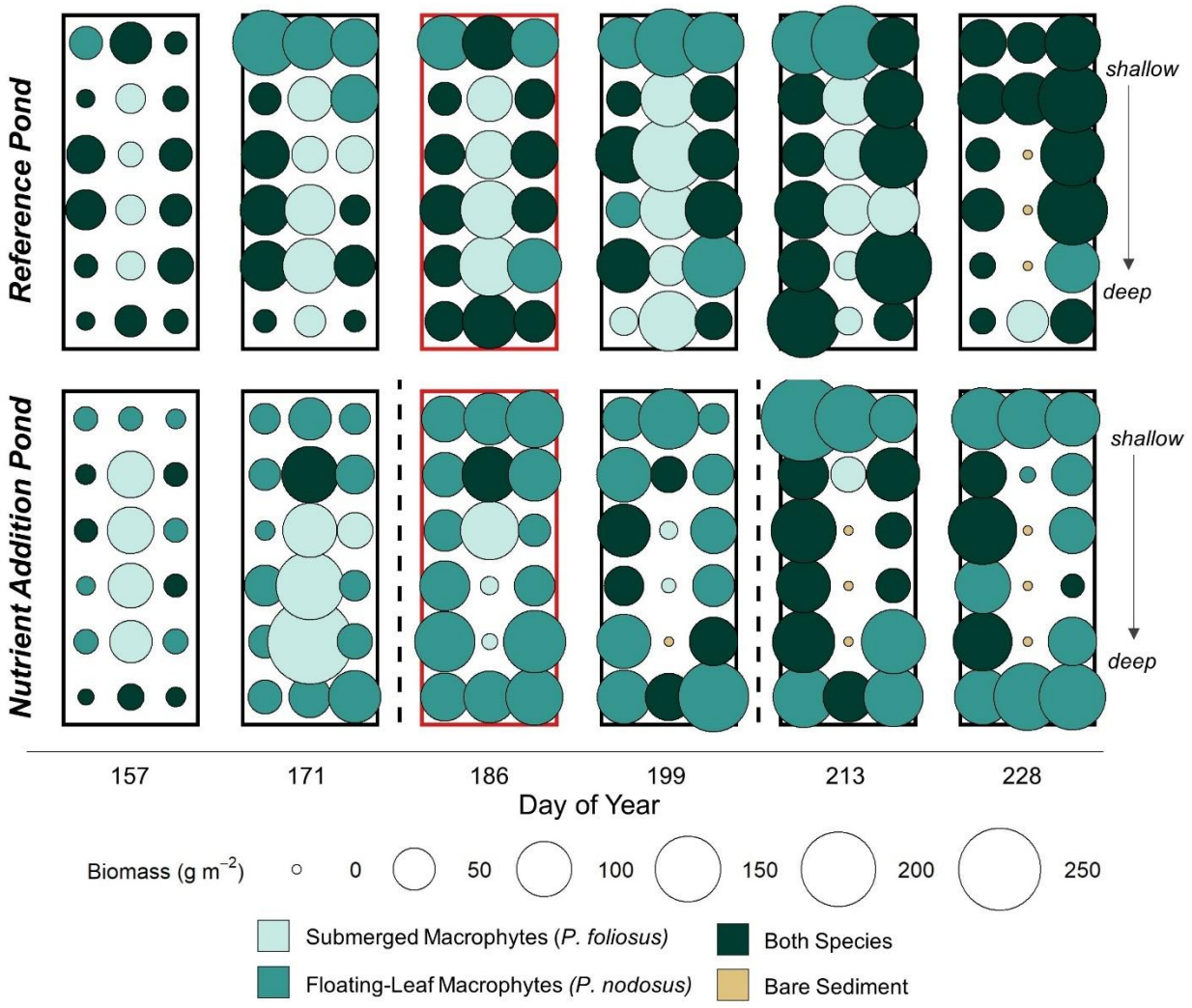

Figure 3. *Spatial and temporal variation in macrophyte dry biomass and community composition.* Biomass was sampled during the aquatic heatwave (DOY 185-190), as noted by the red pond outline on DOY 186. Dashed lines mark nutrient additions on DOY 176 and 211.

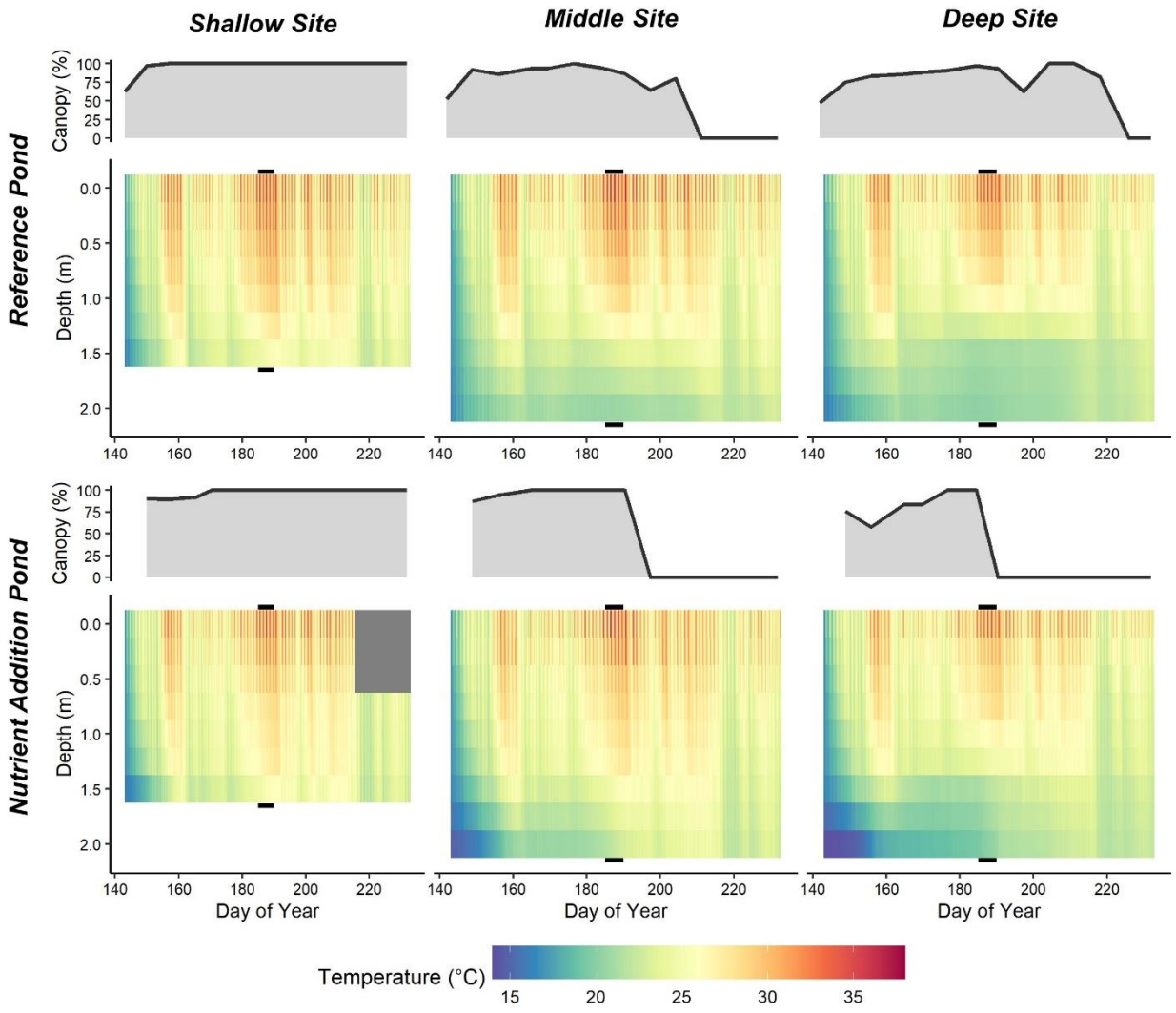

Figure 4. *Spatial and temporal variation in macrophyte canopy height and temperature profiles.* Canopy height is plotted as a percent of the water column height. Black, horizontal lines mark an aquatic heat wave from DOY 185-190. High frequency water temperature loggers were placed every 0.25 m of the water column up to 1.5 m and then every 0.5 m to the bottom. Temperature values at 1.75 m were interpolated for the sake of visualization. Several surface sensors (0-0.5 m) from the shallow site of the nutrient addition pond lost power following DOY 215 (grey box). An initial canopy height measurement is missing from the nutrient addition pond because the water was not sufficiently clear to see and measure the top of the canopy. The canopy height was less than 1 m or 50-75% of the water column at this time.

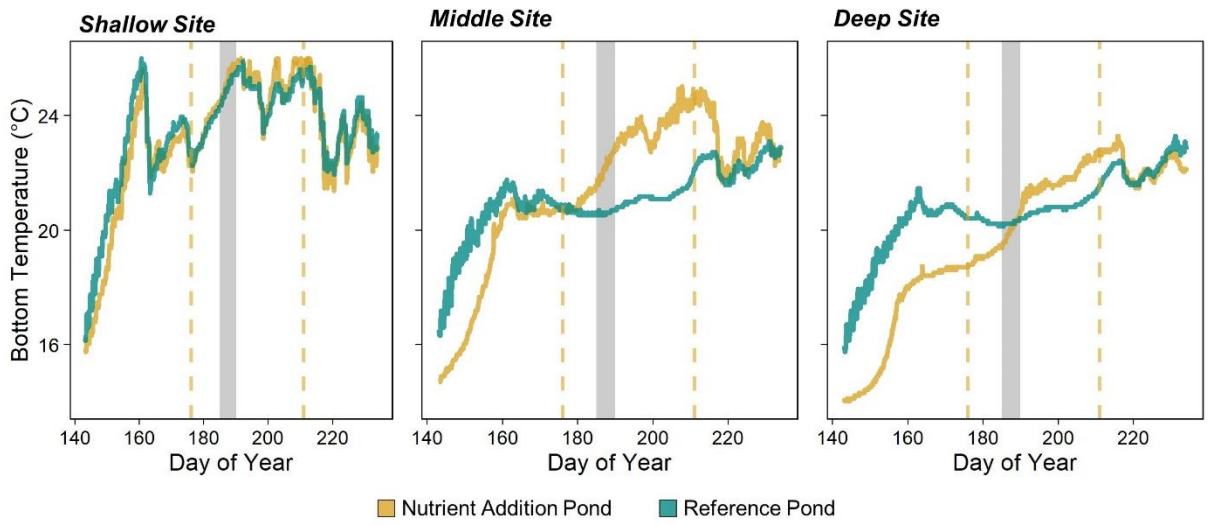

Figure 5. *Bottom water temperature time series across sampling sites.* The grey box marks an aquatic heat wave from DOY 185-190. Yellow dashed lines indicate the nutrient additions on DOY 176 and 211.

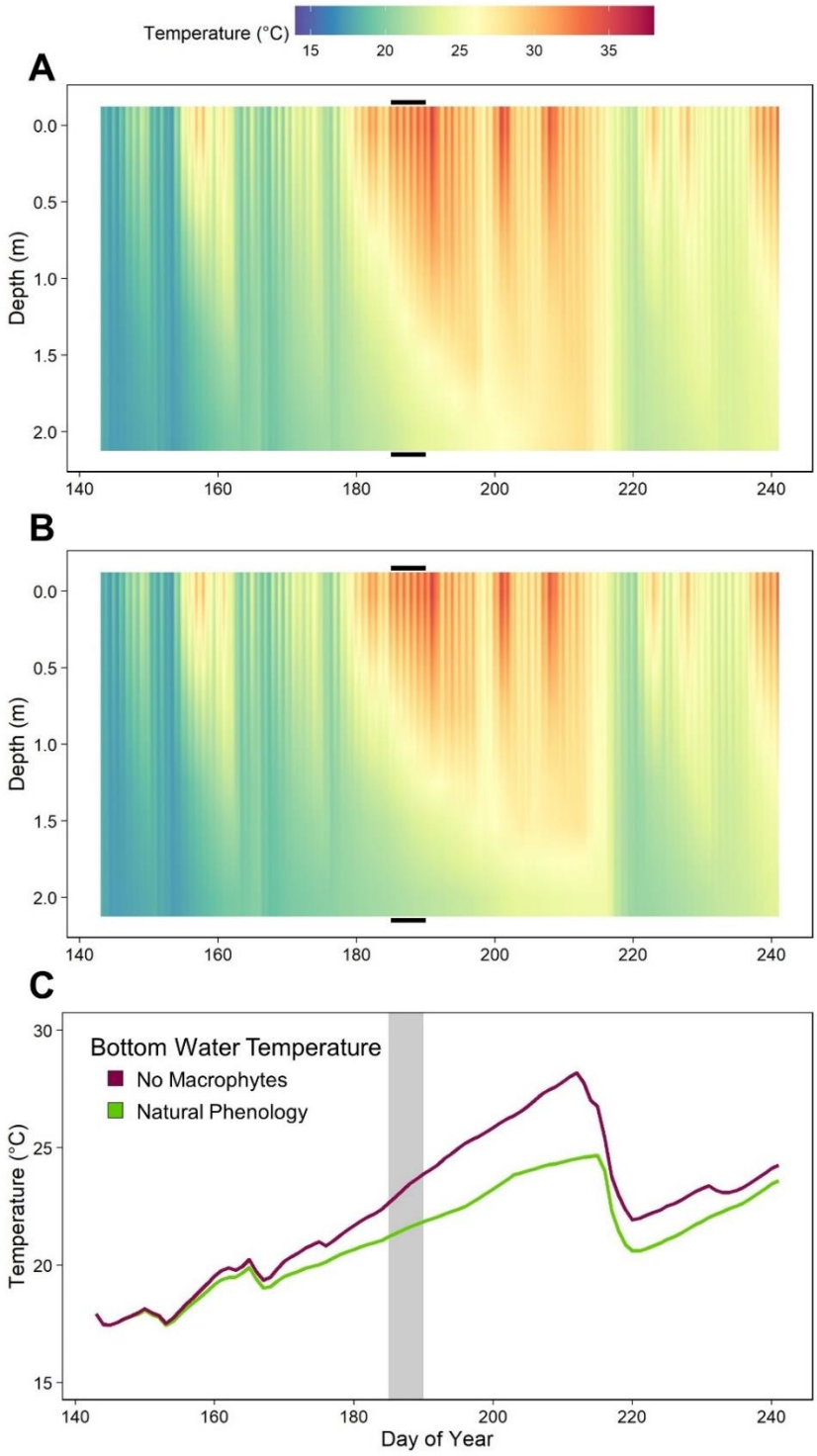

Figure 6. *Model simulation results contrasting no macrophyte coverage with natural phenology*. Predicted temperature profiles with (A) no macrophytes versus (B) the expected seasonal pattern of spring emergence, summer growth, and autumn senescence. Black, horizontal lines mark an aquatic heat wave (DOY 185-190). (C) Timeseries of predicted daily mean bottom water (2m) temperatures with no macrophytes versus expected seasonal patterns in macrophyte coverage.

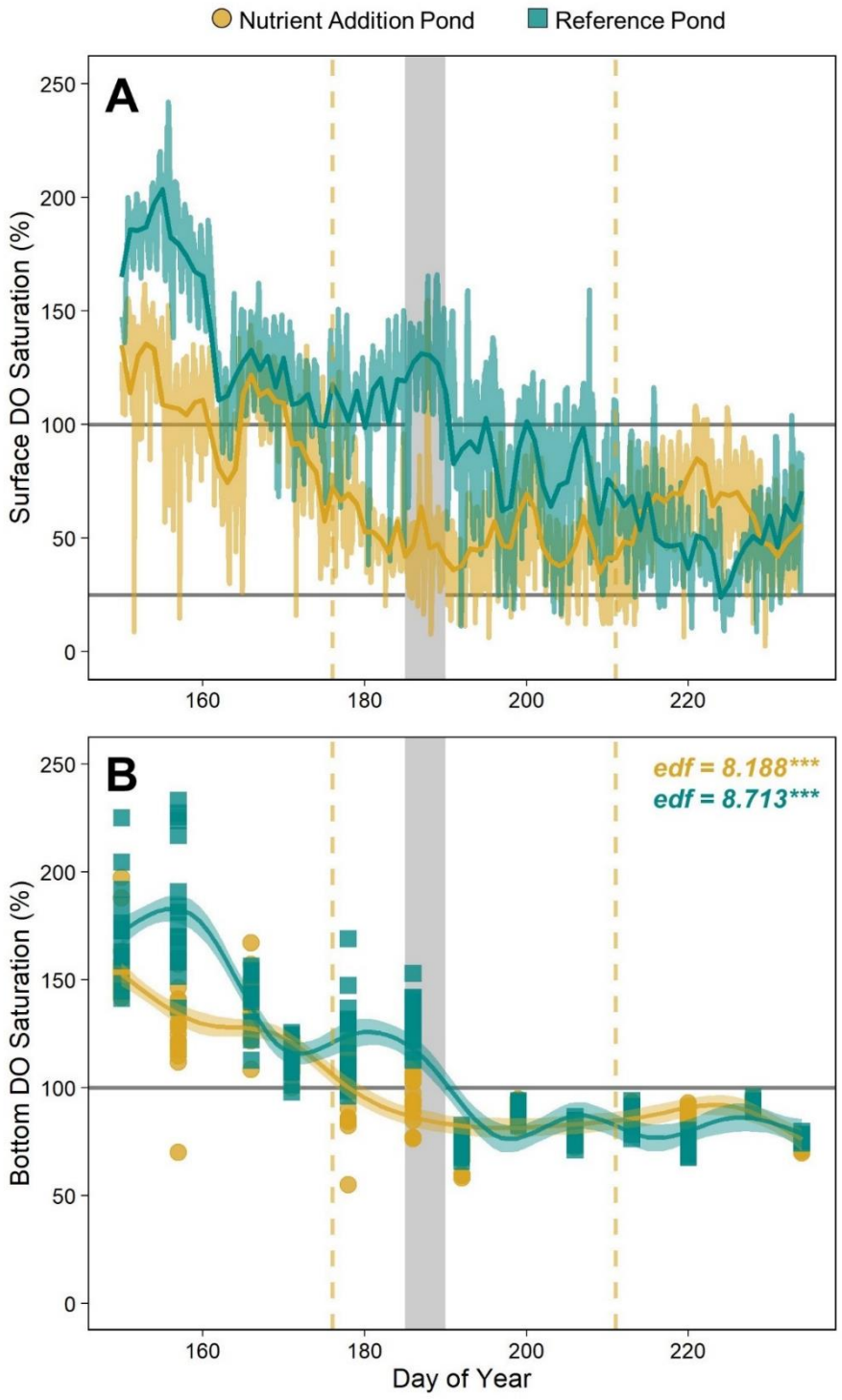

Figure 7. *Surface and bottom DO dynamics.* (A) High frequency surface DO saturation at the deep site of each pond over the study period. The daily mean is plotted in a darker line. Horizontal grey lines mark 100 and 25 percent saturation. (B) Weekly bottom water DO saturation at 18 sites across each pond. Values from each pond were GAM-fit to highlight temporal trends. The asterisks next to the effective degrees of freedom (edf) correspond to the estimated p-value, with *** denoting $p < 0.001$.

SUPPLEMENTARY INFORMATION FOR CHAPTER 4

Introduction

The appendix contains additional methods text detailing the algorithms and approach for the hydrodynamic model as well as an overview of calibrated model parameters (Table S1) and simulation input data for testing heatwave response under variable macrophyte scenarios (Table S2). Model fit is illustrated in Figure S6.

Figure S1 provides an example of individual DO saturation profiles to illustrate there was no evidence of mid-depth DO maxima. We provide time series of estimated thermocline depth (Figure S2), difference between surface and bottom water temperatures (Figure S3), and Schmidt's stability (Figure S4) for each pond. We also illustrate the relationship between macrophyte biomass and canopy height and the Schmidt's stability index (Figure S5). We further provide supplementary visualizations for our DO data, specifically time series of surface DO saturation and the difference between surface and bottom water DO (Figure S7), DO saturation as a function of macrophyte biomass and canopy height (Figure S8), and spatiotemporal variation in bottom water DO saturation (Figure S9).

Model Equations and Approach

Model description

A one-dimensional, integral energy model was developed to simulate the temperature, heat flux and stratification dynamics in small, vegetated ponds. The algorithms are based on the MINLAKE model (Ford and Stefan 1980; Riley and Stefan 1988; Herb and Stefan 2004).

Heat transport is implemented through the one-dimensional temperature diffusion equation:

(Eq. 1) $$\frac{\partial T}{\partial t} = \frac{\partial}{\partial z}\left(K_z \frac{\partial T}{\partial t}\right) + \frac{H(z)}{\rho_w c_p} + \frac{H_{geo}(z)}{\rho_w c_p}$$

where K_z is the vertical turbulent diffusion coefficient, H is internal heat generation due to incoming solar radiation, ρ_w is water density, c_p is specific heat content of water, and H_{geo} is internal geothermal heat generation.

Internal heat generation is implemented as:

(Eq. 2) $$H(z) = (1-\alpha)(1-\beta) I_s{}^{-((k_d+k_m)z)}$$

where α is the fraction of reflected incident solar radiation, β is the fraction of infrared radiation, I_s is total incident short-wave radiation, and K_d is a light attenuation coefficient and k_m is the light attenuation coefficient due to macrophytes.

For the upper, surface boundary condition we assume a Neumann type for the temperature diffusion equation:

(Eq. 3) $$H_{net} = \rho_w c_p \left(K_z \frac{\partial T}{\partial t}\right)$$

where H_{net} is the net heat flux exchange between atmosphere and water column:

(Eq. 4) $$H_{net} = H_{sw} + H_{lw} + H_{lwr} + H_v + H_c$$

where H_{sw} is the incoming solar incident radiation, $H_{sw}=(1-\alpha)I_s$, H_{lw} is the incoming long-wave radiation, H_{lwr} is emitted radiation from the water column, H_v is the latent heat flux, and H_c is the sensible heat flux. Implementations to estimate the respective heat fluxes were taken from Livingstone and Imboden (1989), Goudsmit et al. (2002), and Lerman et al. (1995).

The lower, sediment boundary condition was prescribed as:

(Eq. 5) $$\left(K_z \frac{\partial T}{\partial t}\right) = 0$$

The model algorithm is modularized into five components: (a) heat generation from boundary conditions and vertical diffusion, (b) mixed layer depth, and (c) convective overturn.

(a) Heat generation from boundary conditions and vertical diffusion

In the first step the heat fluxes H, Hg_{eo} and H_{net} are applied over the vertical water column. Simultaneously, vertical turbulent diffusion between adjacent grid cells is calculated. Here, we applied a centered difference approximation for temperature at the next time step using a first-order, explicit Forward Time Centered Space (FTCS) approach. The vertical turbulent diffusion coefficient K_z is calculated based on the empirical equations by Hondzo and Stefan (1993) for lakes in Minnesota as a function of the buoyancy frequency:

(Eq. 6) $$K_z = a_k (N^2)^{-0.43}$$

where a_k is an empirical factor accounting for the surface area of the lake A_s:

(Eq. 7) $$a_k = 0.00706 (A_s)^{0.56}$$

and N^2 is the squared buoyancy frequency:

(Eq. 8) $$N^2 = \frac{g}{\rho_w} \frac{\partial \rho_w}{\partial z}$$

and values of N^2 less than 7.0 10-5 s-2 were set to 7.0 10-5 s-2.

(b) Mixed layer depth

In the third step, we quantify the depth where the amount of external kinetic energy by wind shear stress equals the internal potential energy of the water column. Up to this mixed layer depth, z_{ml}, adjacent layers are subsequently mixed to account for a wind shear stress acting over the vertical water column. Here, the kinetic energy *KE* is described as:

(Eq. 9) $$KE = \tau u^* \Delta t$$

where τ is the surface turbulent shear stress, and u^* is the surface shear velocity, which was calculated from wind velocity as:

(Eq. 10) $$u^* = \sqrt{\frac{C_{10}\rho_a}{\rho_w}} U_2$$

where C_{10} is the wind stress coefficient dependent on the measured wind speed U_2 at 2 m height above the water surface, and ρ_a is the density of air, respectively (Herb and Stefan, 2005).

The dissipation of turbulent kinetic energy (DKE) by macrophytes is incorporated as:

(Eq. 11) $$DKE_z = (\rho_w \hat{a} C_d)(u^*)^3 \Delta z \Delta t$$

where â is the ratio of plant surface area per unit volume water and C_d is the plant form drag coefficient.

The potential energy of the water column for each layer over the depth is calculated as:

(Eq. 12) $$PE_z = g Z_z (Z_{z+1} - Z_{cv}) \Delta \rho$$

where g is gravitational acceleration, z_{cv} is the center of volume depth, and $\Delta\rho$ is a density change from the current layer to the next layer below.

The mixed layer depth z_{ml} is calculated by incrementally increasing the comparison between the difference of total kinetic energy KE to the dissipation of KE by macrophytes, and the internal potential energy PE as:

(Eq. 14) $$z_{ml} \rightarrow PE_{z+1} > (KE - DKE_z)$$

(c) Convective overturn

In the fourth step, any density instabilities over the vertical water column are mixed with a first stable layer below an unstable layer. Here, we applied an area weighed mean of temperature between two layers.

Appendix References

1. Ford, D.E., and H.G. Stefan. 1980. Thermal predictions using an integral energy model. J. Hydraul. Div. ASCE 106(1). 39-55, doi: 10.1061/JYCEAJ.0005358

2. Goudsmit, G.H., H. Burchard, F. Peeters, and A. Wüst. 2002. Application of k-e turbulence models to enclosed basins: The role of internal seiches. J. Geophys. Res. 107. C12. 3230, doi:10.1029/2001JC000954

3. Herb, W.R., and H.G. Stefan. 2004. Temperature stratification and mixing dynamics in a shallow lake with submersed macrophytes. Lake Reserv. Manag. 20(4): 296-308, doi: 10.1080/07438140409354159

4. Herb, W.R., and H.G. Stefan, 2005. Dynamics of vertical mixing in a shallow lake with submersed macrophytes. Water Resour. Res. 41. W02023, doi:10.1029/2003WR002613

5. Hondzo, M., and H.G. Stefan. 1993. Lake water temperature simulation model. J. Hydraul. Eng. 119(11). 1251-1273, doi: 10.1061/(ASCE)0733-9429(1993)119:11(1251)

6. Lerman, A., D. Imboden, and. J. Gat. 1995. Physics and Chemistry of Lakes. 2nd edition. Springer

7. Livingstone, D., and D. Imboden. 1989. Annual heat balance and equilibrium temperature of Lake Aegeri, Switzerland. Aquat. Sci. 51(4): 351-369, doi: 10.1007/BF00877177

8. Riley, M., and H.G. Stefan. 1988. MINLAKE: A dynamic lake water quality simulation model. Ecol. Model. 43. 155-182, doi: 10.1016/0304-3800(88)90002-6

Table S1. *Calibrated model parameter values*

Variable	Description	Value	Parameterization
C_d	Wind momentum drag	0.0013	Calibration to field data
K_m	Macrophyte light extinction coefficient	0.005	Calibration to field data
$C_{d\ plant}$	Macrophyte momentum drag coefficient	1	Herb and Stefan (2004)
â	Macrophyte area to volume	0.5	Calibration to field data
Wind factor	Wind speed multiplier	1	Best field calibration did not use wind speed or shortwave radiation multipliers (so factors equal to 1)
Short wave factor	Shortwave radiation multiplier	1	
Diffusion factor	Diffusion rate multiplier	0.8	Calibration to field data
H_{geo}	Sediment heating coefficient	6	Calibration to field data
ρ_m	Macrophyte density	30	Calibration to field data

Table S2. *Input macrophyte data for model simulations*

Field Data															
DOY	129	143	150	157	166	171	178	186	192	199	206	213	220	228	234
Canopy (m)	0.5	1	1.7	1.7	1.7	1.6	1.6	1.55	1.55	0	0	0	0	0	0
Biomass (g m^2)	NA	NA	NA	36.3	NA	150.1	NA	2.2	NA	0.48	NA	0	NA	0	NA
Simulation – natural macrophyte phenology															
DOY	129	143	150	157	166	171	178	186	192	199	206	213	220	228	234
Canopy (m)	0.5	1	1.7	1.7	1.7	1.6	1.6	1.55	1.55	1	1.6	1.8	1.4	0.2	0.2
Biomass (g m^2)	NA	NA	NA	36.3	NA	150.1	NA	101.4	NA	73.6	NA	15.4	NA	22.4	NA
Simulation – no macrophytes															
DOY	129	143	150	157	166	171	178	186	192	199	206	213	220	228	234
Canopy (m)	0	0	0	0	0	0	0	0	0	0	0	0	0	0	0
Biomass (g m^2)	0	0	0	0	0	0	0	0	0	0	0	0	0	0	0

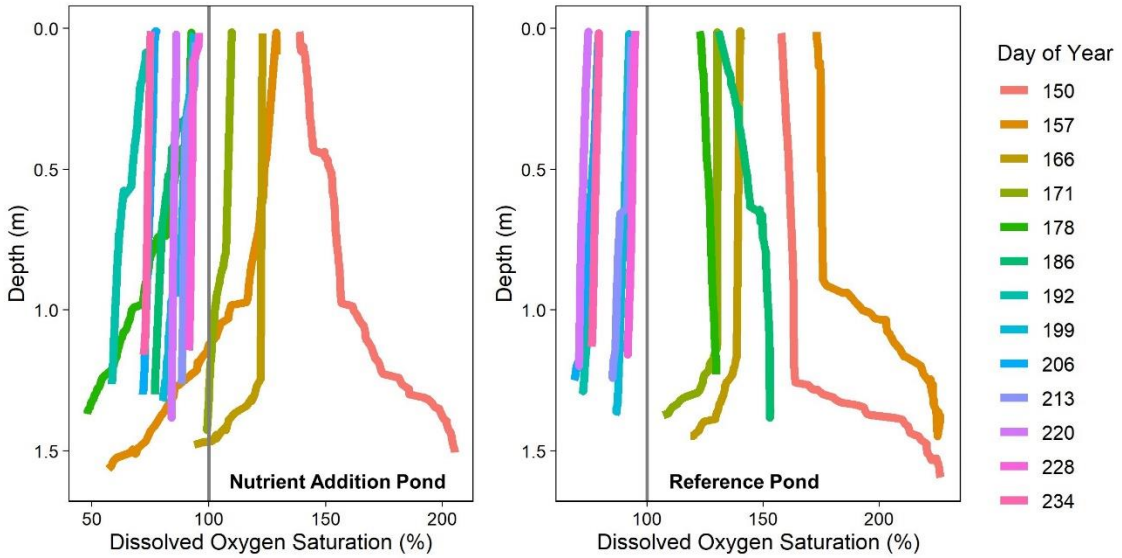

Figure S1. *Examples of individual DO saturation profiles near deep sites.* Profiles are color-coded by the DOY of the sampling event. These profiles were taken in the deeper, central region of the ponds. The vertical grey line highlights 100 percent saturation.

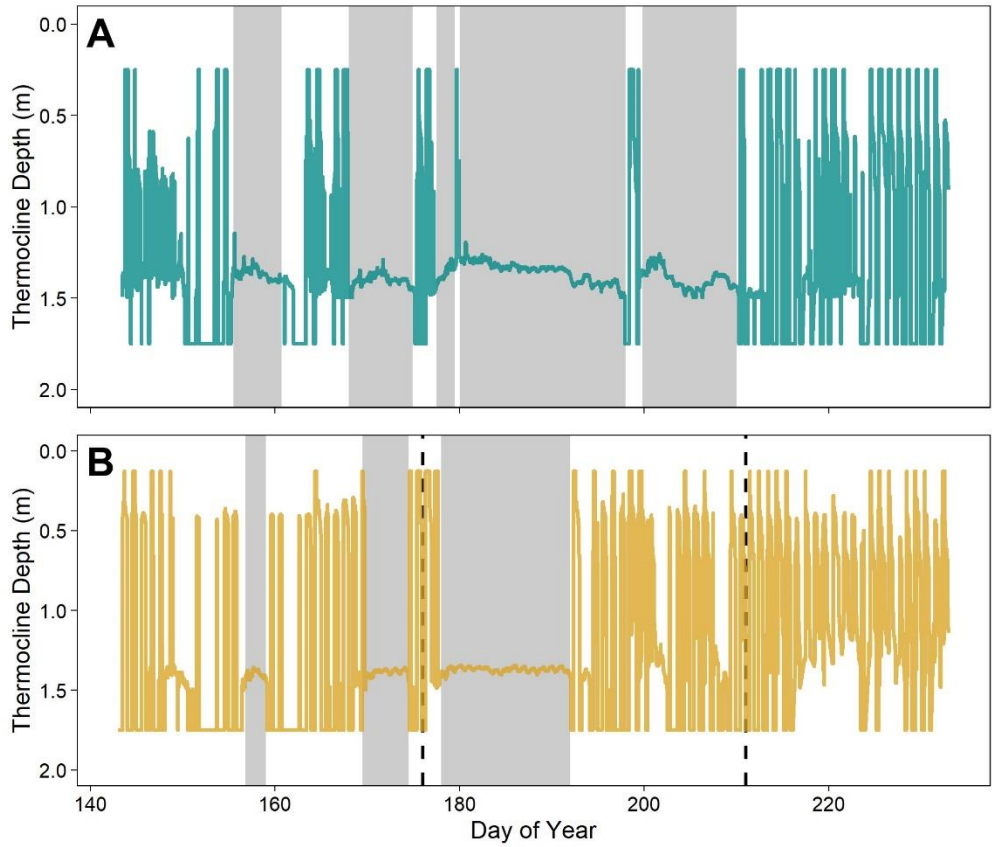

Figure S2. *Estimated thermocline depth by pond.* Periods of a stable thermocline for the reference (A) and nutrient addition (B) ponds are noted in the grey shaded boxes. Nutrient additions are noted with dashed black lines. Estimated thermocline values oscillating rapidly between the near surface and bottom waters were not considered time of stable stratification.

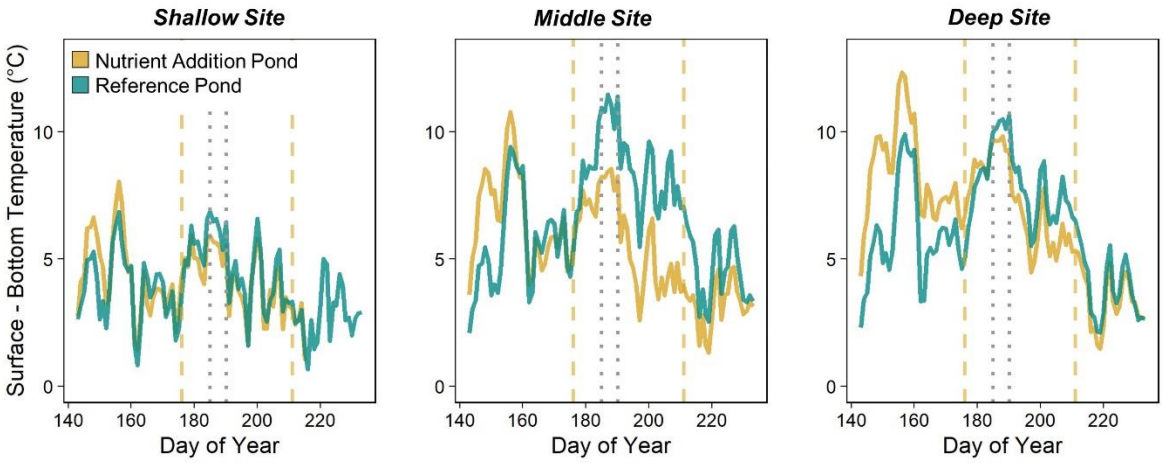

Figure S3. *Time series of the difference in surface and bottom water temperatures.* Daily mean values are plotted. Dashed yellow lines mark nutrient additions. An aquatic heatwave occurred between the dotted, grey lines (DOY 185-190).

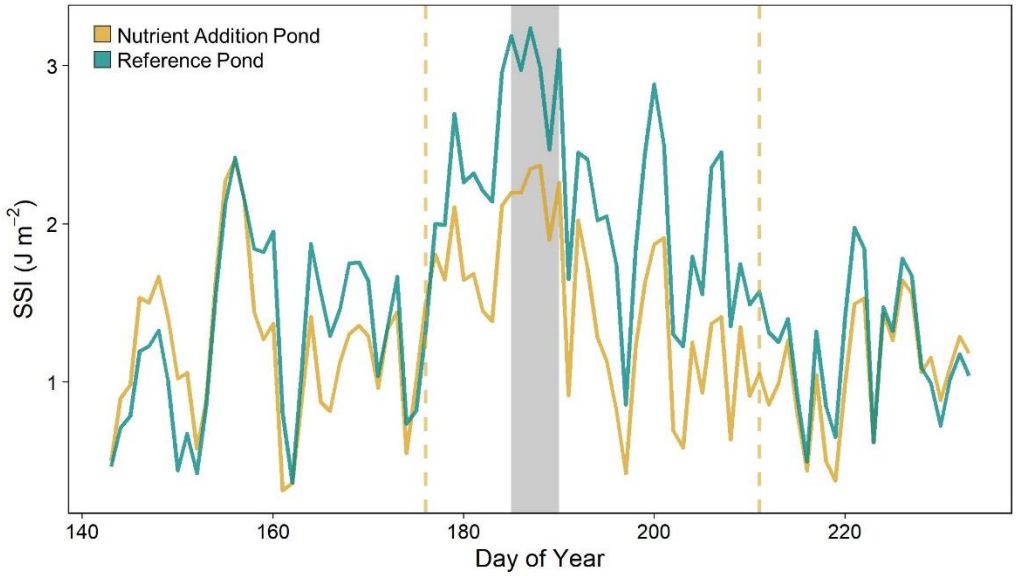

Figure S4. *Pond thermal stability over time.* Schmidt's stability for both experimental ponds. SSI was calculated based on the middle station temperature chain. The grey box marks the aquatic heatwave from DOY 185-190, and dashed yellow lines note nutrient additions.

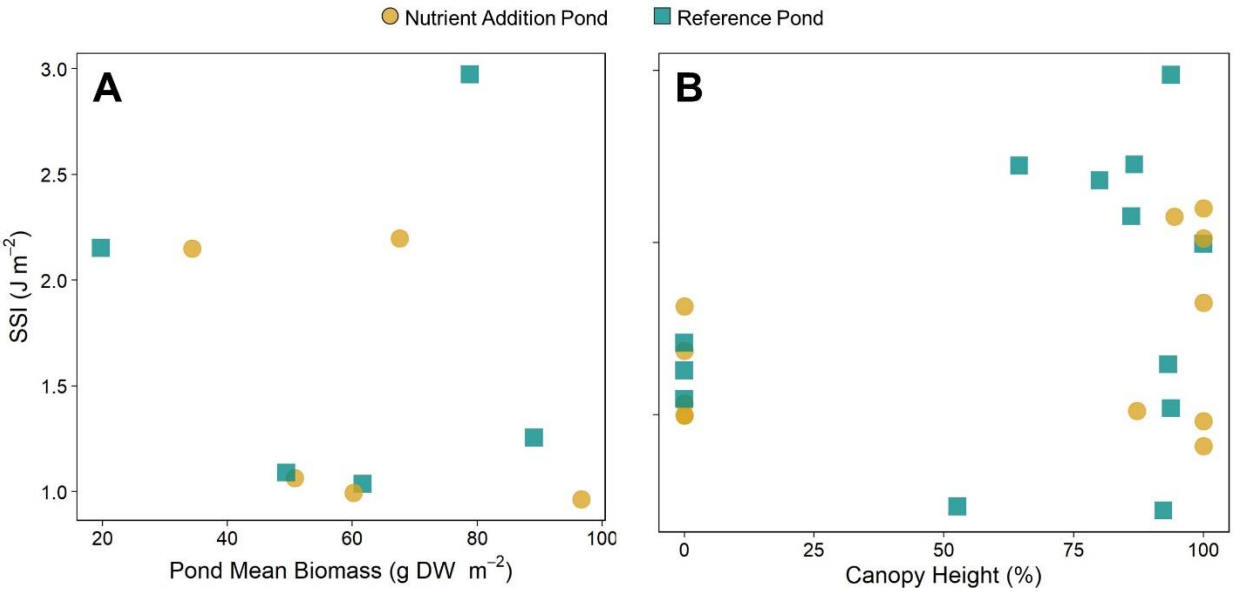

Figure S5. *Schmidt's Stability Index (SSI) and Macrophyte Biomass (A) and Canopy Height (B).* Mean pond biomass is a weighted average across 18 sites, giving shallow (n=14) and deeper (n=4) sites equal weight. Canopy height is reported as a percent of the water column. SSI was calculated based on the middle station temperature chain.

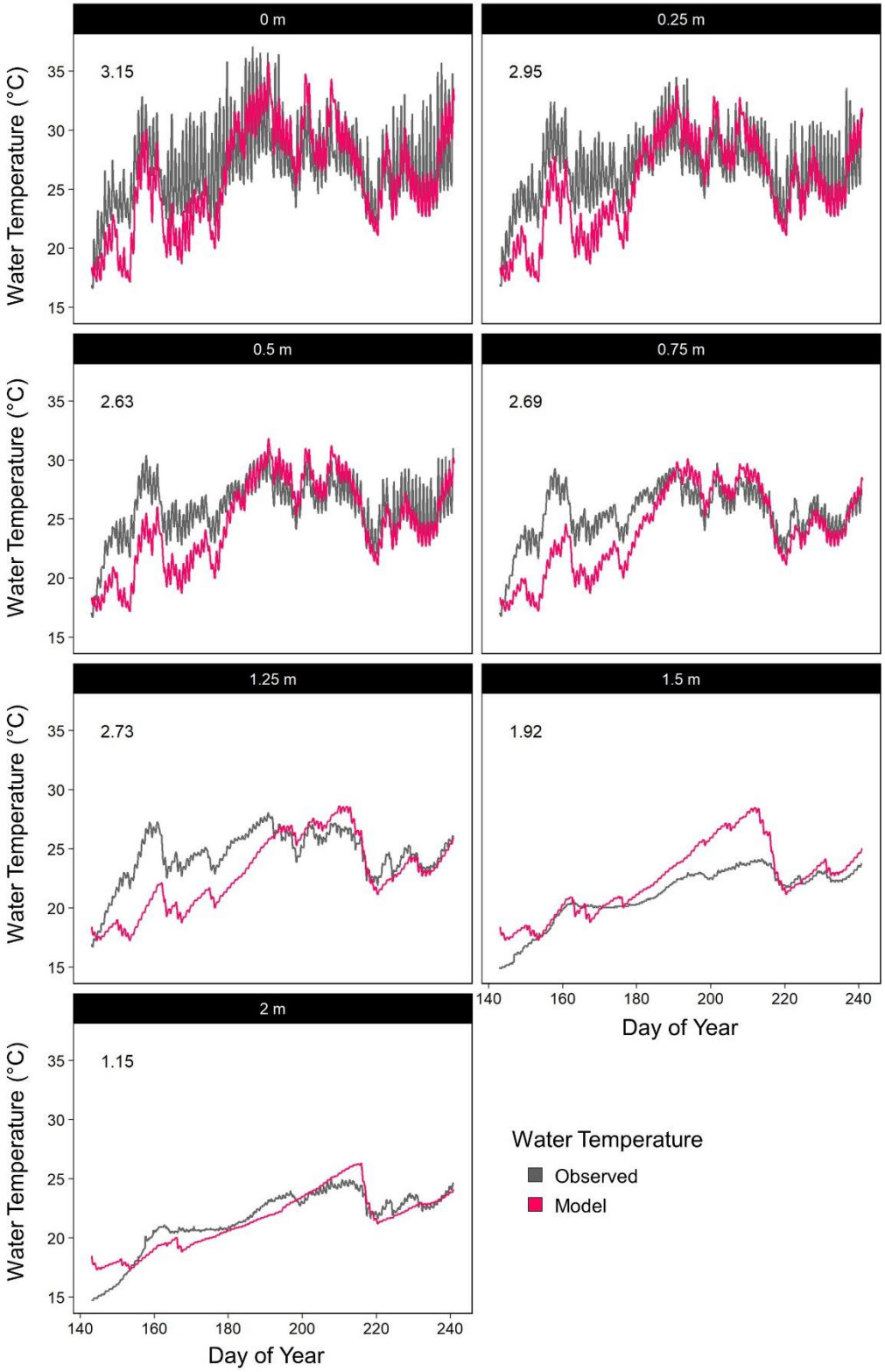

Figure S6. *Model fit at discrete depths.* Predicted water temperatures from the hydrodynamic model are plotted against the observed temperatures at the same depths. The root mean square error (RMSE, °C) are noted in the top left corner.

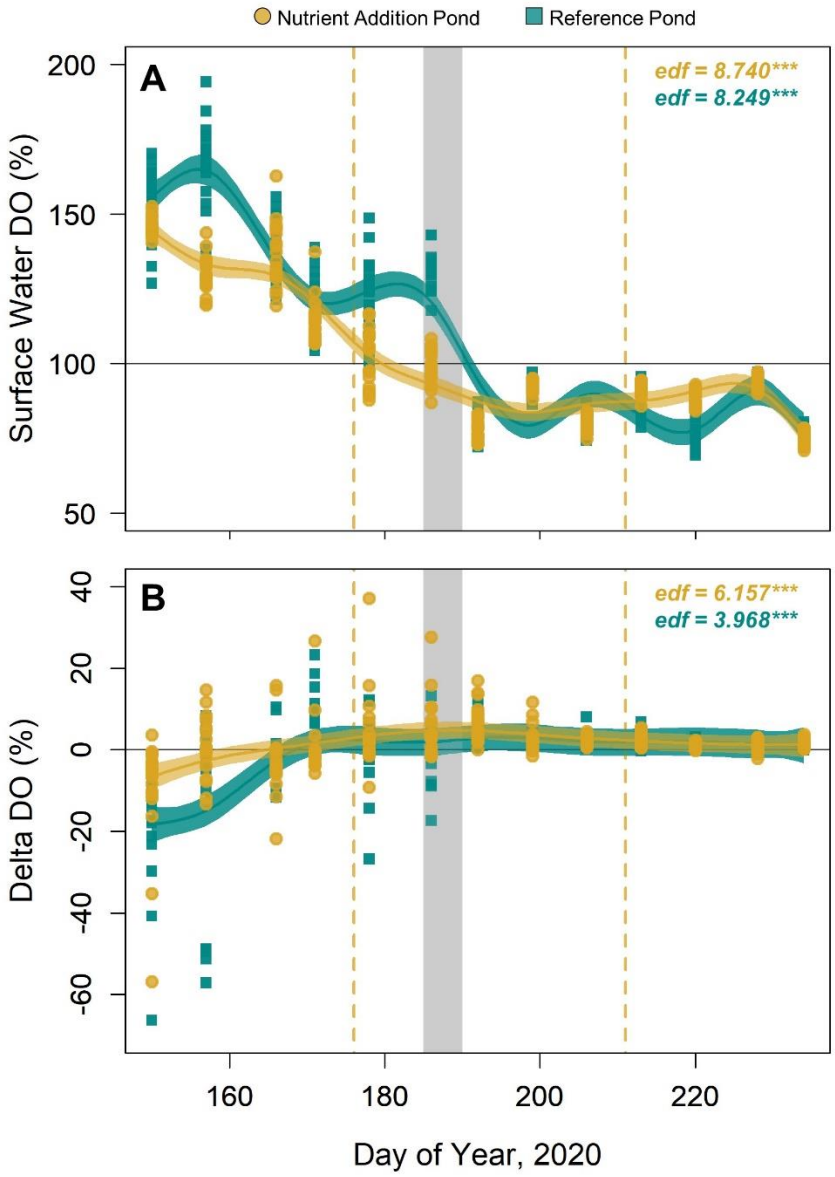

Figure S7. *Time series of surface and delta-DO saturation.* (A) Surface water DO saturation and (B) the difference between surface and bottom water DO saturation based on weekly profiles at 18 sites across each pond. Negative values of delta-DO indicate greater DO saturation in the bottom waters while positive values mean DO is higher in the surface layer. Values from each pond were GAM-fit to highlight temporal trends. The asterisks next to the effective degrees of freedom (edf) correspond to the estimated p-value, with *** denoting $p < 0.001$. Across both panels, dashed yellow lines mark the timing of nutrient additions and the grey box highlights the aquatic heatwave.

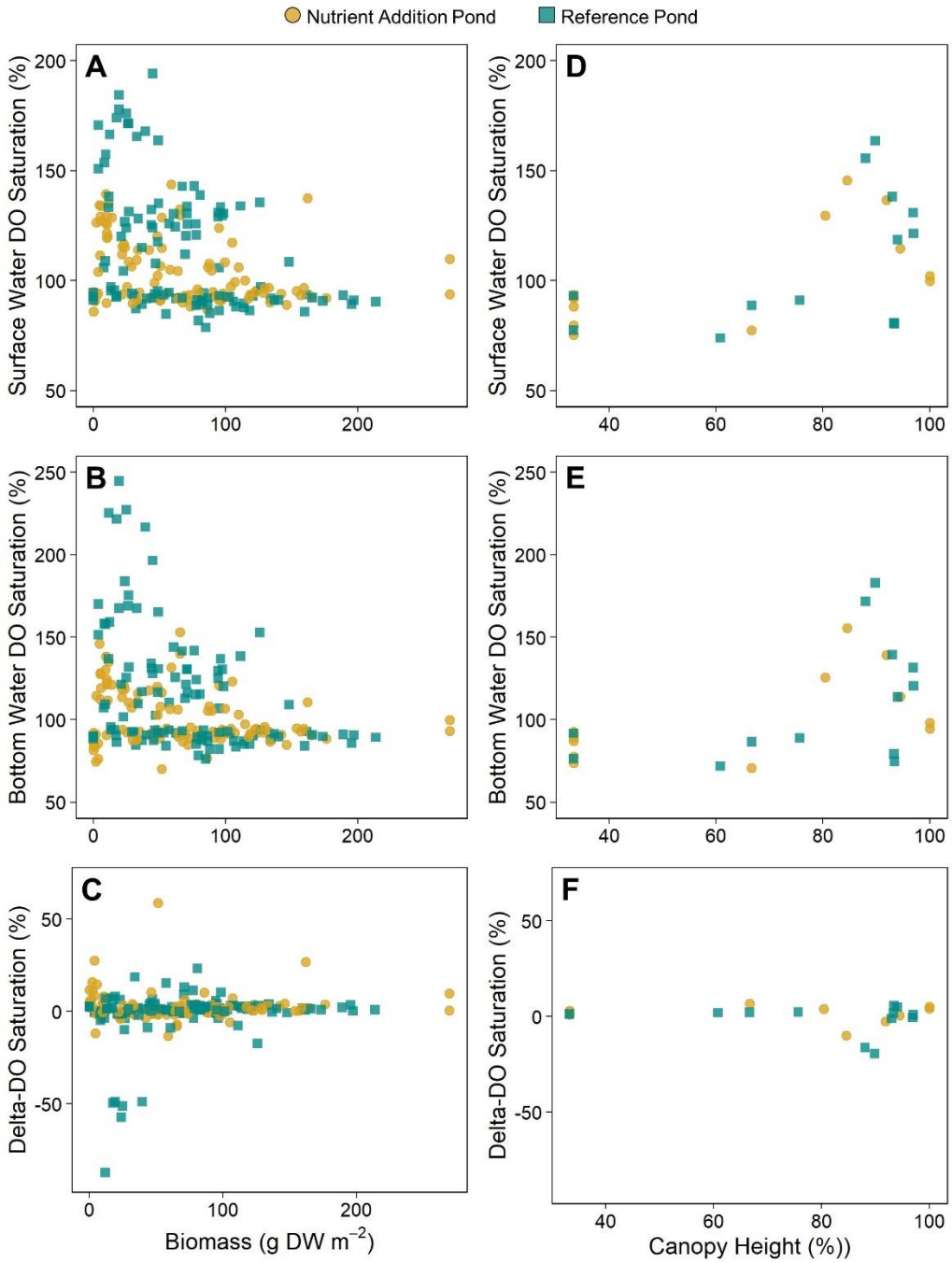

Figure S8. *DO Saturation as a function of macrophyte biomass (A-C) and canopy height (D-F).* Weekly DO profiles at 18 sites across each pond were used for surface and bottom water DO saturation. Delta-DO is the difference between surface and bottom water DO. Biomass samples were taken every two weeks at the same 18 sites. Canopy height is a pond average measured weekly. A pond average DO value from the same DOY was plotted against canopy height.

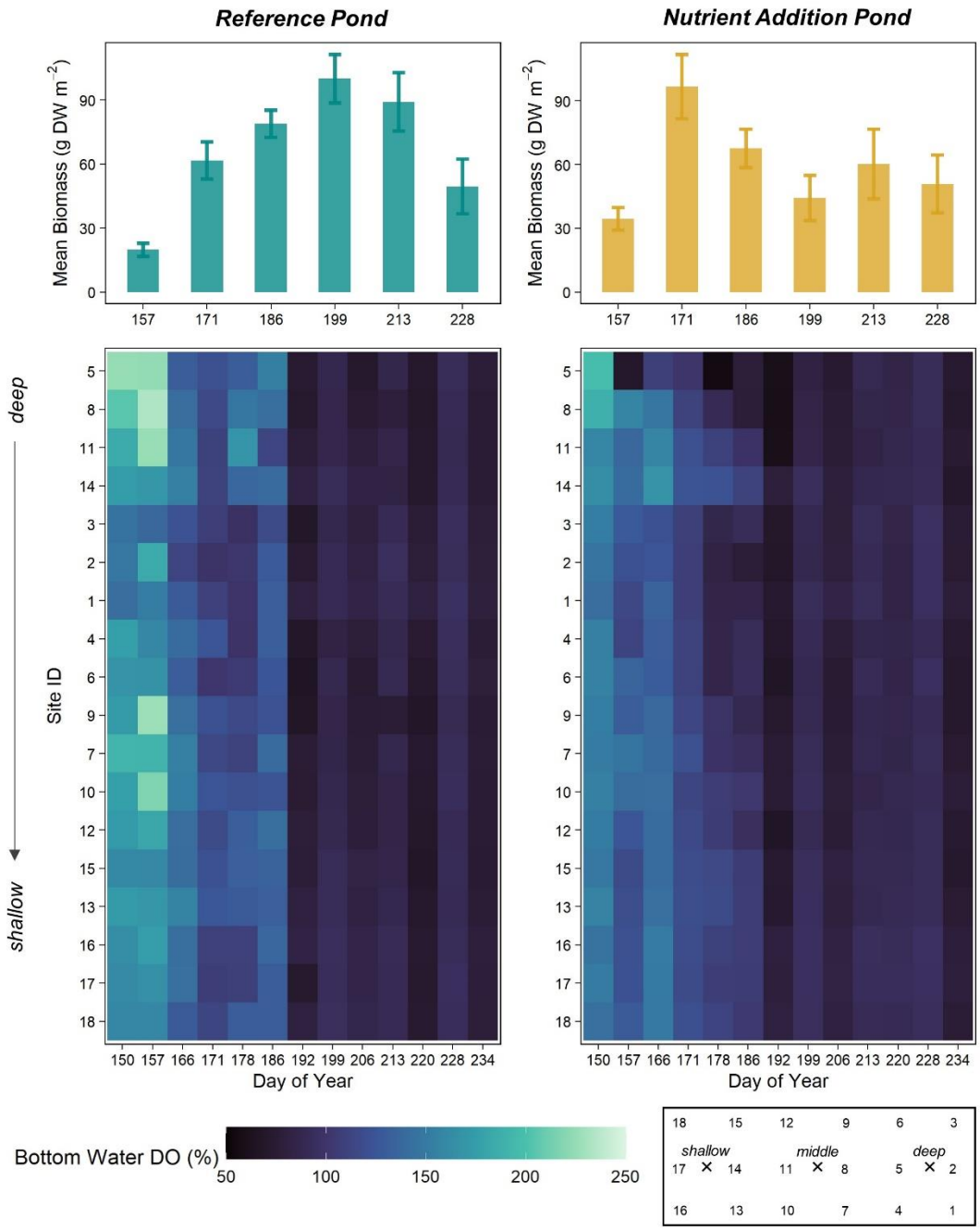

Figure S9. *Spatiotemporal variation in bottom water DO saturation.* Sampling sites are ordered approximately from the deepest to most shallow locations. The pond-averaged biomass values are plotted above. Error bars represent the standard error of the mean.

CONCLUSIONS

Effective management of freshwater eutrophication requires a quantitative and mechanistic understanding of lentic phosphorus (P) cycles and how nutrient enrichment will interact with other external stressors (e.g., climate change). These management needs inspired my dissertation research on internal P loading and compounding stressors in shallow lakes, reservoirs, and ponds. This research has advanced our understanding of lacustrine phosphorus (P) cycles by generating knowledge on spatiotemporal variation in sediment P fluxes and the underlying mechanisms and by synthesizing our current understanding of internal P loading in lentic ecosystems. Chapter 1 employed the tools of systematic literature review and meta-analysis to synthesize findings across studies in order to understand patterns between sediment P flux rates and both ecosystem- and site-scale drivers. By exploring these relationships, this analysis provided guidance for estimating the magnitude and underlying mechanisms of sediment P release for waterbodies in which direct measurements are scarce or unavailable. The literature synthesis also revealed remaining data gaps, which indicated that our current understanding of internal P loading does not fully capture interactions between different mechanisms of sediment P release, particularly interactions between sediments and other biogeochemical conditions.

Chapters 2 and 3 explored the role of sediment P chemistry as a controlling variable for internal P loading. These chapters highlighted the importance of accounting for spatial and seasonal variation in sediment P pools and fluxes, and provided recommendations for capturing this variation in sampling procedures and scaling measurements to the ecosystem-scale. Research findings from these chapters emphasized that single-station or single-season measurements of internal P loading are insufficient to characterize the dominant biogeochemical mechanisms involved. Chapter 3 further emphasized the influence of aerobic sediment P release in productive

waterbodies, in opposition to the persistent idea in the field that oxic conditions at the sediment-water interface will result in sediment P retention. This finding was further supported through the meta-analysis, which revealed that sediment P release occurs under both oxic and anoxic conditions across a broad range of lakes and reservoirs. As such, our mechanistic understanding of internal P loading would benefit from a conceptual shift, specifically from considering the role of dissolved oxygen in sediment P cycling as an oxic versus anoxic dichotomy to a framework that studies dissolved oxygen as a continuous variable, interacting with other chemical and biological conditions in the sediments.

To this end, chapter 4 explored dissolved oxygen dynamics in small waterbodies to understand how this master ecosystem variable responds to compounding stressors of nutrient enrichment and aquatic heatwaves. This analysis underscored the pivotal role that submersed macrophytes play in structuring their physicochemical environment and reinforced that small waterbodies are spatially complex and temporally dynamics systems. Accounting for this spatiotemporal heterogeneity is essential for understanding lentic biogeochemical cycles and how lentic ecosystems will respond to compounding stressors.